

THE UNIVERSITY OF HULL

**Fault-tolerant Load Reduction Control for
Large Offshore Wind Turbines**

being a thesis submitted for the degree of Doctor of Philosophy
in the University of Hull

by

YANHUA LIU

BEng and MSc in Automation (NCEPU, China)

April 2019

Acknowledgements

I am wholeheartedly grateful to my supervisor Prof. Ron J. Patton for supervising me and for his longstanding support. He is such a wise and inspiring teacher. He creates a flexible research environment to let me explore new ideas, while he can always point out the "eigenvalues" of my puzzles at crossroads. His deep insight and broad knowledge of control system provide me many productive and valuable suggestions. I am deeply appreciative of Prof. Ron for his numerous patient discussions.

I am very grateful to my second supervisor Prof. Jim Gilbert for sharing many interesting discussions, and for his fantastic support both academically and financially. I am also thankful to Dr. Bryn Jones and Dr. Wai Hou Lio from the University of Sheffield for their thought-provoking discussions and kind help for the initial study of load reduction methods. Thanks also go to the colleagues including Dr. Fengming Shi, Dr. Zhihuo Wang, Dr. Bingyong Guo, Dr. Jianglin Lan, Dr. Siya Jin, Mustafa Abdelrahman, Chun Liu and Shuo Shi in the Control and Intelligent Systems Engineering Lab. It is really my great honour to meet them in Hull.

I gratefully acknowledge the financial support of the PhD study from Chinese Scholarship Council and the University of Hull.

Finally, I want to give my special gratitude to my respectful parents especially my mother-in-law Yufeng Li, my loving husband Shuo Shi and my beloved son Xilin Shi, who always love me and give me their unwavering support.

Abstract

Offshore wind turbines suffer from asymmetrical loading (blades, tower etc.), leading to enhanced structural fatigue. As well as asymmetrical loading different types of faults (pitch system faults etc.) can occur simultaneously, causing degradation of load mitigation performance and enhanced fatigue. Individual pitch control (IPC) provides an important method to achieve mitigation of rotor asymmetric loads, but this may be accompanied by a resulting enhancement of pitch movement leading to increased possibility of pitch system faults, which negative effects on IPC performance.

This thesis focuses on combining the fault tolerant control (FTC) techniques with load reduction strategies by a more intelligent pitch control system (i.e. collective pitch control and IPC) for offshore wind turbines in a system level to reduce the operation & maintenance costs and improve the system reliability. The scenario of load mitigation is analogous to the FTC problem because the action of rotor/tower bending can be considered as a fault effect. The essential concept is to attempt to account for all the "fault effects" in the rotor and tower systems which can weaken the effect of bending moment reduction through the use of IPC.

Motivated by the above, this thesis focuses on four aspects to fill the gap of the combination between FTC and IPC schemes. Firstly, a preview control system using model predictive control with future wind speed is proposed, which could be a possible alternative to using LiDAR technology when using preview control for load reduction. Secondly, a multivariable IPC controller for both blade and tower load mitigation considering the inherent couplings is investigated. Thirdly, appropriate control-based fault monitoring strategies including fault detection and fault estimation FE-based FTC scheme are proposed for several different pitch actuator/sensor faults. Furthermore, the combined analysis of an FE-based FTC strategy with the IPC system at a system level is provided and the robustness of the proposed strategy is verified.

Table of Contents

List of Figures	vi
List of Tables	ix
List of Abbreviations and Symbols	x
List of Publications	xiv
1 Introduction	1
1.1 Background	1
1.2 Control of Wind Turbines	2
1.3 Typical Faults of Wind Turbine Systems	8
1.4 Challenges and Objectives	12
1.5 Outline of the Thesis	15
2 Load Reduction Control for Wind Turbines	18
2.1 Introduction	18
2.2 The Aero-elastic Simulation Tool FAST	19
2.2.1 Mathematical Model	20
2.2.2 Blade Pitch System	21
2.2.3 Wind Modelling	22
2.2.4 Baseline Wind Turbine Control	22
2.3 Structural Loading in Wind Turbines	24
2.4 Load Mitigation Control	26
2.5 Literature Review of IPC Methods	32
2.5.1 Traditional Feedback Control	32
2.5.2 Feed-forward / Preview Control	34
2.5.3 Smart Rotor Control	36
2.6 Conclusion	37

3	Fault Diagnosis and Fault-tolerant Control for Wind Turbine Systems	38
3.1	Introduction	38
3.2	Overview of Fault Diagnosis and Fault-tolerant Control	40
3.2.1	Fault Classification	40
3.2.2	Fault Diagnosis	42
3.2.3	Fault-Tolerant control	45
3.3	Fault Diagnosis and Fault-tolerant Control for Wind Turbines	48
3.4	A Tutorial Example of FDI for Pitch Actuator Stuck Fault	50
3.4.1	Problem Statement	50
3.4.2	FDI by Kalman Filter	54
3.4.3	Simulation Results	56
3.5	Conclusions	62
4	Rotor Load Reduction using MPC with Gaussian Wind Speed Prediction	63
4.1	Introduction	63
4.2	Wind Turbine Model	65
4.2.1	FAST Linearization	65
4.2.2	Actuator Dynamics	67
4.3	Model Predictive based IPC Design	68
4.3.1	Principle of MPC	69
4.3.2	Feed-forward MPC-IPC Design	70
4.4	Gaussian Wind Speed Prediction	74
4.4.1	Rotor Effective Wind Speed	74
4.4.2	Gaussian Prediction Model	76
4.5	Simulation Results	79
4.5.1	Very Short-term Wind Speed Forecasting using GP	79
4.5.2	MPC-IPC Load Mitigation with Wind Preview	81
4.6	Conclusion	86
5	Fault-tolerant Individual Pitch Control using Adaptive Fault Estimation	88
5.1	Introduction	88
5.2	Problem Statement	91
5.3	FTC-IPC System Design	94
5.3.1	Traditional IPC Strategy for Load Mitigation	94
5.3.2	FE-based FTC Design for Fault Compensation	99
5.3.2.1	FE Design	99
5.3.2.2	FTC Design	101

5.4	Simulation Results	102
5.4.1	Load Reduction in the Fault-free Case	102
5.4.2	Load Reduction in the Faulty Case	103
5.5	Conclusion	110
6	Rotor and Tower Structural Load Mitigation in Presence of Pitch Sensor Fault	113
6.1	Introduction	113
6.2	Problem Formulation	116
6.2.1	Wind Turbine Structural Load Analysis	116
6.2.2	Pitch System Modelling with Sensor Faults	118
6.3	Proposed strategy	122
6.3.1	LQR-based IPC for Blade and Tower Load Mitigation	122
6.3.2	FE-based FTC using Robust UIO	126
6.4	Simulation Results	131
6.4.1	Structural Load Reduction in Fault-free Case	131
6.4.2	Fault Estimation Results	133
6.4.3	Combination between Load Reduction with FE-based FTC	137
6.5	Conclusion	143
7	Summary and Future Work	145
7.1	Summary	145
7.2	Recommendations for Future Research	149
	Appendix A Baseline controllers	151
	Appendix B Frequency Splitting of Coleman transformation	153
	Appendix C Lemmas in the Thesis	156
C.1	Schur Complement	156
C.2	LMI Regional Pole Placement Complement	156
	References	157

List of Figures

1.1	Growth trend of WTs over time and future projects (Koh and Ng, 2016)	2
1.2	Different wind turbine blade failures (from google images).	3
1.3	Main components of a HAWT (Esbensen and Sloth, 2009)	3
1.4	Typical wind turbine sensors (Connectivity, 2019)	5
1.5	Power curve and operation modes for the 5MW NREL wind turbine system (Jonkman et al., 2009)	6
1.6	Power coefficient curve of the 5MW NREL wind turbine	7
1.7	Typical faults and problems from different wind turbine subsystems and assemblies	9
1.8	Percentage distribution of standardized downtime per year per turbine caused by the WT subsystem and assembly faults from various manufacturers in the ReliaWind study (Wilkinson et al., 2010)	10
1.9	Hydraulic pitch system of wind turbine system (from google images)	10
1.10	One hydraulic pitch system with the CPC and IPC controllers	11
1.11	Fault tolerant control of wind turbines with sustainable controllers	12
1.12	Structure of the thesis	16
2.1	The simplified 5MW NREL wind turbine simulation model in MATLAB/Simulink	24
2.2	Horns Rev wind farm in Denmark (Technology, 2017)	25
2.3	Vertical wind shear effect and turbulence from the left side view of a upwind wind turbine (Houtzager et al., 2013)	26
2.4	Different common loads of wind turbine	27
2.5	General wind turbine control system with common load mitigation strategies (Körber, 2014)	27
2.6	Traditional IPC scheme (Bossanyi, 2005)	29

2.7	Illustrations of the blade rotational reference frame {B} and the fixed hub reference frame {F} (referred to as tilt-yaw coordinate system) (Zhang et al., 2014a)	30
2.8	Frequency spectra of the blade 1 flapwise bending moment and main bearing tilt moment	31
2.9	Frequency spectra of the tower fore-aft and side-side bending moments	32
3.1	A control system with actuator, component and sensor faults (Patton, 2015)	41
3.2	A control system with abrupt, incipient and intermittent faults (Patton, 2015)	42
3.3	General schematic diagram of model-based fault diagnosis (Chen and Patton, 2012)	44
3.4	General architecture of FTC strategy (Blanke et al., 2006)	45
3.5	Classification of the AFTC methods	46
3.6	Proposed Kalman filter-based FDI strategy	56
3.7	Wind speed profile	57
3.8	Three pitch angle measurements in both fault-free case and single PAS fault on blade 1	58
3.9	Flapwise bending moment of blade 1 and generator power in both fault-free case and single PAS fault on blade 1	58
3.10	Tower fore-aft and side-side bending moments in both fault-free case and single PAS fault on blade 1	59
3.11	Fault detection result in the case of single PAS fault on blade 1	59
3.12	Three pitch angle measurements in both fault-free case and multiple PAS faults on three blades	60
3.13	Flapwise bending moment of blade 1 and generator power in both fault-free case and multiple PAS faults on three blades	60
3.14	Tower fore-aft and side-side bending moments in both fault-free case and multiple PAS faults on three blades	61
3.15	Fault detection result in the case of multiple PAS faults on three blades	61
4.1	Proposed control strategy in Region 3	69
4.2	The MPC strategy in discrete time	70
4.3	Nominal LiDAR strategy for the EWS prediction	75
4.4	The power output span-wise change	76
4.5	Proposed EWS prediction strategy by GP	77

4.6	Comparison between the wind speed at the hub-height and the rotor EWS	80
4.7	Proposed GP wind speed prediction scheme	81
4.8	Comparison between the real and wind speed prediction by proposed GP (1s ahead)	82
4.9	Comparison between the real and wind speed prediction by proposed GP (5s ahead)	82
4.10	Flapwise bending moments of blade 1	84
4.11	Pitch angle of blade 1	85
4.12	Generator power	85
5.1	Nominal pitch system strategy by CPC	91
5.2	Nominal pitch system strategy by IPC	92
5.3	Step response of one pitch actuator system in different situations . . .	93
5.4	Fault-tolerant pitch system	94
5.5	The designed IPC system for load mitigation	96
5.6	Comparison between pitch angle 1 (CPC) and the three pitch angle vaules in the PI-IPC case under the <i>Wind I</i> condition	103
5.7	The comparison between results with CPC and two different IPC cases under the <i>Wind I</i> condition	104
5.8	Pitch angle of blade 1 under the <i>Wind I</i> condition	107
5.9	Pitch rate of blade 1 under the <i>Wind I</i> condition	107
5.10	Tilt moment of main bearing system under the <i>Wind I</i> condition . . .	108
5.11	Flapwise bending moment of blade 1 under the <i>Wind I</i> condition . . .	108
5.12	Generator power output under the <i>Wind I</i> condition	109
5.13	Fault estimation results of three pitch systems in the PI-IPC case and H_∞ loop-shaping-based IPC case under the <i>Wind I</i> condition	110
5.14	Comparison results of STD for blade 1 flapwise bending moments, main bearing tilt/yaw moments and generator power under the <i>Wind I</i> condition	111
6.1	Effective forces on the tower top for structural load mitigation (Fischer and Shan, 2013)	117
6.2	Considered pitch system with sensor redundancy	122
6.3	Proposed UIO framework	123
6.4	Pole locations of the open-loop and closed-loop system (with designed LQR controller) of the 5MW NREL wind turbine	126

6.5	Comparisons between three pitch controllers in terms of blade 1 flap-wise bending moment M_1 and generator power output P	132
6.6	Comparisons between three pitch controllers in terms of tower fore-aft bending moments T_f and tower side-side bending moments T_s	133
6.7	Frequency spectrum comparison of M_1 in three different pitch controllers	134
6.8	Frequency spectrum comparison of T_f in three different pitch controllers	134
6.9	Sensor faults in the CPC case	137
6.10	Fault estimation results by designed UIO in the CPC case	138
6.11	A zoom-in figure of sensor bias fault estimation in the CPC case	138
6.12	Sensor faults in the LQR-IPC case	140
6.13	Fault estimation results by designed UIO in the LQR-IPC case	140
6.14	Spider figure of normalized performance comparison under 4 different faults of pitch sensor 1 with CPC controller	141
6.15	Spider figure of normalized performance comparison under 4 different faults of pitch sensor 1 with PID-IPC controller	142
6.16	Spider figure of normalized performance comparison under 4 different faults of pitch sensor 1 with LQR-IPC controller	142
A.1	Baseline Torque Controller in MATLAB/Simulink (continued with Fig. A.2)	151
A.2	The detailed torque controller designed in MATLAB/Simulink	152
A.3	Baseline Pitch Controller in MATLAB/Simulink (continued with Fig. A.4)	152
A.4	The detailed pitch controller in MATLAB/Simulink	152

List of Tables

2.1	Parameters of the NREL 5MW wind turbine model	20
2.2	Redistribution of harmonics between the rotating blade loading and main bearing tilt/yaw loading	31
3.1	Time update equations for Kalman filter	54
3.2	Measurement update equations for Kalman filter	55
4.1	RMSE of the wind speed forecasting by proposed GP model	81
4.2	Comparisons between different pitch controllers	84
5.1	Pitch system parameters in different conditions	93
5.2	Designed system parameters	98
5.3	Considered incipient pitch actuator faults	105
5.4	Standard deviation of the simulation results in 7 cases	106
6.1	Different variants for structural load mitigation	117
6.2	Definition of 11 state variables	124
6.3	Open-loop & Closed-loop pole locations	125
6.4	The STD of simulation results in the time domain	132
6.5	Summary of simulation results	139

List of Abbreviations and Symbols

Abbreviations

AFTC	Active Fault Tolerant Control
ANN	Artificial Neural Network
ARE	Algebraic Riccati Equation
BEM	Blade Element Momentum
CPC	Collective Pitch Control
CoE	Cost of Energy
CM	Condition Monitoring
DOF	Degree of Freedom
DEL	Damage-equivalent Load
EWS	Effective Wind Speed
FDD	Fault Detection and Diagnosis
FTC	Fault Tolerant Control
FDI	Fault Detection and Isolation
FDD	Fault Detection, Isolation and Identification
FD	Fault Diagnosis
FE	Fault Estimation
FAST	Fatigue, Aerodynamic, Structure and Turbulence
GP	Gaussian Process
GH	Garrad Hassan
HAWT	Horizontal Axis Wind Turbines
IPC	Individual Pitch Control
IBC	Individual Blade Control
LTV	Linear Time-varying
LTI	Linear Time-invariant

LMI	Linear Matrix Inequality
LQR	Linear Quadratic Regulator
LQG	Linear Quadratic Gaussian
LiDAR	Light Detection and Ranging
LCOE	Levelized Cost of Energy
MPC	Model Predictive Control
MHE	Moving Horizon Estimation
MBC	Multi-blade Coordinate
MIMO	Multi-input Multi-output
NREL	National Renewable Energy Laboratory
NWP	Numeric Weather Predictors
OWTs	Offshore Wind Turbines
O&M	Operation and Maintenance
PFTC	Passive Fault Tolerant Control
PAS	Pitch Actuator Stuck
PSF	Pitch Sensor Fixed
PI	Proportional - Integral
RMSE	Root Mean Square Error
SISO	Single Input Single Output
SMO	Sliding Mode Observer
SMC	Sliding Mode Control
STD	Standard Deviation
SVM	Support Vector Machines
TSR	Tip Speed Ratio
UIO	Unkown Input Observer
WT	Wind Turbine
1P 2P 3P	Once/twice/thrice Per Revolution

Symbols

$\ \cdot\ $	the Euclidean 2-norm of a vector
$\ \cdot\ _\infty$	the Euclidean ∞ -norm of a vector
$He(X)$	$He(X) = X + X^T$

\star	Transpose of elements in the symmetrical position in a matrix
\mathbb{C}	Set of complex numbers
\mathbb{R}	Set of real numbers
\mathbb{R}^m	An m-dimensional real matrix
$\mathcal{L}_2[0, \infty)$	2-norm space
X^T	Transpose of matrix X
I	Identity matrix
$sign(s)$	Signum function with variable s . $sign(s) = \frac{s}{\ s\ }$ with $s \neq 0$, otherwise $sign(s) = 0$

List of Publications

1. **Liu, Y.**, Patton, R. J., and Lan, J. Fault-tolerant Individual Pitch Control using Adaptive Sliding Mode Observer, *IFAC Safeprocess 2018*, pp.1127-1132, 2018.
2. **Liu, Y.**, Patton, R. J., and Shi S. Wind Turbine Load Mitigation using MPC with Gaussian Wind Speed Prediction, In *Proceedings of the UKACC 12th International Conference on Control*, pp.32-37, IEEE, 2018.
3. Shi S. , Patton, R. J., and **Liu, Y.**. Short-term Wave Forecasting using Gaussian Process for Optimal Control of Wave Energy Converter, *IFAC-PapersOnLine*, 51(29), 44-49.
4. **Liu, Y.**, Patton, R. J. Wind Turbine Structural Load Reduction with Pitch Sensor Fault Compensation, *Wind Energy (In Preparation)*, 2019, based on PhD thesis Chapter 6.
5. **Liu, Y.**, Patton, R. J. Fault Tolerant Blade Load Reduction using Adaptive Sliding Mode Observer, *Control Engineering Practice (In Preparation)*, 2019, based on the IFAC Safeprocess paper.

Chapter 1

Introduction

1.1 Background

As an economical and sustainable energy source, wind energy is taking an increasing share of the energy market to satisfy the growing energy demand and overcomes environmental pollution-related problems, as well as reduces dependence on the declining fossil fuel reserves in recent years. Wind turbines (WTs) tend to have larger rotor diameters, higher towers and be built offshore to capture more wind energy and decrease the levelized cost of energy (LCOE) (Kumar et al., 2016b). In order to make wind energy more competitive, it is necessary to improve the offshore WT performance, whilst at the same time enhancing reliability and service life. Fig. 1.1 presents the WT growth trend and future projects. It can be seen that the rotor diameter has increased impressively from 17m for a 75KW wind turbine to 125m for a 5MW wind turbine, which will keep increasing for more power output in the future.

There are two major challenges that offshore WTs face with. On the one hand, the large WT components such as blades and tower are subject to significant unbalanced and fluctuating loading arising from complex wind flows over the rotor and additional imbalance owing to wind shear, gravity, yaw misalignment, tower shadow etc. On the other hand, unexpected failures of WT components can result in expensive repairs and typically months of machine unavailability, thus increasing the operation and maintenance (O&M) costs and subsequently LCOE (Walford, 2006). However, the WT operation and maintenance are also challenged by the fact that offshore WTs are located at sea, sometimes 100 kms from land. Due to this, offshore WTs usually suffer

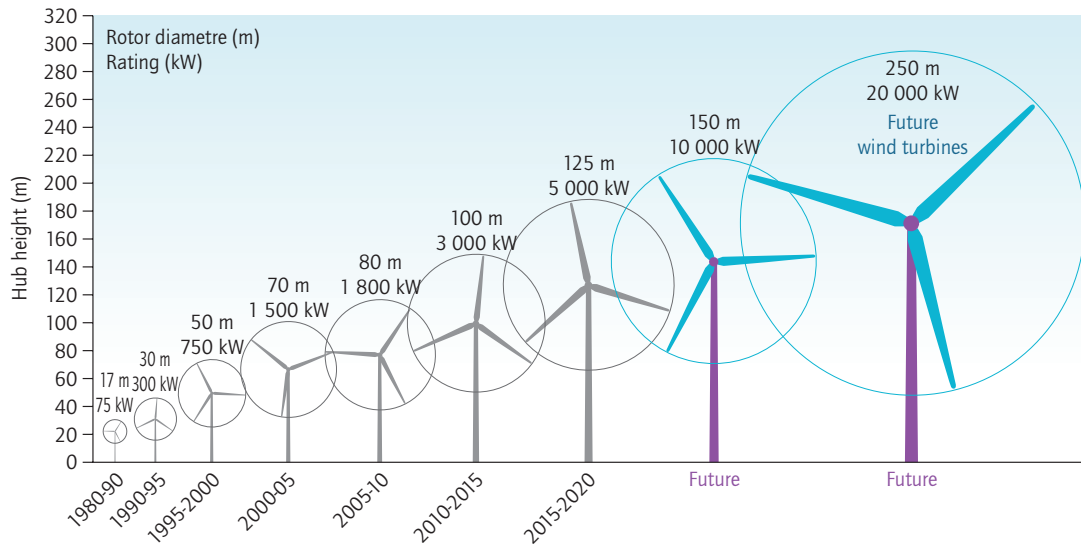


Figure 1.1: Growth trend of WTs over time and future projects (Koh and Ng, 2016)

from long-term maintenance waiting, costly travel and increased downtime, which will amplify the impact of minor failures on the availability and reliability. To summarize, the high level of blade fatigue and loading will contribute to predominant blade failures because of faults, illustrated in Fig. 1.2. Therefore, it is of fundamental importance to design sustainable control strategy and predictive maintenance that helps to reduce the asymmetrical mechanical turbine loading and avoid unnecessary faults. This will contribute to decrease the O&M expenses, enhance the reliability and prolong the lifetime of offshore WTs.

1.2 Control of Wind Turbines

Among the various WT configurations (two or three bladed, downwind or upwind rotor, vertical or horizontal axis etc.), the three bladed upwind horizontal turbine (HAWT) represents the state-of-the-art multi-megawatt WTs and dominates the wind energy market (Körber, 2014), illustrated in Fig. 1.3.

The changing wind flow is the driving force of the turbine, which exerts aerodynamic torque and thrust on the rotor. It causes rotor blades to rotate as the wind passes by. Blades are designed to have a specific aerodynamic curved shape to obtain as much wind energy as possible. These blades are connected to the turbine hub that turns as



Figure 1.2: Different wind turbine blade failures (from google images).

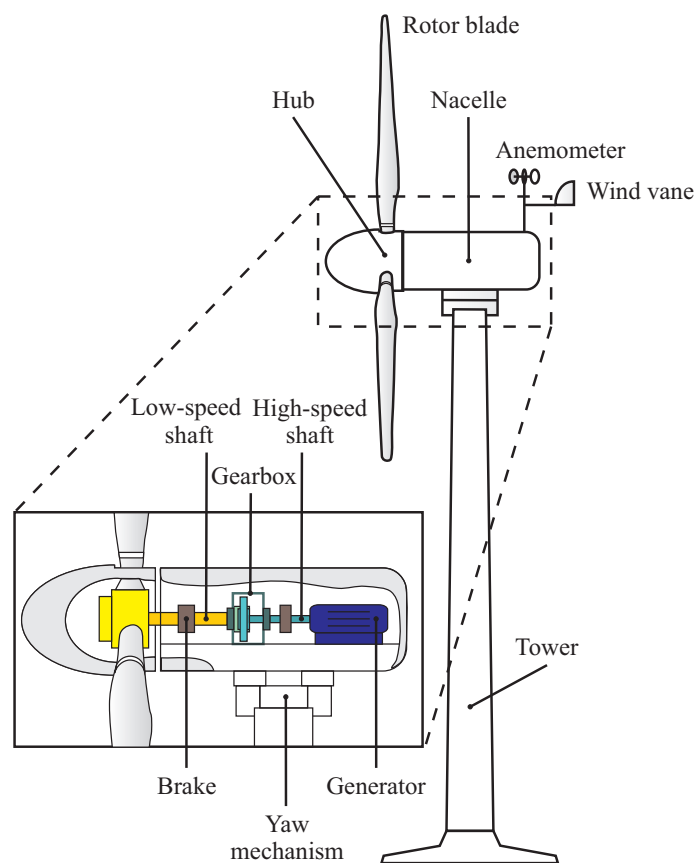


Figure 1.3: Main components of a HAWT (Esbensen and Sloth, 2009)

blades rotate. The WT rotor is composed of both the hub and blades. The rotation of rotor drives the low speed shaft, which is attached to the high speed shaft through the gearbox, enhancing the rotating speed to a certain level needed by the turbine generator. Furthermore, the high speed shaft spins the generator, thus converting the kinetic energy from the incident wind into electrical power. The wind power cannot be fully captured by a WT, which is subject to the rotor diameter and the incoming wind speed that propels the blades. The theoretical optimal aerodynamic efficiency of wind turbine is 0.593 (known as Betz limit) (Betz, 1926), which represents the available wind energy that can be extracted. The power captured by a WT is typically defined as:

$$P(t) = \frac{1}{2} \rho A C_p(\beta, \lambda) v^3(t) \quad (1.1)$$

where $\rho, A, v \in \mathbb{R}$ represent the air density, rotor swept area and wind speed, respectively. C_p is the power coefficient, that is the ratio between the power extracted by the wind turbine to the available wind power. It is a function of the pitch angle β and tip speed ratio λ . It is typically expressed by a look-up table achieved from the real field test dataset. The tip speed ratio (TSR) presents the ratio of the rotor tip speed wr to the wind speed, shown as

$$\lambda = \frac{wr}{v} \quad (1.2)$$

with w, r denote the rotor angular velocity and rotor radius, respectively.

The blade pitch angles are regulated by pitch actuators at the root of blades, which are normally electrical or hydraulic motors. Turbine brakes are critical for emergencies, maintenance and risk management under high or extreme wind speeds, including different types of mechanical, electrical, or hydraulic brakes. The nacelle is located atop the tower and includes the low and high speed shafts, gearbox, generator, controller and brake assembly. A tower (made from concrete, steel etc.) supports the nacelle and rotor. As wind speed increases with the height, the taller towers allow wind turbine to extract more wind energy. The tower is supported by the fixed or floating foundation for OWTs. Fixed OWTs are limited to shallow water depths of up to 50m. Floating foundations provide greater flexibility for site location and make it accessible to superior wind resources (Roddier et al., 2010).

In the modern WTs, different types of sensors are accessible for turbine control and monitoring purposes (Burton et al., 2011), illustrated in Fig. 1.4. In order to provide the wind information for supervisory control, anemometers are used atop the nacelle to measure the hub-height wind speed to determine if the wind speed is strong enough to start the turbine operation. Recently, there is a growing interest in using the remote sensing techniques including the light and detection ranging (LiDAR) systems to obtain the real-time incident wind knowledge (Schlipf, 2016). The wind vane sensor obtains the wind direction, which is used by yaw controllers to adjust the turbine facing into or out of the wind. The blade load sensors, normally optical fibres or strain gauges, are employed at the blade roots to achieve the blade flapwise or edgewise bending measurements for the load reduction control. The pitch position sensors are adopted to measure pitch angles for the generator speed control. Accelerometers are used in the tower to measure the tower accelerations for tower damping control. Rotor and generator speed sensors are employed to measure the rotational speed for the speed regulation and drive train damping control scheme. Several sensors are employed to indicate the temperature and oil level of the gearbox and bearings (Pao and Johnson, 2011).

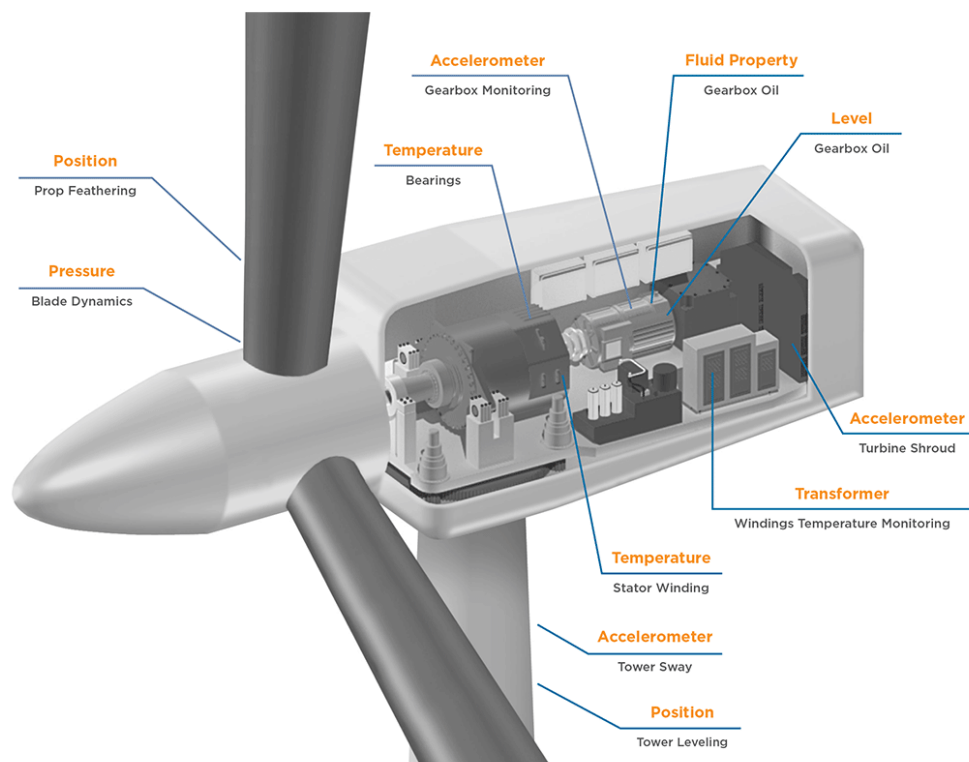


Figure 1.4: Typical wind turbine sensors (Connectivity, 2019)

The main goal of WT control is to maximize wind energy capture and guarantee good power quality while keeping the turbine within operating limits including the cut-out wind speed, rated speed/power etc. Furthermore, load reduction controllers are expected to prevent wind turbines from excessive mechanical loading generated by the time-varying wind force (Burton et al., 2011).

Commercial multi-megawatt wind turbines are typically operated based on the variable-speed variable-pitch strategy. The turbine is designed to have a variable generator speed and a fixed pitch angle below rated wind speed with a variable pitch angle above rated wind speed (Bianchi and Mantz, 2006). Generator torque control ensures the efficient turbine operation and power capture maximization in a wide range of wind speeds. Variable pitch allows blades to pitch along the longitudinal axis for power regulation above rated wind speed and aerodynamic braking by blade feathering (turns towards parallel to wind direction with 0° pitch) in the event of wind gusts. In addition, variable pitch strategy provides another advantage of dynamical load alleviation. The optimal power curve and operation modes of for the National Renewable Energy Laboratory (NREL) 5MW wind turbine system (Jonkman et al., 2005) mainly consists of 4 regions according to the wind speed (Savvidis, 2017), shown in Fig.1.5.

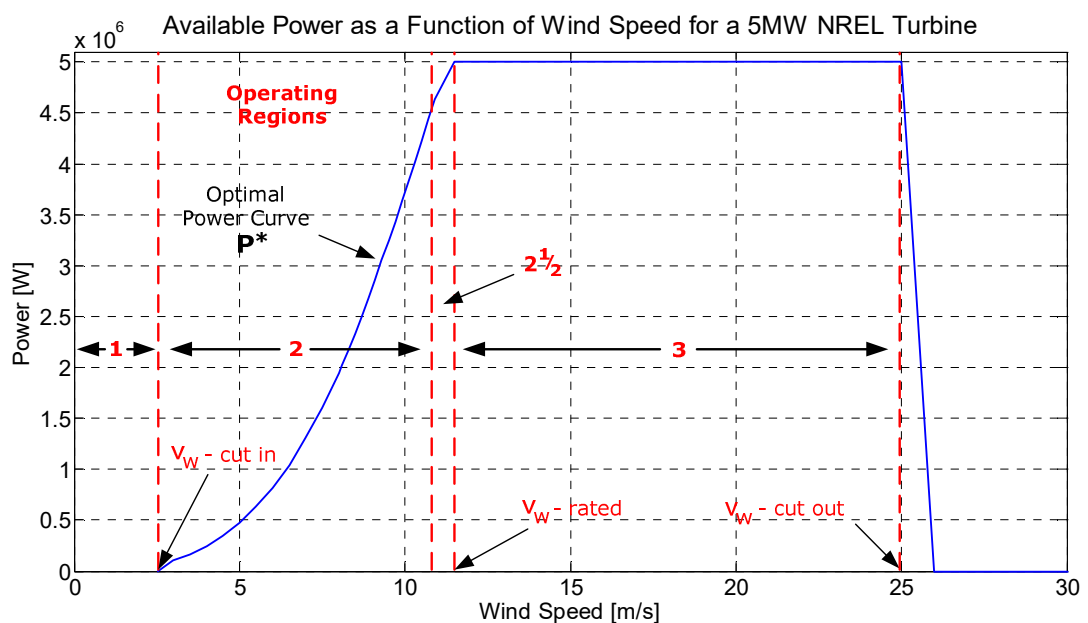


Figure 1.5: Power curve and operation modes for the 5MW NREL wind turbine system (Jonkman et al., 2009)

In **Region 1** (0 - 3 m/s), the turbine is prepared to start and no power is generated when

the wind speed is lower than the cut-in speed. **Region 2** (3 - 10.9 m/s) and **Region 2 $\frac{1}{2}$** (10.9 - 11.4m/s) are control regions for maximizing the power extraction based on the generator torque control strategy when the wind speed is lower than the rated speed. The constant (optimal) TSR is maintained until Region 2 $\frac{1}{2}$, which is a transition region from the fixed TSR strategy to the fixed rotor speed until the rated power is generated at the rated speed. From the power coefficient curve of the 5MW NREL WT (Jonkman et al., 2005) illustrated in Fig. 1.6 , the maximum power coefficient C_p of 0.4852 is achieved at $\beta = 0^\circ$, $TSR = 7.55$. Therefore, the blade pitch angle reference is typically maintained constant at zero. The generator torque control strategy is commonly adopted to track the optimal TSR. The uncaptured power is a result of variations in the TSR around the design value. This accounts for an inherent loss of efficiency in various wind turbine designs.

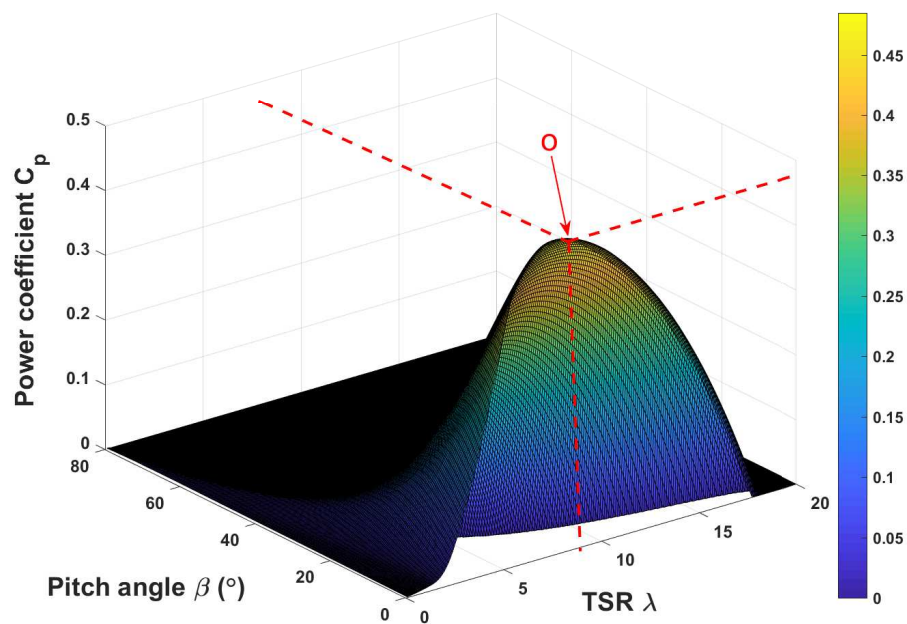


Figure 1.6: Power coefficient curve of the 5MW NREL wind turbine

In the full load region of **Region 3** (11.4 - 25 m/s), the rated power generation and load mitigation are achieved by pitching blade angles to regulate the rotor efficiency via the proposed pitch controller. The Region 3 is maintained until arriving at the cut-off wind speed of 25 m/s, where the rotor rotation terminates and power production stops (Liniger et al., 2017).

In this thesis, only the operation in region 3 is considered. Pitch control system is one of the most crucial control strategies in offshore WTs (Gao and Gao, 2016). Specifically, collective pitch control (CPC) means that 3 blade pitch angles are regulated collectively by the same size in order to adjust the turbine rotor speed. In contrast, the use of the individual pitch control (IPC) means that the pitch angle reacts to load measurements individually and instantaneously to mitigate the blade unbalanced loading, which requires an independent pitch actuator in each blade (Lio et al. (2017)). The goal of CPC is typically to regulate the power output and reduce the tower loading, whilst the principal purpose of IPC is to reduce or mitigate the asymmetric loading of all 3 blades. The idea of IPC originally comes from the helicopter individual blade control (Arnold, 2003), which aims to achieve low rotor blade induced vibration level, better flight performance and lower noise level emission. Motivated by this, the idea of individually allocating three pitch actuators is used in the wind turbine system (Bossanyi, 2003a).

1.3 Typical Faults of Wind Turbine Systems

There exists two typical types of WT system faults including temporary faults and wear-out failures (Qiao and Lu, 2015a). Temporary faults tend to be short-term and random, which could be caused by the environmental and internal factors including wind flow turbulence, accumulated dirt and ice, severe weather conditions (i.e. lightning, storm, hail, gusts etc.), grid disturbances, thermal problems, sensor reading errors, etc. Temporary faults can be compensated by the predictive maintenance performed before the consequent failures (Daneshi-Far et al., 2010). Wear-out failures are normally permanent and irreversible, requiring timely repairs or failed component replacements, which may result in the consequent failures of other assemblies or even the total WT system. The typical faults and problems of different turbine subsystems and assemblies are summarized in Fig. 1.7, inspired by (Hameed et al., 2009; Badihi et al., 2013; Feng, 2014, etc.).

However, these faults and problems exert different impacts on turbine systems (Liu et al., 2015). Fig. 1.8 provides a comparison of the percentage distribution of turbine downtime due to these faults and problems. It is worth noting that the pitch systems contribute approximately 22% of the annual turbine downtime just after the electrical subsystem. Therefore, it becomes very important to design appropriate predictive

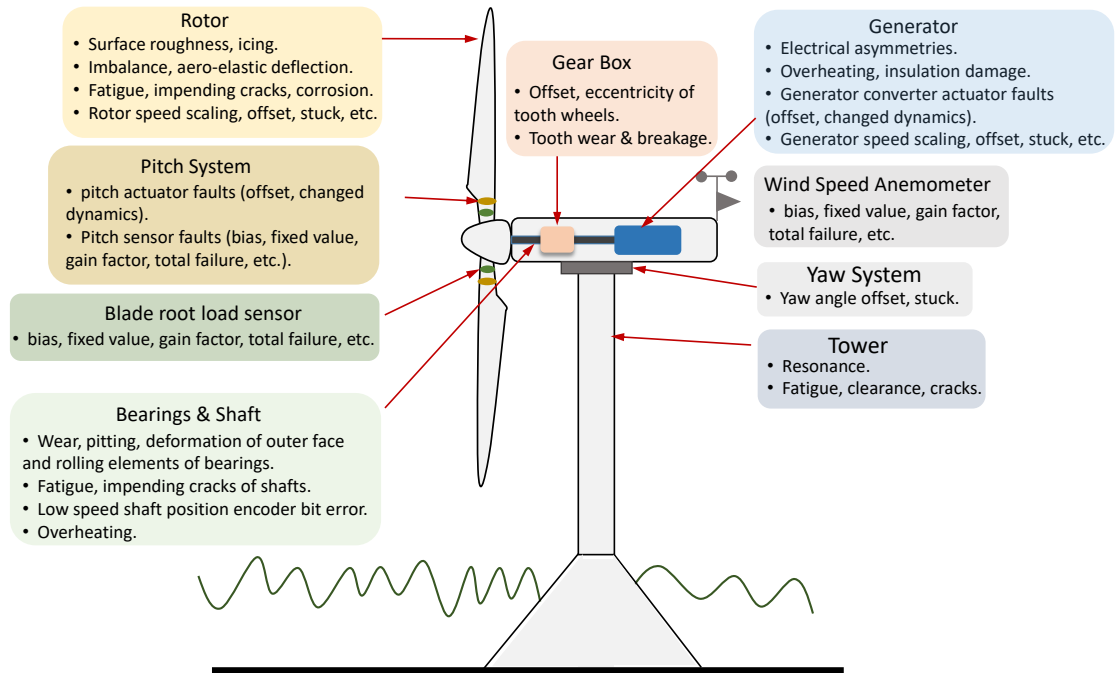


Figure 1.7: Typical faults and problems from different wind turbine subsystems and assemblies

maintenance strategies for pitch systems to enhance the WT reliability and sustainability.

The practical use of individual pitch actuation for each blade is typical for large commercial offshore WT systems for the sake of safety, including hydraulic and electric types with their respective strengths and weaknesses (Burton et al., 2011). Pitch systems driven by the electric motor present wider operating bandwidths that is suitable for the situation requiring faster pitching motions. Compared to this, hydraulic pitch systems have a slower response and bearing greater stiffness, exhibiting a higher level of reliability (Lu et al., 2009). For large offshore WTs suffering from extreme aerodynamic loading, hydraulic pitch systems are considered easy-maintenance and fail-safe. Therefore, this thesis focuses on the study of hydraulic pitch systems, illustrated in Fig. 1.9.

Moreover, a simplified sketch of one hydraulic pitch system with the designed pitch controller (CPC and IPC) is illustrated in Fig. 1.10. The CPC generates the pitch angle reference according to the error of generator speed and the IPC controller adds extra pitch angle to reduce the blade bending moments. The final pitch angle reference is

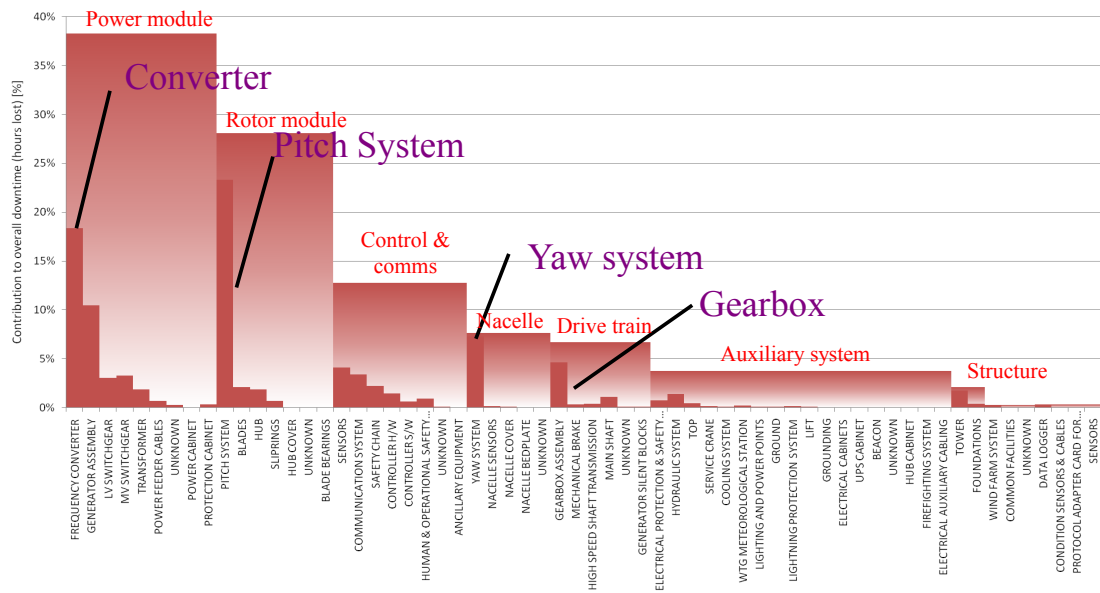


Figure 1.8: Percentage distribution of standardized downtime per year per turbine caused by the WT subsystem and assembly faults from various manufacturers in the ReliaWind study (Wilkinson et al., 2010)



Figure 1.9: Hydraulic pitch system of wind turbine system (from google images)

then compared with the pitch position measurement. The resulting error of pitch angle is transferred into a pitch rate requirement, implemented by the proportional valve (V1) (Burton et al., 2011). That is, the flow of hydraulic fluid (i.e. oil) to the pitch differential cylinder (C1) is controlled by V1 based on the required pitch rate demand. The cylinder C1 is connected to the corresponding blade, adjusting the pitch angle to match the controller demands with the piston in C1 is extended or retracted. Hydraulic pumps can ensure the quick response and high efficiency to satisfy the demanding oil

pressure. Furthermore, the accumulator is hydraulically connected to C1 and supplies the backup flow pressure to maintain the hydraulic pressure from the pump station (Esbensen and Sloth, 2009).

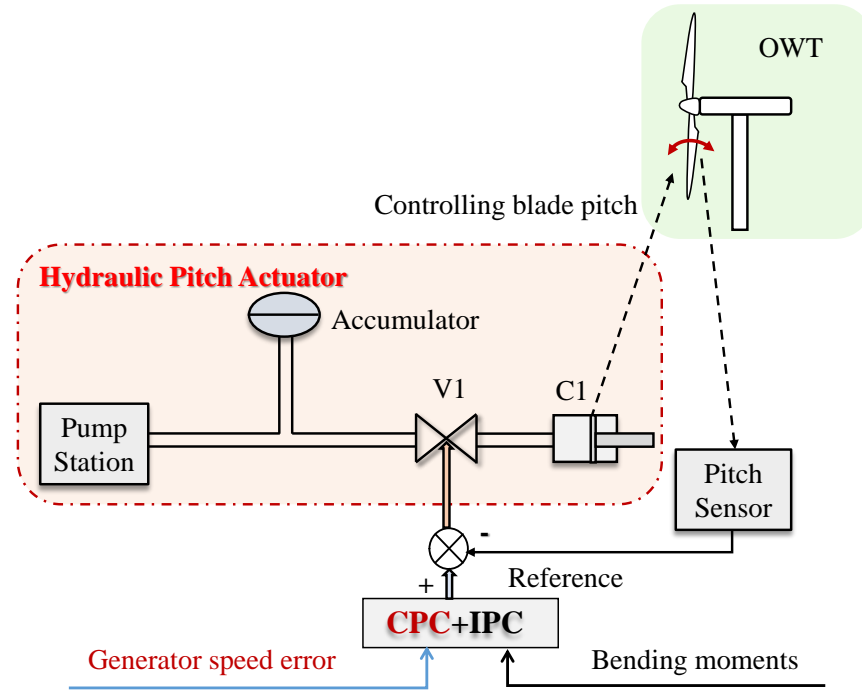


Figure 1.10: One hydraulic pitch system with the CPC and IPC controllers

The hydraulic pitch systems (including actuators and sensors) are prone to faults by various reasons. A very small quantity of air contamination can significantly reduce the effective bulk modulus of oil, which cause the variations of pitch system dynamics (Lu et al., 2009). Similar issues occur when oil in the hose leaks and the pump station gets blocked. Moreover, the pitch actuator will get stuck due to the blockage of valves (i.e. V1) or pumps. Once a valve or pump blockage occurs, the piston in the cylinder C1 cannot move and lose the ability to pitch the corresponding blade, which can lead to the wind turbine system out of control (Cho et al., 2018). In terms of pitch sensor faults, calibration drift (known as bias), stuck readings, no outputs and scaling measurements etc. are typical modes. Therefore, the pitch controller that depends on the faulty sensor output should be robust enough or the faults are compensated accurately. If not handled properly, these faults may cause WT operation instability.

1.4 Challenges and Objectives

The major aim of this thesis is to combine FTC techniques with sustainable controller (i.e. load reduction schemes by IPC) for offshore wind turbines in a more integrated manner to enhance the WT unbalanced load reduction performance in either the fault-free or faulty case and compensate the fault effects, illustrated in Fig. 1.11. Therefore, the O&M expenses will be significantly reduced as well as the reliability and lifetime of offshore WTs are enhanced.

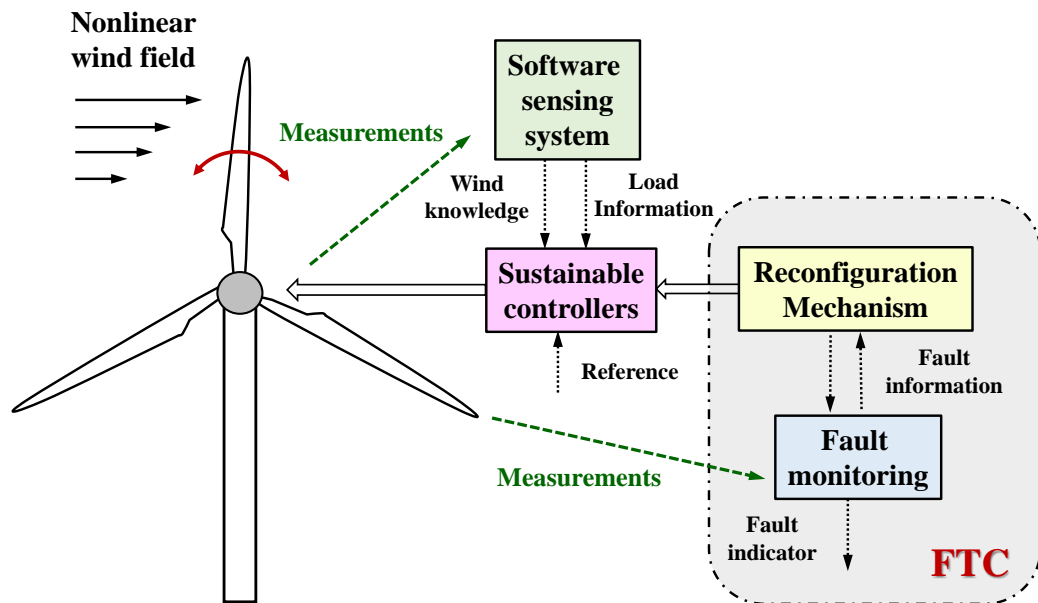


Figure 1.11: Fault tolerant control of wind turbines with sustainable controllers

One way to reduce the O&M expenses and improve operation reliability is the use of more intelligent pitch control systems (e.g. individual pitch control, known as IPC) to attenuate the turbine unbalanced structural loading while maintain the nominal generator power output. Another approach to decrease the expenses is to improve the WT system maintenance schedules. The requirement is to reduce the number and frequency of scheduled maintenance services as well as reduce the downtime caused by faults. Therefore, the implementation of condition monitoring (CM) system and control-based fault monitoring strategy are of paramount significance to increase the operating life of offshore WTs and enhance sustainable operation. Especially, the fault detection and isolation (FDI) scheme as well as fault estimation (FE)-based FTC algorithms can be adopted to detect faults and make compensations to fault effects according to the type of faults.

Possible candidates for costly and non-universal LiDAR used by the preview control-based IPC

There is a growing interest in the study of preview control-based IPC (i.e. model predictive control, called as MPC) using the future wind speed knowledge to enhance the load mitigation performance. However, the used future wind information is either just assumed to be known perfectly or can be estimated from the LiDAR system in these extensive studies. If the future wind information can be achieved from the wind speed prediction through popular data-driven methods using the history data, how reliable is the designed preview control system with this future wind knowledge? This idea is going to be investigated in Chapter 4.

Potential IPC strategy for both blade and tower loading mitigation

Mitigating the blade and tower loading are important for reducing the offshore WT O&M costs. However, there is a general limitation for the current load mitigation techniques, which mitigate the blade loading and tower loading in the separate controllers. It is demonstrated that there exists strong couplings between the blade and tower bending moments. Therefore, it is interesting to deal with these two load mitigation loops in a multi-objective manner. This part of work is presented in Section 6.3.1, which presents a multivariable IPC controller using LQR method.

On-line FDI/FE-based FTC strategy for pitch system faults

Condition monitoring system is essential for WTs to avoid severe failures. CM is mainly an off-line method of monitoring the health of system components at a mechanical system level from sensor measurements based on signal processing approaches. For example, during an inspection procedure the drive train can be rotated and an operator can use vibration testing methods to "listen" for unusual imbalance in the gearbox, drive shaft or hub main bearing. On the other hand, the control approach to fault monitoring based on fault diagnosis and fault tolerant strategies is necessarily on-line by the very fact that all control system operate on-line. Furthermore, CM is only a local method of inspecting individual components, whilst FDI/FE-based FTC control system can monitor both on-line components and also monitor the whole system (with its components) from a global perspective. In this sense, it is important to design appropriate control-based fault monitoring strategy for WT system.

Moreover, under the accumulated operating conditions and harsh environments, the

pitch system suffers from different types of faults and exhibits unsatisfactory pitch dynamics. This has a further adverse impact on the turbine operational stability which in turn enhances the rotor blade fluctuations and hence an increase in bending and fatigue. As stated in Section 1.3, the pitch system faults exert significant impacts on the WT down-time. Therefore, on-line FDI/FE-based FTC strategies are investigated for various pitch system faults as follows:

- (1) In Section 3.4, a pitch actuator stuck fault (PAS) is detected by a Kalman filter FDI strategy,
- (2) In Section 5.3.2, incipient pitch actuator faults are estimated and compensated using a combined sliding mode observer-based fault estimation (FE) and FTC strategy,
- (3) In Section 6.3.2, a robust unknown input observer is used to estimate pitch sensor faults within an FE-based FTC scheme.

Combined analysis of FE-based FTC strategy with IPC system

It is shown that the IPC system can mitigate the turbine loading. However, this load reduction performance comes with the sacrifice of enhanced pitch movements, which increases the pitch system fatigue and thus increases the likelihood of pitch system faults. The resulting pitch system faults will in turn deteriorate the load reduction performance by the IPC. To the best knowledge of the author, there exists two ways to reduce the negative impacts of pitch faults. That is, on the one hand trying to decrease the pitch travel caused by the additional pitch angle from the proposed IPC system, and on the other hand enhancing the robustness and reliability of pitch controllers with the help of FE-based FTC strategies, to compensate the undesirable effects on the IPC system caused by pitch faults. In this sense, it is of paramount significance to consider the pitch system faults within the IPC system in a more systematic way, by asking the following questions. Firstly, do different IPC strategies have the same ability to maintain the load reduction performance when one same pitch fault occurs? Secondly, does the proposed fault tolerant control (FTC) strategy have the same performance when using different IPC schemes in the system? These problems will be investigated in Section 5.4.2 and Chapter 6.4.3.

Furthermore, this scenario of load mitigation is analogous to the FTC problem because the action of rotor bending (caused by wind loading) and considered as a fault effect. A fault acting in a system is an unwanted effect causing a deterioration in performance

and this is precisely what happens with rotor blade bending (see Chapter 5). An extension to the idea can also be considered for tower bending, or even a combination of both (see Chapter 6 for more discussion). So, it is quite attractive to consider all the "fault effects" acting in the rotor system or both the rotor and tower system, i.e. sensor faults, actuator faults and bending moment effects. The bending moment changes are effectively component faults acting in the rotor/tower system. Hence, the work on FTC is a valid contribution in this context as these various effects can be handled together and it can be noted that in the subject of FTC three general forms of faults are considered namely actuator, sensor and component faults (Patton, 2015). All FTC schemes use redundancy of various kinds to achieve fault tolerance. Actually, IPC involves the use of dissimilar actuator redundancy which is a powerful tool for FTC. This is a prime motivation of this PhD work.

1.5 Outline of the Thesis

Based on the aforementioned objectives, the thesis structure is illustrated in Fig. 1.12. The remainder of this thesis is summarized as follows.

Chapter 1 provides an introduction to the modern offshore WT control strategies and some typical faults occur in the practical system. The challenges and objectives of offshore WTs focused on this thesis are discussed.

Chapter 2 provides a brief background of the common WT load sources and introduction of used wind turbine simulator (i.e. 5MW NREL wind turbine, containing the corresponding baseline control systems) for the simulation validation. Moreover, a general literature review of the typical WT load reduction strategies as well as the current different IPC methods is given.

Chapter 3 illustrates some background knowledge about the fault diagnosis and FTC as well as the state-of-art developments of the wind turbine FTC system. Furthermore, a tutorial example about designing a FDI system for the WT PAS fault is presented, where the effects of PAS on the structural loading and power output are also analysed.

Chapter 4 proposes a preview control system using the model predictive control with the future wind speeds to achieve better performance of blade load reduction. Here, the future wind characteristics are provided from a very short-time wind speed prediction

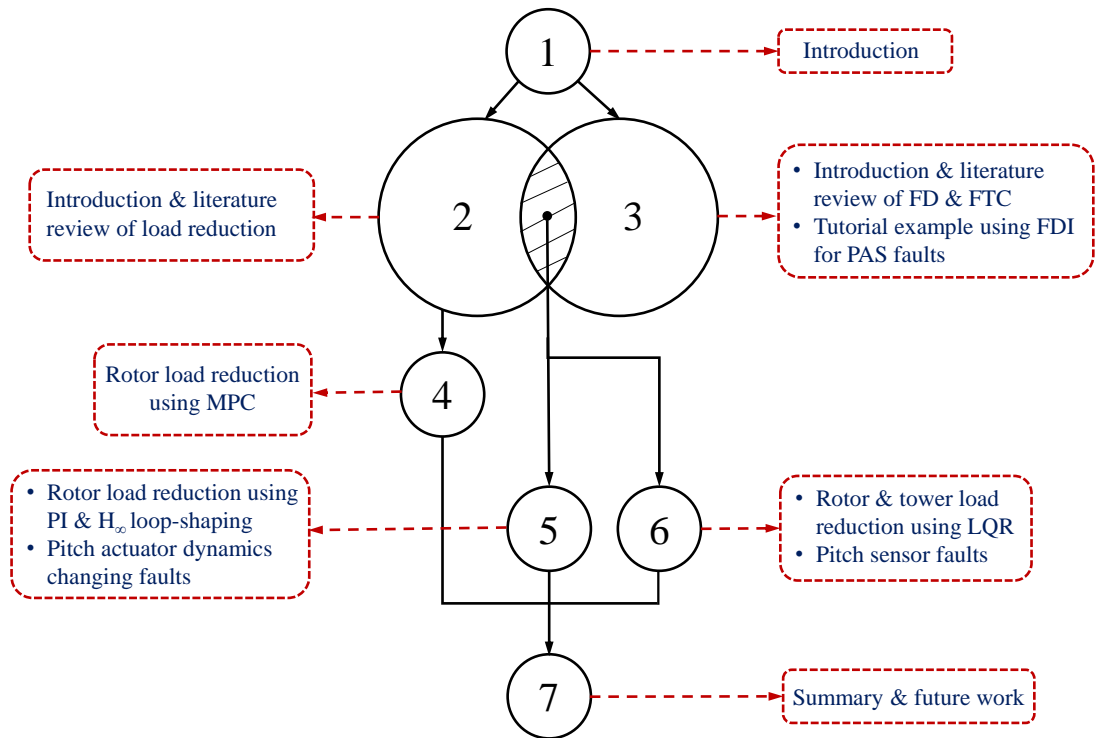


Figure 1.12: Structure of the thesis

strategy through a well-designed Gaussian process model rather than the expensive and non-universal LiDAR system. The proposed strategy has the superiority of not requiring additional hardware, which could be a promising alternative method to the existing LiDAR system when considered for the preview control-based load reduction.

Chapter 5 designs a universal and robust FTC system for three different pitch actuator incipient (component) faults, which is combined with a Coleman transformation-based IPC system using PI or H_∞ loop-shaping control approach. It gives some general understanding of the origin of the unbalanced blade loading and power deterioration, in the event of pitch actuator incipient faults. It can be seen that the proposed sliding mode observer based FTC strategy can achieve the compensation of fault effects and maintain the nominal asymmetrical load mitigation performance.

Chapter 6 proposes a multivariable LQR-based IPC system to mitigate the blade and tower loading together, considering pitch sensor faults with the uncertainties and measurement noise. An UIO-based FE system is proposed to achieve the estimation of four types of sensor faults and thus the FTC compensation is implemented. The designed UIO is validated under three different pitch control cases and the performance

of designed LQR-based IPC controller is also compared in different faulty cases.

Chapter 7 provides a thesis summary and recapitulates the main contributions as well as the future research.

Chapter 2

Load Reduction Control for Wind Turbines

2.1 Introduction

As mentioned in Chapter 1, this thesis makes some contributions on the load reduction of wind turbine unbalanced loading. Before considering the design of different control strategies to achieve the load mitigation, this chapter aims to introduce (i) some background of the common turbine fatigue loads, (ii) the used wind turbine software for validation, (iii) a brief literature review about several load reduction strategies.

The rest of this Chapter is organized as follows. Section 2.2 gives a detail introduction about the use of the 5MW NREL (National Renewable Energy Laboratory) wind turbine including the mathematical turbine model, blade pitch model, wind modelling and the baseline control system. Section 2.3 provides some knowledge of the sources of common wind turbine fatigue loading. Section 2.4 presents the general wind turbine load mitigation strategies. Furthermore, Section 2.5 gives a detailed literature review of current individual pitch control (IPC) methods. Finally, Section 2.6 provides a summarization of this Chapter.

2.2 The Aero-elastic Simulation Tool FAST

Over the last few decades, several wind turbine simulators including wind turbine benchmark model (Odgaard et al., 2013), Garrad Hassan (GH) Bladed model (Bladed, 2019), (Fatigue, Aerodynamics, Structure and Turbulence) FAST (Jonkman et al., 2005), Flex5 (Øye, 2001) etc., have been developed to meet the growing demand for a common research platform for the sustainable control and predictive maintenance research. Unlike the GH Bladed or Flex5, the wind turbine benchmark model and FAST are free and have the available source codes, which make these two models the most commonly used turbine prototypes.

However, the wind turbine benchmark model (Odgaard et al., 2013) is a reduced-order simulator based on the first principle modelling with only drive train motion and actuator dynamics. In contrast, the second simulator FAST contains higher-fidelity and more realistic modelling, which needs more sophisticated control and fault diagnosis strategies, making the proposed strategies more desirable to the real wind turbine system. Therefore, the FAST is chosen as the wind turbine simulator in this thesis.

FAST is a nonlinear aero-elastic structural-dynamic model developed by the NREL from United States for horizontal-axis wind turbines. FAST incorporates the AeroDyn module (Laino and Hansen, 2002) using the Blade Element Momentum (BEM) theory for the aero-dynamic modelling, which simulates the wind turbine response and loading. The FAST structural models include the flexible and rigid bodies. The turbine blades, tower, and drive-train are flexible whilst other turbine components are assumed to be rigid. FAST is incorporated in the MATLAB/Simulink as an S-Function, so that more flexible access to the turbine control development and design is achievable. The relevant controller codes can be included using either a dynamic link library or by running the system in Matlab with the provided Simulink interface (Jonkman et al., 2005).

FAST features 24 degrees of freedom (DOF) to express the main dynamics, including the blade first/second flapwise and first edgewise modes, tower fore-aft and side-side motion, drive train torsion, generator azimuth angle, nacelle and platform modes, etc. (Jonkman et al., 2005). Any combinations of the DOFs can be enabled in the simulation according to users' requirements. All available DOFs except the platform-related modes are enabled throughout this study.

Hence, the NREL 5MW reference turbine (Jonkman et al., 2009) is adopted as the turbine simulator, which is a theoretical wind turbine model designed to represent a modern turbine with the same capacity. It is considered a well-known standard modelling tool for the mainstream wind turbine research (Houtzager et al., 2013). This is a conventional variable-speed, pitch-regulated turbine system (see Section 1.2). The detailed parameters are described in Table. 2.1.

Table 2.1: Parameters of the NREL 5MW wind turbine model

Power rating	5 MW
Rotor orientation, structure	Upwind, three-bladed
Rotor, hub diameter	126 m, 3 m
Hub height	90 m
Gearbox ratio	97
Cut-in, rated, cut-out wind speed	3 m/s, 11.4 m/s, 25 m/s
Rated rotor, generator speed	12.1 rpm, 1173.7 rpm
Rated generator torque	43093.55 Nm
Electrical generator efficiency	94.4%
Rotational frequency (1P)	0.2 Hz (at rated speed)

2.2.1 Mathematical Model

The wind turbine aerodynamics are highly and inherently nonlinear due to the time-varying and complicated incident wind flow. It is hard to achieve a perfect mathematical model, which can represent all the relevant turbine dynamics. Currently, there are two main different methods to achieve a mathematical model that is applicable for turbine control design:

(1) One popular method is the use of a first principle mathematical model and obtain the relevant parameters from the high-fidelity wind turbine simulator through the system identification, which is used by many research works (Van Engelen, 2006; Sloth et al., 2011; Zhang et al., 2013; Körber, 2014; Gao and Gao, 2016; Jones et al., 2018, etc.). A simple mathematical model with a few states can be generated by selecting the relevant system dynamics for the specific control objective. One advantage of this method is the nonlinearities of turbine model can be included explicitly and conveniently, allowing greater flexibility in dealing with the nonlinearities in the control system design.

(2) Some wind turbine simulators (i.e. GH Bladed and FAST) provide the linearization capability that automatically generate the linear state space model at a given operation point, which is extensively used by (Laks et al., 2011; Spencer et al., 2013; Xiao et al., 2013; Li et al., 2014; Hassan et al., 2012; etc.). The generated linear model can be quite large if all the system dynamics are considered, but can be simplified either by using the model order reduction or ignoring some irrelevant DOFs. The main advantage of this approach is that the linear model can be easily obtained, which contains all the dynamic interactions if required.

The second approach is selected in this thesis because the proposed pitch control system (i.e. IPC) focuses on using linear control strategies. The FAST linearization property (see more in Section 4.2.1) is implemented to achieve the linear wind turbine model in the later work.

2.2.2 Blade Pitch System

Furthermore, the model of pitch actuators dynamics is not provided in the FAST. Here, each hydraulic pitch actuator is modelled as a second-order closed-loop system with pitch angle range $[0^\circ, 90^\circ]$ and pitch rate limits $[-8^\circ/s, 8^\circ/s]$ (Odgaard et al., 2013), expressed as

$$\frac{\beta(s)}{\beta_r(s)} = \frac{w_n^2}{s^2 + 2\xi w_n s + w_n^2} \quad (2.1)$$

where the nominal natural frequency is $w_n = 11.11 \text{ rad/s}$, the damping ratio is $\xi = 0.6$. $\beta(s)$ is the pitch angle, and $\beta_r(s)$ is the control reference for the pitch system. To facilitate the subsequent controller design, the state space model for the three pitch systems is illustrated as:

$$\begin{aligned} \begin{bmatrix} \dot{\beta} \\ \ddot{\beta} \end{bmatrix} &= \begin{bmatrix} 0 & 1 \\ -w_n^2 & -2\xi w_n \end{bmatrix} \begin{bmatrix} \beta \\ \dot{\beta} \end{bmatrix} + \begin{bmatrix} 0 \\ w_n^2 \end{bmatrix} \beta_r(t) \\ \begin{bmatrix} \dot{\beta} \end{bmatrix} &= \begin{bmatrix} 0 & 1 \end{bmatrix} \begin{bmatrix} \beta \\ \dot{\beta} \end{bmatrix} \end{aligned} \quad (2.2)$$

In this thesis, the Fault detection and isolation (FDI) and Fault Tolerant Control (FTC) schemes for the pitch system are developed using the local pitch mathematical model (2.2). The global wind turbine dynamic model from the FAST linearization is used for the IPC controller design. However, whilst the FDI/FTC is based on the local pitch system dynamics uncertainties from changing aerodynamics, unknown wind speed and modelling errors must be taken into account through a robust approach. It is important to include a robustness aspect in the FDI/FTC design since the uncertainties can degrade the fault detection and isolation as well as FTC performance. This robustness aspect is considered in Section 6.3.2. However, from Section 5.3.2 an alternative to FDI is also used which is fault estimation (FE) in which the detection and isolation roles are simplified.

2.2.3 Wind Modelling

The NREL TurbSim stochastic inflow simulator (Jonkman, 2009) is adopted to provide the realistic 3D wind field for the wind turbine closed-loop simulation. It provides a simulated full-field turbulent wind environment by a statistical model to drive the FAST simulations. This statistical model incorporates several significant hydrodynamic features that are known to have adverse effects on wind turbine aero-elastic response and loading. The generated 3-dimensional turbulent wind dataset is characterised by the mean wind speed at the reference height, the Kaimal turbulence intensity (Kaimal et al. (1972)) and the wind vertical shear exponent, which can be determined by the user as inputs. The vertical shear exponent is calculated according to the mean wind speed values at the top and bottom of the turbine rotor disk (Jonkman, 2009).

2.2.4 Baseline Wind Turbine Control

The baseline generator torque and blade pitch controllers for the 5MW NREL wind turbine are illustrated in the report (Jonkman et al., 2005). The goal of generator torque controller is to optimize the power extraction when operating below the rated wind speed (Region 2). The generator torque reference is calculated as a tabulated function of the filtered turbine generator speed. In Region 3, the generator torque is designed to be inversely proportional to the filtered generator speed.

Furthermore, the pitch control becomes important in Region 3 and the pitch angles are regulated (from 0 degree) to constrain the generator power output (Gao and Gao, 2016). This is important to keep the turbine from the excessive loading and damage. In region 3, a gain-scheduling proportional-integral (PI) pitch controller is adopted to change three pitch angles simultaneously and hence to decrease the rotor lift and torque, illustrated in (2.3). This is the so-called Collective Pitch Control (CPC). Here, this pitch controller is reviewed briefly as its performance will be considered in the thesis as the baseline CPC system for both FTC and load mitigation control. The FTC and load mitigation systems also use individual pitch control (IPC) in which 3 pitch angles are adjusted individually, giving an opportunity for redundant control to achieve a degree of load balancing (Bossanyi, 2005).

$$\Delta\beta_r(t) = GK(\beta)(K_p(t)\Delta w(t) + K_I(t) \int_0^t \Delta w(t)dt) \quad (2.3)$$

where $\Delta\beta_r$ denotes small perturbations of the pitch angle reference around the operation condition. Δw means the error between the rated generator speed set value and the corresponding measurement. K_p , K_I represent the proportional and integral gains. The gain correction factor $GK(\theta)$ is to adjust the values of K_p , K_I with respect to the time-varying wind speed because the sensitivity between aerodynamic power and blade pitch angle is nonlinear over Region 3.

The overall Simulink implementation is illustrated in Fig. 2.1, where the 5MW NREL model is incorporated in the green block *FAST Nonlinear Wind Turbine* and the red block *Baseline Generator Torque Controller* and blue block *Baseline Pitch Controller* are the proposed baseline controllers (Details illustrated in **Appendix A**). The control inputs of this 5MW NREL turbine model includes three pitch angle references, the generator torque reference together with the yaw angle rated value. The yaw angle is typically a constant 0° , which means the orientation of average wind flow is assumed to be constant. In FAST, various measurements of wind turbine components can be accessed, e.g. the generator speed, wind speed at the hub height, blade flapwise/edgewise bending moments, tower fore-aft/side-side bending moments etc., expressed as the yellow block *OutData*.

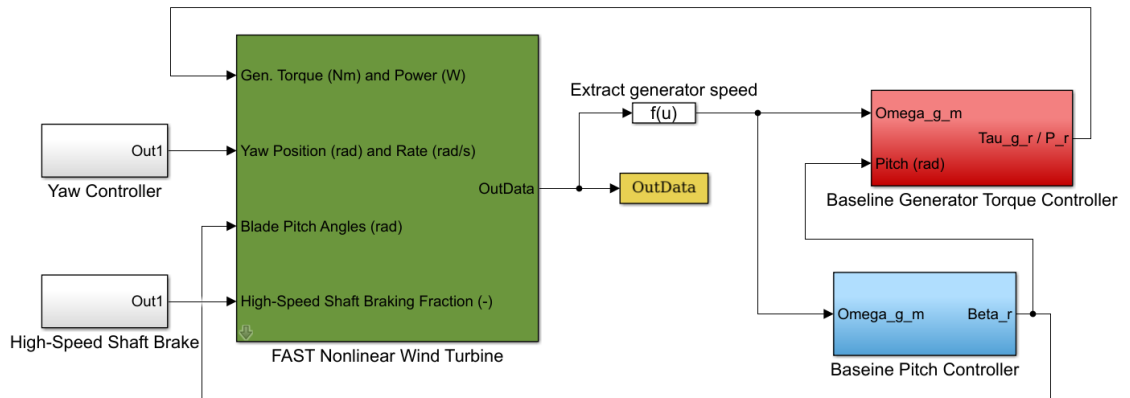


Figure 2.1: The simplified 5MW NREL wind turbine simulation model in MATLAB/Simulink

2.3 Structural Loading in Wind Turbines

Wind turbines not only extract useful wind energy but also suffer from the mechanical loads due to the time-varying incident wind flow. The unbalanced loading typically includes two different kinds: extreme and fatigue loads. Extreme loads are considered to be caused by the sudden strong wind gusting (even up to 113 m/s wind speed) and wind turbines should be able to withstand such extreme conditions that last for about 10 minutes once every 50 years (Association, 2003). One approach that has been proposed to mitigate the gust loads is by means of remote wind sensing techniques known as light and detection ranging (LiDAR) systems, which can obtain wind speed measurements of several hundred meters in front of the turbine rotor to provide sufficient time to respond to potential incoming gusts (Schlipf et al., 2013).

Fatigue loading normally accumulate over time and can cause the turbine damage after long periods of operation. Asymmetric cyclic loading is the dominating source of the rotor and tower fatigue. These are due to the deterministic and stochastic wind phenomena (Körber, 2014). Deterministic wind processes (that can be determined and no statistical approaches required) including wind shear, yaw misalignment, tower shadow and gravity etc. result in the turbine periodic loading. More explanation of these wind properties are illustrated as follows (Burton et al., 2011):

1. Wind Shear.

Wind shear refers to the variation in the average wind velocity or direction with height.

2. Tower Shadow.

Tower shadow denotes the wind speed distortion (i.e. wind speed reduction) caused by the presence of front tower in the incident wind stream.

3. Yaw Misalignment.

Yaw misalignment represents a difference between the wind orientation and the turbine rotor axis direction, which will affect the turbine angle of attack and further power output.

4. Gravity Loads.

Due to the gravity, it exerts a sinusoidally varying edgewise bending moments on the blades and gravitational loading on both the tower and nacelle. The gravity loading on the rotor blade will reach a peak as the blade is in a horizontal position.

Furthermore, rapid variations in the wind speed and orientation (termed as turbulence) along with wake effects typically make the dominating contribution to the turbine unbalanced loading. This is because the scale of a rotor blade and the size of eddies (or vortices) due to turbulence are comparable. In the wind farms, individual wind turbine also suffers from the wake effect from the upstream turbine blades, i.e. a long trailing wake develops behind one wind turbine affecting the lift performance of downstream turbines (González-Longatt et al., 2012). The phenomenon of wake is illustrated in Fig. 2.2.



Figure 2.2: Horns Rev wind farm in Denmark (Technology, 2017)

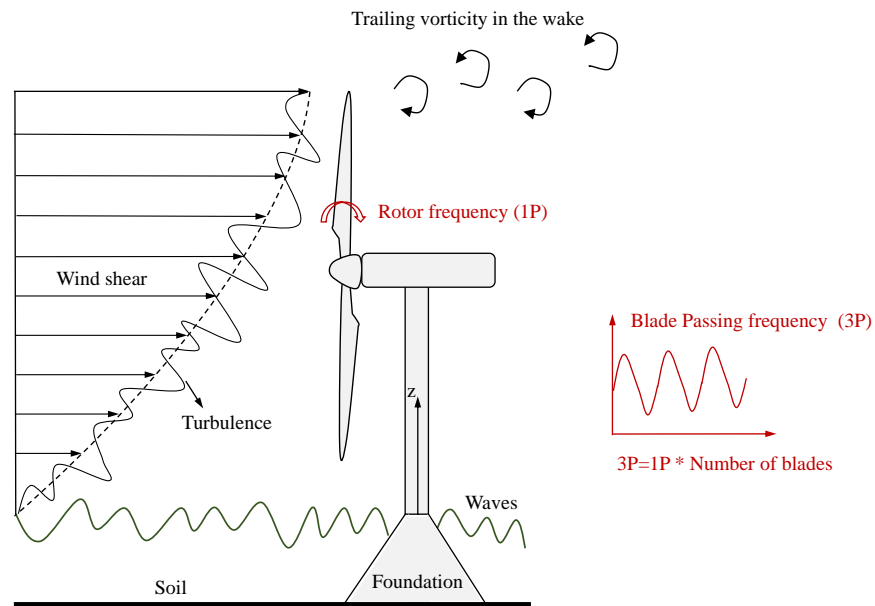


Figure 2.3: Vertical wind shear effect and turbulence from the left side view of a up-wind wind turbine (Houtzager et al., 2013)

Moreover, Fig. 2.3 illustrates the vertical wind shear effect and turbulence. It can be seen from Fig. 2.3, rotor blades slice the incoming wind field at a frequency decided by the blade number and rotor speed. This leads to the development of dynamic rotor blade loading with major frequencies corresponding to the rotor frequency (known as 1P) and its multiples (2P, 3P, ... nP). These fatigue loading exerts adverse effects on the major components including the rotor blades, tower and drive train system. The wind turbine tower system is not rigid in reality. Fluctuating rotor loading cause tower fore-aft oscillations, which will affect the rotor blade dynamics in turn (Burton et al., 2011). The common wind turbine loading are shown in Fig. 2.4. The bending moments in the fore-aft orientation refer to the vibrations in the plane orthogonal to the rotor blade, while the plane parallel to the blade is known as the side-side orientation. The most pivotal eigenmode for both the blade and tower loading is usually the first eigenmode (Jonkman et al., 2005).

2.4 Load Mitigation Control

Except the baseline generator torque controller and CPC system introduced in Section 2.2.4, the modern commercial wind turbines have different control loops to mitigate

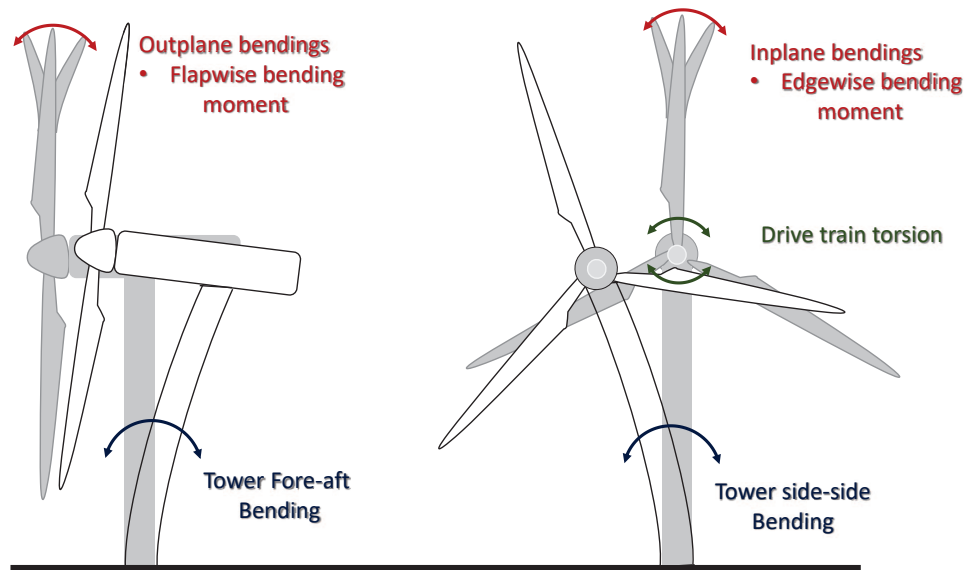


Figure 2.4: Different common loads of wind turbine

the structural loading, illustrated in Fig. 2.5:

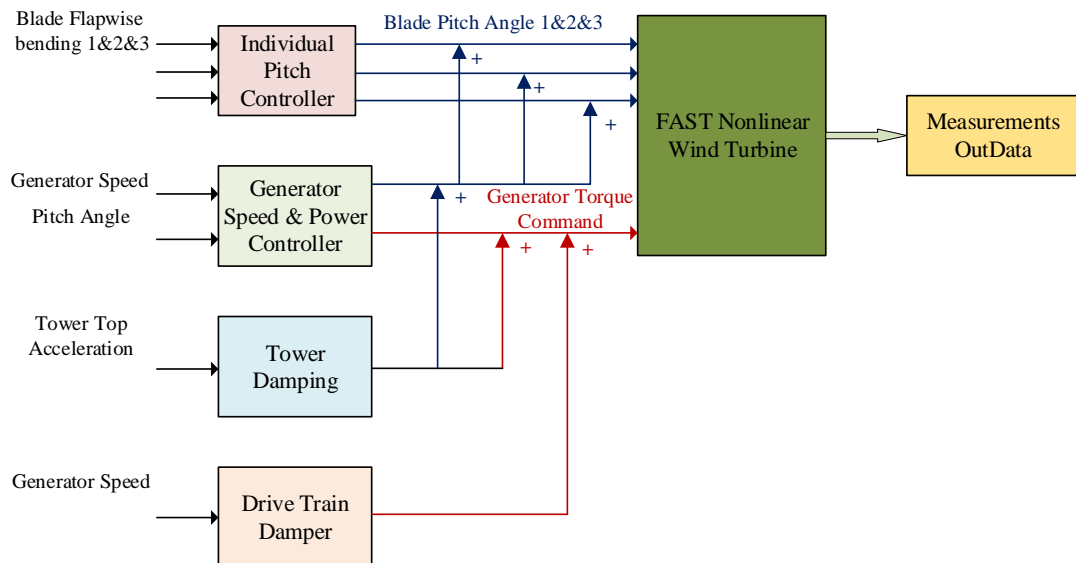


Figure 2.5: General wind turbine control system with common load mitigation strategies (Körber, 2014)

Drive Train Damper It aims to reduce the fatigue loading because of the drive train vibrations. The measured generator speed is adopted to generate an extra zero-mean generator torque signal to dampen the torsional fluctuations of drive train (Van Kuik

et al., 2016). It is typically designed as a bandpass or highpass filter to produce small ripples of generator speed at the drive train frequency.

Active Tower Damping The tower loading is typically dominated by the tower fore-aft oscillations. To dampen the tower fore-aft vibrations, an active tower damping controller is adopted to generate an extra zero-mean collective pitch offset added to the CPC loop based on the tower top fore-aft velocity/acceleration measurements. The tower side-side oscillations are normally more lightly damped than the tower fore-aft vibrations, since the aerodynamic damping from the turbine rotor is relatively smaller in the side-side orientation. In principle, the proper control of generator torque can increase the side-side vibration damping and an additional torque command is derived from the tower side-side acceleration measurements (Wright et al., 2007).

The tower damping controller is usually considered as an independent control loop from the pitch control system for the generator speed regulation (Bossanyi, 2000; Bossanyi, 2003b). However, according to the vibration mechanisms, the blade flapwise fluctuations present significant couplings with tower fore-aft oscillations. Also, both the blade edgewise vibrations and tower side-side fluctuations are shown to have strong couplings with the drive train torsional mode (Körber, 2014). That is, any pitch motion to adjust the generator speed will excite tower vibrations whilst any control signal to reduce tower vibrations will affect the generator speed. Hence, it is of great significance to pay attention to the dynamic couplings when designing these load reduction controllers (Leithead and Dominguez, 2005).

Individual pitch control (IPC) In order to minimize the unbalanced loading of blades and the main bearing system, a zero-mean pitch command for each blade is generated on top of the pitch angle from CPC using the measured blade flapwise/root bending moments. The three blades of most modern wind turbines are pitched individually. Although there exists various IPC designs, many follow the basic principle of the traditional Coleman transformation-based IPC from the work by Bossanyi (2005), shown in Fig. 2.6.

In this strategy, the mitigation of main bearing yaw and tilt loading is treated as two independent loops and achieved by the single-input single-output (SISO) controllers (Bossanyi, 2005). This IPC scheme for yaw and tilt moment compensation is usually referred to as the conventional form of Coleman transformation-based IPC sys-

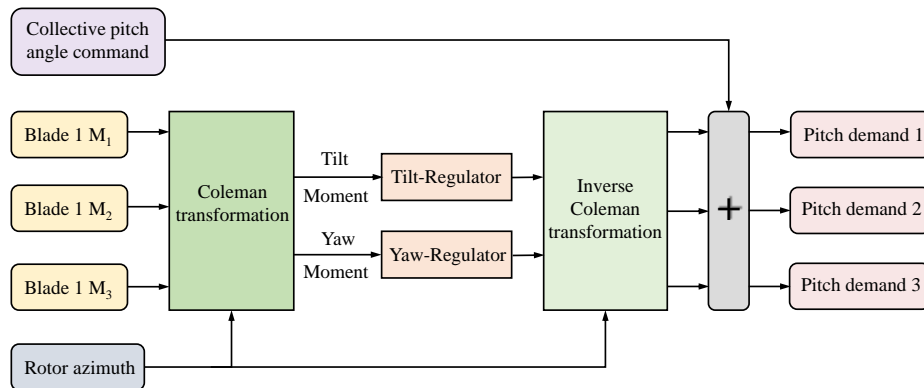


Figure 2.6: Traditional IPC scheme (Bossanyi, 2005)

tem, which has demonstrated to work reliably and effectively in reality (Shan et al., 2013). The blade rotation brings a significant challenge to the load mitigation control, causing the blade loading rotating with blade azimuth angles. Furthermore, the wind turbine model between the flapwise bending moments and pitch angles are typically periodic linear time-varying (LTV) systems, increasing the difficulty in designing appropriate controllers compared with the linear time-invariant (LTI) system (Houtzager et al., 2013). The Coleman transformation also known as d-q transformation (Bossanyi, 2003a), multi-blade coordinate transformation (MBC) (Schuler et al., 2010) has been employed by a large quantity of researchers to achieve the mapping of 3 blade flapwise bending vibrations with phase difference of 120° from the rotating frame B to the fixed hub system F (Van Engelen, 2006). The related coordinate systems are illustrated in Fig. 2.7.

After Coleman transformation, each of the three blade load signals is split into three components including a collective part, together with a cosine and sine component changing with the blade angle in the fixed hub system (Zhang et al., 2011b). The collective component is the mean value of three blade load signals and is same for three rotor blades. The loading acting on the main bearing (i.e. the cosine and sine components) are usually known as the tilt and yaw moments. The tilt moment is in the horizontal direction whilst the yaw moment is in the vertical orientation. This transformation naturally accomplishes the decouplings between the symmetrical (collective) and asymmetrical (cosine and sine) blade unbalanced loading. Since the majority of blade loading comes from the asymmetrical wind inflows, the collective loading are normally ignored by the IPC design.

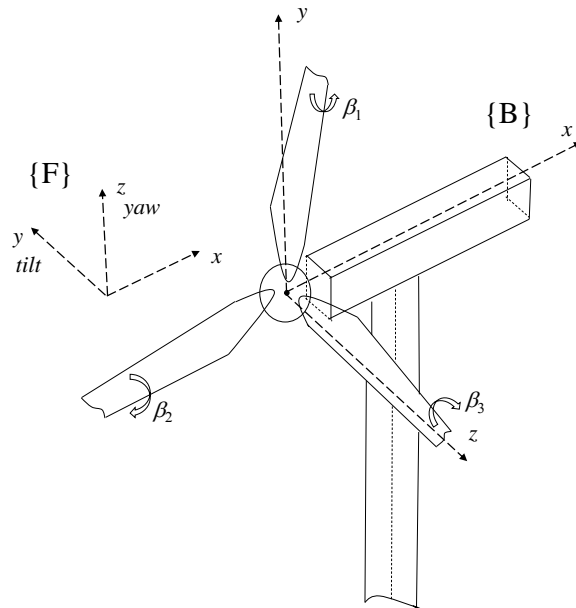


Figure 2.7: Illustrations of the blade rotational reference frame $\{B\}$ and the fixed hub reference frame $\{F\}$ (referred to as tilt-yaw coordinate system) (Zhang et al., 2014a)

However, another significant issue that comes with the Coleman transformation is the problem of frequency splitting (Bossanyi, 2003a; Van Engelen, 2006; Selvam et al., 2009; Zhang et al., 2013). According to the demonstrations in **Appendix B**, the effects from direct components (0P) and the frequency components $3iP$ ($i = 1, 2, \dots, n$) of the flapwise bending moments on the tilt and yaw moments disappear. Moreover, the 1P frequency of the flapwise bending moments is transformed to 0P component of the tilt and yaw moments in the fixed hub coordinate system. The other harmonics in the rotating blade coordinate system contribute to the nearest frequency harmonic, which is the integer multiple of 3P in the fixed reference frame. That is, the blade loading with 2P & 4P frequency are modulated to 3P load on the main bearing yaw and tilt moments, similarly 5P & 7P contribute to 6P. The redistribution of harmonics due to the Coleman transformation is illustrated in Table 2.2.

To visualise these various loading, Fig. 2.8 and Fig. 2.9 provide the frequency analysis of blades, main bearing and tower loading of the 5MW NREL wind turbines, which is performed only with the baseline control systems (Section 2.2.4). Since the frequency spectra of main bearing yaw and tilt moments have quite similar performance, the figure of the tilt moment frequency analysis is omitted here for brevity. It can be seen that the blade loading principally focuses on the 0.2 Hz (the rotor speed is approximately 12.1 rpm \approx 0.2 Hz), 0.4 Hz etc. Furthermore, the loading on the turbine main bearing

Table 2.2: Redistribution of harmonics between the rotating blade loading and main bearing tilt/yaw loading

Harmonics in rotating frame	Harmonics in non-rotating frame
0P	N/A
1P	0P
2P, 4P	3P
3P	N/A
5P, 7P	6P

is dominated by the loading of 0P, 3P, 6P etc., whilst the excessive tower loading occurs primarily at the resonant frequency (0.32 Hz). It is worth noting that the deterministic wind phenomena appears as spikes on the power spectrum, while stochastic properties spread as small burrs over a wider frequency range.

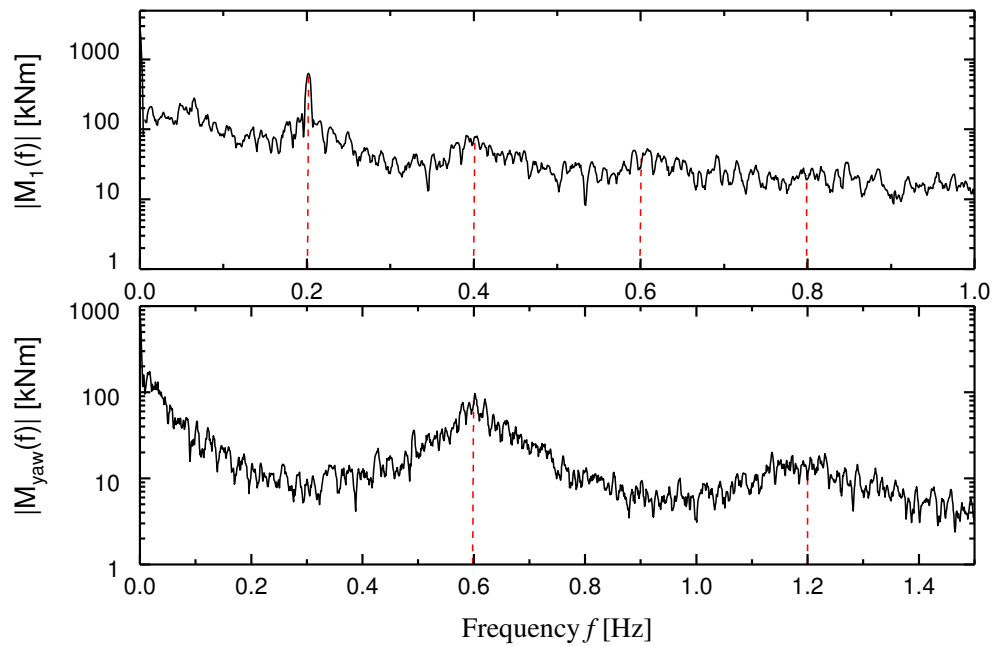


Figure 2.8: Frequency spectra of the blade 1 flapwise bending moment and main bearing tilt moment

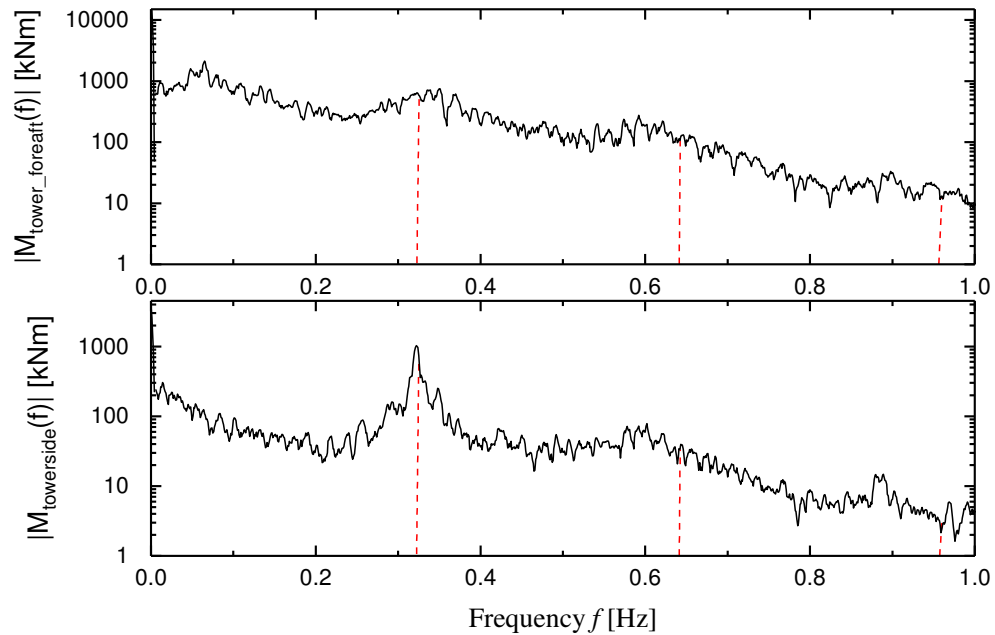


Figure 2.9: Frequency spectra of the tower fore-aft and side-side bending moments

2.5 Literature Review of IPC Methods

2.5.1 Traditional Feedback Control

Early IPC strategies are based on the feedback control with measurements from the structural sensors (Bossanyi, 2005). The most commonly used IPC strategy is the Coleman transformation-IPC strategy based on azimuth angle and blade root loads feedback, in which each pitch angle is periodically regulated to mitigate the 1P blade loading, illustrated in Fig. 2.6 (Bossanyi, 2003a, 2005; Van Engelen, 2006; Selvam et al., 2009; Schuler et al., 2010; Lu et al., 2015; Liu et al., 2016, etc.). If the pitch actuator dynamics respond to higher harmonics of the measured blade bending, these high frequency moments can also be compensated by IPC. In the work of (Van Engelen and Van der Hooft, 2005; Van Engelen, 2006; Houtzager et al., 2013), the authors extend the 1P-IPC concept to the mitigation of higher harmonic wind turbine loading (2P, 3P) with each control loop using a different Coleman transformation. Careful design is needed to handle the couplings between the different load reduction loops. However, the requirement of higher harmonic load reduction leads to increased pitch actuation motion and causes more wear, thus increasing the possibility for potential faults and limiting the useful pitch system service life. Given that 1P loading is the primary sources of blade fatigue, the 1P loading mitigation is the main subject of this

thesis. The IPC system should be carefully designed to decouple from the CPC loop at the relevant active frequencies, which also maintains the generator power output at a desired level (as required in Region 3).

When using the Coleman transformation in IPC methods, it is required to measure the rotor azimuth angle. Some researchers (Zhang et al., 2013) propose a proportion resonance (PR) control strategy with the Clarke transformation. It is a substitute for the Coleman transformation, which does not require the azimuth angle. This proposed scheme can mitigate the blade loading of both the 1P and higher harmonics along with 3P loading on the main bearing system. Another approach of mitigating the asymmetric blade loading by pitch control is called as "single blade control" (Leithead et al., 2009), also known as individual blade control (IBC) (Han and Leithead, 2014). In IBC, each blade is equipped with one actuator, sensors and controller so that each blade responds to the measured blade load independently, without any communications within three blades, which results in three identical SISO controllers. Despite the seeming differences, fundamental similarities has been demonstrated to exist between the Coleman transformation-based IPC, Clarke transform-based IPC and IBC (Lio et al., 2017).

Since there is couplings between various control loops and disturbances, it is appealing to apply the optimal multivariable control methods in the IPC design. To improve the robustness of control system with turbine uncertainties, a multivariable IPC has been designed using H_∞ loop-shaping theory (Lu et al., 2015), which handles the load mitigation directly in the frequency domain and simultaneously achieves impressive damping performance on the blade loading. Similarly, an optimal multivariable IPC is designed to attenuate the blade periodic loading under the premise of penalizing control inputs by H_∞ optimization based on a frequency-domain multi-input multi-output plant in (Vali et al., 2016). Since sliding mode control (SMC) is robust to the matched parameter disturbances, it has been studied by (Xiao et al., 2013; Han and Liu, 2014) to verify its effectiveness in the IPC system. Furthermore, other optimal multivariable approaches such as linear quadratic regulator (LQR) (Wright, 2004) and l_1 optimal multivariable controller (Schuler et al., 2010) are also studied. Moreover, in terms of the real wind turbine validation, an IPC system based on PI control approach is designed by GH and has been validated on the two or three-bladed wind turbines (namely CART2 or CART3) provided by the NREL (Bossanyi and Wright, 2009; Bossanyi et al., 2012; Bossanyi et al., 2013).

2.5.2 Feed-forward / Preview Control

There is usually an inherent delay before the forthcoming wind flow exerts effects on wind turbines. From the perspective of control system, wind speed variations serve as disturbances which require the control action from the closed-loop controller to handle them, which is often referred to as disturbance feed-forward control (Selvam et al., 2009). The load reduction performance can be enhanced by the feed-forward control strategy especially with the measured wind disturbances (Körber, 2014). Since wind speed measurements from the anemometer cannot sufficiently represent the effective wind speed (EWS) driving the wind turbine dynamics, it stimulates the related research on the EWS estimation (Østergaard et al., 2007; Soltani et al., 2013). Further improvements can be achieved if the wind information can not only be known at the current moment, but also if the future wind speed is obtained before it affects the turbine system, referred to as "preview control" (Laks et al., 2010). Currently, the LiDAR systems can provide future wind flow knowledge even several hundred meters ahead of the rotor plane, which measures not only one point in space but also an area or volume of wind flow (Schlipf, 2016). The wind preview knowledge can then be provided to the feedback control loop, allowing the control system to have preventive actions before the wind flow arrives. The combinations between the feed-forward / preview control loop and feedback controller is usually used to tackle multivariate control goals simultaneously, including the wind disturbances rejection, generator speed regulation and load reduction (Selvam et al., 2009; Dunne et al., 2010; Dunne et al., 2011; Wang et al., 2012, etc.).

In Selvam et al. (2009), an optimal linear quadratic Gaussian (LQG) feedback controller is proposed to mitigate the 1P and 3P blade fatigue loading through IPC. Moreover, a feed-forward controller with the wind speed estimation provided by a Kalman filter is proposed to reject the effects of wind low-frequency components on the blade moments. In Dunne et al. (2011), 2 feed-forward control loops containing collective-pitch model-inverse and an individual pitch gain-scheduled shaped compensator are combined with a standard feedback control system, respectively. The results show that the blade and tower fore-aft loading can be further reduced by sacrificing enhanced pitch motions. The incident wind speed is assumed to be provided by LiDAR. In Laks et al. (2010), load reduction performances of preview-based feed-forward control strategies with both the multi-blade coordinate (MBC) and non-MBC based models by H_∞ optimization are explored. The results show that the accuracy of wind preview can

affect the performance of preview-based feed-forward scheme and even eliminate the advantages it brings.

Furthermore, the feed-forward characteristics can also be directly integrated into the feedback control loop by model predictive control (MPC) for multi-objective optimization without the increased complexity, where future wind predictions are required. Therefore, MPC maintains the optimality and constraint handling performance when using a combined feed-forward-feedback control system. The work in (Körber and King, 2010) proposes a well-designed linear MPC control strategy using future wind speeds, which can perform well on the tower load mitigation whilst maintaining good stability of power output. The work in Koerber and King (2013) proposes a MPC control strategy for the collective pitch control and generator torque control issue with considering the turbine state constraints (i.e. rotor speed limits). The results show that preview control with state constraints can avoid unnecessary shut-down caused by the over-speed limit violations. The authors in Spencer et al. (2013) study the effects of the different parameters for upcoming wind flows and wind prediction horizon lengths on the proposed MPC controllers in mitigating turbine loading. It is worth noting that obvious mitigation results can be obtained under the premise of knowing the future wind information and considering a limited variance of wind shear operating in Region 3. Perfect incoming wind measurements are assumed. In Raach et al. (2014), a nonlinear MPC with IPC is presented and the results present an impressive blade fatigue loading mitigation. In Laks et al. (2011), it is proposed that a time-varying MPC scheme using the incoming wind characteristics can outperform the classical controllers (e.g. PI) without wind preview in terms of blade load reduction. Instead of assuming ideal wind measurements, a more realistic model from the LiDAR system for preview measurements is assumed. The LiDAR preview strategy with local blade inflow measurements are employed to obtain a more accurate MPC control system in Kragh and Hansen (2011). Similarly, Schlipf et al. (2013) studies a nonlinear MPC-based preview controller with future wind speeds from LiDAR. Several field tests conducted by NREL on the CART2 and CART3 wind turbine have verified the effectiveness of feed-forward control system along with LiDAR not only in simulations but also in actual conditions (Scholbrock et al., 2013; Schlipf et al., 2014; Fleming et al., 2014). It is worth noting that although feed-forward control systems can benefit from the LiDAR measurements, the errors of LiDAR wind measurements from the wind evolution and distortion will exert inverse effects on its performance which requires post processing i.e. optimal filters with the obtained wind measurements (Simley and Pao, 2013).

2.5.3 Smart Rotor Control

There is an increasing interest in more advanced load control strategies such as the locally distributed aerodynamic control strategy with built-in intelligent aerodynamic actuators located directly in the blades, referred to as "smart rotor control" (Bernhammer et al., 2016; Van Wingerden et al., 2008). Rather than adjusting the entire blade through the pitch actuator system, the smart rotor changes the incident airflow and blade loading by employing special actuators located span-wise along the blade (Menezes et al., 2018). Compared to the IPC system, the smart rotor control makes turbine rotors more intelligent, to enable them responding to the periodic and extreme loading events (i.e. wind gusts) faster and more accurately. This is because only small mass not the total blade mass is regulated in the smart rotor control scheme, thereby influencing the blade local force distribution.

Potential techniques include the trailing-edge flaps (Castaignet et al., 2011; Ng et al., 2016), microtabs (Johnson et al., 2010), active twist (Chen and Chopra, 1997), as well as specific actuators for the boundary layer control, e.g. synthetic jets or plasma actuators (Ebrahimi and Movahhedi, 2017). Comprehensive review papers (Barlas and Van Kuik, 2007; Barlas and van Kuik, 2010) provide the illustrative introduction of the state-of-the-art wind turbine smart rotor control strategies. Promising simulation results have been demonstrated in Plumley et al. (2014), in which a smart rotor control system with the distributed trailing edge flaps is compared to a conventional IPC system. The similar load reduction performance can be achieved using trailing edge flaps, also reducing both the pitch actuator motion and rates simultaneously. The modern control methods (e.g. MPC) are employed with trailing edge flaps in Castaignet et al. (2011). Currently, few papers about field tests of the turbine smart rotor control (Castaignet et al., 2014; Berg et al., 2014) are presented, which mostly employ the relatively mature technique with trailing edge flaps. This is because there are several difficulties in implementing the smart rotors on modern wind turbines (Menezes et al., 2018). That is, the actuator devices mounted on blades should be reliable to avoid the increasing maintenance and operation costs. Furthermore, implementing these specific actuator devices need an expensive blade redesign.

2.6 Conclusion

The purpose of this Chapter is to provide a thorough introduction to the motivation of IPC in the modern wind turbine system and a literature review of current IPC methods. Because of the requirement to minimize the operation and maintenance expenses, there has been a surging interest on the design of different IPC schemes on a global scale. This has evolved from the understanding of traditional feedback control to develop a suitable feed-forward/preview control strategy using the LiDAR techniques. This is followed by a more complicated and expensive load reduction system (i.e. smart rotor control). The load reduction results are being continuously improved. However, these control strategies can inevitably lead to the enhanced pitching motions and fatigue, which will increase the possibility of pitch system faults and in turn affect the IPC performance. Therefore, a fault tolerant control (FTC) system is required to deal with the pitch system faults. Chapter 3 details the motivation and development of the use of FTC system to handle the pitch system faults on-line.

Chapter 3

Fault Diagnosis and Fault-tolerant Control for Wind Turbine Systems

3.1 Introduction

As described in Chapter 1, the wind turbine pitch system plays a crucial role in the strategy to minimise the effects of wind and turbulence loading on the turbine blades and tower. Clearly, this system must be reliable and should be tolerant to certain faults that can occur in pitch system sensors or in the actuators themselves. In other words the action of this control system must be sustainable in all operating conditions and even when some faults occur. For example, we can define a "load reduction performance" to be a certain percentage reduction in standard deviation of flapwise bending with control action compared with the bending without the control. We can also use this performance measure to compare the performance of different control strategies. If a fault occurs in a pitch actuator we must therefore be able to understand the effect of this fault on the load reduction. Actually, this is precisely the concept of "fault tolerant control" (FTC) considering load reduction. In the fault tolerant pitch actuation system the percentage of bending moment reduction should be maintained even in the event of an actuator fault. The same principle can be applied to fault tolerance in the presence of pitch sensors or blade sensors.

The way to achieve fault tolerance is to use redundancy, either using repeated identical hardware (sensors, etc.) or repeated dissimilar redundancy. However, the redundancy can also be generated using "soft" redundancy, i.e. by using analytical methods to replicate the action of sensors. A suitable combination of both types of redundancy will

provide a very powerful mechanism for achieving the sustainable system operation. To make redundancy effective enough, it is essential to monitor the presence of any fault or developing faults before they have a significant effect on the system - in this case the load reduction performance.

So, the purpose of FTC is to ensure that a control system has satisfactory control performance in the event of faults. The faults cannot be total "failures" in other words only certain "recoverable" faults can be considered. Then the important question is what is recoverable? A suitable method fault monitoring is required to answer this question. To monitor the faults one of two control-based procedures can be used (i) fault detection and isolation (FDI), or (ii) fault estimation (FE). In (i) residual (or "error" signals) are used to give the indication of the onset of a fault. Once detected (using a threshold) the nature, type and location of the fault can be determined to isolate the fault. The FDI scheme is usually model-based and the performance of this type of diagnosis scheme is dependent on the likelihood that the model or models used are accurate, since modelling errors will affect the performance of the detection and isolation (Chen and Patton, 2012). In (ii) an alternative method is based on the principle of robustly estimating each fault. The robustness takes into account the modelling uncertainty and each of the "detection" and "isolation" functions are considered automatically within the fault estimation role.

So the FTC uses FDI or FE to recover or reconfigure the system to an acceptable operating level once a fault has been detected. This can either be done by reconfiguring the control system as well as the sensors and/actuators, based on a provided level of redundancy. Alternatively, redundancy is still used but the estimated faults (in FE) are used to compensate for the fault effects acting in the control system. It is desirable to account for the robustness of the "FDI and FTC" or "FE and FTC". It turns that the FDI-based approach to FTC is exceedingly complex and difficult to implement in a real system. In this thesis, the FE approach to FTC is preferred.

FTC is thus an important control strategy for achieving the sustainable operation of wind turbines. The sustained operation means that a sufficient level of reliability of the control system function must be reached. Based on the acquired knowledge of the "health" of a sensor or actuator (from the FDI/FE and FTC combined system) it is very attractive to use this information as a form of "prognostic" knowledge from which predictive and optimal maintenance strategies can be employed to reduce maintenance expenses and system downtime or failure.

The purpose of this Chapter is to illustrate some background knowledge about fault diagnosis and FTC as well as the current developments in wind turbine FTC system. The remainder of this Chapter is shown as follows. Section 3.2 provides an overview of the background knowledge about fault diagnosis and FTC. Next, a quick review of different wind turbine fault diagnosis and FTC strategies is presented in Section 3.3. Section 3.4 provides a detailed tutorial example about designing a fault detection and isolation (FDI) system for the turbine pitch actuator stuck fault. Finally, the summary is provided in Section 3.5.

3.2 Overview of Fault Diagnosis and Fault-tolerant Control

3.2.1 Fault Classification

As explained in Isermann (2011), "A fault is an un-permitted deviation of at least one characteristic property or parameter of the system from the acceptable /usual /standard condition". Faults in the process equipments can cause substandard production and increase the possibility of system downtime, operating expenses, as well as potential detrimental effects on the environment (Patton et al., 2013). A fault is distinguished from a failure. The term "failure" is adopted when a fault is severe enough that the related system function (actuator, sensor or internal function) cannot work properly (Isermann, 2006). This usually results in system downtime, unless it occurs in a non-critical component or in a system that has redundancy (to enable the system to recover from the failure). For example, the failure of one wind turbine pitch actuator usually requires an immediate system shut-down. Although the wind turbine can maintain an operating mode, the discrepancies between three rotor blade pitch angles can cause enhanced power output fluctuations and severe mechanical damage on the rotor. On the other hand the redundancy that can occur between three healthy but independent actuators (in the so-called "individual pitch control") forms a very powerful basis for both load mitigation and rotor system fault tolerance.

Generally, faults are categorised as actuator, component or sensor faults in accordance with the fault location (Chen and Patton, 2012; Blanke et al., 2006). The typical faults of a closed-loop control system is presented in Fig. 3.1.

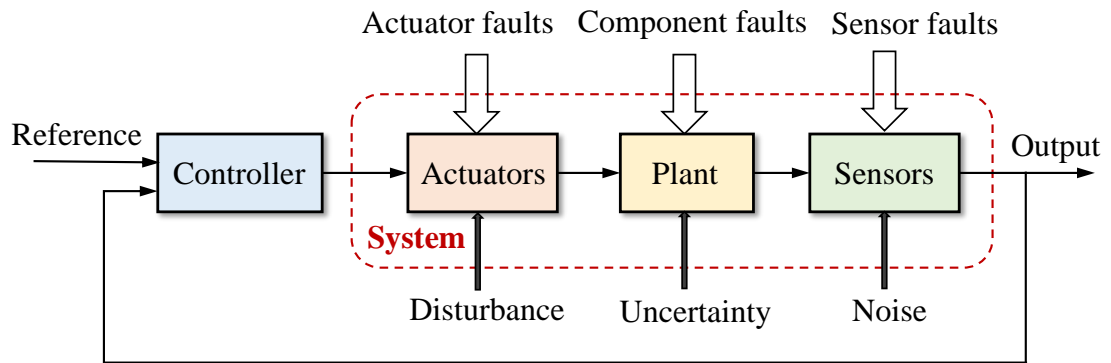


Figure 3.1: A control system with actuator, component and sensor faults (Patton, 2015)

An *actuator fault* implies that the control action applied to the controlled system changes either partially or completely, which corresponds to any malfunction of concerned equipments that actuate the system. The partial actuator fault indicates that the actuator performs less effectively and only provides the system with only a part of the nominal actuation signal, e.g. as a result of rusty or clogged valves. For a complete actuator failure, no actuation is generated regardless of the provided inputs, e.g. due to the burnout and breakage of wiring or stuck at a specific position. This can not be directly compensated by control actions, usually detected and isolated by fault diagnosis techniques.

A sensor is an equipment that measures or observes the real system, e.g. accelerometers, potentiometers, strain gauges, pressure gauges, etc. A *sensor fault* indicates that the obtained system measurements are incorrect, which can be divided into partial or complete sensor fault. When sensors suffer from faults, the sensor measurements are subject to serious errors but the system dynamics are unaffected. Sensor faults usually come from the bias, poor calibration, scaling error or sensor dynamic variations.

A *component fault* (also termed as process fault) directly affects the system parameters, which in turn changes the system input/output dynamics. Component faults refer to variations in the parameters or structure employed during the physical system modelling, and cover a big range of potential faults including aerodynamic coefficients variations, mass changes, ageing, temperature changes, or environmental impacts.

Furthermore, faults are also divided into additive or multiplicative fault type in terms of how they are modelled (Isermann, 2006):

An *additive fault* implies that the fault affects system signal by adding an additional fault signal, such as offset actuator and sensor faults.

A *multiplicative fault* means that the fault affects system signal by multiplying an additional fault signal, such as parametric faults.

According to the time dependency of fault signals, faults are divided into (a) abrupt faults, (b) incipient faults and (c) intermittent faults (Isermann and Ballé, 1997), illustrated in Fig. 3.2.

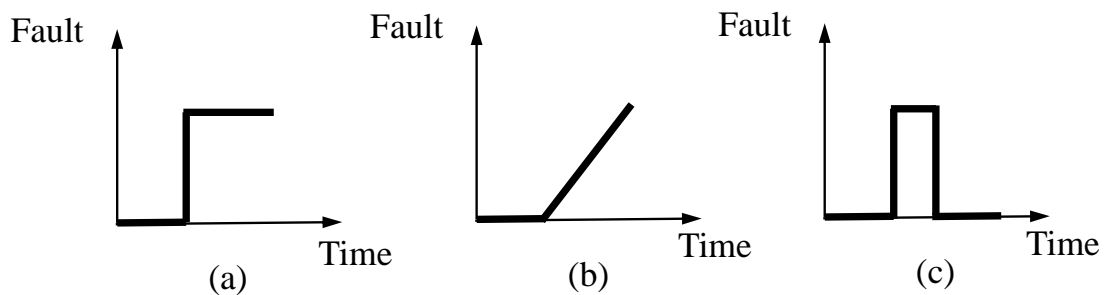


Figure 3.2: A control system with abrupt, incipient and intermittent faults (Patton, 2015)

An *abrupt fault* means that the change occurs faster than the nominal system dynamics and demands quick fault detection. Conversely, *incipient fault* develops slowly, e.g. clogging of valves. *Intermittent fault* exhibits the repetitive pattern of occurrence and disappearance. The different methods of fault classification described above are related and the different fault categories can overlap. For example, a sensor bias fault can be considered as belonging to the sensor fault or additive fault type.

3.2.2 Fault Diagnosis

For the safety-critical systems, the safe operation and supervision requires detection and diagnosis of faults, which introduces the description of following terminologies (Isermann and Ballé, 1997; Gao et al., 2015a).

Fault detection: "Determination of the faults present in a system and the time of detection."

Fault isolation: "Determination of the kind, location and time of detection of a fault. Follows fault detection."

Fault identification: "Determination of the size and time-variant behaviour of a fault. Follows fault isolation."

Fault estimation: "Determination of magnitude of a fault signal on-line."

Fault detection as the most basic category only provides the binary decisions indicating is a fault exists in the physical system or not. Fault isolation provides the fault position, type as well as the occurring time. Furthermore, fault identification provides the fault magnitude and time of fault occurrence. Fault detection and isolation is known as FDI and fault detection and diagnosis (FDD) represents fault detection, isolation and identification, or simply termed as fault diagnosis (FD) (Isermann and Ballé, 1997). Fault estimation (FE) achieves the accurate fault information including type, size, onset and location. As stated in Section 3.1, the FDI and FE mechanism have become the mainstream techniques to achieve the fault diagnosis (Gertler, 1998; Chen and Patton, 2012).

The FDI mechanism achieves the fault information including the onset, location and severity and provides an early fault detection before them become critical (Patton, 1997a). The FDI can be implemented by means of hardware redundancy, which represents multiple independent replications of hardware channels (e.g., sensors, actuators, computers, etc.) and requires consistency comparisons between outputs from the same components (Chen and Patton, 2012). On the other hand, as stated in Section 3.1, analytical information about the monitored physical system can be adopted to implement the FDI based on a mathematical system model, referred to as analytical redundancy (Patton et al., 2013). Analytical redundancy exhibits more system independence compared with the hardware redundancy (Patton, 1997a). It turns out to be very appealing to combine the hardware redundancy with analytical redundancy to realize the on-line fault detection and diagnosis. In the FDI scheme, after obtaining the fault information, the supervision system reconfigures the feedback control and maintains the system nominal operation by replacing the faulty component (sensor, actuator etc.) with redundant components or analytical redundancy (non-critical faults) or requires stopping the system (critical faults).

Generally speaking, the main fault diagnosis technologies can be divided into: (1) model-based (2) data-based (model-free) methods (Zhang and Jiang, 2008; Gao et al.,

2015a; Gao et al., 2015b). The basic principle of model-based fault diagnosis is make a comparison between the measured outputs and estimates achieved from measured system inputs through a mathematical model (Gertler, 2015). A residual as fault indicator is normally derived from the deviations between system output measurements and model-based estimates. The residual indicates the faulty condition, which is typically zero in the absence of faults and is distinguishably different from zero in the event of faults. The general schematic diagram of two-stage model-based FDD is explained in Fig. 3.3.

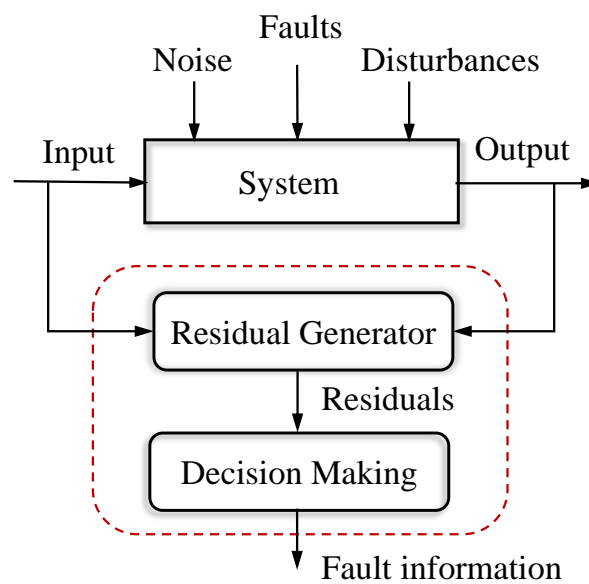


Figure 3.3: General schematic diagram of model-based fault diagnosis (Chen and Patton, 2012)

For linear dynamic systems, there exists three main approaches for generating residuals (Gertler, 2015): (i) direct consistency (parity) relations (Gertler, 1998), (ii) parity space (Chow and Willsky, 1984), and (iii) diagnostic observers (Chen and Patton, 2012). A residual evaluation process follows after the residual generation stage, which monitors whether and where a fault occurs.

In some control applications (such as complete actuator faults), the fault information provided by FDI is sufficient. Nonetheless, the FDI mechanism cannot provide direct fault reconstructions, involving the size and "direction" of faults. When the faults are tolerable, fault estimates become very important to achieve a comprehensive fault diagnosis of wind turbine system and more advanced fault handling methods including fault-tolerant strategy are required (Georg and Schulte, 2014).

AFTC can provide a system with more fault tolerant capability, which has two conceptual steps (Zhang and Jiang, 2008; Blanke et al., 2006; Gao et al., 2015a):

(1) **Fault diagnosis scheme.** This mechanism can robustly and accurately detect the system fault occurrence or estimate faults by using the measured inputs and outputs. It presents a nominal baseline controller in the absence of faults, which attenuates the effects of system disturbances as well as guarantees the satisfactory stability and required closed-loop tracking performance.

(2) **Reconfiguration mechanism.** The controller parameters are adapted or reconfigured such that the acceptable performance of closed-loop system is guaranteed in the event of one or more bounded faults.

Therefore, it is the AFTC approach that can fit well with a wider range of methods, rather than PFTC. A classification of the principal AFTC approaches (Lan, 2017; Zhang and Jiang, 2008; Lunze and Richter, 2008) is presented in Fig. 3.5. The red lines represent the relevant approaches studied in this thesis.

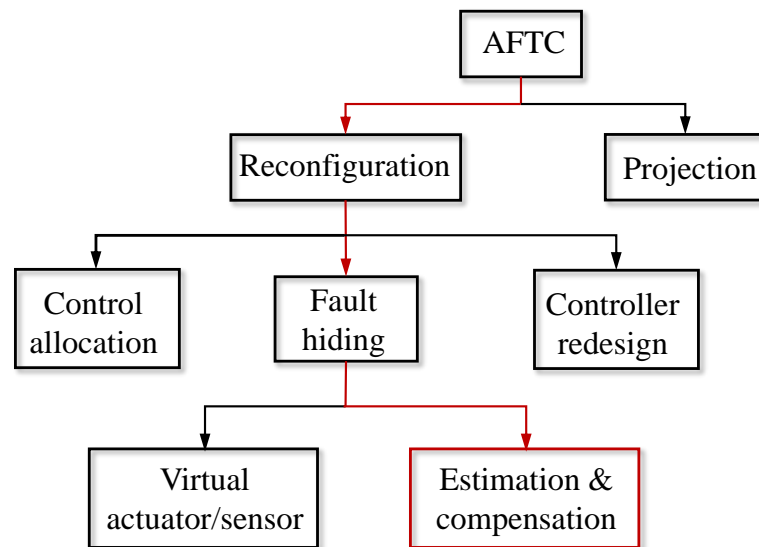


Figure 3.5: Classification of the AFTC methods

As shown in Fig. 3.5, the AFTC strategy involves the projection and reconfiguration approaches. The projection method (known as multiple-model approach) obtains the fault knowledge from the FDI block, switches between the pre-designed controller sets and selects an appropriate controller to compensate fault effects based on the fault condition (Maybeck and Stevens, 1991; Zhang and Jiang, 2001).

The reconfiguration method is categorised into three main approaches including control allocation, fault hiding and controller redesign. Controller allocation realizes the reallocation of control signals from faulty actuators to the redundant healthy actuators without reconfiguring the controller structure (Buffington et al., 1999; Alwi and Edwards, 2008). Controller allocation is less acceptable for the industry due to the physical redundancy requirements of system components, but is still promising for severe system faults. Fault hiding aims to hide faults from the nominal controller through involving an additional reconfiguration block for the faulty plant, which includes virtual actuator/sensor, and estimation & compensation (Richter, 2011). A reconfigured system with a virtual actuator/sensor block is placed between the real actuator/sensor and the baseline system controller. It performs indistinguishably from the nominal system and masks the fault effects. Virtual actuators change the control signal to handle the fault while virtual sensors can replace the practical faulty sensors (Lunze and Steffen, 2006). Controller redesign discards the nominal system control strategy and proposes a new controller for the system with faults (Lunze and Richter, 2008).

Furthermore, the estimation & compensation approach implements the on-line fault compensation through a reconfigurable controller with fault information from FE. FE accurately estimates the fault information including type, magnitude, location and occurrence time. It is a more direct approach to obtain the fault knowledge compared with other alternatives (e.g. FDI and FD). The FE is embedded with the reconfigurable controller, estimating system faults and then forwarding the fault estimations to the FTC controller. Currently, different estimation approaches have been studied for the FE, e.g. sliding mode observer (Huang et al., 2016; Yan and Edwards, 2007; Tan and Edwards, 2002), augmented state observer (Gao and Ding, 2007), adaptive observer (Wang and Daley, 1996; Zhang et al., 2008), and unknown input observer (Odgaard and Stoustrup, 2012a; Gao et al., 2016), and also robust integrated FTC design (Lan and Patton, 2016) etc.

There are similarities between the model-based FDI and FE approaches, whose performance relies on the precision of system mathematical model (Patton, 1997b). Meanwhile, the performance of FDI/FE-based FTC strategies is directly influenced by the precision of fault estimates and the presence of simultaneous faults. The attention should be devoted to the system model uncertainties and the situation of simultaneous faults. It is important to propose a robust FDI/FE-based FTC system that is insensitive to unknown uncertainties, disturbances as well as the measurement noise. Furthermore, the FDI involves standard procedures of fault detection and fault isolation, while

FE estimates accurately the actual fault information by system observer methods. The FE intrinsically accomplishes the fault detection and isolation without any design of supervisor, residual and switching mechanisms. Thus, FE turns out to be a powerful alternative of the FDI method in the FTC system.

3.3 Fault Diagnosis and Fault-tolerant Control for Wind Turbines

The last decade has witnessed a number of research studies on designing fault diagnosis and FTC schemes for wind turbines. The majority of researches have been driven by the open competitions launched by KK-electronic a/c and Mathworks between 2009 and 2015 (Odgaard et al., 2013). Therefore, several review papers of condition monitoring, fault diagnosis and FTC for wind turbines have summarized the relevant technologies (Hameed et al., 2009; Lu et al., 2009; Pourmohammad and Fekih, 2011; Odgaard and Stoustrup, 2012b; Badihi et al., 2013; Qiao and Lu, 2015a; Liu et al., 2015; Habibi et al., 2018).

In terms of fault diagnosis for wind turbines, the proposed schemes range from model-based to data-driven approaches. For wind turbine model-based FDI schemes, the principal methods are based on Kalman filter (Wei et al., 2008; Kiasi et al., 2011), observers (Odgaard and Stoustrup, 2009; Zhang et al., 2011a) and parity space equation (Pisu and Ayalew, 2011), etc. A FDI strategy using Kalman filter is used to detect and isolate the blade root loading sensor faults with considering dual sensor redundancy (Wei et al., 2008). In the work (Odgaard and Stoustrup, 2009), a FDI strategy using unknown input observer is designed to estimate converter faults and isolate them to be a sensor or an actuator fault. In Pisu and Ayalew (2011), separate parity equations are used to detect and isolate the pitch actuator and drive-train subsystem faults. Residual filters are proposed to make the generated residuals robust to system uncertainties and noise while being sensitive to the specific faults. For data-driven based FDI techniques, various approaches are studied (Dong and Verhaegen, 2011; Simani et al., 2011; Yin et al., 2014; Qiao and Lu, 2015b). The work by Simani et al. (2011) presents a data-driven diagnosis scheme using fuzzy prototypes for converter faults detection and isolation. In Yin et al. (2014), a data-driven fault detection strategy is presented using a parity-space-based residual generator, which is directly based on system measurements. With proper evaluation approach and decision logic, fault detection results

for a turbine benchmark are obtained. The majority of these strategies are typically based on the use of generated residuals.

The FTC strategies can be integrated with different control techniques including Takagi-Sugeno (T-S) fuzzy modelling based methods (Kamal et al., 2012; Sami and Patton, 2012b; Sami and Patton, 2012c), linear parameter varying (LPV) control based methods (Sloth et al., 2011; Chen et al., 2013), sliding model-based methods (Georg and Schulte, 2014; Sami and Patton, 2012a), predictive control based methods (Yang and Maciejowski, 2012; Feng and Patton, 2014), as well as H_∞ based methods (Qi et al. (2014)) etc. A multi-observer switching control-based robust active fault-tolerant fuzzy control for wind turbines with considering sensor faults, wind disturbance and system uncertainties is presented in Kamal et al. (2012). The T-S fuzzy model with parametric uncertainties is used and fuzzy state observers are established for fault construction. In Sloth et al. (2011), a linear parameter-varying passive and active FTC controllers are proposed to accommodate hydraulic pitch actuator faults with changed dynamics based on the LPV wind turbine models. It is concluded that the AFTC scheme significantly outperforms PFTC when system dynamics change dramatically due to the fault impact. A observer-based FTC strategy for wind turbines using active FTC is studied by Georg and Schulte (2014). The pitch actuator faults and generator sensor faults are estimated by a T-S sliding mode observer and then compensated by subtracting the reconstructed faults from the demanded control inputs or measurement outputs. An extended Kalman filter is proposed to obtain the estimations of turbine states and system fault information in Yang and Maciejowski (2012). A group of MPC pre-compensators can be used to further compensate the impacts of various faults with the fault estimates and a global MPC optimises the overall system performance. The work by Qi et al. (2014) presents a H_∞ based FTC scheme for actuator faults based on a stochastic piecewise affine wind turbine model. The strategy is verified under normal and faulty situations with different wind fields. Most of these references adopt on-line fault estimation & compensation strategy to achieve the active FTC.

Except the above different control methods-based FTC strategies, FTC can be implemented with other schemes. In the work by Rotondo et al. (2012), a FE strategy using batch least squares for several wind turbine actuator and sensor faults is proposed. Virtual sensor/actuator approaches is used to deal with the fault effects. Similarly, an FTC strategy using a set of unknown input observers is presented for estimating different generator and rotor speed measurement faults (Odgaard and Stoustrup, 2012a). Virtual sensor strategy can be easily implemented in real wind turbine systems, while actuator

signal corrections may cause system instability due to low-precision fault reconstruction (Blesa et al., 2014). The work by Kim et al. (2012) proposes a scheme based on control allocation to tolerate pitch actuator incipient faults with changed parameters through reconfiguration law. The principal strategy is to redistribute the torque loss into normal blade actuators to maintain the power output in the event of pitch actuator faults. Each blade is provided with an individual pitch angle using control allocation strategy.

The FDI and FTC strategies have their own characteristics and are applicable to different or even the same situations. Appropriate fault diagnosis and prognostic strategy should be selected, according to specific issues. Particularly, the work of this thesis adopts the FDI approach and FE combined with fault compensation within the AFTC mechanism to handle different faults in the wind turbine pitch system.

3.4 A Tutorial Example of FDI for Pitch Actuator Stuck Fault

3.4.1 Problem Statement

In a wind turbine system, the pitch actuator is internally adjusted by a designed pitch controller (i.e. collective pitch control, individual pitch control). The pitch measurement value is obtained by the blade related pitch sensors. Generally, each blade pitch system is equipped with two sensors, and the average of these two values is used as the measurement value of the corresponding blade pitch position (Odgaard et al., 2013). This hardware redundancy guarantees the reliability and accuracy of the obtained pitch measurements.

The pitch systems faults will affect the closed-loop system performance as well as wind turbine dynamics, including power output, structural loads etc. (Etemaddar et al., 2014). Pitch actuator stuck faults (PAS) are investigated here. After the PAS occurs, the pitch measurement will be a fixed value. In the case of a stuck sensor fault with a fixed measurement (PSF), the associated pitch measurement of the faulty sensor also remains constant, similar to PAS. However, the difference between the PAS and PSF is the final pitch angle measurement output which in the PSF case is not a constant value, due to the ubiquitous presence of hardware redundancy of the pitch sensors. Since the

pitch regulation system is a critical function of the blade operation, a pitch system fault must either be corrected or the pitch system should change to a fail-safe mode using the remaining actuators. Clearly, the early detection of this stuck fault is an essential role in safe wind turbine operation.

In this study, a FDI system is designed by standard Kalman filter to detect the PAS fault and the impact of PAS on the turbine loading and power output is discussed in this Chapter.

The Kalman filter is a discrete-time processing system which is applied to the sampled inputs and outputs of the (assumed) wind turbine system. Hence, the wind turbine system model itself (as in the case of a real wind turbine system) has continuous dynamics. As a part of this the state space model of 3 pitch actuators is added to the FAST 5MW wind turbine system and represented as follows.

$$\begin{aligned} \begin{bmatrix} \dot{\beta}_i(t) \\ \ddot{\beta}_i(t) \end{bmatrix} &= \begin{bmatrix} 0 & 1 \\ -w_n^2 & -2\xi w_n \end{bmatrix} \begin{bmatrix} \beta_i(t) \\ \dot{\beta}_i(t) \end{bmatrix} + \begin{bmatrix} 0 \\ w_n^2 \end{bmatrix} \beta_{r,i}(t) + \begin{bmatrix} w_{i,1}(t) \\ w_{i,2}(t) \end{bmatrix} \\ \beta_{m,i}(t) &= \begin{bmatrix} 1 & 0 \end{bmatrix} \begin{bmatrix} \beta_i(t) \\ \dot{\beta}_i(t) \end{bmatrix} + v_i(t) \end{aligned} \quad (3.1)$$

where w_n is the nominal natural frequency and ξ is the damping ratio. The nominal parameters in the fault-free case are $w_n = 11.11$ rad/s and $\xi = 0.6$, respectively. $\beta_{r,i}(t)$ denotes the pitch reference from the pitch controller, $\beta_{m,i}(t)$ indicates the blade pitch angle measurement. $v_i(t), w_i(t)$ denote the measurement noise and process noise, respectively. These noise sequences are assumed to be spectrally white, zero-mean as well as uncorrelated.

For brevity, the system time index is removed. The pitch system (3.1) is illustrated as:

$$\begin{aligned} \dot{x} &= Ax + Bu + w \\ y_m &= Cx + v \end{aligned} \quad (3.2)$$

with

$$A = \begin{bmatrix} 0 & 0 & 0 & 1 & 0 & 0 \\ 0 & 0 & 0 & 0 & 1 & 0 \\ 0 & 0 & 0 & 0 & 0 & 1 \\ -w_n^2 & 0 & 0 & -2\xi w_n & 0 & 0 \\ 0 & -w_n^2 & 0 & 0 & -2\xi w_n & 0 \\ 0 & 0 & -w_n^2 & 0 & 0 & -2\xi w_n \end{bmatrix}, \quad (3.3)$$

$$B = \begin{bmatrix} 0 & 0 & 0 \\ 0 & 0 & 0 \\ 0 & 0 & 0 \\ w_n^2 & 0 & 0 \\ 0 & w_n^2 & 0 \\ 0 & 0 & w_n^2 \end{bmatrix}, \quad C = \begin{bmatrix} 1 & 0 & 0 & 0 & 0 & 0 \\ 0 & 1 & 0 & 0 & 0 & 0 \\ 0 & 0 & 1 & 0 & 0 & 0 \end{bmatrix}, \quad (3.4)$$

$$x = \begin{bmatrix} \beta_1 \\ \beta_2 \\ \beta_3 \\ \dot{\beta}_1 \\ \dot{\beta}_2 \\ \dot{\beta}_3 \end{bmatrix}, \quad u = \begin{bmatrix} \beta_{r,1} \\ \beta_{r,2} \\ \beta_{r,3} \end{bmatrix}, \quad y = \begin{bmatrix} \beta_1 \\ \beta_2 \\ \beta_3 \end{bmatrix} \quad (3.5)$$

$$w = \begin{bmatrix} w_{1,1} \\ w_{2,1} \\ w_{3,1} \\ w_{1,2} \\ w_{2,2} \\ w_{3,2} \end{bmatrix}, \quad v = \begin{bmatrix} v_1 \\ v_2 \\ v_3 \end{bmatrix} \quad (3.6)$$

$$E[ww^T] = Q, \quad E[vv^T] = R \quad (3.7)$$

where $x \in R^n$, $u \in R^m$ and $y_m \in R^p$ represent the system state, control input vector and system measurement output, respectively. $w \in R^l$ indicates the process noise with known covariance Q . $v \in R^q$ denotes the measurement noise with known covariance R . $A \in R^{n \times n}$, $B \in R^{n \times m}$, $C \in R^{p \times n}$ are known constant system matrices. In this case,

$n = 6$, $m = 3$, $l = 6$, $p = 3$, $q = 3$. For the design of the Kalman filter for system (3.2), (A, C) is observable.

The pitch actuator stuck fault is illustrated as

$$\beta_i = \beta_{AS_i}, \quad \dot{\beta}_i = \ddot{\beta}_i = 0$$

Because $\dot{\beta}_i$ and $\ddot{\beta}_i$ are totally decoupled, f_a is a matrix with size 6×1 . The three pitch system state-space model with actuator fault f_a is represented as:

$$\begin{aligned} \dot{x} &= Ax + Bu + f_a + w \\ y_m &= Cx + v \end{aligned} \quad (3.8)$$

where

$$f_a = \begin{bmatrix} \beta_{AS_1} - \beta_1 - w_{1,1} \\ \beta_{AS_2} - \beta_2 - w_{2,1} \\ \beta_{AS_3} - \beta_3 - w_{3,1} \\ w_n^2 \beta_1 + 2\xi w_n \dot{\beta}_1 - w_n^2 \beta_{r,1} - w_{1,2} \\ w_n^2 \beta_2 + 2\xi w_n \dot{\beta}_2 - w_n^2 \beta_{r,2} - w_{2,2} \\ w_n^2 \beta_3 + 2\xi w_n \dot{\beta}_3 - w_n^2 \beta_{r,3} - w_{3,2} \end{bmatrix}$$

with

$$A = \begin{bmatrix} 0 & 0 & 0 & 1 & 0 & 0 \\ 0 & 0 & 0 & 0 & 1 & 0 \\ 0 & 0 & 0 & 0 & 0 & 1 \\ -123.43 & 0 & 0 & -13.332 & 0 & 0 \\ 0 & -123.43 & 0 & 0 & -13.332 & 0 \\ 0 & 0 & -123.43 & 0 & 0 & -13.332 \end{bmatrix},$$

$$B = \begin{bmatrix} 0 & 0 & 0 \\ 0 & 0 & 0 \\ 0 & 0 & 0 \\ 123.43 & 0 & 0 \\ 0 & 123.43 & 0 \\ 0 & 0 & 123.43 \end{bmatrix}, \quad C = \begin{bmatrix} 1 & 0 & 0 & 0 & 0 & 0 \\ 0 & 1 & 0 & 0 & 0 & 0 \\ 0 & 0 & 1 & 0 & 0 & 0 \end{bmatrix},$$

3.4.2 FDI by Kalman Filter

The Kalman filter technique is firstly proposed for obtaining state estimates from noisy and inaccurate measurements by (Kalman, 1960). The Kalman filter achieves the optimal state estimates through obtaining a minimum of the mean value of estimated errors sum (normally linear combinations, such as squared errors), which combines the prediction and measurement recursively (Hua et al., 2017). As an optimal and recursive linear estimator, the Kalman filter assumes that the system dynamics are linear and subject to the Gaussian white noise. Whiteness means that the noise level is irrelevant with time and has equal power at each frequency (Maybeck, 1979).

Since the Kalman filter is a discrete-time system, the discrete-time model for the fault-free pitch system (3.2) is illustrated as:

$$\begin{aligned}x_k &= Ax_{k-1} + Bu_{k-1} + w_{k-1} \\y_{m_k} &= Cx_k + v_k\end{aligned}\tag{3.9}$$

The proposed observer using Kalman filter in the fault-free condition is represented as:

$$\begin{aligned}\hat{x}_k &= A\hat{x}_{k-1} + Bu_{k-1} + K_k(y_{m_{k-1}} - C\hat{x}_{k-1}) \\ \hat{y}_{m_k} &= C\hat{x}_k\end{aligned}\tag{3.10}$$

where \hat{x}_k , \hat{y}_{m_k} , K_k denote the system state estimate, output estimate and designed Kalman filter gain, respectively.

The Kalman filter algorithm is performed in two steps: the prediction step wherein the next system state is predicted from previous measurements, the correction step wherein the current state estimate is achieved with the help of current system measurements (Bishop et al., 2001). These two steps are represented by recursive equations including time update equations (Table 3.1) and measurement update equations (Table 3.2).

Table 3.1: Time update equations for Kalman filter

State prediction:	$\hat{x}_k^- = A\hat{x}_{k-1} + Bu_{k-1}$
Predicted state estimate error covariance:	$P_k^- = AP_{k-1}A^T + Q$

\hat{x}_k^- is a priori estimate, which is the estimation of x_k before the present measurement y_{mk} is considered. The above equations are in charge of predicting the system state and estimate error covariance of the next time step. The initialization is established once including initial state \hat{x}_0 (with $\hat{x}_0 = E(x_0)$) and initial state uncertainty P_0 (with $P_0 = E[(x_0 - \hat{x}_0)(x_0 - \hat{x}_0)^T]$) (Simon, 2006). P_0 is the covariance of the initial estimate of x_0 . If the initial state is known very well, then P_0 is quite small and vice versa.

Table 3.2: Measurement update equations for Kalman filter

Kalman filter gain:	$K_k = P_k^- C^T [C P_k^- C^T + R]^{-1}$
Measurement residual:	$e_k = y_{mk} - C \hat{x}_k^-$
State update:	$\hat{x}_k = \hat{x}_k^- + K_k e_k$
Estimate error covariance update:	$P_k = (I - K_k C) P_k^-$

The measurement update equations implement the feedback by injecting new system measurements y_{mk} into the *priori* state estimate and achieve the updated *posteriori* state estimate \hat{x}_k , which is the estimation of x_k after considering the current measurement (Zuluaga et al., 2015). Firstly, the Kalman gain K_k (the weight designed for measurements) is computed. When the measurement uncertainty is quite large and the estimate uncertainty is very small, K_k is close to zero and vice versa. Afterwards, the measurement estimate error e_k can be obtained by incorporating the real measurement y_{mk} . Finally, a *posteriori* state estimate error covariance of the current state is achieved, which normally reduces with each iteration. After the complete process shown in Table 3.2, the current state estimate could be achieved, which is located between the *priori* estimate and measured state.

After each pair illustrated in Table 3.1 and Table 3.2, the procedure is repeated with the previous *posteriori* state estimates and error covariance for predicting the new *priori* state estimates and error covariance in the next iteration. The diagram of proposed Kalman filter-based FDI scheme for the pitch system is illustrated in Fig. 3.6.

As illustrated in Fig. 3.6, errors between the system output estimates y_{mk} and real measurements \hat{y}_{mk} are adopted as the residual to detect faults, which is illustrated as

$$r_i = y_{mi} - C \hat{x}_i \quad (3.11)$$

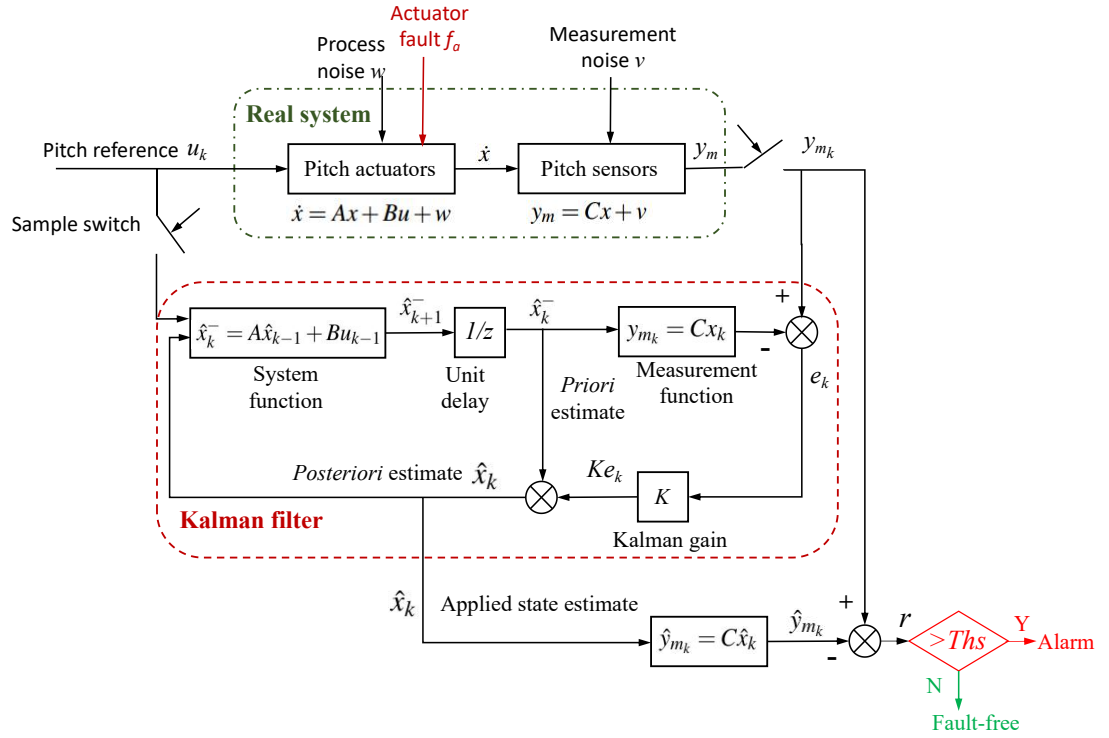


Figure 3.6: Proposed Kalman filter-based FDI strategy

A simple threshold strategy using the achieved residual is adopted to detect faults and defined as (Chen and Patton, 2012):

$$\begin{cases} \|r_i\| < \text{Threshold } Ths & \text{for fault-free case} \\ \|r_i\| > \text{Threshold } Ths & \text{for faulty case} \end{cases}$$

When the residual r is above the designed threshold Ths , the fault alarm becomes 1, indicating that a fault has been detected, and vice versa.

3.4.3 Simulation Results

In this section, simulation results in the FAST 5MW NREL wind turbine system are presented to investigate the PAS effects on the turbine dynamics and verify the performance of proposed FDI strategy. The simulations are under a stochastic wind speed with mean value of 18 m/s at the hub-height, turbulence intensity 14% and vertical shear exponent 0.2, illustrated as Fig. 3.7. The process noise and measurement noise of the real system are modelled as Gaussian white noise with power $1e^{-5}$, which almost

lies between $[-0.01, 0.01]$. The total simulation time is $1000s$. Because the pitch system model used here is linear and time-invariant, the Kalman filter gain K_k will converge towards a steady value. The pre-calculation of parameters Q and R can be performed by performing the Kalman filter offline. By trial and error, the threshold Ths is selected as 1.1° .

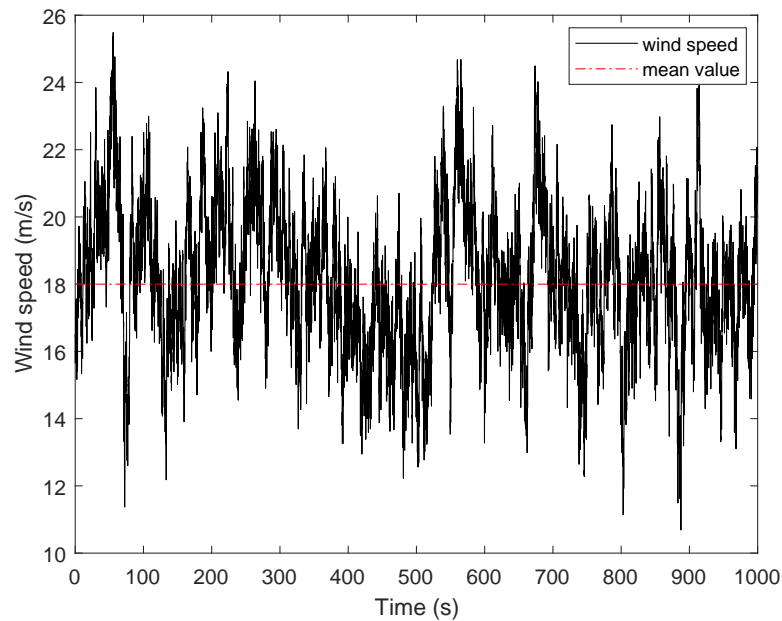


Figure 3.7: Wind speed profile

Two different fault conditions are considered here including a single actuator stuck fault in blade pitch 1 and multiple actuator stuck faults. First of all, an actuator fault occurs in blade pitch 1 during $[300, 700]s$ and the pitch actuator 1 stuck at 18.05° (called Fault 1), shown in Fig. 3.8.

Due to Fault 1, the generated difference between the pitch reference command and the measured blade 1 pitch value does influence the pitch reference command of other fault-free blades during the time range of Fault 1. The PAS faults in the blade pitch system also exert detrimental effects on the wind turbine power output and structural dynamics, shown in Fig. 3.9 and Fig. 3.10. The fault detection result is illustrated in Fig. 3.11. It should be noted that the detection time of Fault 1 is around $12.1s$ and there are no faults detected for blade 2 and 3.

Furthermore, the case of multiple pitch actuator stuck faults is considered. The pitch actuator 1 is stuck at 19.4° during $[250, 500]s$ (named as Fault 2), actuator 2 is stuck

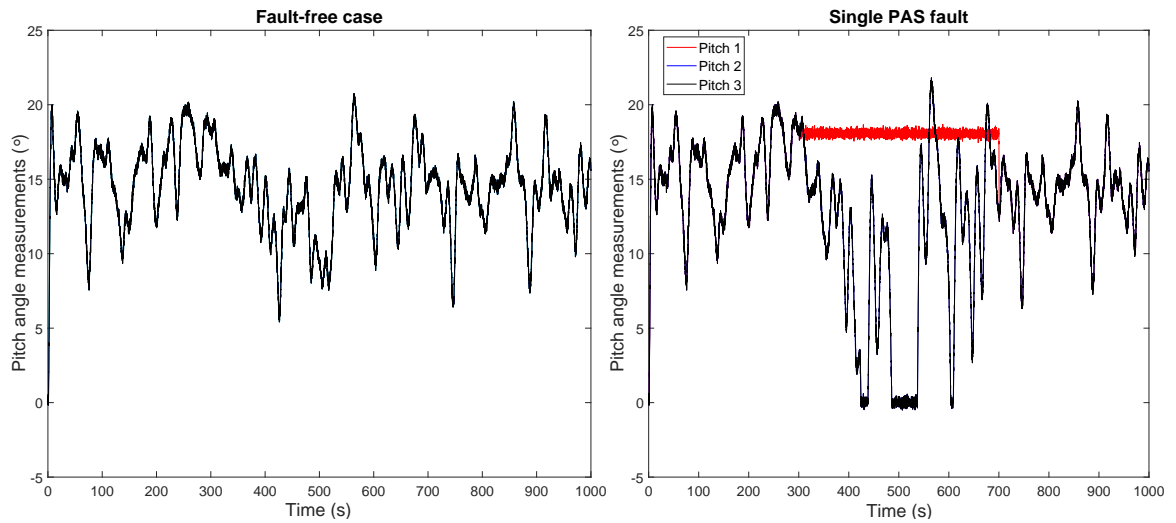


Figure 3.8: Three pitch angle measurements in both fault-free case and single PAS fault on blade 1

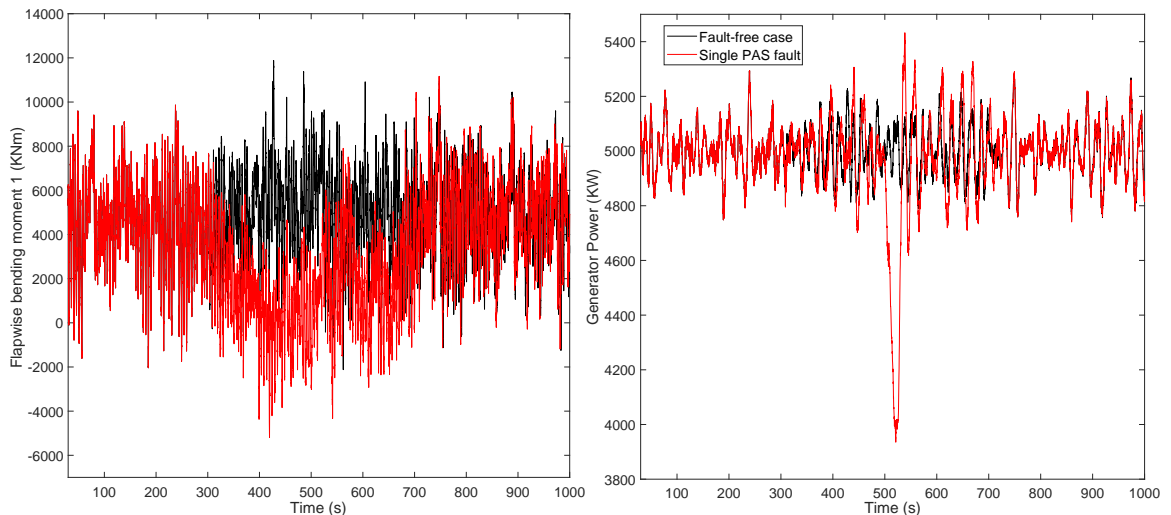


Figure 3.9: Flapwise bending moment of blade 1 and generator power in both fault-free case and single PAS fault on blade 1

at 10.6° within $[600, 700]s$ (termed as Fault 3), and actuator 3 is stuck at 12.9 during $[800, 1000]s$ (called Fault 4), shown as Fig. 3.12. The structural analysis is illustrated in Fig. 3.13 and Fig. 3.14.

The fault detection result is explained in Fig. 3.15. The detection time for these three actuator faults are approximately $16.7s$, $7.1s$, $3.4s$, respectively. The proposed residual is demonstrated to be robust against both process and measurement noise. Interestingly,

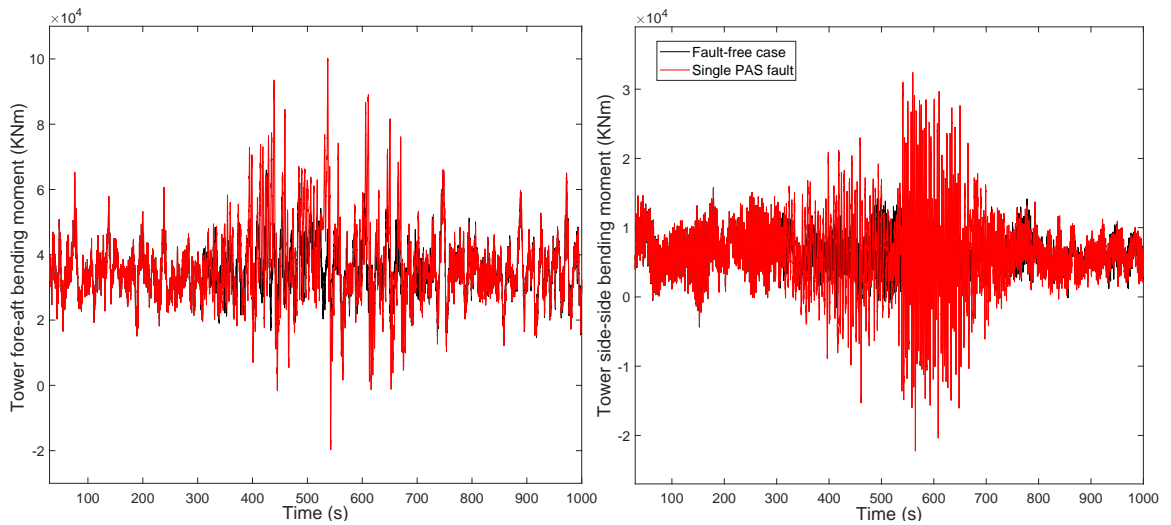


Figure 3.10: Tower fore-aft and side-side bending moments in both fault-free case and single PAS fault on blade 1

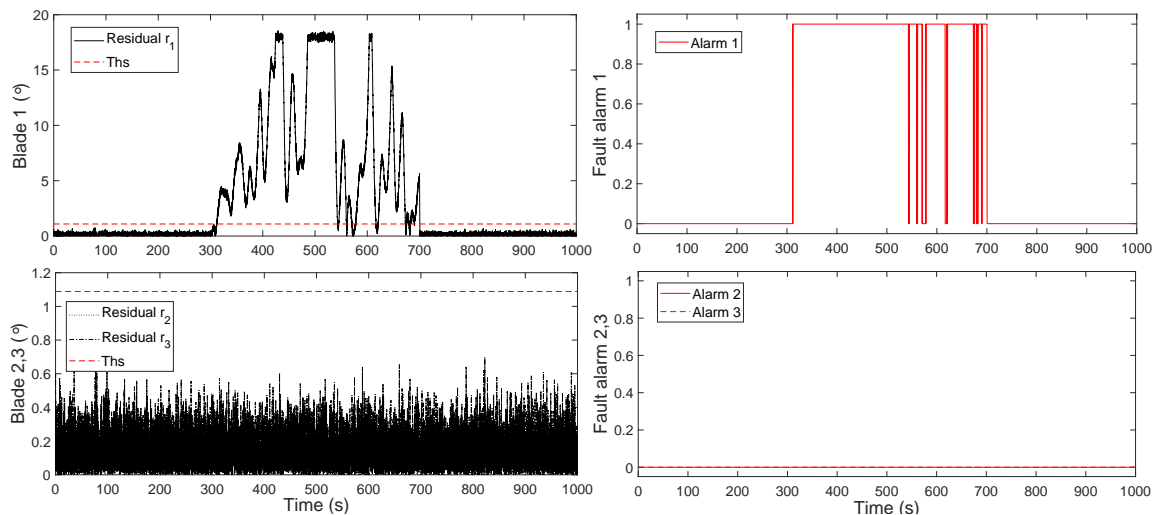


Figure 3.11: Fault detection result in the case of single PAS fault on blade 1

the fault detection time depends on the speed of wind speed changes when the fault occurs. From Fig. 3.12, it is found that if the wind speed changes rapidly and drastically, the detection time tends to become shorter (e.g. Fault 3, Fault 4).

From Fig. 3.8 and Fig. 3.12, due to the existence of PAS faults, the faulty pitch actuator cannot adjust the corresponding blade, while the other blades are also affected. The pitch angle measurement feedback of the faulty blade is clearly different from the pitch angle reference. From Fig. 3.9, Fig. 3.10, Fig. 3.13 and Fig. 3.14, it is clear that

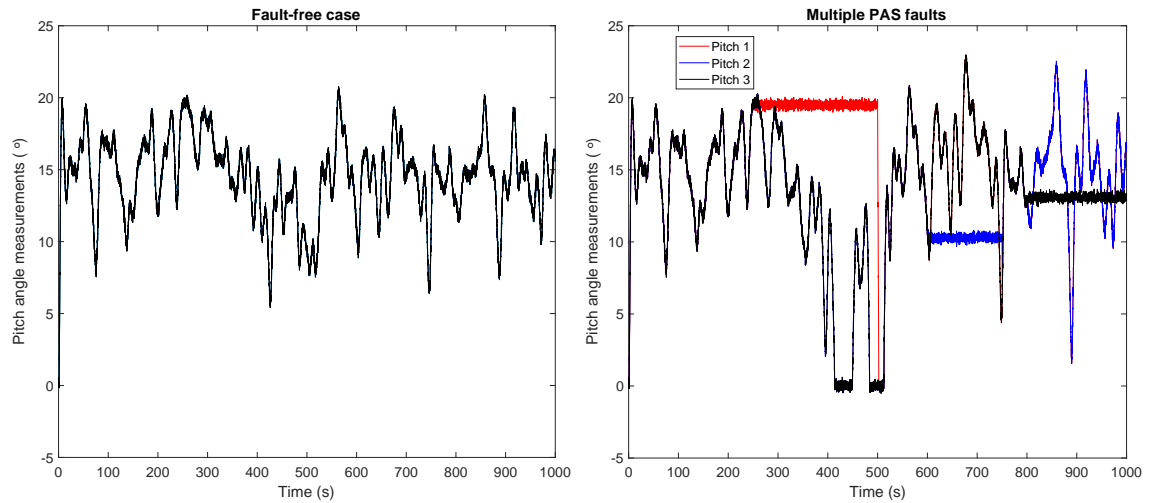


Figure 3.12: Three pitch angle measurements in both fault-free case and multiple PAS faults on three blades

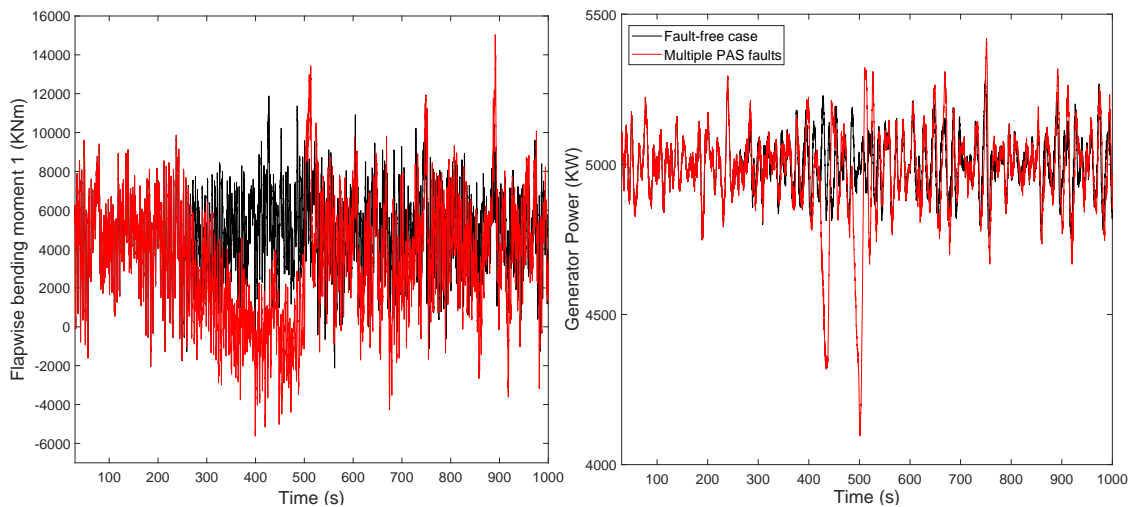


Figure 3.13: Flapwise bending moment of blade 1 and generator power in both fault-free case and multiple PAS faults on three blades

actuator stuck faults have a critically detrimental impact on the mechanical structure of wind turbine systems. The angle at which the faulty blade is stuck plays a significant role in the degree of the wind turbine structural unbalanced load variations and generator output change. If this stuck pitch angle is far away from the nominal pitch angle in the absence of faults (e.g. Fault 1, Fault 2), it causes a large difference between the measured value and the pitch reference which will lead to large fluctuations of the pitch reference. Then it leads to drastic fluctuations of generator speed, resulting in

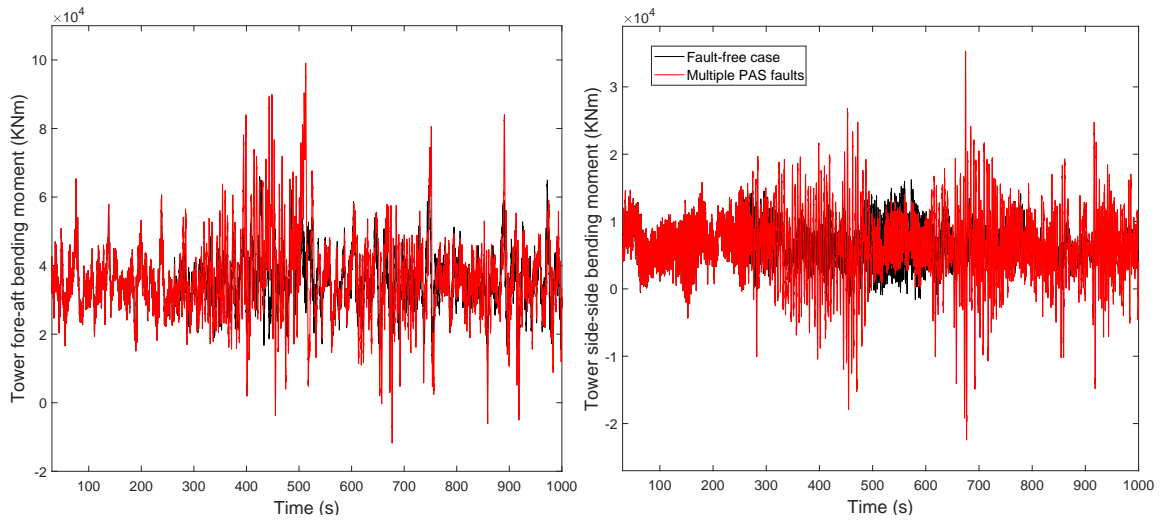


Figure 3.14: Tower fore-aft and side-side bending moments in both fault-free case and multiple PAS faults on three blades

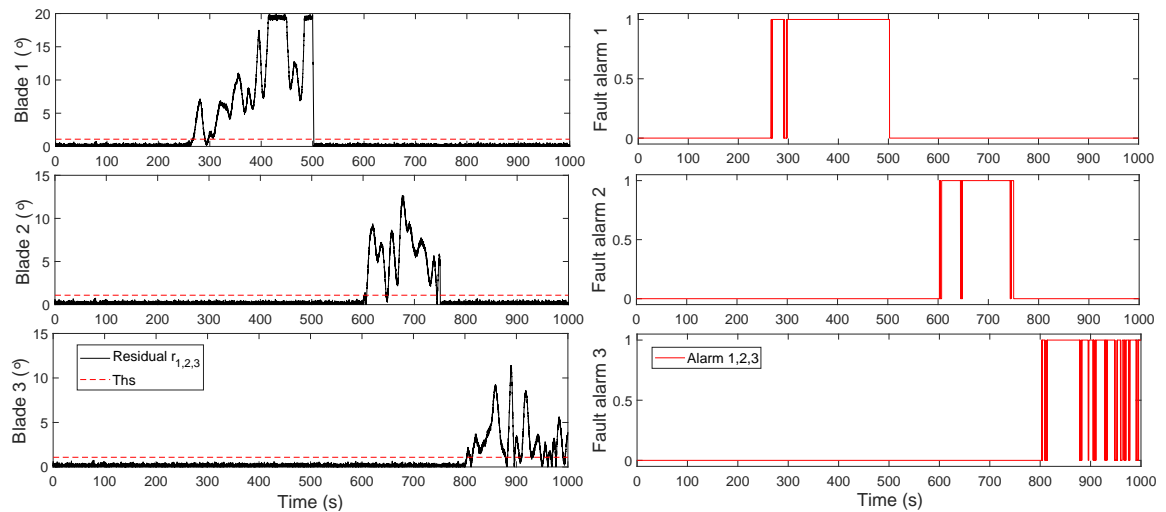


Figure 3.15: Fault detection result in the case of multiple PAS faults on three blades

unstable output power. Furthermore, discrepancies between the three blades enhances large asymmetrical blade loading as well as tower fore-aft and side-side bending moments. On the contrary, if the stuck angle is near to the value of blade pitch angle in the fault-free situation (e.g. Fault 3, Fault 4), the enhancement of rotor imbalance and generator power as well as the tower loads tend to be weak, although still more severe than the fault-free case.

The aim of this proposed FDI is to implement an emergency shut-down of the wind

turbine system as soon as possible when the PAS occurs. Fig. 3.8 and Fig. 3.12 demonstrate that the designed fault detection strategy can detect PAS faults and present a fault alarm reliably and accurately at a very early stage. Once a PAS fault is detected, the wind turbine should have an emergency shut-down to avoid further damage and failure if there is no hardware redundancy available.

3.5 Conclusions

In this Chapter, introduction to the knowledge about fault diagnosis and FTC are given firstly. The related definitions, principles and classifications are clarified and explained. Then a quick literature review of the current fault diagnosis and FTC methods for wind turbine systems is presented. Furthermore, a model-based FDI scheme for wind turbine pitch actuator stuck fault is designed and verified on the NREL 5MW wind turbine simulator. From the detailed results, it can be concluded that the proposed FDI method can provide early fault detection effectively and make it accessible for wind turbine predictive maintenance. Following this, Chapter 4 investigates a possible candidate approach of (light detection and ranging) LiDAR system using preview control for rotor load mitigation.

Chapter 4

Rotor Load Reduction using MPC with Gaussian Wind Speed Prediction

4.1 Introduction

As discussed in Chapter 2, the model predictive control (MPC) based preview strategy for wind turbine load reduction has drawn wide attention due to the systematic process of constraints and easy combination with future wind speed knowledge within multi-variable control problems. However, it is found that the wind flow conditions are just assumed ideal in several papers (Körber and King, 2010; Spencer et al., 2013; Dunne et al., 2011, etc.). Furthermore, a significant scheme to realize preview control is to employ the light detection and ranging system - LiDAR, providing real-time measurements of the approaching wind speeds near the blades (Laks et al., 2011). Although various experiments in the next-generation of LiDAR designs are active, the LiDAR system is still expensive and is not always affordable for individual wind turbine (Laks et al., 2011). It is essential to provide alternative technique candidates for LiDAR.

It is impressive to use the cascaded control-based IPC system with additional local blade inflow measurements instead of LiDAR system in the work by Jones et al. (2018). Another possible useful method when adopting the MPC-based preview control strategy is to achieve the very short-term wind speed forecasting (i.e. several seconds in advance) from past measurement datasets (Körber and King, 2010). Though the benefits of preview control for load mitigation have been demonstrated, little consideration has focused on studying the combination of very short-term wind speed forecasting

with the MPC-based preview control strategy for blade load reduction, which is exactly the focus of this Chapter .

Therefore, this Chapter involves some innovative research on very short-term wind speed forecasting by the Gaussian Process (GP) method. This study follows the popular studies of wind speed forecasting, which are subject to the intermittent and uncertain wind aerodynamics (e.g. Jiang et al.,2010; Kani and Ardehali, 2011). It is demonstrated by statistical analysis that a strong correlation exists between the future wind speed and historical statistics in a very short time (Tascikaraoglu and Uzunoglu, 2014). Meanwhile, machine learning-based method characterized by describing the underlying patterns from the training data is receiving increased attention for the wind speed prediction (Kani and Ardehali, 2011). According to the underlying forecasting principles, the techniques are mainly divided into numeric weather predictors (NWP), statistical approaches and machine learning based methods including Support Vector Machines (SVM), Artificial Neural Networks (ANN) etc. (Soman et al., 2010). Furthermore, GP as a prevailing kernel-based learning approach represents potential for dealing with complex nonlinear regression issues with non-parametric models (Shi et al., 2018; Xie et al., 2010). In Jiang et al. (2010), the designed adaptive GP scheme for predicting very short-term (10min) wind speed sequence surpasses other candidate statistical approaches (e.g. Mycielski method). Nonetheless, the recent investigations turn out to focus on wind prediction with the time scale of at least 30 mins or more whilst few studies emphasize the very short-term wind speed prediction several seconds in advance for control. Therefore, it is worthwhile to implement the GP algorithm to the very short-time wind speed prediction.

The remainder of this Chapter is explained as follows. Section 4.2 represents the linear wind turbine model for the proposed MPC controller. The model predictive-based IPC strategy is illustrated in Section 4.3. In Section 4.4, a very short-term wind speed forecasting strategy using the GP regression model with Matérn class covariance function is presented. Section 4.5 gives the illustrative simulation results on the FAST NREL 5MW wind turbine simulator and the summary is provided in Section 4.6.

4.2 Wind Turbine Model

4.2.1 FAST Linearization

The FAST linearization capability (Jonkman et al., 2005) is carried out at a specific wind condition to obtain the reduced-order linearized numerical model from the non-linear 5MW NREL wind turbine. Considering that the main focus of this study is on the IPC system design above the rated wind speed, a wind flow with mean value 18 m/s at the hub height and a vertical shear exponent of 0.2 is chosen because of its proximity to the centre of the wind speed range in Region 3. The following degrees of freedom (DOFs) are chosen:

- Generator rotational flexibility DOF (q_1).
- The 1st blade flapwise mode DOF for each of three blades (q_2, q_3, q_4).

These structural DOFs are selected by considering the target blade loads. The second blade bending modes are excluded in order to maximize the model fidelity and minimize the corresponding computational complexity. The generator torque is typically kept constant above the rated wind speed and is not chosen as a system input. The control inputs of 3 pitch angles are incorporated in the linearization process. The effective horizontal wind speed at the hub height is selected as the system disturbance input.

The nonlinear aeroelastic model for describing the wind turbine motion can be expressed as (Yuan and Tang, 2017; Jonkman et al., 2005):

$$M(q, u, t)\ddot{q} + f(q, \dot{q}, u, u_d, t) = 0 \quad (4.1)$$

where M denotes the mass matrix, f is the nonlinear "forced function" vector, q , \dot{q} , \ddot{q} are the DOF displacements, velocities and accelerations, respectively, u represents the control inputs, u_d is the wind disturbance vector, t denotes the time sequence. The vector f is simulated by the aerodynamic model AeroDyn, which calculates the aerodynamic loading and forces acting on the wind turbine blade components from the blade element momentum (BEM) wake model (Laino and Hansen, 2002). The above nonlinear aeroelastic equation is linearized numerically by the FAST simulator in the

specific operation condition based on the small perturbation theory. The achieved linear model is periodic and defined in rotating coordinates, given that the periodicity of rotor azimuth angle (Li et al., 2014). The linear periodic motion equation obtained is illustrated as (Hassan et al., 2012):

$$M(\varphi)\underline{\ddot{q}} + C(\varphi)\underline{\dot{q}} + K(\varphi)\underline{q} = F(\varphi)\underline{u} + F_d(\varphi)\underline{u}_d \quad (4.2)$$

where $M(\varphi)$, $C(\varphi)$, $K(\varphi)$, $F(\varphi)$, $F_d(\varphi)$ indicate the changing matrices of the mass, damping, stiffness, control inputs and wind input disturbance, respectively. Underline (e.g. \underline{q}) denotes the perturbations from their respective operating point values. Let $\underline{x} = [\underline{q}, \underline{\dot{q}}]^T$, the state-space representation of the system is illustrated as:

$$\begin{aligned} \dot{\underline{x}} &= A(\varphi)\underline{x} + B(\varphi)\underline{u} + B_d(\varphi)\underline{u}_d \\ \underline{y} &= C(\varphi)\underline{x} + D(\varphi)\underline{u} + D_d(\varphi)\underline{u}_d \end{aligned} \quad (4.3)$$

where $A(\varphi)$, $B(\varphi)$, $B_d(\varphi)$, $C(\varphi)$, $D(\varphi)$, $D_d(\varphi)$ represent the matrices of state, control input, wind input disturbance, output state, control input transmission and wind input disturbance transmission varying with the rotor azimuth position, respectively. \underline{x} , \underline{u} , \underline{u}_d , \underline{y} denote the perturbations of the state vector, control action, input disturbance and output measurement sequence in the operating point rather than the absolute value.

A more straightforward linearized system representation defined in the rotating frame (i.e. ignoring the $D_d(\varphi)\underline{u}_d$) is considered here:

$$\begin{aligned} \dot{\underline{x}} &= A(\varphi)\underline{x} + B(\varphi)\underline{u} + B_d(\varphi)\underline{u}_d \\ \underline{y} &= C(\varphi)\underline{x} + D(\varphi)\underline{u} \end{aligned} \quad (4.4)$$

where $\underline{x} \in \mathbb{R}^{7 \times 1}$, $\underline{u} \in \mathbb{R}^{3 \times 1}$, $\underline{u}_d \in \mathbb{R}^{1 \times 1}$, $\underline{y} \in \mathbb{R}^{3 \times 1}$. $\underline{u} = [\beta_1, \beta_2, \beta_3]$ is the control input reference vector of three individual blade pitch angles.

The periodicity of achieved linear model (i.e., a series of linear turbine models with dissimilar rotor azimuth positions) increase the controller design. Therefore, Coleman transformation (see Section 2.4) is adopted to transform the wind turbine dynamics from the rotating coordinate to the non-rotating frame (identical with the static tower coordinate) and naturally realize the interconnection between the rotors and the fixed

nacelle with the tower. Coherently, the linear time invariant (LTI) model with averaged system matrices in the non-rotating coordinate system for the 5MW NREL wind turbine is represented as (Liu et al., 2018b):

$$\begin{aligned}\dot{\underline{x}}_{NR} &= \bar{A}_{NR}\underline{x}_{NR} + \bar{B}_{NR}\underline{u}_{NR} + \bar{B}_{dNR}\underline{u}_d \\ \underline{y}_{NR} &= \bar{C}_{NR}\underline{x}_{NR} + \bar{D}_{NR}\underline{u}_{NR}\end{aligned}\quad (4.5)$$

where $\{\bar{A}_{NR}, \bar{B}_{NR}, \bar{B}_{dNR}, \bar{C}_{NR}, \bar{D}_{NR}\}$ are achieved through averaging $\{A_{NR}(\varphi), B_{NR}(\varphi), C_{NR}(\varphi), C_{NR}(\varphi), D_{NR}(\varphi)\}$ over the changing range of azimuth angle φ . State vector $\underline{x}_{NR} = [x_{flo} \ x_{flc} \ x_{fls} \ w_r \ x_{flo} \ x_{flc} \ x_{fls}]^T$, control input $\underline{u}_{NR} = [u_o \ u_c \ u_s]^T$, disturbance input $\underline{u}_d = [v_d]$, output measurements $\underline{y}_{NR} = [w_r \ M_{yc} \ M_{ys}]^T$. The subscripts of o, c, s represent the collective, cosine and sine components, x_{fl} indicate the flapwise tip displacements, w_r is turbine rotor speed, M_y denotes the blade flapwise bending moments.

4.2.2 Actuator Dynamics

In the commercial large offshore wind turbines, every blade is usually equipped with one pitch actuator system at the root of blades to pitch the blade individually and compensate for the asymmetric blade loading (see Section 2.2.2). The three hydraulic pitch actuators are modelled as:

$$\begin{aligned}\begin{bmatrix} \dot{\beta}_i \\ \ddot{\beta}_i \end{bmatrix} &= \begin{bmatrix} 0 & 1 \\ -w_n^2 & -2\xi w_n \end{bmatrix} \begin{bmatrix} \beta_i \\ \dot{\beta}_i \end{bmatrix} + \begin{bmatrix} 0 \\ w_n^2 \end{bmatrix} [u_i] \\ \begin{bmatrix} \dot{\beta}_i \end{bmatrix} &= \begin{bmatrix} 0 & 1 \end{bmatrix} \begin{bmatrix} \beta_i \\ \dot{\beta}_i \end{bmatrix}\end{aligned}\quad (4.6)$$

where $i = 1, 2, 3$, the nominal natural frequency $w_n = 11.11 \text{ rad/s}$ and damping ratio $\xi = 0.6$. The Coleman transformation is implemented to the three pitch system dynamics according to the work in Bir (2008), which is realized by MATLAB, resulting in:

$$\begin{aligned}\dot{x}_p &= A_p x_p + B_p u_{com} \\ u_p &= C_p x_p\end{aligned}\quad (4.7)$$

where the pitch system states $x_p \in \mathbb{R}^{6 \times 1}$, the pitch actuator control commands $u_{com} \in \mathbb{R}^{3 \times 1}$ and $u_{com} = [u_{com_o} \ u_{com_c} \ u_{com_s}]^T$, pitch system output $u_p \in \mathbb{R}^{3 \times 1}$ (consistent with \underline{u}_{NR} in (4.5), representing as $\underline{u}_{NR} = C_p x_p$). Given that the FAST simulator fails to present the pitch actuator dynamics, the linear wind turbine model (4.5) is augmented with the pitch actuator dynamics (4.7) here. Therefore, the complete extended linear wind turbine model can be represented as (4.8), where $A_c \in \mathbb{R}^{13 \times 13}$, $B_c \in \mathbb{R}^{13 \times 3}$, $B_{dc} \in \mathbb{R}^{13 \times 1}$, $C_c \in \mathbb{R}^{3 \times 13}$ represent the system state, control input vector, wind disturbance input vector as well as output state vector, respectively.

$$\begin{aligned} \begin{bmatrix} \dot{x}_{NR} \\ \dot{x}_p \end{bmatrix} &= \underbrace{\begin{bmatrix} \bar{A}_{NR} & \bar{B}_{NR}C_p \\ \mathbf{0} & A_p \end{bmatrix}}_{A_c} \begin{bmatrix} x_{NR} \\ x_p \end{bmatrix} + \underbrace{\begin{bmatrix} \mathbf{0} \\ B_p \end{bmatrix}}_{B_c} \begin{bmatrix} u_{com_o} \\ u_{com_c} \\ u_{com_s} \end{bmatrix} + \underbrace{\begin{bmatrix} \bar{B}_{dNR} \\ \mathbf{0} \end{bmatrix}}_{B_{dc}} v_d \\ \underline{y}_{NR} &= \underbrace{\begin{bmatrix} \bar{C}_{NR} & \bar{D}_{NR}C_p \end{bmatrix}}_{C_c} \begin{bmatrix} x_{NR} \\ x_p \end{bmatrix} \end{aligned} \quad (4.8)$$

4.3 Model Predictive based IPC Design

Based on the achieved extended linear wind turbine model, a feed-forward MPC control system with the future wind knowledge is proposed to mitigate the blade flapwise bending moments, which are the principal source of the blade asymmetric loading and fatigue. The schematic diagram of designed MPC-based IPC strategy with very short-term wind speed forecast is represented in Fig. 4.1, which consists of three systems: (i) a baseline pitch controller (CPC) using gain-scheduled PI approach for generator power output control (introduced in Section 2.2.4), (ii) a very short-term wind speed forecasting system using the GP model, (iii) the MPC-based IPC system for blade unbalanced loading reduction. The inverse MBC transformation transforms the additional pitch signals from the proposed MPC-IPC system and then transmitted to each of the pitch actuator systems. In conclusion, the collective pitch angles $\beta_{collective}$ together with the individual pitch commands $\beta_{individual}$ constitute the complete set of three pitch angle references β_r .

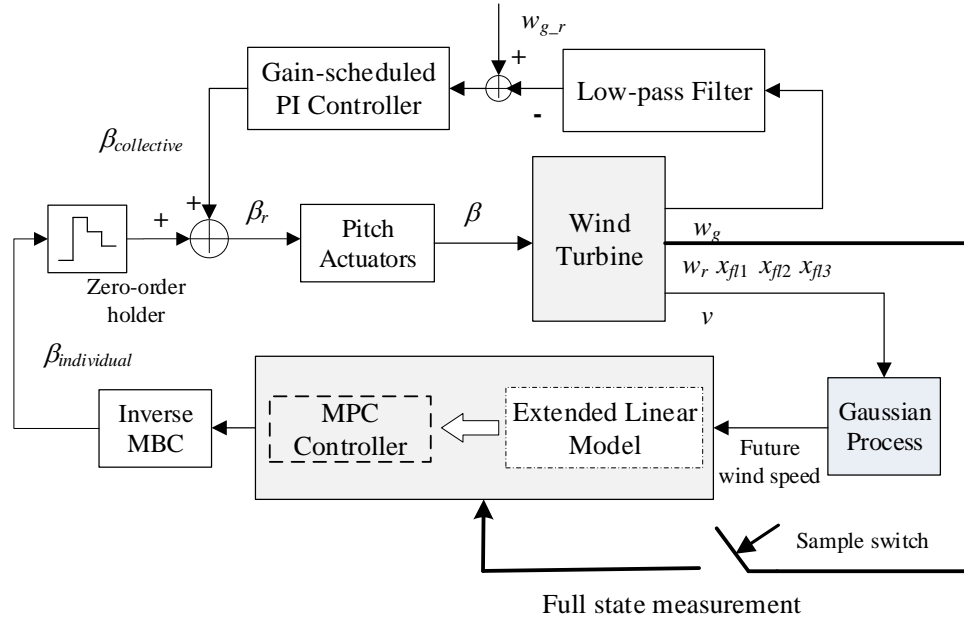


Figure 4.1: Proposed control strategy in Region 3

4.3.1 Principle of MPC

MPC (also referred to as receding horizon control) as a valid and advanced algorithm of processing multivariable control problems with satisfying system constraints has been extensively applied in the industrial practical issues (Qin and Badgwell, 2003). MPC uses an internal prediction model of the target system to forecast the future output dynamics and computes the pitch angle control signals by optimising a finite-time quadratic cost-function (one for each controller) on line (Morari and Lee, 1999). The MPC strategy in discrete-time is depicted in Fig. 4.2. The prediction capability is carried out over a specific time period, which is referred to as the preview horizon N_p . Usually, a quadratic cost function describing the discrepancy between predicted outputs and the reference trajectory is used and optimized within N_p subject to the system constraints with physical meaning (including input, output and state constraints) (Bemporad and Morari, 1999). The control horizon N_c is the optimal control vector length (normally $N_c \leq N_p$). Only the first of the optimal control inputs is implemented in the system and the remaining signals are discarded according to the receding horizon philosophy. This process is repeated with the updated state information in the next iteration. Since the system state knowledge is required for every iteration, this mechanism implements the feedback properties for the MPC (Savvidis, 2017). In the wind

turbine load reduction problem, the principle of MPC naturally provides the advantage of incorporating both the wind disturbance prediction and pitch actuator limitations in this optimization system. The prediction horizon N_p indicates the length of the provided wind information for the MPC to improve the controller performance (usually $N_p > N_d$).

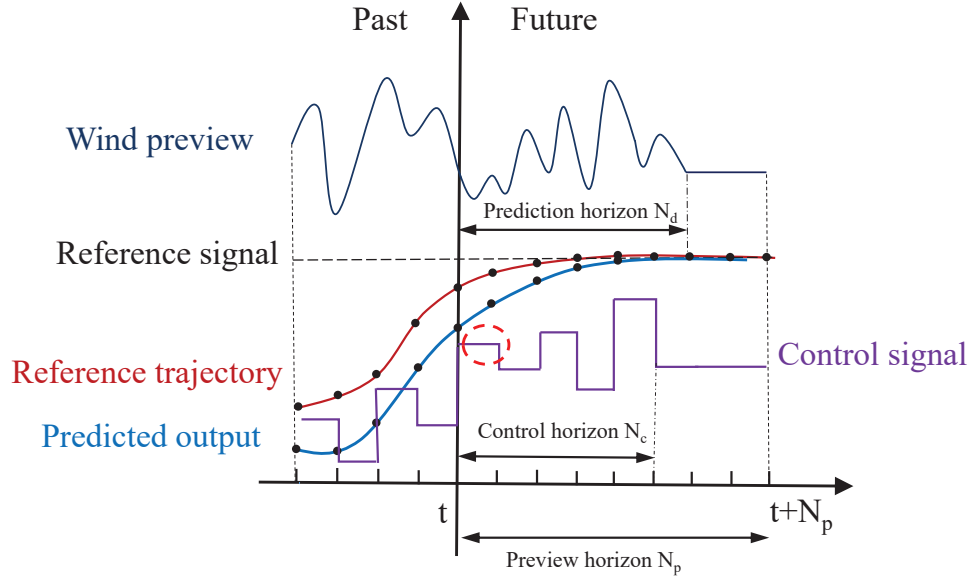


Figure 4.2: The MPC strategy in discrete time

4.3.2 Feed-forward MPC-IPC Design

The principal turbine dynamics are assumed to be presented by a LTI model. The discrete-time system (with sampling time T_s) corresponding to the augmented model (4.8) (with the same matrix size) is shown in:

$$\begin{aligned} x_{k+1|k} &= Ax_{k|k} + Bu_{k|k} + B_d u_{d_{k|k}} \\ y_{k|k} &= Cx_{k|k} \end{aligned} \quad (4.9)$$

where $A = e^{A_c T_s}$, $B = (\int_0^{T_s} e^{A_c t} dt) B_c$, $B_d = (\int_0^{T_s} e^{A_c t} dt) B_{d_c}$, $C = C_c$, this discretization process can be performed by Matlab. The cost function J usually contains the penalties both on the tracking error and on the system actuation in a quadratic mode. The MPC controller aims at optimizing the performance index and achieve the best individual pitch angle commands u limited by linear inequality constraints over appropriate

preview and control horizons. The optimization problem is given by (Privara et al., 2011):

$$\arg \min_{u(\cdot)} J(k) \quad (4.10)$$

$$\text{with } J(k) = \sum_{i=1}^{N_p} (y_{k+i|k} - r_{k+i})^T Q (y_{k+i|k} - r_{k+i}) + \sum_{j=0}^{N_c} (u_{k+j|k})^T R u_{k+j|k}$$

$$\text{s.t. } x_{k|k} = x_0 \quad (4.10.a)$$

$$u_{min} \leq u_{k+j|k} \leq u_{max} \quad j = 0, 1, \dots, N_c \quad (4.10.b)$$

$$\Delta u_{min} \leq u_{k+j+1|k} - u_{k+j|k} \leq \Delta u_{max} \quad (4.10.c)$$

Let $y_{k+i|k}$ represent the prediction of y at sample $k+i$ where the prediction is achieved at sampling time k . r_{k+i} (here set as zero) includes the reference input for the fluctuations of rotor speed (i.e. the difference between the real rotor speed and rated value in Region 3) and the reference value of the mean blade flapwise bending moment. This has the purpose of minimising the unbalanced blade loading and guarantees the rated energy output. $u_{k+j|k}$ is the optimal control input at sample $k+j$ obtained at sample k , Q and R are the weighting matrices denoting the importance values imposed on the tracking error and control inputs. R is typically a symmetric positive definite matrix (defined as $R \succ 0$) and matrix Q is a symmetric positive semi-definite matrix (defined as $Q \succeq 0$) (Raković, 2016). (4.10.a) indicates the initial knowledge of states, (4.10.b) and (4.10.c) represent the control input constraints $u_{min} = 0^\circ$, $u_{max} = 90^\circ$ and the pitch rate limits $\Delta u_{min} = -8^\circ/s$, $\Delta u_{max} = 8^\circ/s$. The turbine state measurements x_0 are considered to be provided by sensors and available for the MPC controller here, which could be estimated by a Kalman filter or other state estimators (Wright et al., 2007) at every simulation step.

This cost function (4.10) can be represented in the matrix formulation:

$$J = \mathbf{x}_{\rightarrow k+1}^T Q \mathbf{x}_{\rightarrow k+1} + \mathbf{u}_{\rightarrow k}^T R \mathbf{u}_{\rightarrow k} \quad (4.11)$$

where $Q = C^T Q_x C$, $Q_x \succ 0$ which means that the output vector y is required to be regulated to the reference, the subscript arrow denotes a set of predictions, $\mathbf{x}_{\rightarrow k+1}$ represents the state prediction vector of x beginning from $k+1$ to $k+N_p$ sample interval. The

predicted state sequence for the linear state-space model (4.9) is illustrated in a more compact way (Rossiter, 2003):

$$\underline{\mathbf{x}}_{\rightarrow k+1} = \mathbf{M}x_k + \mathbf{P}\underline{\mathbf{u}}_{\rightarrow k} + \mathbf{E}\underline{\mathbf{u}}_{\rightarrow k}^d \quad (4.12)$$

where

$$\underline{\mathbf{x}}_{\rightarrow k+1} = \begin{bmatrix} x_{k+1|k} \\ x_{k+2|k} \\ \vdots \\ x_{k+N_p|k} \end{bmatrix}, \mathbf{M} = \begin{bmatrix} A \\ A^2 \\ \vdots \\ A^{N_p} \end{bmatrix} \quad (4.13)$$

$$\mathbf{P} = \begin{bmatrix} B & 0 & \cdots & 0 \\ AB & B & \cdots & 0 \\ \vdots & \vdots & \ddots & \vdots \\ A^{N_c-1}B & A^{N_c-1}B & \cdots & B \end{bmatrix}, \underline{\mathbf{u}}_{\rightarrow k} = \begin{bmatrix} u_{k|k} \\ u_{k+1|k} \\ \vdots \\ u_{k+N_c|k} \end{bmatrix}$$

$$\mathbf{E} = \begin{bmatrix} B_d & 0 & \cdots & 0 \\ AB_d & B_d & \cdots & 0 \\ \vdots & \vdots & \ddots & \vdots \\ A^{N_d-1}B & A^{N_d-1}B_d & \cdots & B_d \end{bmatrix}, \underline{\mathbf{u}}_{\rightarrow k}^d = \begin{bmatrix} v_{d_{k|k}} \\ v_{d_{k+1|k}} \\ \vdots \\ v_{d_{k+N_d|k}} \end{bmatrix}$$

where $\underline{\mathbf{u}}_{\rightarrow k}$ denotes the optimal input vector between k and $k + N_c$ sampling time. x_k denotes the current and past measurements. The optimal control signal is assumed to be unchanged beyond N_c . The size of \mathbf{P} depends on the length of N_c , which is flexible and can be changed. The effective wind vector within the preview range of N_d samples acts as the disturbance term $\underline{\mathbf{u}}_{\rightarrow k}^d$, which is predicted by the designed GP model (introduced in the Section 4.4). Note that the preview horizon N_p is normally considered larger than the wind speed prediction horizon N_d , which implies the future wind speed is considered unchanged beyond the N_d sample.

Substituting $\underline{\mathbf{x}}_{\rightarrow k+1}$ (4.12) into (4.11) and collecting similar terms, the achieved formulation is given by:

$$J = \underline{\mathbf{u}}_{\rightarrow k}^T H \underline{\mathbf{u}}_{\rightarrow k} + 2 \underline{\mathbf{x}}_{\rightarrow k}^T F_1^T \underline{\mathbf{u}}_{\rightarrow k} + 2 \underline{\mathbf{v}}_{\rightarrow k}^d T F_2^T \underline{\mathbf{u}}_{\rightarrow k} + G \quad (4.14)$$

with

$$H = \mathbf{P}^T \tilde{\mathbf{Q}} \mathbf{P} + \tilde{\mathbf{R}}, F_1 = \mathbf{P}^T \tilde{\mathbf{Q}} \mathbf{M}, F_2 = \mathbf{P}^T \tilde{\mathbf{Q}} \mathbf{E} \quad (4.15)$$

$$\tilde{\mathbf{Q}} = \begin{bmatrix} Q_1 & 0 & \cdots & 0 \\ 0 & Q_2 & \cdots & 0 \\ \vdots & \vdots & \ddots & \vdots \\ 0 & 0 & \cdots & Q_{N_p} \end{bmatrix}, \tilde{\mathbf{R}} = \begin{bmatrix} R_1 & 0 & \cdots & 0 \\ 0 & R_2 & \cdots & 0 \\ \vdots & \vdots & \ddots & \vdots \\ 0 & 0 & \cdots & R_{N_c} \end{bmatrix}$$

$$G = \mathbf{x}_{\rightarrow k}^T \mathbf{M}^T \tilde{\mathbf{Q}} \mathbf{M} \mathbf{x}_{\rightarrow k} + \mathbf{x}_{\rightarrow k}^T \mathbf{M}^T \tilde{\mathbf{Q}} \mathbf{E} \mathbf{v}_{d \rightarrow k} + \mathbf{v}_{d \rightarrow k}^T \mathbf{E}^T \tilde{\mathbf{Q}} \mathbf{M} \mathbf{x}_{\rightarrow k} + \mathbf{v}_{d \rightarrow k}^T \mathbf{E}^T \tilde{\mathbf{Q}} \mathbf{E} \mathbf{v}_{d \rightarrow k} \quad (4.16)$$

From (4.16), it can be seen that G is independent of the control input sequence and can be neglected during the process of finding the optimal control input. $\tilde{\mathbf{Q}}$ and $\tilde{\mathbf{R}}$ represent the expanded sets of weighting matrices Q and R in the preview horizon N_p and control horizon N_c , respectively.

In the proposed MPC-IPC system, the minimisation of the performance index J turns out to be an optimization problem consisting of the pitch control activity, the generator power output regulation and the blade asymmetric load mitigation, restricted by the limits of pitch angle and rate that can be calculated using a standard quadratic programming method. For the purpose of optimisation, the interior-point-convex algorithm is adopted in the simulation and implemented by the "quadprog" command in the MATLAB.

Guaranteeing the closed-loop feasibility and stability of the proposed MPC controller with physical constraints is quite important. It has been demonstrated that the linear system MPC can maintain the nominal stability by introducing terminal weights in the performance index and the use of terminal constraints (Mayne et al., 2000; Feng, 2014). In this Chapter, the wind turbine model used is linear and stable. Meanwhile, no state constraints are introduced. Therefore, the proposed MPC could keep stable without the terminal cost and constraints with the help of sufficiently large preview horizon N_p (Körber and King, 2010). Given that the excessive constraint requirements are not included, the proposed MPC strategy is shown to be unaffected by the infeasible problem.

4.4 Gaussian Wind Speed Prediction

4.4.1 Rotor Effective Wind Speed

The LiDAR system is a mature technique for prediction of remote wind field properties as well as for rotor effective wind speed (EWS) forecasting (Raach et al., 2014). Nonetheless, the raw LiDAR measurements only provide the line-of-sight wind information and this is disturbed by directional bias errors. The prediction accuracy depends closely on the obtained LiDAR data and the adopted reconstruction approaches to model the wind characteristics in the interested locations (Guillemin et al., 2018). Different wind reconstruction approaches are proposed to obtain the wind field characteristics including future effective wind speed, direction, horizontal and vertical linear shear etc. It has been demonstrated that a potential technique can be used to obtain the detailed and reliable prediction knowledge of the oncoming wind speed especially gusts for contributing to enhanced wind turbine fatigue and extreme load mitigation from the typical nacelle-mounted LiDAR measurements with the synthesis of a Kalman filter (Towers and Jones, 2016). The work by Borraccino et al. (2017) proposes a model-fitting wind field reconstruction technique providing wind speed estimations designed to be suitable for power performance verification. The nominal LiDAR strategy for the EWS prediction is represented in Fig. 4.3. However, LiDAR is known to be an expensive technique and not available for commercial wind turbine operation. Therefore, it is natural to attempt to find some alternative method to obtain the future wind characteristics instead of LiDAR.

Generally, the wind speed measurement is achieved by an anemometer located at the hub of wind turbine system (Riahy and Abedi, 2008; Jena and Rajendran, 2015). This measured wind speed fails to denote the effective wind flow affecting the complete rotor and also suffers from high disturbances. Therefore, there is an increasing demand for the estimation of rotor EWS. Currently, there are several model-based methods including Kalman filtering and unknown input observers (Soltani et al., 2013) are proposed to estimate the precise EWS with the help of some common wind turbine measurements such as the turbine power output.

In this Chapter, the rotor EWS is achieved from the TurbSim wind flows with a discrete weighting function at each sampling interval. The achieved EWS is the weighted average of the matrix elements rather than a direct average over the rotor range (Schlipf

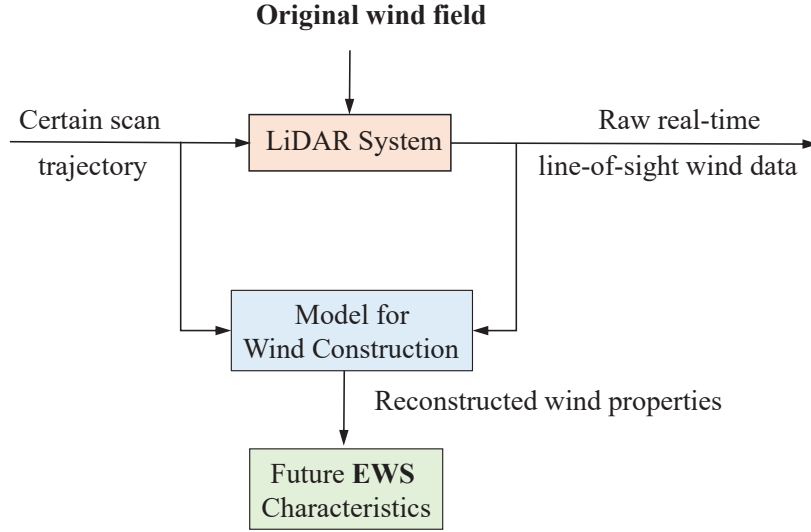


Figure 4.3: Nominal LiDAR strategy for the EWS prediction

et al., 2013). The original wind flows from the TurbSim simulator $[u_i, v_i, w_i]$ are characterized by a 3-D matrices of wind components, including the vertical, lateral and horizontal wind portions in the Cartesian coordinate system. The horizontal wind component u_i is employed to obtain the rotor EWS. A weighted average method in the polar coordinates (r, ϕ) is adopted here considering the effects of root and tip losses (Schlipf, 2016) and the rotor EWS is represented as:

$$v_0 = \sqrt{\frac{\int_0^{2\pi} \int_0^R u_i^2 \frac{\partial C_p}{\partial r}(r) r dr d\phi}{\int_0^{2\pi} \int_0^R \frac{\partial C_p}{\partial r}(r) r dr d\phi}} \quad (4.17)$$

where R means the turbine rotor radius, $r \in [0, R]$ denotes the distance from the hub centre, $R \frac{\partial C_p}{\partial r}$ function represents the power output span-wise change with the effects of root and tip losses. The adopted $R \frac{\partial C_p}{\partial r}$ model (Burton et al., 2011) is illustrated in Fig. 4.4, compared with the case without tip and root loss $\frac{32}{27} \frac{r}{R}$. The $\frac{32}{27} \frac{r}{R}$ function denotes the maximum power output with the Betz efficiency limit of $\frac{16}{27}$ (Soltani et al., 2013). In the discrete wind conditions, (4.17) is reduced to (4.18):

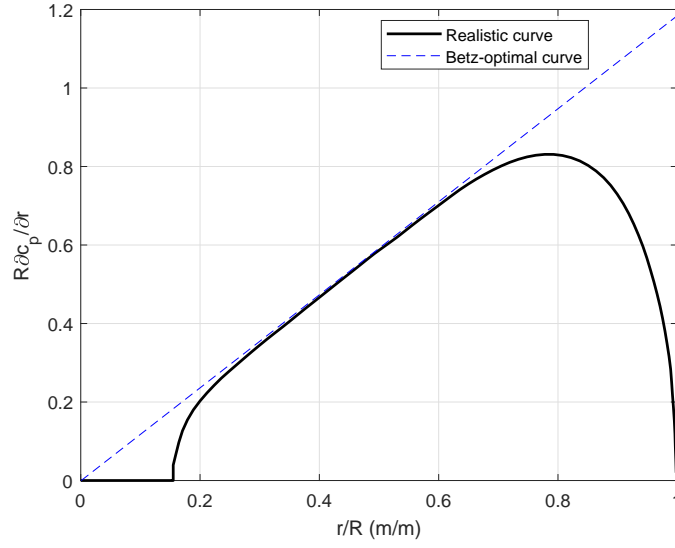


Figure 4.4: The power output span-wise change

$$v_0 = \frac{\sum_{j=1}^{n_R} C_{P,j} u_{i,j}}{\sum_{j=1}^{n_R} C_{P,j}}, \quad \text{with } C_{P,j} = \frac{\partial C_p}{\partial r}(r_j) \quad (4.18)$$

where $C_{P,j}$ evaluated at the distance r_j from the hub.

The full field wind profile is not available/measurable for the evaluation of the field tests. So here the EWS at the current time interval is calculated from the (4.18) based on the measurements from the FAST. This estimated rotor EWS is adopted as a basis for providing the future wind speed over the required simulation time by the proposed GP prediction model in the next section. An EWS prediction strategy is used in this thesis as illustrated in Fig. 4.2. The used GP model is illustrated in Section 4.4.2.

4.4.2 Gaussian Prediction Model

A Gaussian process is a non-stationary stochastic modelling procedure in which set(s) of Gaussian random variables change with time. Any limited quantity of which presents a joint Gaussian distribution relationship (Chen et al., 2014; Deisenroth, 2010). A random function $f(x)$ could be defined by a GP distribution with a mean function (nor-

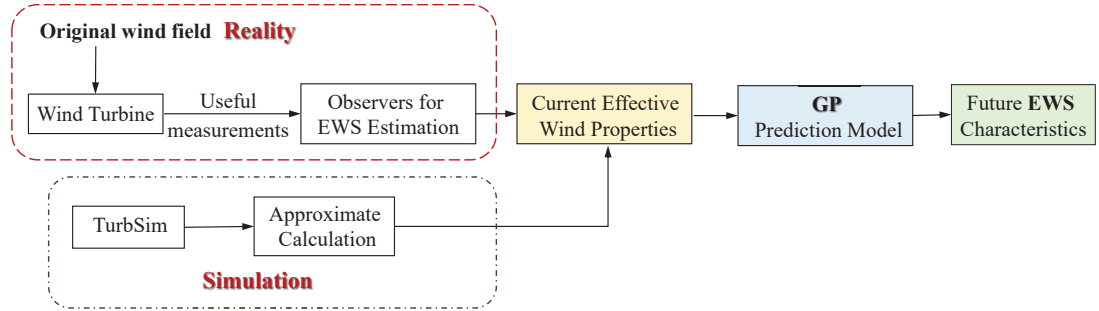


Figure 4.5: Proposed EWS prediction strategy by GP

mally supposed to be zero) and covariance function (also known as kernel function), constituting a *prior* (Williams and Rasmussen, 2006), is shown in

$$\begin{aligned}
 f(x) &\sim \mathbf{GP}(m(x), k(x, x^*)) \\
 m(x) &= \mathbb{E}[f(x)] \\
 k(x, x^*) &= \text{cov}(f(x), f(x^*))
 \end{aligned} \tag{4.19}$$

where $x \in \mathbb{R}$ denotes an arbitrary input, $f(x)$ and $f(x^*)$ are random variable pairs indexed by different inputs x and x^* . $k(x, x^*)$ means a covariance function with different forms and is parametrized by several specific parameters θ . The kernel function defines the behaviour of a process and describes the proximity between any arbitrary points of the random function, which is used by the GP algorithm to achieve the prediction of both value and uncertainty knowledge for an unknown required point from the training set (Wilson and Adams, 2013).

For regression problems solved by GPs, a set of training data $\mathbf{D} = (X, y)$ is considered with X, y denoting observations of the input sequence and corresponding scalar outputs. GPs realize the exploration of implicit functional relations between the inputs and outputs for the specified training dataset, and then acquire an *a posterior* distribution over the overall function $f(x)$.

A joint Gaussian distribution exists in any combination of function values $f(x_i)$ (Wilson and Adams, 2013):

$$[f(x_1), f(x_2), \dots, f(x_n)]^T \sim \mathcal{N}(\mu, K + \sigma^2 I) \tag{4.20}$$

where n denotes the index number, covariance function $K = K_{ij} = k(x_i, x_j)$ with size of $n * n$, as well as mean function $\mu = \mu_i = m(x_i)$. The type of covariance function turns out to be important for a GP regression model dominating the kernel function's performance including smoothness and periodicity (Williams and Rasmussen, 2006). The specific task of the GP is to select an appropriate type of covariance function and obtain the corresponding θ parameters by optimization methods.

Considering the obtained wind speed measurement is a physical process suffering from unknown uncertainties, the kernel function of Matérn class (Roberts et al., 2013) is adopted here, is defined by

$$k(x_i, x_j) = h^2 \frac{1}{\Gamma(\nu) 2^{\nu-1}} (2\sqrt{\nu} \frac{|x_i - x_j|}{\lambda}) \mathbb{B}_\nu(2\sqrt{\nu} \frac{|x_i - x_j|}{\lambda}) \quad (4.21)$$

where $h, \Gamma, \mathbb{B}, \lambda$ represent the output scale, the standard Gamma, a second-order improved Bessel function and the input scale defining how far away the two points x and x' are where there is a significant influence between each other, respectively. In this kernel function, the parameter ν denotes the differentiability order of the achieved GP regression model (here $\nu = \frac{1}{2}$) with $\nu + \frac{1}{2}$ times differentiable. The remaining learning hyperparameters $\theta = (h, \lambda)^T$ can be estimated by the optimization of the log marginal likelihood function (Williams and Rasmussen, 2006):

$$\log p(y|\theta) = -\frac{1}{2} \log |K| - \frac{1}{2} y^T K^{-1} y - \frac{n}{2} \log(2\pi) \quad (4.22)$$

The goal is to forecast the target output f^* for a new system input X^* according to the achieved GP *posterior* distribution from the associated training dataset \mathbf{D} . The augmented joint distribution by (X^*, f^*) is represented as:

$$\begin{bmatrix} f^* \\ y \end{bmatrix} \sim \left(\begin{bmatrix} m(X^*) \\ m(X) \end{bmatrix}, \begin{bmatrix} k(X^*, X^*) & k(X^*, X) \\ k(X, X^*) & K + \sigma^2 I \end{bmatrix} \right) \quad (4.23)$$

with $k(X^*, X) = k(X, X^*)^T = [k(X_1, X^*), \dots, k(X_n, X^*)]$. With the help of mathematical manipulation, the prediction result for the new input X^* is defined by (Williams and

Rasmussen, 2006):

$$\begin{aligned}\mu(f^*) &= m(X^*) + k(X^*, X)[K + \sigma^2 I]^{-1}(Y - m(X)) \\ \text{var}(f^*) &= k(X^*, X^*) - k(X^*, X)[K + \sigma^2 I]^{-1}k(X, X^*)\end{aligned}\quad (4.24)$$

Finally, the GP regression model is complete. From the above explanations, the Gaussian prediction model for the EWS is proposed. The forecast performance is evaluated by Root Mean Square Error (RMSE) (Draxl et al., 2015):

$$RMSE = \sqrt{\frac{1}{n} \sum_{t=1}^n (v_t - \hat{v}_t)^2} \quad (4.25)$$

where v_t, \hat{v}_t mean the actual and predicted wind speed, n denotes the quantity of available prediction pairs.

4.5 Simulation Results

The designed strategy is assessed by the 5MW NREL turbine simulator with the main DOFs activated in the above rated wind condition. In this Chapter, the initial realistic 3D wind flow characterized by the mean value of 18 m/s, 14% turbulence intensity and a vertical power law exponent of 0.2 is achieved from the TurbSim software (Jonkman, 2009).

4.5.1 Very Short-term Wind Speed Forecasting using GP

According to the analysis in Section 4.4.1, the EWS achieved from TurbSim is adopted as the wind disturbance input. The obtained EWS record v_d has a length of 1200s with a sampling interval of 0.0125s. The comparison between the wind speed at the hub-height and the estimated rotor EWS is shown in Fig. 4.6. The EWS is composed of two parts including *Part I* during $[0, 200]s$ which is used as the training dataset for fitting the GP model and *Part II* over $[200, 1200]s$ requiring prediction and for the simulation of MPC-IPC controller.

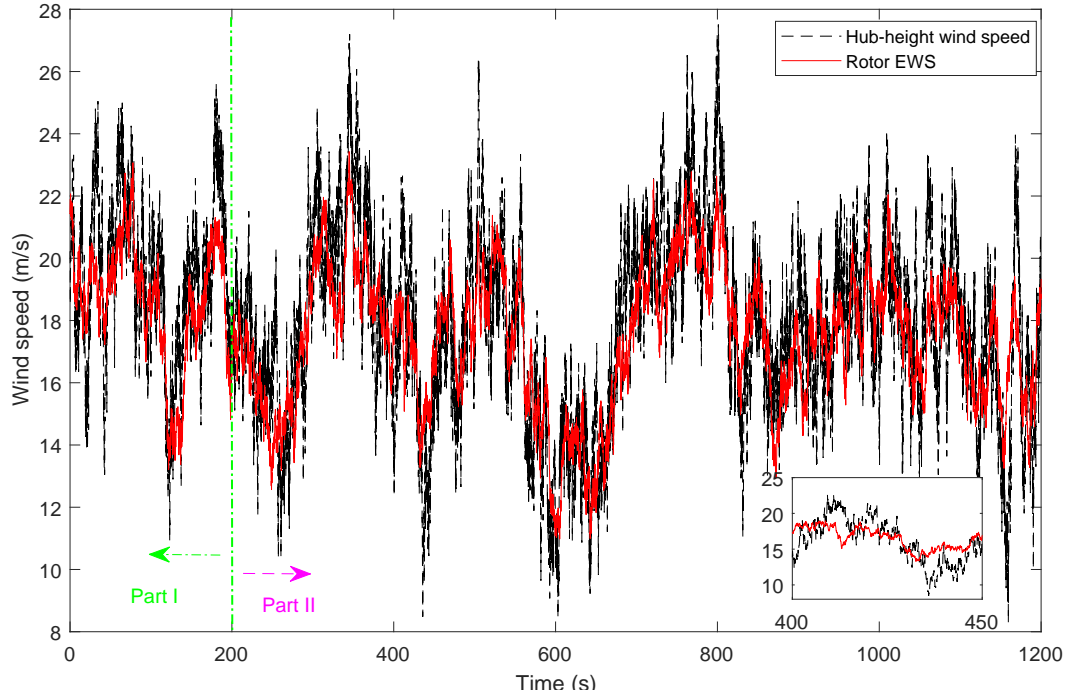


Figure 4.6: Comparison between the wind speed at the hub-height and the rotor EWS

The proposed GP wind speed prediction scheme for a very short-time range includes the following steps, which is shown in Fig. 4.7. Given that the proposed MPC controller performed with a frequency of 5 Hz (explained in the next section), the prediction step length is 0.2 s . Then, the beginning 200 s record of wind speed (namely *Part I* in Fig. 4.6) are employed as the training dataset for GP model-fitting. With the help of this step, the final GP model (*posterior*) is achieved from the initial GP model (*prior*) through updating the related hyper-parameters. Moreover, the subsequent 1000 s of wind data (i.e. *Part II*) are utilised for both the prediction tests and the next MPC-IPC simulation work. In the proposed GP prediction model, the 50 data points preceding each point to be predicted in *Part II* are used as inputs. Determining the prediction length of future wind speed is quite important. The longer the prediction time, the larger workload, and the more complex the model for MPC. Here, a maximum predicted length of 5 s for the wind speed is studied. The resulting RMSEs for the 1000 s wind speed of *Part II* with several prediction time are illustrated in Table 4.1. Specifically, the wind speed prediction with preview time of 0.2 s and 1 s are illustrated in Fig. 4.8 and Fig. 4.9. The grey area represents uncertainties of the predicted points. From the simulation results, it can be concluded that the prediction error of wind speed is increasing with the prediction length. The results verify the feasibility and validity

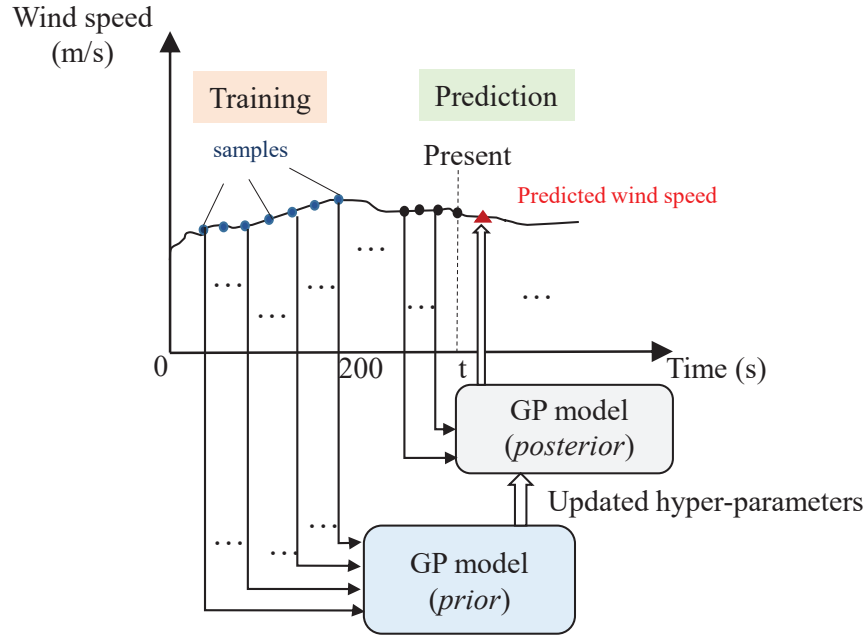


Figure 4.7: Proposed GP wind speed prediction scheme

of the designed GP predictor for very short-term wind speed forecasting.

Table 4.1: RMSE of the wind speed forecasting by proposed GP model

Preview Time (s)	0.2	1	2	3	4	5
RMSE (m/s)	0.3255	0.4162	0.5201	0.6861	0.9122	1.096

4.5.2 MPC-IPC Load Mitigation with Wind Preview

It is of great significance to decide the following MPC parameters containing the sampling interval T_s , control horizon N_c , output preview horizon N_p together with wind prediction horizon N_d to obtain the trade-off between the system complexity, simulation speed and result accuracy (Spencer et al., 2013).

- The sample interval T_s is usually as small as possible to demonstrate the natural frequencies of principal turbine structural DOFs and it is set as $0.2s$ here.
- The preview horizon N_p should be large enough to maintain the nominal stability of the proposed MPC for the stable wind turbine system (Körber and King,

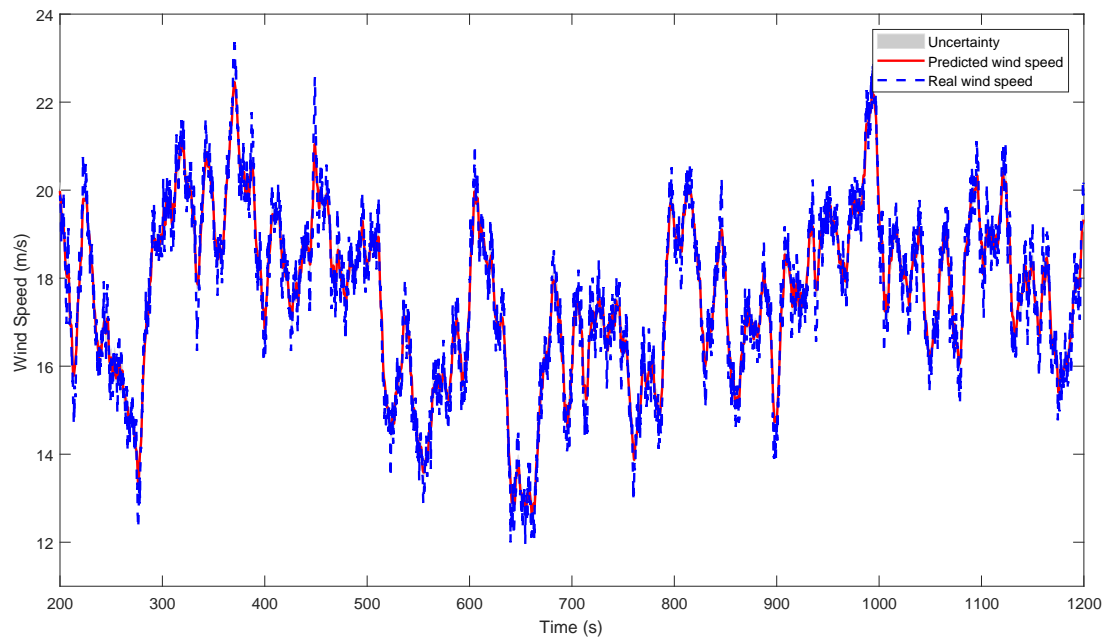


Figure 4.8: Comparison between the real and wind speed prediction by proposed GP (1s ahead)

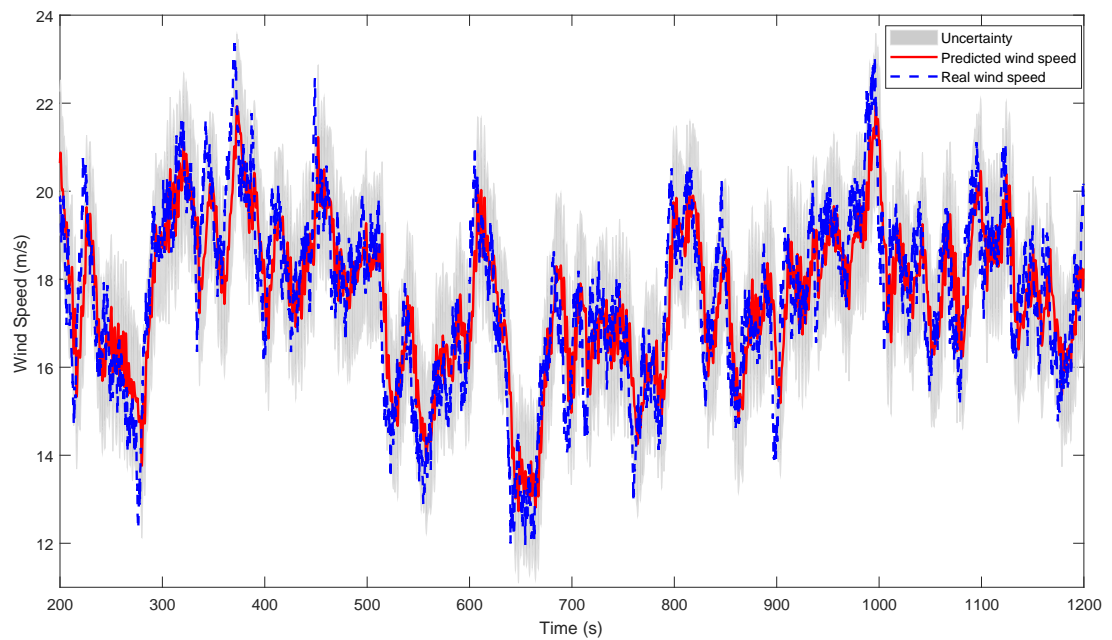


Figure 4.9: Comparison between the real and wind speed prediction by proposed GP (5s ahead)

2010). Here, $N_p = 15$ which results in a preview period of $3s$ presenting the main dynamics of the wind turbine.

- The control horizon N_c is related to the system computation complexity. The larger the N_c is, the more complex the computation is. Here, $N_c = 5$ ($1s$) aims at achieving a balance between the forecasting accuracy and system computational burden.
- The wind prediction horizon N_d is flexible, which is decided by the user. Excessive future wind information will slow the MPC operational process and the exaggerated wind speed errors may generate counter-productive effects. According to the work (Spencer et al., 2013), the proposed MPC with the knowledge of wind speed prediction exceeding $1s$ fail to improve the control effect obviously. In order to obtain a trade-off between the accuracy and complexity, the wind preview horizon of $1s$ is carried out with the proposed MPC controller. Given that the MPC operates at $5 Hz$, the prediction step for future wind speed used by MPC should be at intervals of $0.2s$. So $N_d = 6$ is selected here requiring 1 to 5 steps ahead of wind speed prediction.

The considered constraints for the MPC-IPC controller includes the blade pitch angle restrictions $[0^\circ, 90^\circ]$ and pitch rate limits $[-8^\circ/s, 8^\circ/s]$. The tuned weighting matrices Q_x , R are designed properly and have the same parameters in the different simulation cases (Table 4.2). The proposed MPC controller is evaluated under the wind condition (*Part II*). The performance measures contain standard deviations (STD) of the blade 1 flapwise bending moments M_1 , pitch rate $\dot{\theta}$ and generator power P . The calculation is from $230s$ to $1200s$ to avoid the effects of starting transients. The rainflow counting approach is used to estimate the lifetime damage-equivalent load (DEL) with different material-specific parameters of 4 and 10 for steel and composite materials (Selvam, 2007) for evaluating the fatigue damage level of wind turbine components. Here, a Matlab-base tool MLife designed by the NREL lab is adopted to generate the wind turbine lifetime DEL (Hayman and Buhl Jr, 2012).

The detailed simulation results are represented in Table 4.2 and Figs. 4.10 - 4.12, which contain the baseline CPC controller (expressed as, Baseline), PI case representing the IPC using PI controller, together with (MPC) meaning the MPC controller without any wind speed previews (i.e. all the future wind speed values are assumed to be 0), (MPC+w_r) denoting the MPC has ideal wind speed previews, and the MPC with

achieved wind forecasting called as (MPC+ w_p) where w_p represents the wind speed forecasting explained in Section 4.5.1.

Table 4.2: Comparisons between different pitch controllers

Parameters	Baseline	PI	MPC	MPC+ w_p	MPC+ w_r
std(M_1) [kNm]	2051.3	1405.6	1390.5	1310.2	1341.3
std($\dot{\theta}$) [deg/s]	0.43	2.50	3.05	3.27	3.84
std(P) [KW]	91.5	98.9	76.4	64.1	69.5
DEL(M_1) [m=4]	2800	2290	2120	2000	2020
DEL(M_1) [m=10]	7690	7560	6550	5530	5520

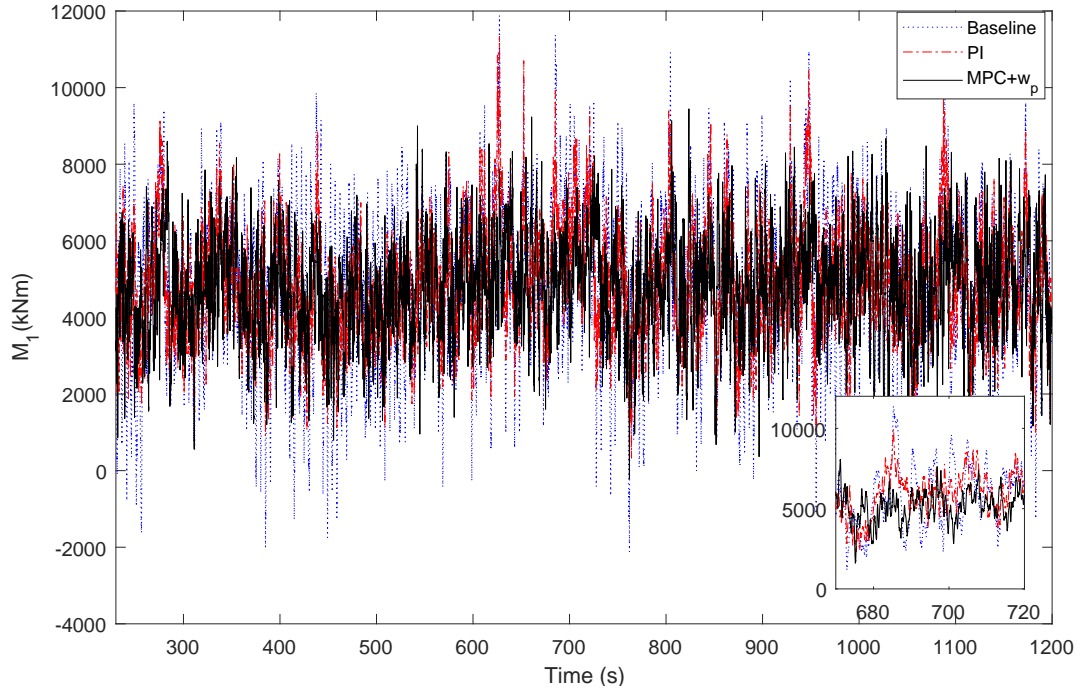


Figure 4.10: Flapwise bending moments of blade 1

From the above simulation results, it is shown that the designed MPC controller without wind preview knowledge obtains 32.2% loading mitigation of the blade flapwise bending moments (compared with Baseline case) and 16.5% drop of power output oscillation during the simulation running time, which is impressively better than the PI case with enhanced power fluctuation. Meanwhile, the results are improved by a further 3.9% for loads mitigation and by a further 13.4% drop for generator power fluctuations with the condition of perfect wind speed prediction. It should be noted

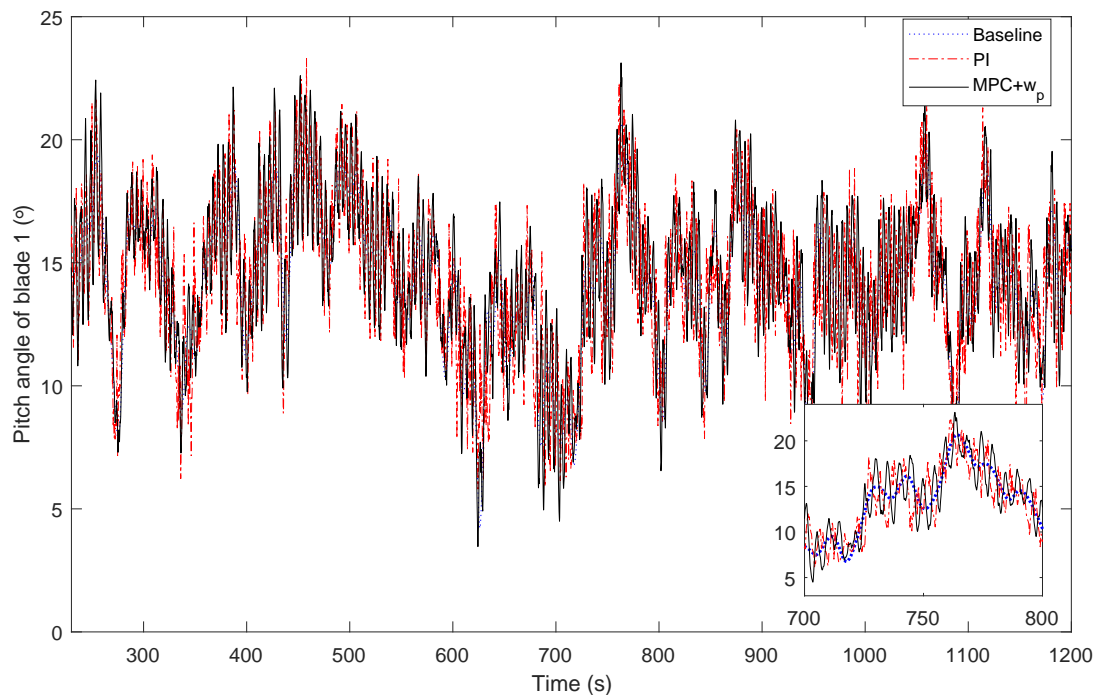


Figure 4.11: Pitch angle of blade 1

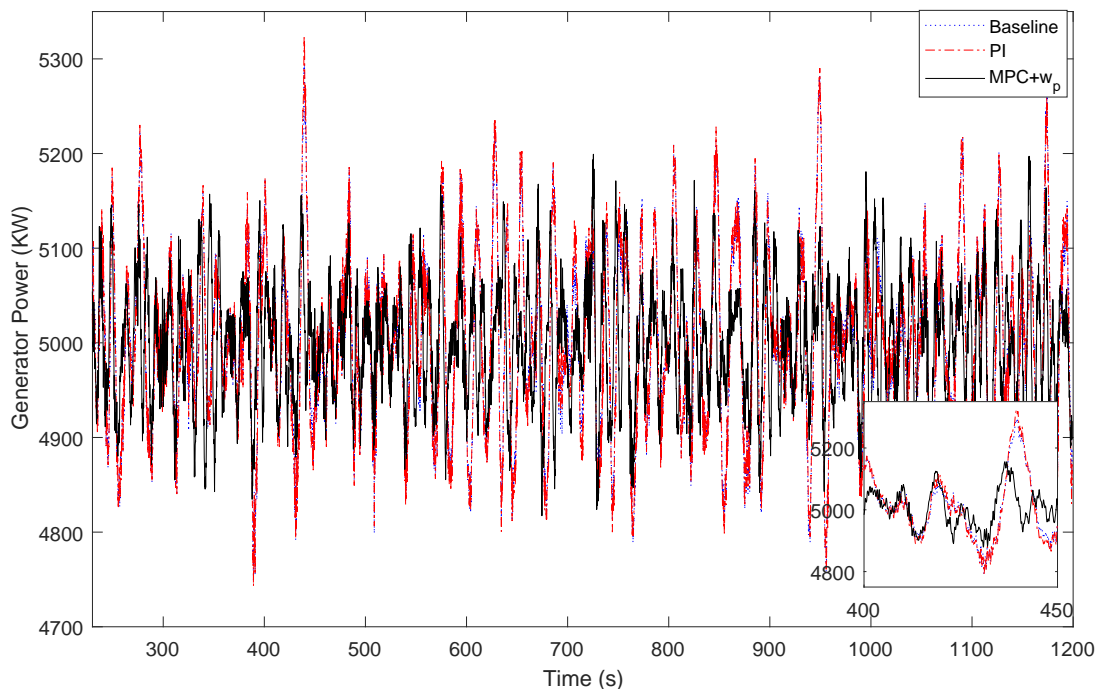


Figure 4.12: Generator power

that the life DEL also decreases most in the (MPC+w_p) case. Nonetheless, while the blade unbalanced loading reduction performs best in the (MPC+w_p) case, the pitch actuation motion is excessive compared to the baseline CPC. The reason for achieving the smoother power output is the performance index for the MPC controller including the weighting knowledge for generator power. Due to the inclusion of future wind speed information, the wind turbine model used for proposed MPC strategy is closer to the real turbine. In this sense, the MPC controller could have more optimal control outputs based on the future knowledge. It is worth noting that MPC with predicted wind speed achieves marginally better results compared with the case when adopting ideal wind speed forecast, which shows that the accuracy of 1s wind speed forecasting is good enough. Overall, the simulation results demonstrate the validity of designed strategy and the load mitigation performance is less sensitive to the rotor effective wind speed forecasting errors. Further investigations are under way to include more wind characteristics (including vertical shear, wind direction etc.) in the MPC controller model in future.

4.6 Conclusion

In this Chapter, an innovate GP model with Matérn class kernel for very short-term wind speed forecasting is designed for the control purpose. This is further combined with the MPC-based IPC system, constituting a wind turbine preview control aiming at blade loading mitigation. The detailed simulation results on the NREL 5MW turbine simulator verify the effectiveness of designed strategy. Since no additional hardware system is needed, this method is suggested to serve as a promising alternative technique to the pricey LiDAR in terms of providing future wind knowledge. That is, it could be used without extra LiDAR measurements. It is worth noting that the sensitivity between wind speed forecasting and the MPC-based IPC load reduction performance is relatively low. The designed scheme sheds new light on the study of combining very short-term wind speed forecasting and preview control for blade unbalance load mitigation without the LiDAR system.

From the simulation results, it can be concluded that the pitch movements have been enhanced due to the extra pitch angle introduced by the MPC-based IPC system, which will increase the possibility of pitch system faults. Therefore, it is important to design

effective and robust fault tolerant control strategies to compensate the pitch faults in the IPC system, which is studied in Chapter 5.

Chapter 5

Fault-tolerant Individual Pitch Control using Adaptive Fault Estimation

5.1 Introduction

As described in Chapter 1, the significance of combined analysis of the fault tolerant control (FTC) strategy with individual pitch control (IPC) has been emphasized, which is exactly the focus of this Chapter. Two traditional IPC systems for blade load reduction and incipient pitch actuator faults (including hydraulic leakage, high oil content, pump wear) are combined and studied, observing different IPC system performance under the same fault condition and the robustness of FTC strategy in different IPC systems.

Fault estimation (FE) and FTC are demonstrated to achieve incipient fault estimation and compensation for fault effects. In FTC it is important for the system to give a warning when faults first develop and before they become serious or even malfunctions (Patton, 2015; Blanke et al., 2006; Gao et al., 2015a; Zolghadri et al., 2014). The FTC concept is introduced in Section 3.2.3 where more description is given. This detection and isolation of early or "incipient" faults is an important by-product of an FTC strategy, providing potential fault information to the operators. Faults which are not severe are compensated in the FTC system in order to maintain the control performance, so even when some faults occur the FTC system can maintain energy production operation until a maintenance event is planned.

As discussed in Section 3.2.3, FTC is divided into two strategies (1) Passive FTC which is none other than the use of robust control without any action to reconfigure or compensate for faults, and (2) Active FTC which is concerned with active configuration of the control system, subsequent to fault occurrence and detection/estimation. This work makes use entirely of the Active FTC approach and Fig. 3.5 shows a classification of these methods. This Chapter is concerned with the fault hiding and compensation strategy illustrated in Fig. 3.5 by the red line.

It is of great value to combine FTC with designs used for load mitigation, i.e. making use of IPC control methods (PI, etc). Within this framework, the FTC strategy based on FE has been proven to be suitable for achieving the pitch actuator fault reconstruction compared to the FDI technique (Chen et al., 2013; Shi and Patton, 2015). Nonetheless, the research involving IPC in wind turbines combined with FTC in the presence of faults (referred to as "fault-tolerant individual pitch control") are rarely considered. A fault diagnosis and accommodation technique for enabling or disabling the IPC algorithm according to the fault detection result of the azimuth angle sensor is proposed in the work (Fogh Odgaard et al., 2015). A fault detection strategy for blade root bending moment sensor faults with the help of LIDAR technique is integrated to the existing IPC system (Stotsky, 2014). Although these two sensors are important measurements requiring for the IPC system, the pitch actuator system faults are equally important. A fault detection and diagnosis (FDD) and automatic signal correction algorithm for a pitch actuator fault within an IPC scheme is proposed in another paper (Badihi and Zhang, 2018) which focuses on one hydraulic oil leak fault (giving rise to a pressure drop). There are two main weaknesses of that work: (1) it uses an FDI-based FTC which is exceedingly complex to implement in real practice and involves switching delay and detection delay all of which are very much affected by uncertainty, (2) the FTC design is only tested for one simulated wind condition, which is unrealistic for practical application since the wind conditions are constantly varying.

On the other hand this Chapter proposes a universal and robust fault-tolerant IPC strategy based on FE scheme for large wind turbines which aims to mitigate for bending blade moment variations caused by uneven wind loading. It is planned to make the load mitigation system also tolerant to pitch system faults and hence the work describes a combination of the use of IPC with FE-based FTC. The idea of using IPC is that the 3 pitch actuators can form a type of actuator redundancy (actually dissimilar redundancy) with resulting different pitch angles enabling a re-balancing of the rotor to be

established. There are actually two forms of wind loading that act on the rotor, symmetrical and asymmetrical loads. In the symmetrical case the loading acts equally on the three rotor blades and this may be the case for low wind speeds, e.g. in Region 2 operation. At higher wind speeds, in Region 3, the loading across the blades become more asymmetrical due to turbulence and vortex effects. More description of these phenomena are given in Section 2.3. In fact the symmetrical loading can be handled well using conventional Collective Pitch control (CPC) as for lower wind speeds in Region 3 but still close to the critical speed the wind flow into the rotor is more uniform. At higher wind speed as the turbulence increases the asymmetrical loading should be compensated using the IPC actuator redundancy.

The forces and moments acting on the rotor are rotating and to facilitate a procedure of analysis and design for IPC it is conventional to use the so-called Coleman Transformation (Bossanyi, 2005) (see also Section 2.4). This transforms the periodic system forces and moments into a fixed coordinate axis system. It is fortuitous that this mathematical operation also separates the effects of the symmetrical and asymmetrical force and moment components to enable the appropriate compensation (for asymmetrical loads) to be applied through appropriate IPC control action.

Hence, of the various IPC strategies, Coleman transformation-based IPC attenuates the non-rotating tilt and yaw loads from the blade load projection effectively. The most commonly used control approach for IPC is Proportional-Integral (PI) control which has the advantage of ease of implementation (Bossanyi, 2005; Van Engelen, 2006). A second IPC approach H_∞ loop-shaping control can be used for comparison with IPC based on PI control (Lu et al., 2015).

Section 1.4.1 discusses how the scenario of load mitigation is analogous to the FTC problem because the action of rotor bending (caused by wind loading) and considered as a component fault effect (Patton, 2015). An extension to this can be considered for tower bending, or even a combination of both (see Chapter 6 for more discussion). The idea of considering all the "fault effects" acting in the rotor system fits well with the work described in this Chapter. Hence, work on FTC is a valid contribution in this context of handling blade loading and actuator faults, as these various effects can be handled together.

As a review, this Chapter initially provides some general insight into the concept of unbalanced blade load deterioration based on the use of different IPC control methods

for the pitch actuator faulty case. Issues considered are: how they can be affected by three different pitch actuator system faults, and how the undesirable effects are compensated by a suitably designed FE-FTC strategy. The proposed FE based FTC strategy integrating with different IPC schemes is validated on the NREL 5MW turbine simulator in two different wind conditions in order to evaluate important robustness properties.

This Chapter is constructed as follows. Section 5.2 gives a detailed illustration of the issue being considered. In Section 5.3, two Coleman transformation based IPC systems using PI and H_∞ loop-shaping control methods are proposed. Next, a step-by-step sliding mode observer (SMO) (Lan et al., 2018) strategy is adopted to obtain the estimation of pitch system states and faults. Furthermore, it also presents the FE-based FTC scheme to compensate the faults. Finally, the detailed simulation results and conclusions are presented in Section 5.4 and Section 5.5, respectively.

5.2 Problem Statement

In this Chapter all the work focuses on Region 3 operation (above the rate wind speed of 11.2 m/s). More description about the so-called baseline CPC system is given in Section 2.2.4. The CPC strategy is shown in Fig. 5.1. $w_{g,r}$, β_r represent rated values of the generator speed and three collective pitch angles, respectively. w_g , β denote the real measurements, respectively.

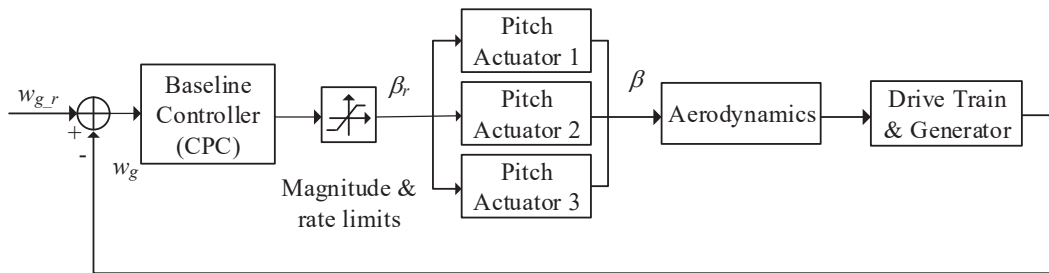


Figure 5.1: Nominal pitch system strategy by CPC

An extra pitch angle generated by the designed IPC system is then added to the collective pitch angles individually in order to mitigate the blade unbalanced loading. The nominal pitch system with the IPC strategy is shown in Fig. 5.2.

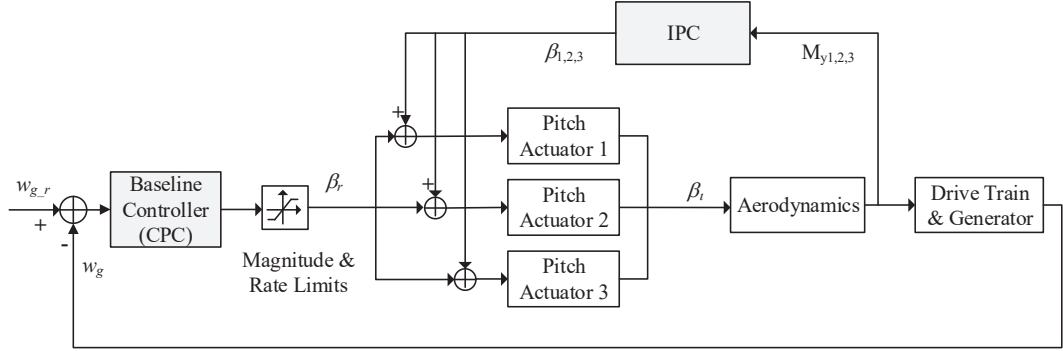


Figure 5.2: Nominal pitch system strategy by IPC

The hydraulic pitch system is modelled as (see Section 2.2.2):

$$\frac{\beta(s)}{\beta_r(s)} = \frac{w_n^2}{s^2 + 2\xi w_n s + w_n^2}. \quad (5.1)$$

where w_n and ξ are the nominal natural frequency and damping ratio parameters, respectively. In the case without faults, $w_n = 11.11 \text{ rad/s}$ and $\xi = 0.6$. Some potential faults of hydraulic pitch systems contain the oil leakage due to improper management of hydraulic fluids, the pump damage resulting from continuous pump operation, as well as the high air content in oil. These will lead to that the blade pitch system has changed dynamics (ξ and w_n), causing slow pitching performance and unstable wind turbine outputs. The open-loop performance of various faulty cases are evaluated and shown in Fig. 5.3.

The faulty parameters with changed dynamics can be modelled as convex combinations of ξw_n , w_n^2 and the fault level f , illustrated as (Liu et al., 2018a):

$$\begin{aligned} w_n^2 &= w_{n_0}^2 + (w_{n_f}^2 - w_{n_0}^2)f, \\ \xi w_n &= \xi_0 w_{n_0} + (\xi_f w_{n_f} - \xi_0 w_{n_0})f. \end{aligned} \quad (5.2)$$

where ξ_0 and w_{n_0} are the nominal pitch actuator damping ratio and frequency respectively, whilst ξ_f and w_{n_f} denote the dynamic parameters in the faulty case. Parameter $f \in [0, 1]$ represents the fault level. Table 5.1 illustrates the corresponding dynamic parameters with different pitch system faults.

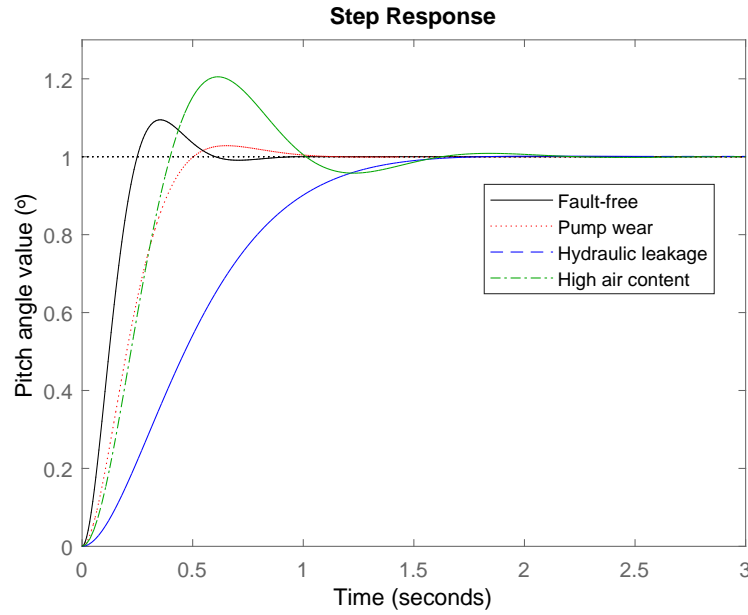


Figure 5.3: Step response of one pitch actuator system in different situations

Table 5.1: Pitch system parameters in different conditions

Fault type	Dynamic parameters	Reversible
Fault-free	$w_{n_0} = 11.11 \text{ rad/s}$, $\xi_0 = 0.6$	N/A
Hydraulic leakage	$w_{n_f} = 3.42 \text{ rad/s}$, $\xi_f = 0.9$	×
Pump wear	$w_{n_f} = 7.27 \text{ rad/s}$, $\xi_f = 0.75$	×
High air content	$w_{n_f} = 5.73 \text{ rad/s}$, $\xi_f = 0.45$	✓

The fault of pump wear will cause 25% pressure reduction from the rated hydraulic pressure as a consequence of approximately 20 years' operation. This fault is irreversible and requires manual maintenance. Hydraulic leakage resulting in low hydraulic pressure normally occurs quicker than the pump wear. If the flow pressure turns out to be too low, the pitch system will fail in pitching the corresponding blade to the required position. This will lead to the pitch actuator stuck fault (namely blade seize, see more in Section 3.4), requiring reparation during wind turbine shut-down (Naik, 2017). The high air content in the oil can restore the nominal air content level without any repair, but will cause transient response overshoot in the open-loop system (Luo et al., 2014). It should be noted that these three faults are characterized by incipient faults and causing variations (even uncertainty) in the pitch system dynamics,

which could be treated together. Therefore, it is important to compensate for the pitch actuator faults on-line and recover the nominal pitch system performance quickly.

5.3 FTC-IPC System Design

The diagrammatic sketch of the proposed FTC-IPC system is illustrated in Fig. 5.4, which contains the following systems (i) a baseline pitch control (CPC) system for regulating the power output (see Section 2.2.4), (ii) an IPC scheme using PI or H_∞ loop-shaping control approach aiming at the mitigation of asymmetrical blade loading, (iii) observers using SMO for the fault estimation of three different pitch actuator faults, and (iv) FTC schemes for pitch actuator fault compensation.

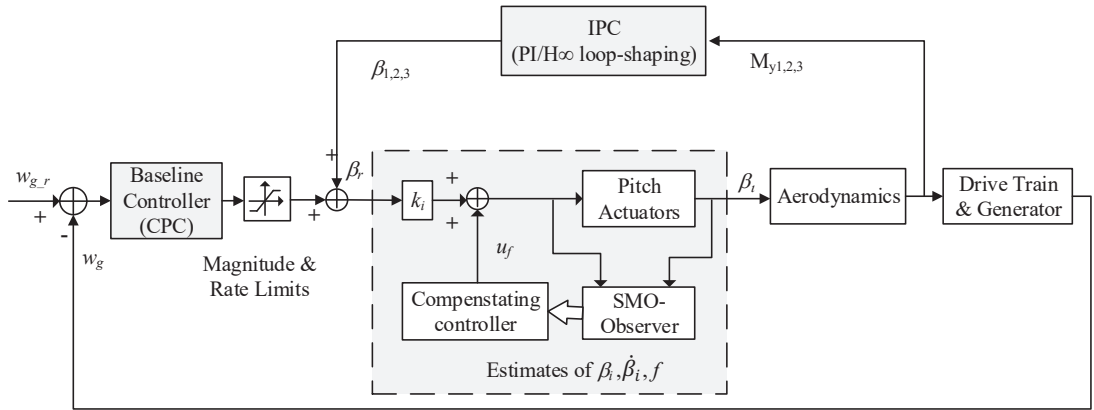


Figure 5.4: Fault-tolerant pitch system

5.3.1 Traditional IPC Strategy for Load Mitigation

The concern of this Chapter is focused on combining the IPC with FTC and discussing the pitch actuator fault effects on different IPC systems, with the blade bending moments considered as separate fault effects (see more in Section 1.4 and Section 5.1). Therefore, the traditional Coleman transformation-based IPC strategy using two different control approaches including PI and H_∞ loop-shaping control is studied to compensate the main bearing tilt and yaw moments, and thus reducing the rotor blade unbalanced loading.

Assuming the 1st blade is in the horizontal direction, the Coleman $P^{-1}(\varphi)$ and inverse Coleman transformations $P(\varphi)$ for 1P are illustrated by:

$$\begin{bmatrix} M_o \\ M_c \\ M_s \end{bmatrix} = \begin{bmatrix} M_{mean} \\ M_{yaw} \\ M_{tilt} \end{bmatrix} = \underbrace{\begin{bmatrix} \frac{1}{3} & \frac{1}{3} & \frac{1}{3} \\ \frac{2}{3} \cos(\varphi) & \frac{2}{3} \cos(\varphi + \frac{2\pi}{3}) & \frac{2}{3} \cos(\varphi + \frac{4\pi}{3}) \\ \frac{2}{3} \sin(\varphi) & \frac{2}{3} \sin(\varphi + \frac{2\pi}{3}) & \frac{2}{3} \sin(\varphi + \frac{4\pi}{3}) \end{bmatrix}}_{P^{-1}(\varphi)} \begin{bmatrix} M_{y1} \\ M_{y2} \\ M_{y3} \end{bmatrix} \quad (5.3)$$

with

$$P(\varphi) = \begin{bmatrix} 1 & \cos(\varphi) & \sin(\varphi) \\ 1 & \cos(\varphi + \frac{2\pi}{3}) & \sin(\varphi + \frac{2\pi}{3}) \\ 1 & \cos(\varphi + \frac{4\pi}{3}) & \sin(\varphi + \frac{4\pi}{3}) \end{bmatrix} \quad (5.4)$$

where o, c, s denote the collective, cosine, sine components respectively, φ means the blade azimuth angle. The relationships between the three azimuth angles are illustrated in (5.5) (Van Engelen, 2006):

$$\varphi_1 = \varphi; \quad \varphi_2 = \varphi + \frac{2\pi}{3}; \quad \varphi_3 = \varphi + \frac{4\pi}{3} \quad (5.5)$$

The designed Coleman transformation-based IPC strategy is illustrated in Fig. 5.5, where g contains the wind inflow conditions and generator torque reference etc. It can be seen from the Fig. 5.5, a notch filter is proposed to remove the $3P$ -harmonics of the yaw and tilt moments, thus avoiding the enhancement of $3P$ loading on the fixed wind turbine components. Meanwhile, a low-pass filter with cut-off frequency of 1.2 Hz is adopted to smooth the generated additional individual pitch angle $\beta_{11}(t), \beta_{12}(t), \beta_{13}(t)$ (coming from the IPC system) before being combined with the pitch angle reference $\beta_c(t)$ from the CPC system, thereby reducing the potential pitch actuator movements at high frequency.

First of all, the PI-based IPC system is studied. Two single-input-single-output (SISO) pitch control loops with same PI parameter values are designed for the main-bearing tilt and yaw moment compensation. The PI controller parameters are tuned manually and

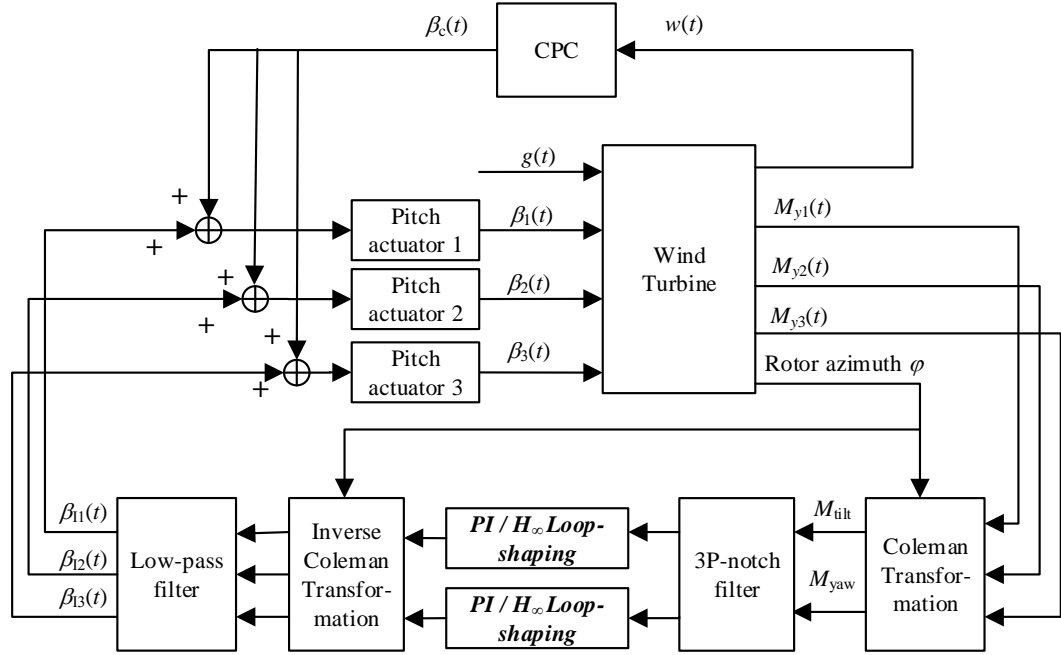


Figure 5.5: The designed IPC system for load mitigation

appropriately by trial and error. In this study, extra pitch angles from the IPC system are typically with frequency more than 0.1Hz. The frequency of collective pitch angles from the CPC is less than 0.1Hz. In this sense, the IPC strategy is decoupled from the CPC system, thereby avoiding the impact of additional introduced pitch angles on generator power instability.

The achieved PI-IPC control system can be illustrated by

$$\begin{aligned}
 C_{PI-IPC}(s) = & \underbrace{\frac{w_l^2}{s^2 + 2\xi_l w_l s + w_l^2}}_{\text{Low-pass filter}} \underbrace{P(\varphi)}_{\text{Inverse Coleman}} \\
 & \underbrace{\begin{bmatrix} K_p + \frac{K_{i,yaw}}{s} & 0 \\ 0 & K_p + \frac{K_{i,tilt}}{s} \end{bmatrix}}_{\text{PI controller}} \\
 & \underbrace{\frac{s^2 + 2\xi_{n1} w_n + w_n^2}{s^2 + 2\xi_{n2} w_n + w_n^2}}_{\text{3P-notch filter}} \underbrace{P^{-1}(\varphi)}_{\text{Coleman}}
 \end{aligned} \tag{5.6}$$

So as to have a more comprehensive study of fault effects and the robustness of the later designed FE-FTC system in different IPC cases (explained in Section 5.3.2), an alternative control technique with the same design layout (Fig. 5.5) is required. Here, an H_∞ loop-shaping method with better robustness is selected to be combined with the conventional IPC system (Panagopoulos and Åström, 2000). The H_∞ loop-shaping approach aims to achieve a controller that provides robustness to system uncertainties and minimizes the effects of external disturbances and noise (Mendiratta and Jayapal, 2010). A linear wind turbine model $G(s)$ describing the connection between pitch angle fluctuations and flapwise bending moment perturbations is adopted for the controller design (Lio et al., 2017), illustrated as:

$$G(s) = G_a(s)G_b(s) \quad (5.7)$$

where $G_a(s)$, $G_b(s)$ represent the blade pitch actuator system (same with (5.1)) and the blade dynamics (defined as (5.8)), respectively.

$$G_b(s) = \frac{dM_{flap}}{d\theta} \frac{2\pi f_b^2}{s^2 + 2\pi d_b f_b s + 2\pi f_b^2} \quad (5.8)$$

The design procedure includes the following two main steps (Lio, 2018):

- Propose a appropriate pre-compensator $W(s)$ for shaping the singular values of targeted loop shape $G_s(s) = G(s)W(s)$, which should have relative large loop gain at the target frequency and small gain at higher frequency for better noise suppression.
- Synthesize $K_s(s)$ and obtain the greatest robust stability margin of $G_s(s)$, then the complete loop-shaping controller $K_H(s) = W(s)K_s(s)$.

Considering the frequency splitting problem and the objective of 1P flapwise bending moments mitigation, an H_∞ loop-shaping based IPC system is proposed to mitigate the main bearing tilt and yaw loads at 3P frequency. Hence, the pre-compensator $W(s)$ is designed as a combination of a PI controller and a 3P inverse notch filter:

$$W(s) = \left(K_p + \frac{K_i}{s}\right) \frac{s^2 + 2\xi_1 w + w^2}{s^2 + 2\xi_2 w + w^2} \quad (\xi_1 > \xi_2) \quad (5.9)$$

The wind turbine model parameters and designed controller parameters including PI-based IPC and H_∞ loop shaping-based system are given in Table 5.2.

Table 5.2: Designed system parameters

Description	Parameter	Value
PI controller (PI-IPC)		
Proportional gain	$K_{p_{yaw}}$	0.00002
Proportional gain	$K_{p_{tilt}}$	0.00002
Integral gain	$K_{i_{yaw}}$	0.00001
Integral gain	$K_{i_{tilt}}$	0.00001
3P-notch filter (PI-IPC)		
Frequency	w_n	$2\pi * 0.6 \text{ rad/s}$
Damping ratio 1	ξ_{n_1}	0.3
Damping ratio 2	ξ_{n_2}	1
Low-pass filter (both)		
Frequency	w_l	$2\pi * 1.2 \text{ rad/s}$
Damping ratio	ξ_l	0.7
PI controller (H_∞ loop-shaping)		
Proportional gain	K_p	0.000003
Integral gain	K_i	0.000005
Frequency	w	$2\pi * 0.2 \text{ rad/s}$
Damping ratio 1	ξ_1	0.5
Damping ratio 2	ξ_2	0.01
Wind turbine model parameters		
Differentiation between flapwise bending & pitch angle	$\frac{dM_{flap}}{d\theta}$	$-1.5e6 \text{ Nm/}^\circ$
Natural frequency of blade 1 st flapwise mode	f_b	0.7 Hz
Aerodynamic damping ratio	d_b	0.47

The H_∞ loop-shaping controller could be obtained with the help of MATLAB by using command `ncfsyn.m`. The final synthesised controller $K_H(s)$ is represented as:

$$K_H(s) = \frac{0.00022s^5 + 0.00509s^4 + 0.06698s^3 + 0.3946s^2 + 0.8909s + 0.6623}{s^5 + 72.3s^4 + 2641s^3 + 60040s^2 + 93070s} \quad (5.10)$$

5.3.2 FE-based FTC Design for Fault Compensation

5.3.2.1 FE Design

The complete faulty pitch system encompassing (5.1) and (5.2) can be illustrated as

$$\begin{aligned} \dot{x}_1 &= x_2 \\ \dot{x}_2 &= G_0(x) + B_0 u + F(x)f \\ y &= x_1 \end{aligned} \quad (5.11)$$

where $x = [x_1 \ x_2]^\top = [\beta \ \hat{\beta}]^\top$, $G_0(x) = -w_{n_0}^2 x_1 - 2\xi_0 w_{n_0} x_2$, $B_0 = w_{n_0}^2$ and fault distribution function $F(x) = (w_{n_0}^2 - w_{n_f}^2)(x_1 - u) + 2(\xi_0 w_{n_0} - \xi_f w_{n_f})x_2$.

The fault distribution $F(x)$ is shown to be a time-varying matrix that inevitably increases the complexity of observer design. An adaptive step-by-step SMO (Lan et al., 2018) is adopted to achieve the estimation of pitch system states and faults simultaneously, represented as (5.12).

$$\begin{aligned} \dot{\hat{x}}_1 &= \hat{x}_2 + v_1 \\ \dot{\hat{x}}_2 &= G_0(\hat{x}) + B_0 u + F(\hat{x})\hat{f} + v_2 \\ \dot{\hat{f}} &= \eta_f \text{sign}(e_f) \end{aligned} \quad (5.12)$$

where \hat{x} , \hat{f} denote the estimates of states and faults, respectively. v_1, v_2 are the proposed SMO switching functions and e_{x_1}, e_{x_2}, e_f are the estimation errors of two states and actuator fault, designed as:

$$\begin{aligned} v_1 &= \eta_{v_1} \text{sign}(e_{x_1}), v_2 = \eta_{v_2} \text{sign}(\tilde{x}_2 - \hat{x}_2) \\ e_{x_1} &= x_1 - \hat{x}_1 \\ e_{x_2} &= x_2 - \hat{x}_2 \\ e_f &= f - \hat{f} \end{aligned} \quad (5.13)$$

where $\tilde{x}_2 = \hat{x}_2 + v_1$. $\eta_{v_1}, \eta_{v_2}, \eta_f$ are designed positive parameters. In order to guarantee the observer stability for achieving the asymptotic estimates, $\eta_{v_1}, \eta_{v_2}, \eta_f$ are defined by:

$$\eta_{v_1} = \sigma_{v_1} \|e_{x_1}\| + \varepsilon_{v_1}, \eta_{v_2} = \sigma_{v_2} \|e_{x_2}\| + \varepsilon_{v_2}, \eta_f = \sigma_f \|e_f\| + \varepsilon_f \quad (5.14)$$

where $\sigma_{v_1}, \sigma_{v_2}, \sigma_f$ are positive learning rates, and $\varepsilon_{v_1}, \varepsilon_{v_2}, \varepsilon_f$ are small positive constants.

By defining $\tilde{G}_0 = G_0(x) - G_0(\hat{x})$ and $\tilde{F} = F(x) - F(\hat{x})$, the estimation error system by subtracting (5.12) from (5.11) can be represented as

$$\begin{aligned} \dot{e}_{x_1} &= e_{x_2} - v_1 \\ \dot{e}_{x_2} &= \tilde{G}_0 + \tilde{F}f + F(\hat{x})e_f - v_2 \\ \dot{e}_f &= \dot{f} - \eta_f \text{sign}(e_f) \end{aligned} \quad (5.15)$$

By designing an appropriate sliding surface for observer and a suitable Lyapunov function, $\dot{e}_{x_1}, \dot{e}_{x_2}, \dot{e}_f$ will approach 0 during the reaching phase of the sliding mode. According to the equivalent output injection concept (Edwards et al., 2000), the estimates of x_1, x_2, f can be obtained. The detailed proof for the existence of designed SMO observer could be referred to the work of Lan (2017).

Remark 5.1 The discontinuity in the sign function will introduce high frequency chattering effects which deteriorate the performance of sliding mode observer. In order to ensure a smooth control action, the above sign function $\text{sign}(s)$ will be approximated by the sigmoid-like function as shown in (5.16), which is often referred to as pseudo-sliding (Zinober, 1990):

$$\text{sign}(s) = \frac{s}{\|s\| + \delta} \quad (5.16)$$

where δ denotes a small positive scalar.

Therefore, the SMO design parameters include $\sigma_{v_1}, \sigma_{v_2}, \sigma_f, \varepsilon_{v_1}, \varepsilon_{v_2}, \varepsilon_f, \delta$. These constant positive parameters are tuned off-line by trial and error. It is worth noting that the designed SMO with the same parameters should be effective for different incipient pitch actuator faults considered in this Chapter.

5.3.2.2 FTC Design

The faulty pitch system (5.11) can be represented as

$$\begin{aligned} \dot{x}_1 &= x_2 \\ \dot{x}_2 &= G_0(x) + w_n^2 u + F_1(x)f \end{aligned} \quad (5.17)$$

where $F_1(x) = (w_{n_0}^2 - w_{n_f}^2)x_1 + 2(\xi_0 w_{n_0} - \xi_f w_{n_f})x_2$.

After obtaining the fault information, an FTC controller is designed for the pitch actuator fault compensation (5.17), designed as

$$u = k_i \beta_r + u_f \quad (5.18)$$

where β_r is the sum of baseline collective pitch angle and the additional pitch angle from the proposed IPC strategy, u_f is the reconfigurable controller for fault compensation, and k_i is proposed to modify the reference signal β_r and hence is referred to as a "modification parameter". The designed active FTC strategy has been illustrated in Fig. 5.4.

The modification matrix k_i with the help of an asymptotic fault estimate is designed as

$$k_i = \frac{w_{n_0}^2}{\hat{w}_n^2} = \frac{w_{n_0}^2}{w_{n_0}^2 + (w_{n_f}^2 - w_{n_0}^2)\hat{f}} \quad (5.19)$$

The compensating controller u_f is proposed as

$$u_f = -\frac{F_1(\hat{x})\hat{f}}{\hat{w}_n^2} \quad (5.20)$$

where $F_1(\hat{x}) = (w_{n_0}^2 - w_{n_f}^2)\hat{x}_1 + 2(\xi_0 w_{n_0} - \xi_f w_{n_f})\hat{x}_2$. The state estimates \hat{x}_1, \hat{x}_2 and the fault estimation \hat{f} can be achieved by the proposed observer (5.12). More detailed explanation about the proposed FE-based FTC scheme can be referred to the work (Lan et al., 2018).

Clearly, as can be seen from the above, the modification parameter $k = 1$ corresponds to the fault-free case. The compensating controller u_f is active if and only if a fault f occurs. The performance of the proposed FTC system relies on the accuracy of FE action. According to the FTC performance analysis in the work (Lan et al., 2018), the proposed FTC controller (5.18) can compensate the faults effectively which enables the faulty pitch system to operate as a normal pitch system, which will be further verified in Section 5.4.2.

5.4 Simulation Results

The validity of designed FTC-IPC system is performed on the NREL 5MW turbine simulator, with the simulation step set as 0.0125s. The simulation is achieved in Matlab. Though there exists some difference when system changes from continuous to discrete time. If the simulation step is selected to be small enough, the simulation results will be very close to the reality. The simulation is performed under 1000s above-rated wind speed condition. Two stochastic and full-field turbulent wind speed flows are obtained by TurbSim (Jonkman, 2009). The first wind flow has the mean wind speed value of 18 m/s at the hub-height, with turbulence intensity 14% and vertical shear exponent 0.2, illustrated in Fig. 3.7. The second wind flow has the mean wind speed 23m/s, turbulence intensity 18%, and a vertical shear exponent of 0.2. For brevity and ease of readability, the resulting figures in Section 5.4.1 and Section 5.4.2 correspond to the first wind condition - *Wind I* (mean wind speed 18m/s) and the results under the second wind flow - *Wind II* (mean wind speed 23m/s) is just reflected in Table. 5.4 and Fig. 5.13.

5.4.1 Load Reduction in the Fault-free Case

The effectiveness of the proposed IPC systems by PI and H_∞ loop-shaping approaches have been validated for the two wind conditions (*Wind I* and *Wind II*), reflected in Table. 5.4. The time domain results of the generator power output, and the flapwise bending moments of blade 1 and the yaw moment of the hub bearing system under the *Wind I* condition are illustrated in Fig. 5.7, Table 5.4 and Fig. 5.14. The simulation results represent an up to 32% load reduction of blade 1 flapwise bending moments using PI-IPC can be achieved in the *Wind I* condition. It is shown that similar

results for load reduction by PI and H_∞ loop-shaping based IPC systems with maintaining the stable generator power output. However, from Fig. 5.6, it can be seen that there exists an extra requirement for the pitch actuator movements in the PI-IPC case (same in the H_∞ loop-shaping based IPC) to achieve the blade load reduction, which could cause potential pitch system fatigue and failure. As listed in Table 5.4, the pitch travel has increased impressively, by nearly 400%. Furthermore, from Fig. 5.7 and Fig. 5.14, the case of PI-IPC slightly outperforms the H_∞ loop-shaping based IPC case to reduce the blade flapwise bending, as well as the main bearing yaw and tilt moments. These improvements come at a cost of increased pitch motions in two wind conditions. It can be concluded that the PI-based IPC system has slightly better load mitigation results compared to the H_∞ loop-shaping based IPC case, with the designed specific controller parameters described in Section 5.3.2.

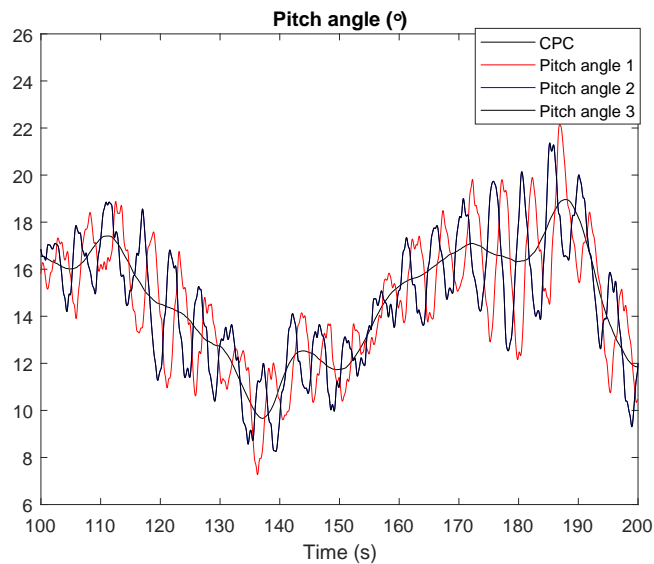


Figure 5.6: Comparison between pitch angle 1 (CPC) and the three pitch angle vaules in the PI-IPC case under the *Wind I* condition

5.4.2 Load Reduction in the Faulty Case

The situation when all 3 pitch actuator systems suffer from different incipient faults (resulting in changing dynamics) is considered here. More information of considered faults is illustrated in Table 5.3.

The pitch measurements usually suffer from disturbance and uncertainties, modelled as a zero mean white Gaussian noise with a variance of $1.0e-7$. The proposed SMO

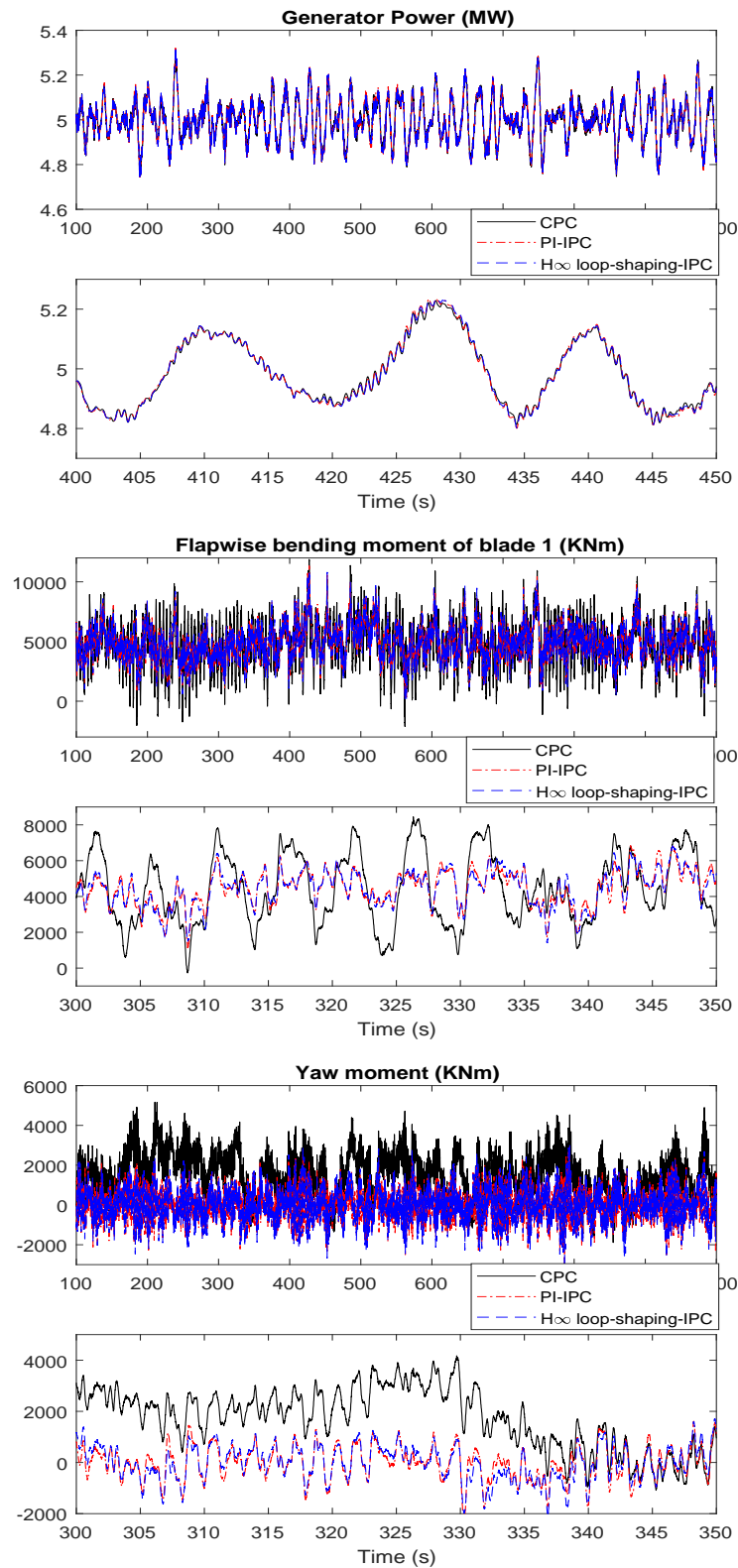


Figure 5.7: The comparison between results with CPC and two different IPC cases under the *Wind I* condition

Table 5.3: Considered incipient pitch actuator faults

Fault class	Occurrence time	Place	Type
F1	$t \in [200, 800]s$	Pitch actuator 1	Hydraulic leakage
F2	$t \in [0, 1000]s$	Pitch actuator 2	Pump wear
F3	$t \in [0, 1000]s$	Pitch actuator 3	High air content

variants are $\sigma_{v_1} = 0.3, \sigma_{v_2} = 0.2, \sigma_f = 0.1, \varepsilon_{v_1} = 0.01, \varepsilon_{v_2} = 0.01, \varepsilon_f = 0.05, \delta = 0.001$, which are tuned by trial and error. Seven different cases are considered in this Chapter. CPC denotes that only the baseline collective pitch controller is involved, PI-IPC and H-IPC are the control systems containing both CPC and the proposed IPC using PI or H_∞ loop-shaping approach. PI-IPC-f and H-IPC-f represent the PI-IPC and H-IPC cases suffering from 3 pitch actuator faults. PI-IPC-FTC and H-IPC-FTC system refer to the PI-IPC and H-IPC cases with the proposed FTC scheme.

The standard deviation (STD) knowledge of different measurements is adopted to compare the load reduction results. Moreover, the concept of absolute pitch travel ($\int_0^t |d\beta/dt| dt$) is adopted to approximate the fatigue exerted on the blade pitch system due to excessive pitching movements. Therefore, the STD of blade 1 flapwise bending moment, the STD of main bearing tilt/yaw moments and the STD of generator output power as well as the pitch travel under two different wind conditions are represented in Table 5.4. The performance calculations range from 20s to 1000s in order to avoid the start-up transients. Detailed simulation results of PI-based IPC system compared with CPC case in the fault-free and faulty cases under the *Wind I* condition are illustrated in Figs. 5.8 - 5.13. The simulation results associated with blade 1 and one of the tilt and yaw moments are presented for the sake of brevity. The comparison between results of PI-IPC and H_∞ loop-shaping approach is presented in Fig. 5.14.

Firstly, the incipient pitch actuator fault effects are explained. As we can see from Fig. 5.8 and Fig. 5.9, the dynamics of pitch system 1 represent sluggish movements during the occurrence time range of the fault F1. It is interesting to note that owing to the other 2 actuator faults (F2 & F3), pitch actuator 1 shows slow movements even with no fault present in this actuator. The pitch travel increases slightly in the faulty case, showing that the faults give rise to larger pitch actuator motion with potential actuator malfunction, after long periods of operation. Due to the undesirably slow pitching response, the pitch angles also present more deviations, which lead to an enhanced imbalance of these 3 pitch actuators. As a consequence, the increasing imbalance

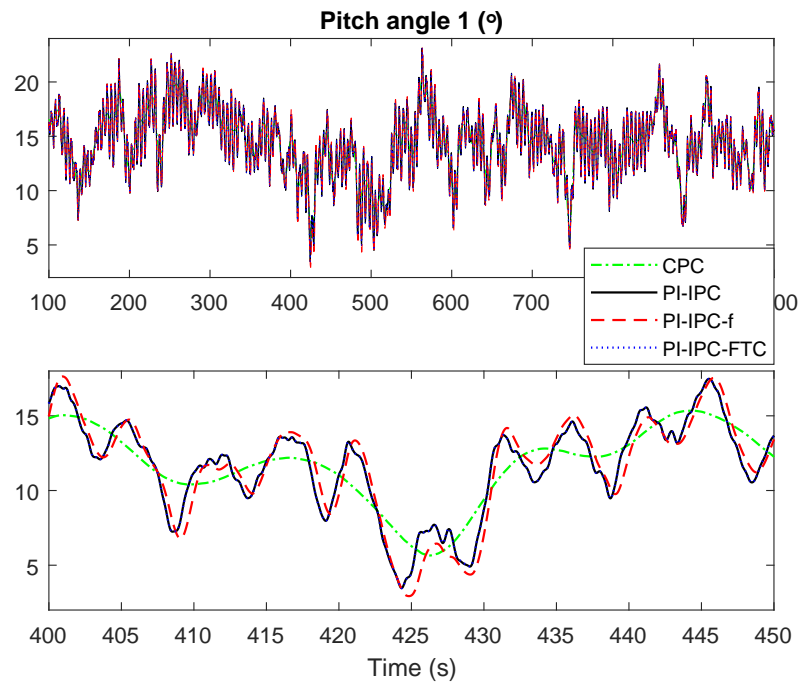
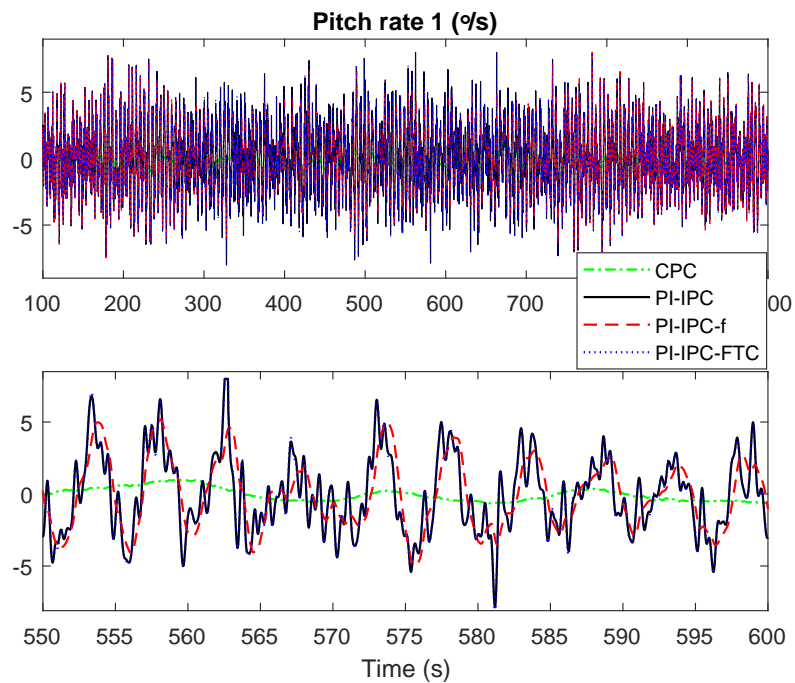
Table 5.4: Standard deviation of the simulation results in 7 cases

Parameters	CPC	PI-IPC	PI-IPC-f	PI-IPC-FTC	H-IPC	H-IPC-f	H-IPC-FTC
<i>Wind I – Mean wind speed (18m/s)</i>							
Flapwise M_1 (KN·m)	2041.1	1410.8	1533.4	1410.0	1444.2	1536.6	1420.5
Yaw (KN·m)	1107.1	746.3	788.4	745.3	807.6	823.5	766.6
Tilt (KN·m)	942.0	686.8	732.5	685.9	763.5	777.2	717.3
Gen-power (KW)	88.8	90.9	98.2	90.8	90.3	97.2	90.3
Pitch 1 travel (rad)	6.7	36.6	38.1	36.6	32.5	35.6	33.1
<i>Wind II – Mean wind speed (23m/s)</i>							
Flapwise M_1 (KN·m)	2733.4	1860.2	2040.4	1860.2	1949.3	2026.5	1879.1
Yaw (KN·m)	1759.4	1247.5	1364.5	1247.5	1382.6	1381.1	1281.0
Tilt (KN·m)	1694.7	1306.7	1416.2	1306.8	1390.4	1404.1	1300.6
Gen-power (KW)	133.5	136.7	143.2	136.7	134.8	141.0	134.8
Pitch 1 travel (rad)	7.2	52.1	54.5	52.1	42.7	45.9	43.7

between three pitch systems has amplified the asymmetric blade root loading, which implies the yaw and tilt moments are enhanced greatly, illustrated in Fig. 5.10. Hence, this amplification of flapwise bending moments results in enhanced blade fatigue as shown in Fig.5.11. Furthermore, it can be seen that the generator power fluctuation is more intense in the pitch actuator faulty case from Fig. 5.12.

From Table 5.4 and Fig. 5.14, it can be concluded that the pitch incipient actuator faults have similar negative effects on the blade asymmetric loading and generator power. However, the H_∞ loop-shaping based IPC system shows slightly better performance in maintaining the nominal load mitigation performance compared with the PI-IPC in the faulty actuator case. It is interesting to note that the H-IPC is equivalent to a form of passive FTC (to some extent) in which the effects of faults are reduced by using appropriate feedback action. See Section 3.2.3 for the definition of passive FTC.

Secondly, it is also very important that the designed FE strategy can function well with different wind fields and different actuator faults. Therefore, the proposed SMO performance is validated in both PI and H_∞ loop-shaping based IPC systems under two different wind conditions, shown in Table 5.4. It is clear that the 3 faults (F1 & F2 & F3) can be estimated very well in both IPC cases under these two wind conditions. Furthermore, the fault estimation results under the *Wind I* condition are shown in Fig. 5.13. It is shown that the fault estimation results are good in both

Figure 5.8: Pitch angle of blade 1 under the *Wind I* conditionFigure 5.9: Pitch rate of blade 1 under the *Wind I* condition

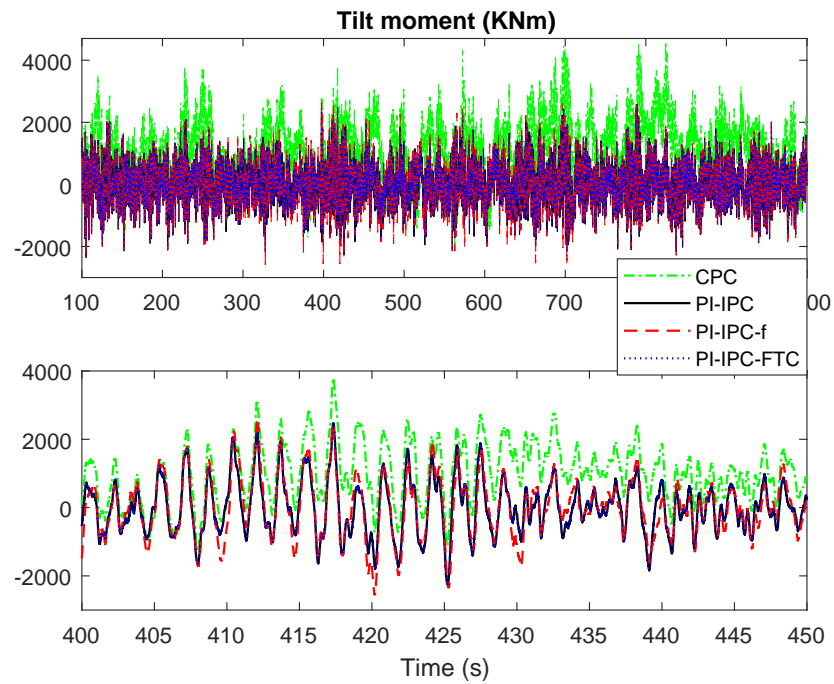


Figure 5.10: Tilt moment of main bearing system under the *Wind I* condition

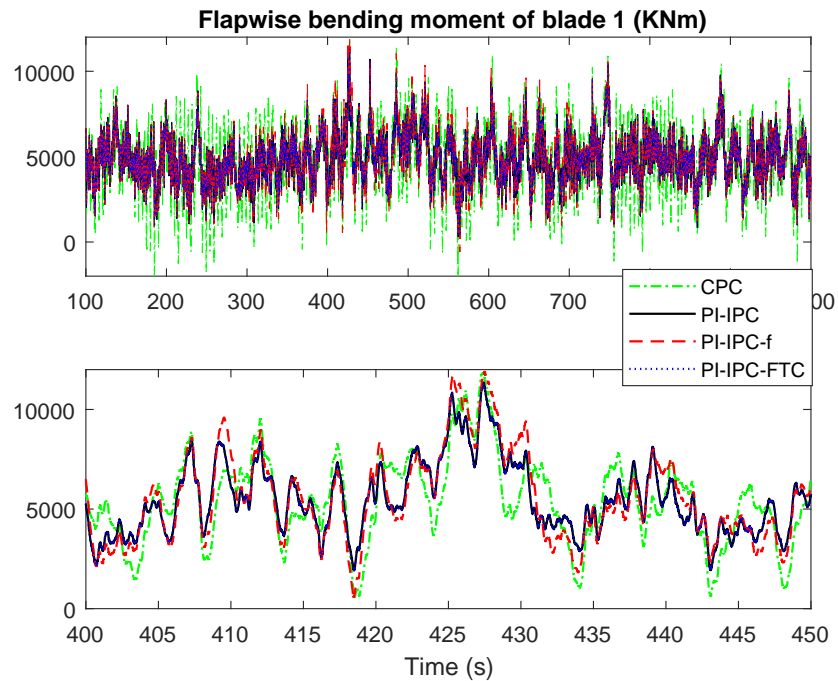


Figure 5.11: Flapwise bending moment of blade 1 under the *Wind I* condition

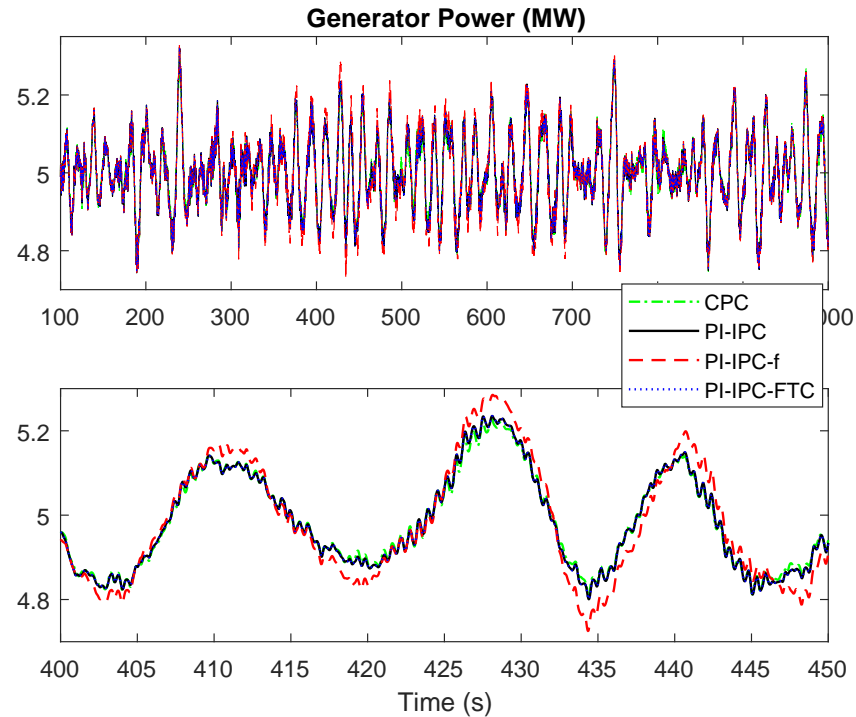


Figure 5.12: Generator power output under the *Wind I* condition

cases of PI-IPC and H-IPC with the same SMO parameters. This serves to validate the strong robustness of the proposed SMO strategy. However, it is interesting to say that the fault estimation performance in the PI-IPC case is marginally better than that in H-IPC (still acceptable), especially when the fault changes. Furthermore, the potential reason for the better fault estimation performance in the PI-based IPC case is that the PI method is dealing with the average error of the reference signal while H_∞ loop-shaping method minimizes the maximum error (i.e. the worst possible case). In this sense, the performance in the PI-based IPC is comparably stable. In conclusion, the proposed SMO parameters do not depend on the turbine operation point and are valid for the studied incipient pitch actuator faults (including high air content, hydraulic leakage, pump wear). Hence, the tuning of the SMO parameters can be made off-line.

Finally, the FE-based FTC strategy should compensate the different pitch actuator fault effects in these two wind conditions. Assisted by Table 5.4, the designed FTC strategy can recover the nominal pitch action and effectively compensate the above negative effects due to three different pitch actuator faults. With the proposed FTC controller, further fatigue damage to the blade and main bearing are thus avoided. It can be seen that the nominal pitch system performance is recovered. The

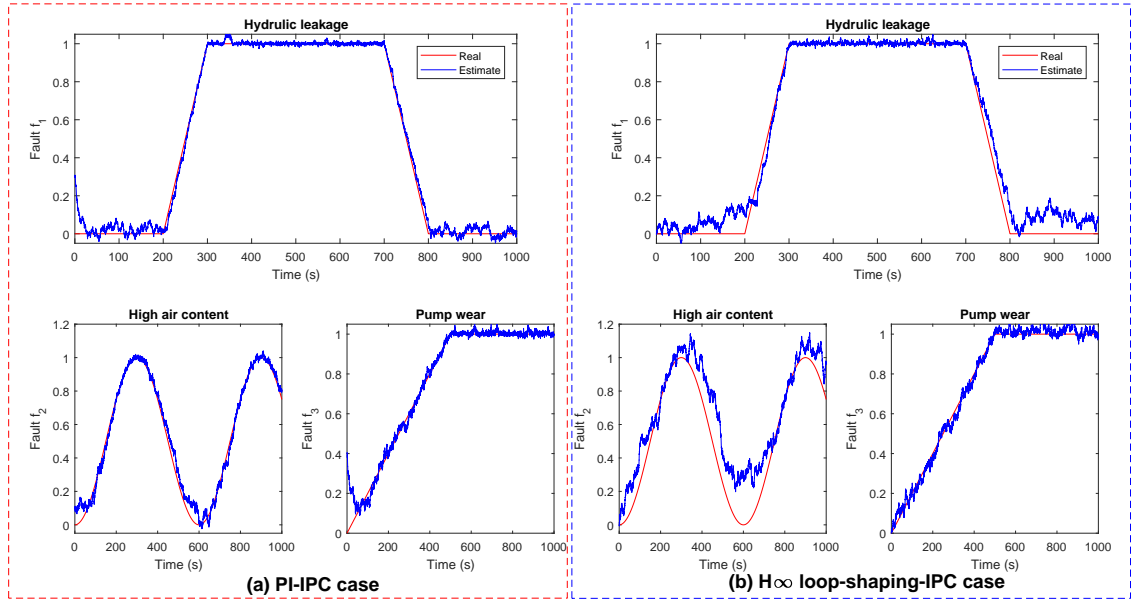


Figure 5.13: Fault estimation results of three pitch systems in the PI-IPC case and H_∞ loop-shaping-based IPC case under the *Wind I* condition

fault effects are removed from the generator output power and the imbalanced blade loads. Fig. 5.14 gives a clear comparison of the percentage performance of these two IPC system in the fault-free and pitch actuator faulty case. From Fig. 5.14, H-IPC performs marginally better in restoring the generator power performance with the help of the proposed FTC strategy compared with the PI-IPC case. Similarly, the simulation results under *Wind II* summarized in Table 5.4 verify the robustness of proposed FTC strategy.

5.5 Conclusion

In this Chapter, a robust SMO-based FTC scheme is combined with a Coleman transformation based IPC system using PI or H_∞ loop-shaping approach, verifying the effectiveness of both the FE-based FTC system and the proposed IPC system. In the meanwhile, mechanisms by which and how much the blade asymmetrical loading responds to the pitch actuator incipient faults within different IPC systems are analysed. This topic is seldom discussed in the current research about IPC system.

From the simulation results, it is concluded that the unbalanced pitch systems due to the incipient actuator faults have adverse impacts on the blade vibrations and then

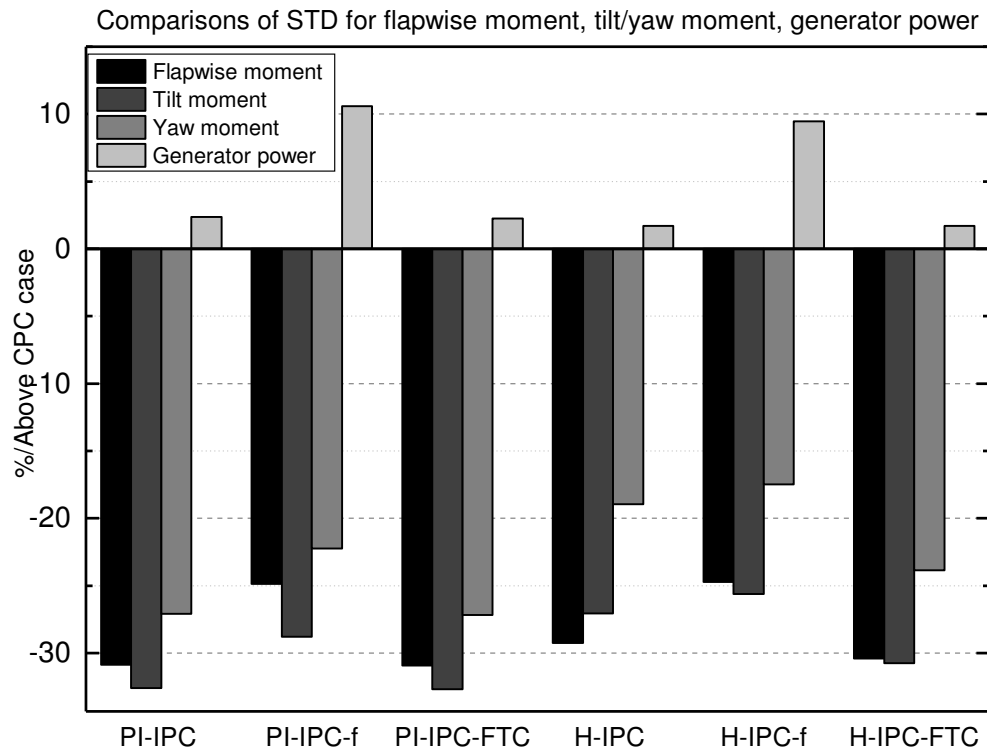


Figure 5.14: Comparison results of STD for blade 1 flapwise bending moments, main bearing tilt/yaw moments and generator power under the *Wind I* condition

deteriorate the main bearing asymmetrical loading. The proposed FTC-IPC scheme has been verified to maintain the nominal pitch system performance and compensate for the fault effects on the generator power and unbalanced loading in the presence of pitch actuator faults. The robustness of designed FE based FTC strategy is validated in different wind operating conditions and for various IPC scenarios. Combined with the previous study on implementing the proposed FTC scheme within the CPC system (Lan et al., 2018), it is concluded that this adaptive SMO-based FTC system can be a universal FTC strategy for offshore wind turbine pitch systems. It can be further deducted that the PI-based IPC strategy performs better in the fault-free case, but H_∞ loop-shaping based IPC strategy performs better in terms of maintaining its own load mitigation performance in the faulty case and also in the case with fault compensation by designed FE-based FTC system. It is worth noting that H_∞ loop-shaping based IPC strategy has more potential to keep good load reduction results compared with PI-based IPC.

However, this Chapter only considers the traditional IPC system for blade load reduction and the incipient dynamic changing faults of a pitch actuator system. On the one

hand, given that the inherent couplings between blade and tower system, it is reasonable to investigate a multivariable control-based IPC system for both blade and tower load mitigation. On the other hand, pitch sensors also suffer from different faults which exert non-negligible influence on the IPC load reduction performance, requires the use of a suitable FTC system. Chapter 6 is motivated by this study and continues to work on these problems.

Chapter 6

Rotor and Tower Structural Load Mitigation in Presence of Pitch Sensor Fault

6.1 Introduction

It has been shown that the maintenance cost for tower and foundations contributes up to 12% of the cost of energy due to the harsh sea conditions (Malcolm and Hansen, 2006). As summarized in Chapter 5, blade fatigue load mitigation and tower vibration control turn out to be important to reduce the maintenance and operation costs as well as reducing fatigue and increasing expected lifetime. Furthermore, given that pitch sensor faults can cause negative effects on the pitch system performance (especially individual pitch control, IPC), physical redundancy and fault-tolerant control (FTC) scheme for wind turbine (WT) pitch system is strongly suggested. Chapter 5 focusses on the load mitigation problem together with FTC for the rotor system. However, this Chapter is an extension of the idea of considering all the "fault effects" together acting in the rotor and tower system including the blade & tower bending reduction and pitch sensor fault compensation, which is introduced in Section 1.4.1 and Section 5.1.

Extensive research has been conducted to suppress the tower fore-aft and side-to-side vibrations (Wright et al., 2007; Perrone and Kühn, 2015; Kumar et al., 2016a). A common approach for achieving the tower load alleviation is to modulate the collective blade pitch angle (CPC) based on the tower acceleration measurements (Bossanyi, 2000). The tower structural bending moments can be compensated by additional col-

lective pitch angle variations occurring at a higher frequency (frequency band depending on the tower structure natural frequency). In Evans et al. (2015), a robust model predictive control system is designed for the fore-aft tower damping of WTs. Good simulation results for the reduction of tower base bending moments is achieved by a passive viscous damper system in Carcangiu et al. (2011). An active generator torque controller with the tower fore-aft vibration measurements for tower loads mitigation is represented by Zhang et al. (2014b). However, as shown in Leithead et al. (2004), due to couplings between the blade flap mode and tower mode, a simple feedback signal proportional to the tower acceleration can be counter-productive, which increases the tower fatigue loading rather than the reduction.

It is clear that a general limitation for the currently understood load mitigation schemes is that the blade asymmetrical loading and the tower bending are handled using separate controllers. The goal of the active tower damping controller is to reduce the tower fluctuations. However, this approach fails to exert an effective impact on the blade fatigue loading alleviation, or even make it worse (Darrow et al., 2011; Wright et al., 2007; Namik and Stol, 2010). On the other hand, the fatigue loading on the rotor blades and yaw bearings are reduced by the designed IPC system, while it comes with no effective tower vibration mitigation. The tower loading can even be enhanced (Bossanyi et al., 2013; Chen and Stol, 2014). Therefore, it is very appealing to integrate the tower damping and blade load reduction into one advanced multi-input multi-output (MIMO) control system.

However, the above load mitigation strategy inevitably exacerbates the pitch system movements, which requires pitch actuators to provide extra damping rate to alleviate the unbalanced loading. It is important to smooth the gap between the requirement for structural loading mitigation and heavy pitch commands. In other words, the negative effects of the tower & blade load reduction need to be reduced. It is thus important to consider the negative effect that pitch sensor faults can have on the load mitigation system performance. An FTC strategy for achieving this is described in this Chapter which whilst based on the work of Chapter 5 nevertheless encapsulates some modifications to account for (i) the pitch sensor faults and (ii) the tower bending.

In this Chapter the pitch position sensor faults are shown to have a significant effect on Region 3 wind turbine performance. These sensor faults will affect the pitch position reference if not handled correctly since the pitch controller is using the measured pitch

position (Naik, 2017). Several research papers are proposed to deal with the pitch sensor faults. In Shi and Patton (2015), the faults considered are estimated by an extended state observer to achieve FTC within a linear parameter-varying (LPV) wind turbine system description. For that study an offshore WT generator speed/pitch sensor faults and generator torque fault are considered. Another paper (Chen et al., 2013) presents an adaptive observer to obtain the fault estimation of pitch sensor fixed fault together with hydraulic system component fault in the presence of disturbance. The model used for both studies is the WT benchmark model of (Odgaard et al., 2009). It is clear that the fault estimation signals from the above two strategies suffer from considerable errors, mostly to do with the fact that the problem descriptions are too general, i.e. are not focussed closely enough on the actual WT problem. In other words insufficient care has been taken to include the true wind induced fluctuations. In this thesis the FAST software Turbsim is included to give a more faithful representation of the effect of wind speed variations and their impact on measurement noise (see Section 2.2 for further explanation). In Cho et al. (2016), a model-based fault detection scheme is designed for WT pitch system fault scenarios by using a Kalman filter for residual generation. Furthermore, it describes an unknown input observer (UIO) strategy to detect and accommodate the WT rotor and generator sensor faults in Odgaard and Stoustrup (2010). However, the above two papers fail to provide useful information about the fault magnitude, which is deemed to be an inadequacy of their work. Furthermore, a robust fault reconstruction strategy for the simultaneous pitch system faults using a modified sliding mode observer is shown to have good fault estimation accuracy in the work (Rahnavard et al., 2019). A similar fault-tolerant tracking control system with a descriptor sliding mode observer for simultaneous WT pitch actuator/sensor fault estimation and compensation is proposed by Wang et al. (2017).

None of the above studies make use of physical redundancy among the sensors. In the realistic WT system application this redundancy is present. The above studies are verified only for the so-called "baseline" pitch control case and do not consider the IPC strategy used in this thesis. The significance of this is that these studies do not consider the mutual effects between pitch sensor faults and the IPC system. These studies also do not consider cases of total sensor failures and multiplicative (component) and hydraulic faults are also not considered (e.g. oil leaks, pump wear, high air content). However, the hydraulic fault types are considered in Chapter 5. This Chapter actually considers 4 fault types (Bias sensor, stuck sensor, sensor failure [total fault], multiplicative - a partial sensor fault), see Section 6.2.2 for more information.

This Chapter addresses a multi-objective design strategy: the primary goal is to propose a linear quadratic regulator (LQR)-based IPC control strategy for simultaneously reducing the blade and tower loading. A further task is to design a robust UIO-based FE system for accurate sensor fault estimation in the presence of measurement noise and unmodelled system uncertainties, which are decoupled and attenuated by the H_∞ optimization. The hardware redundancy of pitch sensor system is considered here. The fault estimates are used for pitch sensor fault compensation, completing the design of pitch sensor FTC scheme. The ultimate purpose is to combine the LQR-based IPC system and the sensor FTC scheme together, obtaining a more comprehensive interactive evaluation of the proposed strategy, which aims to enhance the reliability of WTs.

The remainder of this Chapter is summarised as follows. The WT structural load analysis and the pitch system mathematical modelling with different sensor faults are presented in Section 6.2. Following this, Section 6.3 illustrates the proposed strategies including the LQR-based IPC approach for both blade and tower loading mitigation and a robust fault estimation method using UIO and then the pitch sensor fault effects are compensated by a FTC scheme. Finally, the detailed simulation results and conclusions are illustrated in Section 6.4 and Section 6.5, respectively.

6.2 Problem Formulation

6.2.1 Wind Turbine Structural Load Analysis

From Fig. 2.4 in Section 2.4, it is shown that tower fore-aft bending couples with the blade flapwise bending moments as well as the tower side-side bending interconnects with the blade edgewise bending moments. The tower fore-aft and side-side bending moments contribute to most of the tower bottom fatigue damage, of which the contribution of tower fore-aft bending exceeds 99% (Duckwitz and Shan, 2014). Therefore, the analysis in this Chapter focuses on the damping of 1st flapwise bending moments and 1st fore-aft tower vibrations together using multivariable control design.

Generally, different control structures (in terms of choice of actuators, e.g. pitch only or combined pitch and generator) result in various combinations of effective forces acting on the tower top. Table. 6.1 and Fig. 6.1 show the various possibilities of WT structural load mitigation, depending on actuator strategies:

Table 6.1: Different variants for structural load mitigation

Controlled Variant	Blade Flapwise	Tower Fore-aft	Tower Side-side
Collective Pitch Angle	×	✓	×
Individual Pitch Angle	✓	✓	✓
Generator Torque	×	×	✓

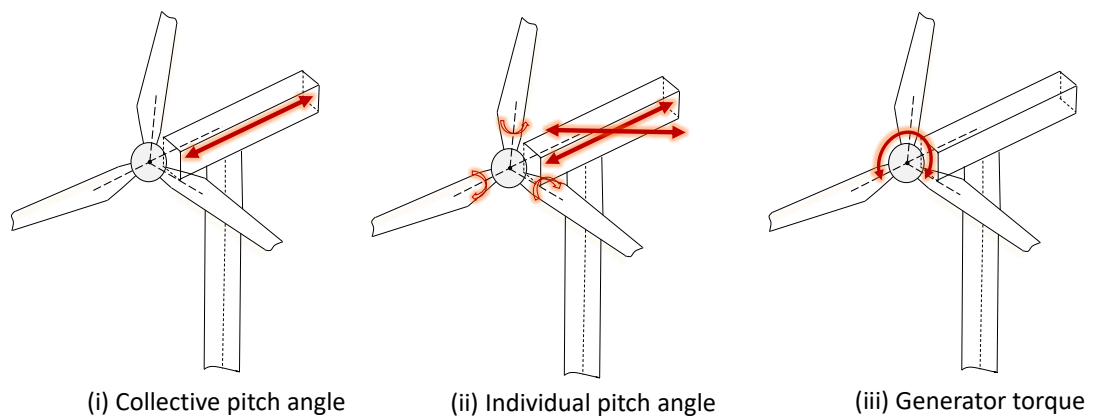


Figure 6.1: Effective forces on the tower top for structural load mitigation (Fischer and Shan, 2013)

An extra generator torque can be used to mitigate the tower side-side mode from the tower side-side acceleration. The most general approach for the standard tower load mitigation controller is to design a decentralized feedback loop with the measured tower top fore-aft oscillations, this is referred to as active tower damping (Shan et al., 2013) (see more information in Section 2.4).

From Table. 6.1 and Fig. 6.1, we can see that the traditional active tower damping for tower fore-aft bending moments is achieved by obtaining an additional collective pitch angle from the measured tower fore-aft acceleration. The proposed controller output is an additional collective pitch reference, complementary and analogous to the standard pitch angle command from CPC. The effectiveness of this approach requires (i) the tower feedback control loop should be decoupled from the CPC loop, and (ii) the tower acceleration signal should contain only tower fore-aft mode (Leithead and Dominguez, 2005). Some success of tower fore-aft bending alleviation using this method is shown in (Bossanyi, 2000; Wright and Fingersh, 2008), whereby it is probably because of smaller WT used where the couplings between the turbine blade flap motion and the tower fore-aft motion are less significant.

Nonetheless, with the increasing height of tower for multi-megawatt offshore WTs, the couplings between the blade flap motion and the tower fore-aft motion become more impressive, making it difficult to achieve good results of tower mitigation (Mohammadi et al., 2018). It turns out to be important to design a multivariable control strategy that can achieve both the blade load reduction and tower fore-aft loading mitigation. Moreover, according to Table. 6.1 and Fig. 6.1, individual pitch control can provide three individual pitch angles which can deal with the first blade flapwise bending moment, first tower fore-aft and tower side-side bending moments together by using the feedback from the useful measurements including the tower top fore-aft and side-side accelerations and flapwise bending moments. Therefore, this Chapter focuses on proposing a multivariable IPC scheme for both tower fore-aft bending load reduction and blade flapwise bending moments together. It is worth noting that the frequency band of the extra pitch angle fluctuations for load alleviation should be kept separate from the bandwidth of the generator speed control loops (CPC).

6.2.2 Pitch System Modelling with Sensor Faults

The WT pitch actuator is adjusted by an internal pitch controller (CPC, or the combination of CPC and IPC) and equipped with pitch sensors for the end pitch angle position feedback of rotor blades. Using the information from sensors (see Fig. 1.4), the pitch control system guarantees that each rotor blade is in the reference position, thereby completing the closed-loop control loop. Pitch sensors require a high level of reliability (through redundancy) and should provide accurate blade position feedback, given that the offshore WTs are subject to the challenging climatic circumstance and constantly changing wind conditions.

Potential pitch sensor faults are caused by a combination of (i) blade pitch bearing maladjustment, (ii) excessive dust on the digital encoder disk, (iii) unreasonable temperature (iv) humidity variations and (v) inaccurate calibration (Cho et al., 2016). These sensor faults will result in incorrect pitch position readings, further exerting bad effects on the pitch control system. The pitch control system is critical in this role as the optimal pitch reference is based on reliable pitch position measurements. If the sensor faults are not handled correctly the WT closed-loop dynamics and stability will be affected. Poor closed-loop action and decreased stability will in turn induce increased load effects. Hence, the choice of appropriate FTC scheme considering pitch sensor faults will have a significant role in enhancing the WT sustainability.

As summarised in Section 6.1, four different types of sensor faults are considered and illustrated as follows:

- *Bias sensor fault.* This is a common drift fault for analogue sensors belonging to the additive type. The measured sensor reading has an extra constant or time-varying offset caused by sensor temperature variations or calibration issues.
- *Stuck with fixed sensor fault.* The sensor output becomes stuck at a constant value and the reading remains fixed after this fault occurs.
- *Total sensor fault.* This is referred to as a hard sensor fault, which is a form of catastrophic system fault or "failure". A sensor fault manifests itself as a sudden cessation of operation, maintaining a constant zero output, which is often caused by electrical issues (e.g. loss of contact or broken wires) (Heredia et al., 2008).
- *Multiplicative-type (partial) sensor fault.* A gain reduction acts on the nominal sensor output and thus the sensor measurement is scaled.

Each hydraulic pitch actuator system is modelled as a second-order system (see Section 2.2.2). The pitch sensor system in the fault-free condition is modelled as:

$$\beta_m(t) = \beta(t) + d_s(t) \quad (6.1)$$

where $d_s(t)$ denotes the measurement noise.

The bias sensor fault is illustrated by adding an additional term β_{bias} to the measured output

$$\beta_m(t) = \beta(t) + \beta_{bias}(t) + d_s(t) \quad (6.2)$$

A fixed sensor fault means that the measured sensor output maintains a constant value β_{fixed} , described as

$$\beta_m(t) = \beta_{fixed} + d_s(t) \quad (6.3)$$

The total sensor fault is modelled as:

$$\beta_m(t) = \beta(t) - \beta(t) + d_s(t) = d_s(t) \quad (6.4)$$

The multiplicative sensor fault with gain f is defined as:

$$\beta_m(t) = f\beta(t) + d_s(t) = \beta(t) + (f - 1)\beta(t) + d_s(t) \quad (6.5)$$

In this study, the hardware redundancy of two sensors for each pitch system is considered to test the potential of designed FE-based FTC system. The measurement of each rotor blade is considered as an average of the two existing pitch sensors. Considering the system modelling uncertainty d , with measurement noise d_s (for both sensors 1 & 2, therefore $d_s \in 6 \times 1$) and sensor faults f_s , three pitch actuator systems (2.2) can be modelled as:

$$\begin{aligned}
 \dot{x}(t) &= Ax(t) + Bu(t) + Dd(t) \\
 y_{m_1}(t) &= Cx(t) + F_s f_s(t) + E_{s_1} d_s(t) \\
 y_{m_2}(t) &= Cx(t) + E_{s_2} d_s(t) \\
 y_m(t) &= \frac{1}{2}(y_{m_1}(t) + y_{m_2}(t)) \\
 &= Cx(t) + \frac{1}{2}F_s f_s(t) + E_s d_s(t)
 \end{aligned} \tag{6.6}$$

where

$$f_s(t) = \begin{cases} \beta_{bias}, & \text{Biased fault} \\ -\beta(t) + \beta_{fixed}, & \text{Fixed output} \\ -\beta(t), & \text{Total failure} \\ (f-1)\beta(t), & \text{Multiplicative fault} \end{cases} \tag{6.7}$$

where $x \in R^n$, $u \in R^m$ and $y \in R^p$ represent the state matrix, control inputs and system outputs, respectively. $d \in R^l$ represents a combined effect of unknown disturbance and modelling uncertainty. $f_s \in R^s$ and $d_s \in R^r$ denote assumed sensor faults and measurement noise, respectively. The constant matrices $A \in R^{n \times n}$, $B \in R^{n \times m}$, $D \in R^{n \times l}$, $C \in R^{p \times n}$, $F_s \in R^{p \times s}$, and the sensor noise distribution matrices $E_{s_{1,2}} \in R^{p \times r}$ are known with $n = 6$, $m = 3$, $l = 1$, $p = 3$, $s = 3$, $r = 6$. The measurement noise is assumed to be the same for each pitch sensor. Therefore, $E_s = E_{s_1}$ is used in $y_m(t)$ after the average of these two measurements. The details are illustrated as:

$$A = \begin{bmatrix} 0 & 0 & 0 & 1 & 0 & 0 \\ 0 & 0 & 0 & 0 & 1 & 0 \\ 0 & 0 & 0 & 0 & 0 & 1 \\ -123.43 & 0 & 0 & -13.332 & 0 & 0 \\ 0 & -123.43 & 0 & 0 & -13.332 & 0 \\ 0 & 0 & -123.43 & 0 & 0 & -13.332 \end{bmatrix},$$

$$B = \begin{bmatrix} 0 & 0 & 0 \\ 0 & 0 & 0 \\ 0 & 0 & 0 \\ 123.43 & 0 & 0 \\ 0 & 123.43 & 0 \\ 0 & 0 & 123.43 \end{bmatrix}, \quad C = \begin{bmatrix} 1 & 0 & 0 & 0 & 0 & 0 \\ 0 & 1 & 0 & 0 & 0 & 0 \\ 0 & 0 & 1 & 0 & 0 & 0 \end{bmatrix}, \quad D = \begin{bmatrix} 0.1 \\ 0.1 \\ 0.1 \\ 0.1 \\ 0.1 \\ 0.1 \end{bmatrix},$$

$$F_s = \begin{bmatrix} 1 & 0 & 0 \\ 0 & 1 & 0 \\ 0 & 0 & 1 \end{bmatrix}, \quad E_s = \begin{bmatrix} 1 & 0 & 0 & 0 & 0 & 0 \\ 0 & 1 & 0 & 0 & 0 & 0 \\ 0 & 0 & 1 & 0 & 0 & 0 \end{bmatrix}$$

It is assumed that the pitch system dynamics (6.6) satisfy the following assumptions to guarantee the feasibility of the designed UIO (in Section 6.3.2).

Assumption 6.1 The pair (A,C) is observable and the pair (A,B) is controllable.

Assumption 6.2 The faults f_s are assumed to be differentiable and thus can be extended into a new (augmented) system state. $f_s = 0$ stands for a fault-free case. Unknown input d is supposed to be bounded by $\mathcal{L}_2[0, \infty)$.

Given that the closed-loop pitch actuator is modelled as a linear system, the error caused by a fault on the blade pitch position measurement moves to the corresponding pitch actuator reference. Therefore, the sensor faults can be modelled as changes in the blade pitch references accordingly (Odgaard et al., 2013), illustrated as:

$$\beta_{r,f,i} = \beta_{r,i} - \frac{\Delta\beta_{m,1} + \Delta\beta_{m,2}}{2}, \quad \Delta\beta_{m,j} = \beta_{m,j} - \beta_{mf,j} \quad (6.8)$$

where $i \in \{1,2,3\}$, $j \in \{1,2\}$, $\beta_{r,f,i}$ is the new pitch reference angle containing the sensor fault, $\beta_{r,i}$ is the nominal pitch reference, $\Delta\beta_{m,j}$ means the change of pitch angle, $\beta_{m,j}$ is the nominal pitch angle measurement, $\beta_{mf,j}$ is the pitch angle measurement with the pitch sensor fault.

In this Chapter, one of the two sensors of the pitch system 1 which suffers from sensor faults is studied. The final pitch system with the considered sensor fault f_s is represented in Fig. 6.2.

The above analysis completes the following problem.

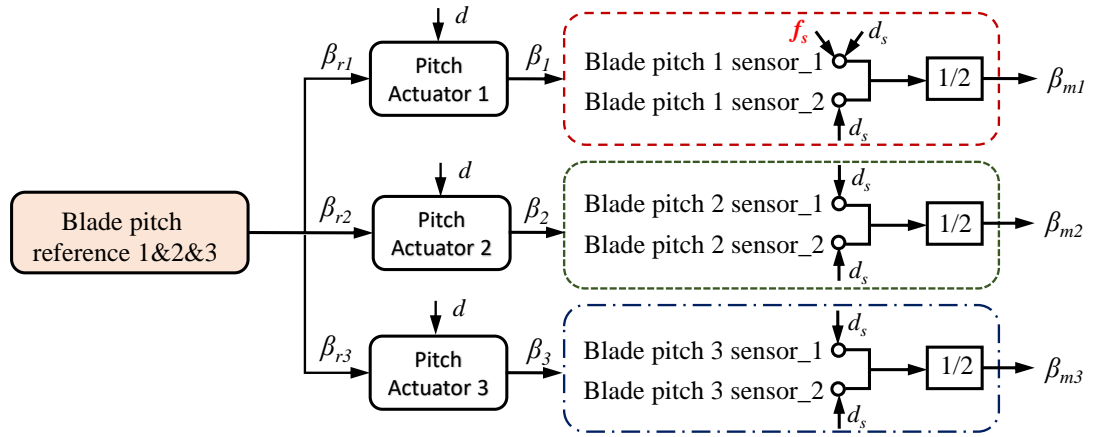


Figure 6.2: Considered pitch system with sensor redundancy

Problem 6.1 Given the pitch system (6.6) subject to bounded sensor faults, unknown uncertainties and measurement noise, a robust FE-based FTC strategy is required to obtain the fault knowledge and compensate for the sensor fault effects to recover the nominal pitch system performance in the event of sensor faults.

6.3 Proposed strategy

In this Section, the framework of the proposed UIO and FTC compensation strategy is shown in Fig. 6.3, which includes: (i) a baseline collective pitch control (CPC) for generator power output regulation (see Section 2.2.4), and (ii) an LQR-based individual pitch controller (IPC) for both blade and tower load mitigation, and (iii) a robust UIO-based fault tolerant strategy for pitch sensor fault estimation & compensation with unknown disturbance and measurement noise. For better comparison, the PI-based IPC controller designed in Section 5.3.1 is also considered.

6.3.1 LQR-based IPC for Blade and Tower Load Mitigation

The FAST linearisation property is carried out under a specific wind condition to achieve the reduced-order linear wind turbine model from the nonlinear FAST 5MW NREL wind turbine simulator for controller design (see Section 4.2.1). Here, the linearized wind turbine is obtained under the wind condition with a hub-height mean

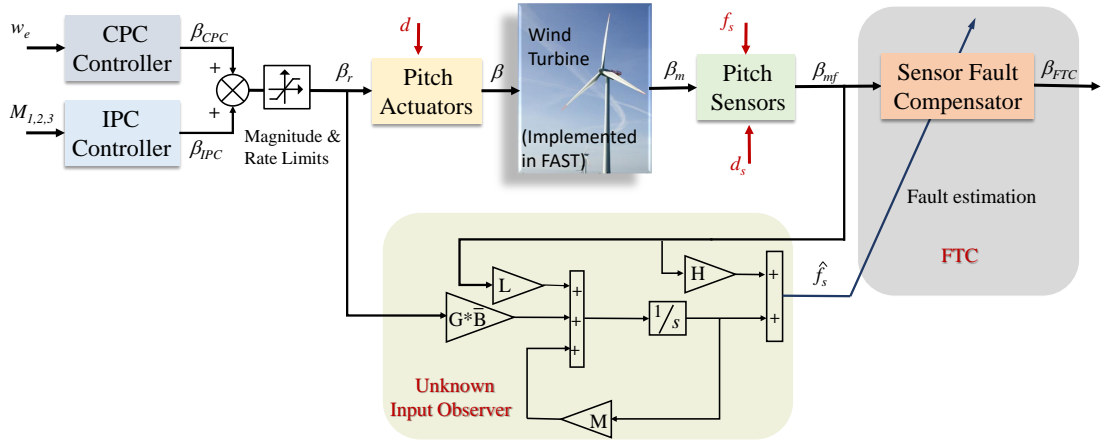


Figure 6.3: Proposed UIO framework

value 18 m/s and a vertical shear exponent of 0.2. Six degrees of freedom (DOFs) including generator rotational flexibility, drive-train rotational mode, first blade flapwise mode for each blade and first fore-aft tower bending mode are activated. Five outputs including generator speed, flapwise bending moments (mean, sine and cosine components) and tower fore-aft acceleration are selected as the system outputs. Three individual pitch angles are set as the inputs of this WT system.

The LQR controller is applicable and efficient for multivariable linearised systems, which aims to optimize a controller by optimizing a specific quadratic cost function with well-designed weighting factors (Duriez et al., 2017). The objective function J is typically a combination of perturbations of desired states and input variables, parametrized by two weighting matrices (i.e. Q and R). The LQR controller attempts to achieve the optimal control inputs by deriving the algebraic Riccati equation based on the state-space linear model (Li et al., 2008). In this Chapter, the LQR controller with assumed full-state feedback is proposed to mitigate the tower 1st fore-aft bending moment and 1st blade flapwise bending moment simultaneously as well as maintain the maximum generator power output.

Based on the linear WT model from the FAST linearization process, defined as

$$\begin{aligned} \dot{x}(t) &= A_s x(t) + B_s u(t) \quad t \geq 0, x(0) = x_0 \\ y(t) &= C_s x(t) \end{aligned} \quad (6.9)$$

where $x(t)$, $u(t)$ represent the system state and input vector, respectively. $A_s \in \mathbb{R}^{11 \times 11}$,

$B_s \in \mathbb{R}^{11 \times 3}$, $C_s \in \mathbb{R}^{5 \times 11}$ are the related wind turbine system matrices. The azimuth angle state is ignored here. The definition of 11 state variables is shown in Table. 6.2:

Table 6.2: Definition of 11 state variables

State variable	Definition
x_1	Displacement of 1 st tower fore-aft bending mode DOF (m)
x_2	Displacement of drivetrain rotational flexibility DOF (rad)
x_3	Displacement of 1 st flapwise bending mode DOF of blade 1 (m)
x_4	Displacement of 1 st flapwise bending mode DOF of blade 2 (m)
x_5	Displacement of 1 st flapwise bending mode DOF of blade 3 (m)
x_6	Velocity of 1 st tower fore-aft bending mode DOF (m/s)
x_7	Velocity of variable speed generator DOF (rad/s)
x_8	Velocity of drivetrain rotational flexibility DOF (rad/s)
x_9	Velocity of 1 st flapwise bending mode DOF of blade 1 (m/s)
x_{10}	Velocity of 1 st flapwise bending mode DOF of blade 2 (m/s)
x_{11}	Velocity of 1 st flapwise bending mode DOF of blade 3 (m/s)

These state variables are assumed known here, which are not always measurable in reality and can be estimated by a well-designed state estimator. The pair (A_s, B_s) is controllable. It is required to find the optimal state feedback control law matrix $K \in \mathbb{R}^{3 \times 11}$,

$$u(t) = -Kx(t) \quad (6.10)$$

which can ensure the closed-loop system robustly stable and minimize the infinite-time quadratic objective function, shown as

$$J(t) = \int_0^{\infty} [x^T(t)Qx(t) + u^T(t)Ru(t)]dt \quad (6.11)$$

The selection of Q and R matrix plays a significant role in deciding the performance of designed load reduction controller. Q is a positive semi-definite diagonal matrix that evaluates the penalty for system state deviations from equilibrium, here $Q = C_s^T Q_1 C_s$ is selected to penalize the system output perturbations from the reference values. R is usually a positive definite matrix that adjusts the degree of emphasis on the control input (Wright, 2004). The larger these parameter values are, the more these signals are penalized. If the parameters in Q are larger, the accurate state (or output) regulation

turns out to be more significant and the system allows for more aggressive control, and vice versa. The following LQR design steps are implemented to achieve the optimal feedback law through pole placement (Kumar and Jerome, 2013):

Step 1: Solve the associated Algebraic Riccati Equation (ARE), return the solution S

$$A_s^T S + SA_s - SB_s R^{-1} B_s^T S + Q = 0 \quad (6.12)$$

Step 2: The optimal control matrix K is derived from S using

$$K = R^{-1} B_s^T S \quad (6.13)$$

Step 3: Hence from (6.10) and (6.13), the optimal full-state feedback control law for the WT system is

$$u^*(t) = -R^{-1} B_s^T S x(t) \quad (6.14)$$

Different weights Q_1 and R are tuned to obtain the optimal control performance by trial and error. $Q_1 = \text{blkdiag}(0.1, 1e-8, 6e-8, 6e-8, 0.4)$, $R = \text{blkdiag}(100, 100, 100)$ are selected here. In this case, the open-loop and closed-loop pole locations using LQR of the wind turbine system (6.9) are shown in Table. 6.3 and Fig. 6.4:

Table 6.3: Open-loop & Closed-loop pole locations

DOF	Open-loop Poles (rad/s)	Closed-loop Poles (rad/s)
Generator speed	-0.242	-0.382
Drive-train 1 st torsion	$-0.734 \pm 14.077i$	$-0.737 \pm 14.073i$
1 st Flapwise blade mean value	$-2.589 \pm 4.046i$	$-3.1057 \pm 4.475i$
1 st Flapwise blade sine component	$-2.654 \pm 4.9924i$	$-3.687 \pm 5.737i$
1 st Flapwise blade cosine component	$-2.644 \pm 2.500i$	$-3.6763 \pm 3.234i$
Tower 1 st fore-aft	$-0.149 \pm 2.088i$	$-0.516 \pm 1.877i$

This results in increased damping for the tower first fore-aft motion and blade first bending motion as well as generator speed output, given that the corresponding real parts of these poles move further to the left part of the complex plane. Only a small weighting is put on the output that related with the drive-train torsion. From the tuning procedure, it can be found that there exists strong couplings between the blade first flapwise mean value and the tower first fore-aft bending motion, which should be dealt with carefully.

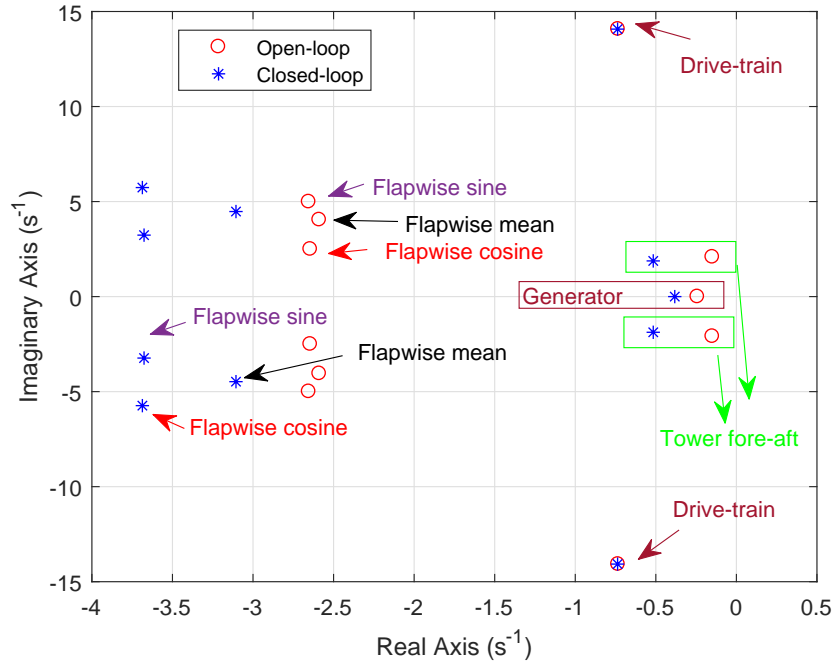


Figure 6.4: Pole locations of the open-loop and closed-loop system (with designed LQR controller) of the 5MW NREL wind turbine

6.3.2 FE-based FTC using Robust UIO

To solve *Problem 6.1*, the 1st order derivative of the sensor faults \dot{f}_s is augmented as a disturbance and the time index is omitted for simplicity, thus completing the extended pitch system as:

$$\begin{aligned}\dot{\bar{x}} &= \bar{A}\bar{x} + \bar{B}u + \bar{D}\bar{d} \\ y &= \bar{C}\bar{x} + E_s d_s\end{aligned}\quad (6.15)$$

where

$$\bar{A} = \begin{bmatrix} A & \mathbf{0} \\ \mathbf{0} & \mathbf{0} \end{bmatrix}, \quad \bar{B} = \begin{bmatrix} B \\ \mathbf{0} \end{bmatrix}, \quad \bar{D} = \begin{bmatrix} D & \mathbf{0} \\ \mathbf{0} & I \end{bmatrix}, \quad \bar{C} = \begin{bmatrix} C & \frac{1}{2}F_s \end{bmatrix}$$

$$\bar{x} = \begin{bmatrix} x \\ f_s \end{bmatrix}, \quad \bar{d} = \begin{bmatrix} d \\ \dot{f}_s \end{bmatrix}\quad (6.16)$$

where $\bar{x} \in \mathbb{R}^{n+s}$, $u \in \mathbb{R}^m$, $y \in \mathbb{R}^p$, $\bar{d} \in \mathbb{R}^{l+s}$ and $\bar{A} \in \mathbb{R}^{(n+s) \times (n+s)}$, $\bar{B} \in \mathbb{R}^{(n+s) \times m}$, $\bar{D} \in \mathbb{R}^{n \times (l+s)}$, $\bar{C} \in \mathbb{R}^{p \times (n+s)}$.

Remark 6.1 For all $s \in \mathbb{C}$ with $s \neq 0$, $\text{Re}(s) \geq 0$, due to (A,C) is observable,

$$\text{rank} \begin{bmatrix} sI_n - A \\ C \end{bmatrix} = n, \quad (6.17)$$

therefore, for the augmented system 6.15,

$$\text{rank} \begin{bmatrix} sI_{n+s} - \bar{A} \\ \bar{C} \end{bmatrix} = \text{rank} \begin{bmatrix} sI_n - A & 0 \\ 0 & sI_s \\ C & F_s \end{bmatrix} = n + s \quad (6.18)$$

Thus, system (6.15) is observable.

To estimate the augmented state vector \bar{x} , the following UIO structure (Chen et al., 1996) is proposed.

$$\begin{aligned} \dot{z} &= Mz + G\bar{B}u + Ly \\ \hat{x} &= z + Hy \end{aligned} \quad (6.19)$$

where $z \in \mathbb{R}^{n+s}$ denotes observer states, and $\hat{x} \in \mathbb{R}^{n+s}$ is the estimate of \bar{x} . $M \in \mathbb{R}^{(n+s) \times (n+s)}$, $G \in \mathbb{R}^{(n+s) \times (n+s)}$, $L \in \mathbb{R}^{(n+s) \times p}$ and $H \in \mathbb{R}^{(n+s) \times p}$ are the designed UIO matrices.

Definition 6.1 The observer (6.19) is termed as a robust and stable UIO for the pitch system (6.15), if the state estimation error $e_x = \bar{x} - \hat{x}$ asymptotically approaches zero during the finite time, in the presence of bounded unknown system disturbance, measurement noise and sensor faults.

Using (6.15) and (6.19), the estimation error dynamics are expressed by:

$$\begin{aligned} \dot{e}_x &= (\Xi \bar{A} - L_1 \bar{C})e_x \\ &\quad + (\Xi \bar{A} - L_1 \bar{C} - M)z \\ &\quad + [(\Xi \bar{A} - L_1 \bar{C})H - L_2]y \\ &\quad + (\Xi - G)\bar{B}u \\ &\quad + \Xi \bar{D}\bar{d} - L_1 E_s d_s - H E_s \dot{d}_s \\ e_y &= \bar{C}e_x + E_s d_s \end{aligned} \quad (6.20)$$

where

$$\begin{aligned} \Xi &= I_{n+s} - H\bar{C} \\ L &= L_1 + L_2 \end{aligned} \quad (6.21)$$

To guarantee the stability of proposed observer, the following necessary conditions are proposed for the error dynamics (6.20):

$$M \text{ is Hurwitz} \quad (6.22)$$

$$\Xi\bar{A} - L_1\bar{C} - M = 0 \quad (6.23)$$

$$(\Xi\bar{A} - L_1\bar{C})H - L_2 = 0 \quad (6.24)$$

$$E - G = 0 \quad (6.25)$$

Remark 6.2 In Sun and Patton (2013), so as to obtain the decoupling between the disturbance and system, the matrix H is solved from $\Xi\bar{D} = 0$ with satisfying the rank demand: $\text{rank}(\bar{C}\bar{D}) = \text{rank}(\bar{D})$. Nonetheless, this restrictive rank requirement fails to be satisfied in this case due to the occurrence of external sensor faults with $\text{rank}(\bar{C}\bar{D}) = 3 \neq \text{rank}(\bar{D}) = 4$. Therefore, a robust and more general UIO strategy is proposed for the pitch system with released rank demand inspired by the work in Lan and Patton (2015). Here, the effects of disturbances and measurement noise are attenuated under a certain level by the H_∞ optimization.

By satisfying these conditions (6.21)-(6.25), the error dynamics (6.20) become

$$\begin{aligned} \dot{e}_x &= (\Xi A - L_1 \bar{C})e_x + \Xi \bar{D} \bar{d} - L_1 E_s d_s - H E_s \dot{d}_s \\ e_y &= \bar{C} e_x + E_s d_s \end{aligned} \quad (6.26)$$

If all the eigenvalues of the system matrix $M = \Xi A - L_1 \bar{C}$ can be assigned to the left half plane of complex plane, e_x will converge to zero when all the disturbances are zero. From (6.26), it is shown that the measurement noise d_s and disturbance \bar{d} in (6.26) exert negative effects on the state and output estimate errors as well as deteriorate the FE performance. The H_∞ optimization is employed to achieve the attenuation of the effects from d_s and \bar{d} , thus enhancing the UIO robustness and stability.

Theorem 6.1 If there exists a symmetric positive definite matrix $P \in \mathbb{R}^{(n+s) \times (n+s)}$, and matrices $M_1 \in \mathbb{R}^{(n+s) \times s}$ and $M_2 \in \mathbb{R}^{(n+s) \times s}$, such that the error system (6.26) is robustly stable with H_∞ performance satisfying $\|e_y\|_\infty < \gamma \|w_d\|_\infty$ for any disturbance $w_d \in \mathcal{L}_2(0, \infty)$ and a specific constant parameter γ ,

$$\begin{bmatrix} \Pi_{11} & (P - M_1 \bar{C}) \bar{D} & -M_2 E_s + \bar{C}^T E_s & -M_1 E_s & C^T \\ \star & -\gamma^2 I & 0 & 0 & 0 \\ \star & \star & E_s^T E_s - \gamma^2 I & 0 & 0 \\ \star & \star & \star & -\gamma^2 I & 0 \\ \star & \star & \star & \star & -I \end{bmatrix} < 0 \quad (6.27)$$

where $\Pi_{11} = He(P\bar{A} - M_1\bar{C}\bar{A} - M_2\bar{C})$, disturbance matrix $w_d = [\bar{d} \ d_s \ \dot{d}_s]^T$. \star represents the transpose of matrix elements in symmetric positions. It is worth noting that the matrices L_1 and H are obtained firstly with the proposed matrices P, M_1, M_2 , and then M, G, H and L_2 can be achieved.

Proof 6.1 Consider the following Lyapunov function $V = e_x^T P e_x$ and P is a symmetric positive definite matrix. Combined with the error dynamics (6.26), the first time derivative of V is represented as:

$$\begin{aligned} \dot{V} &= \dot{e}_x^T P e_x + e_x^T P \dot{e}_x \\ &= e_x^T M^T P e_x + \bar{d}^T \bar{D}^T \Xi^T P e_x - d_s^T E_s^T L_1^T P e_x \\ &\quad - \dot{d}_s^T E_s^T H^T P e_x + e_x^T P M e_x + e_x^T P \Xi \bar{D} \bar{d} \\ &\quad - e_x^T P L_1 E_s d_s - e_x^T P H E_s d_s \end{aligned} \quad (6.28)$$

$$= \begin{bmatrix} e_x \\ \bar{d} \\ d_s \\ \dot{d}_s \end{bmatrix}^T \begin{bmatrix} M^T P + P M & P \Xi \bar{D} & -P L_1 E_s & -P H E_s \\ \star & 0 & 0 & 0 \\ \star & \star & 0 & 0 \\ \star & \star & \star & 0 \end{bmatrix} \begin{bmatrix} e_x \\ \bar{d} \\ d_s \\ \dot{d}_s \end{bmatrix}$$

The H_∞ performance of the output estimation error $\|e_y\|_\infty < \gamma \|w_d\|_\infty$ is illustrated as

$$J = \int_0^\infty (e_y^T e_y - \gamma^2 w_d^T w_d) dt < 0 \quad (6.29)$$

With assumed zero initial conditions, it holds that

$$\begin{aligned} J &= \int_0^\infty (e_y^T e_y - \gamma^2 w_d^T w_d + \dot{V}) dt - \int_0^\infty \dot{V} dt \\ &= \int_0^\infty (e_y^T e_y - \gamma^2 w_d^T w_d + \dot{V}) dt - V(\infty) + V(0) \\ &\leq \int_0^\infty (e_y^T e_y - \gamma^2 w_d^T w_d + \dot{V}) dt \end{aligned} \quad (6.30)$$

One sufficient condition for (6.29) is satisfied is shown as

$$J_1 = e_y^T e_y - \gamma^2 w_d^T w_d + \dot{V} < 0 \quad (6.31)$$

Combining (6.28) with (6.31), the following formula can be obtained:

$$\begin{bmatrix} e_x \\ \bar{d} \\ d_s \\ \dot{d}_s \end{bmatrix}^T \begin{bmatrix} M^T P + PM + \bar{C}^T \bar{C} & P \bar{\Xi} \bar{D} & -PL_1 E_s + \bar{C}^T E_s & -PHE_s \\ * & -\gamma^2 I & 0 & 0 \\ * & * & E_s^T E_s - \gamma^2 I & 0 \\ * & * & * & -\gamma^2 I \end{bmatrix} \begin{bmatrix} e_x \\ \bar{d} \\ d_s \\ \dot{d}_s \end{bmatrix} < 0 \quad (6.32)$$

Note that PL_1 , PH in (6.32) are nonlinear, therefore $M_1 = PH$, $M_2 = PL_1$ are defined for convenience. With the use of Schur Complement Lemma (Boyd et al., 1994), the following LMI can be achieved:

$$\begin{bmatrix} He(P\bar{A} - M_1\bar{C}\bar{A} - M_2\bar{C}) & (P - M_1\bar{C})\bar{D} & -M_2E_s + \bar{C}^T E_s & -M_1E_s & C^T \\ * & -\gamma^2 I & 0 & 0 & 0 \\ * & * & E_s^T E_s - \gamma^2 I & 0 & 0 \\ * & * & * & -\gamma^2 I & 0 \\ * & * & * & * & -I \end{bmatrix} < 0, P > 0 \quad (6.33)$$

This completes the proof of *Theorem 6.1*.

With satisfying the LMI (6.27), the stability and availability of designed UIO has been guaranteed. In addition to this, optimizing the observer dynamic response is also essential to guarantee an acceptable observer performance. It can be achieved by placing all the eigenvalues of observer system matrix within a appropriate sub-domain in the complex plane including discs, vertical strips, conical regions etc. (or combinations thereof) by the LMI optimisation toolbox (Chilali and Gahinet, 1996). So as to achieve the satisfied closed-loop system time response performance of proposed UIO, the LMI regional pole placement complement is adopted to place the observer (6.27) poles within the suitable vertical strip regions.

Here, the observer poles (6.27) can be placed to the vertical region $\mathcal{D} : a < Re(\lambda) < b$ with given negative scalars a and b ($a < b$), such that

$$\begin{bmatrix} He(P\bar{A} - M_1\bar{C}\bar{A} - M_2\bar{C}) - 2bP & 0 \\ \star & -He(P\bar{A} - M_1\bar{C}\bar{A} - M_2\bar{C}) + 2aP \end{bmatrix} < 0 \quad (6.34)$$

Therefore, by designing suitable positive constant γ , negative parameters a , b and solving the LMIs (6.27) and (6.34), P , M_1 , M_2 can be achieved. According to $H = P^{-1}M_1$, $L_1 = P^{-1}M_2$ and (6.21)-(6.25), the matrices M , G , H , L are obtained subsequently. In conclusion, *Problem 6.1* can be solved by the above analysis and design of a robust UIO system.

Finally, the FTC system for fault compensation is realized by subtracting the achieved fault estimate from the proposed robust UIO, shown in

$$\beta_{FTC} = \beta_{mf} - \hat{f}_s \quad (6.35)$$

where the fault compensation quality is related to the accuracy of the sensor fault estimation \hat{f}_s , that is whether the estimate error $f_s - \hat{f}_s$ approaches zero.

6.4 Simulation Results

6.4.1 Structural Load Reduction in Fault-free Case

The proposed LQR-based IPC strategy is validated on 5MW NREL WT simulator under the three-dimensional turbulent wind field with a hub-height mean speed 18 m/s , turbulence intensity 14% and a vertical shear exponent of 0.2, shown in Fig. 3.7. Comparisons are carried out between the baseline pitch controller (CPC) and LQR-based IPC as well as the PI-based IPC case. The performance measures including standard deviations (STD) of generator power P , pitch rate $\dot{\theta}$, the blade 1 flapwise bending moments M_1 , tower fore-aft bending moment T_f and tower side-side bending moment T_s calculated from 30s to 1000s are used to compare these three control strategies, illustrated in Table 6.4.

Figs. 6.5 - 6.6 present an overview of the simulation results of three different pitch controllers in the time domain. As can be seen from Table 6.4, compared with the CPC case, the proposed LQR-IPC controller can improve the smoothness of generator power fluctuation by approximately 42% whilst the PI-IPC enhances the power

Table 6.4: The STD of simulation results in the time domain

Cases	P (KW)	$\dot{\theta}$ (rad/s)	M_1 (kNm)	T_f (kNm)	T_s (kNm)
CPC	88.8	0.0081	2041.1	7816.8	2867.4
PI-IPC	90.9	0.0445	1410.8	8135.7	2981.9
LQR-IPC	51.3	0.0496	1535.0	6778.7	2496.8

vibration by 1.1%. Furthermore, the LQR-IPC achieves nearly 24.8% mitigation of blade flapwise bending moments as well as 13.3% reduction of tower fore-aft bending moments, without the expense of enhanced tower side-side bending moments. The PI-based IPC controller achieves a marginally better performance on the mitigation of blade unbalanced loads (6% more compared with LQR-IPC) but with increased fluctuations of the tower fore-aft (4.1%) and side-side bending moments (4.0%). Figs. 6.5 - 6.6 also validate the aforementioned conclusions. It is apparent from Table 6.4 that both PI-IPC and LQR-IPC controllers represent some similarities with the enhanced pitching motion to achieve the goal of structural load reduction, which will lead to potential pitch system faults.

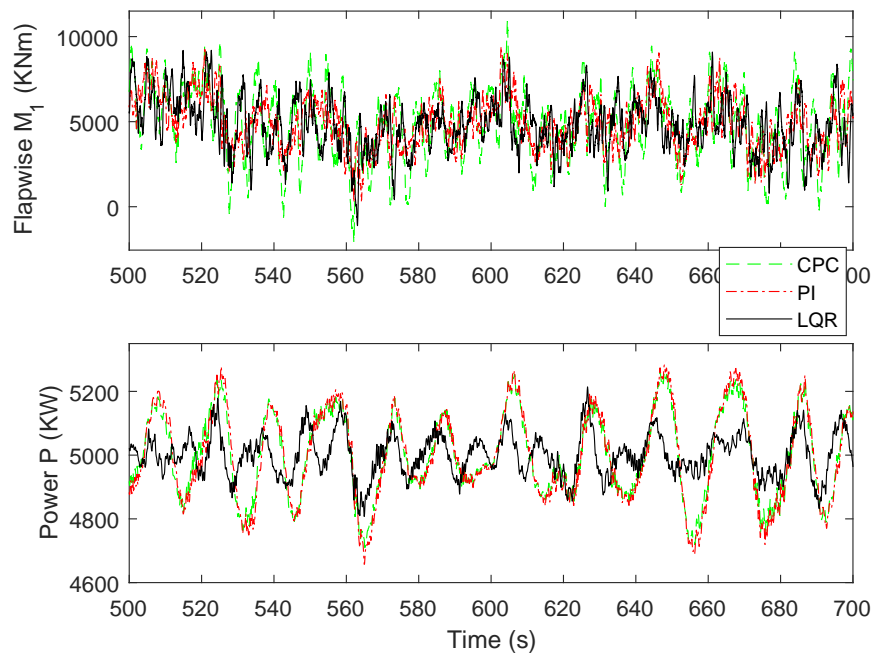


Figure 6.5: Comparisons between three pitch controllers in terms of blade 1 flapwise bending moment M_1 and generator power output P

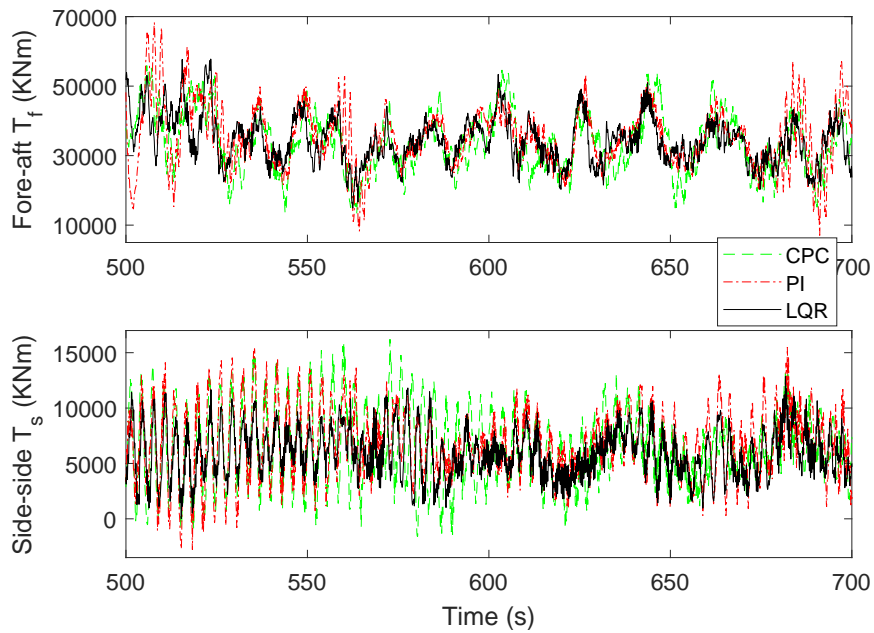
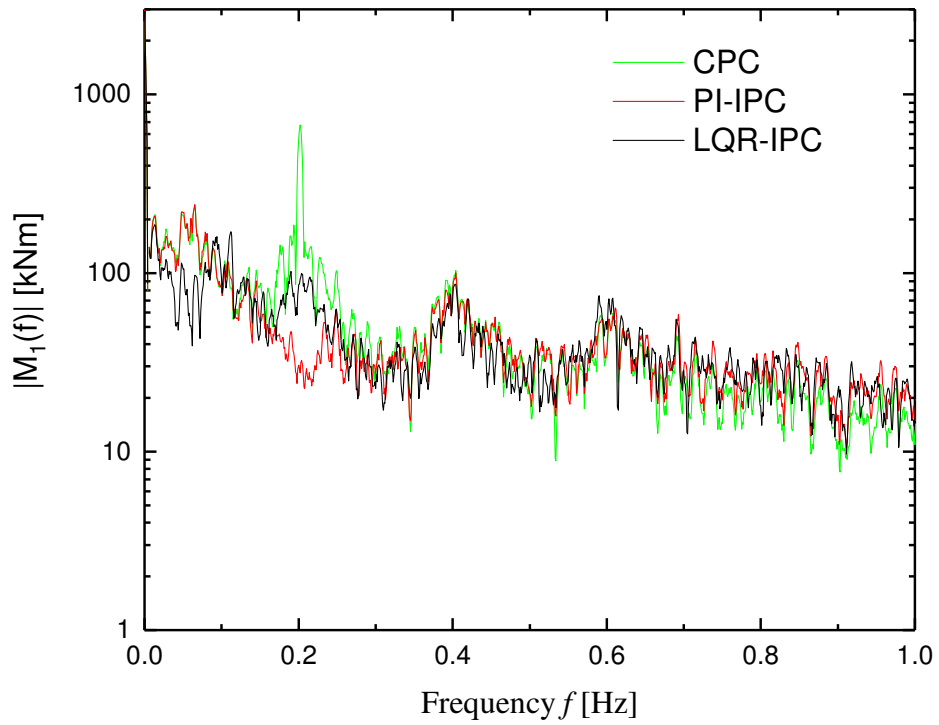
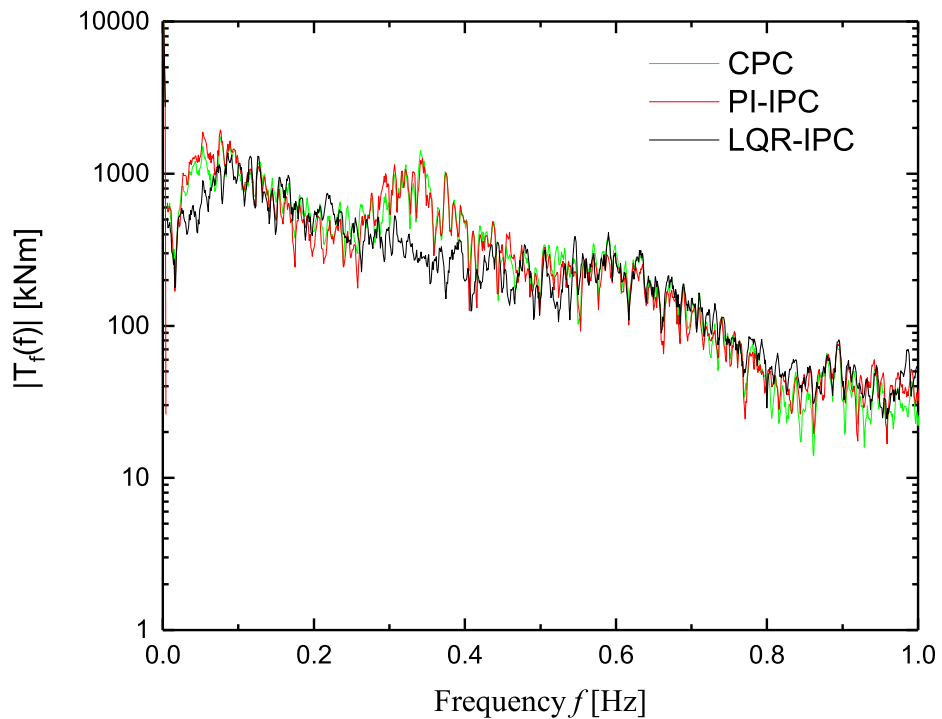


Figure 6.6: Comparisons between three pitch controllers in terms of tower fore-aft bending moments T_f and tower side-side bending moments T_s

The frequency analysis of the blade 1 flapwise bending moments M_1 and tower fore-aft bending moment T_f are represented in Figs. 6.7 – 6.8. It can be seen that the most prominent component of the blade asymmetrical loads is the first harmonic of frequency 1P whilst the most significant part of tower fore-aft loading is 0.3Hz. It is shown that the PI-IPC can obtain better 1P blade loading mitigation than the designed LQR-based IPC, whilst the LQR-IPC can mitigate the unbalanced blade loads around 0.1Hz. Furthermore, some enhancements of the higher frequency blade loading components have been noted in the both cases. On the other hand, the LQR-IPC controller is observed with notable mitigation of tower fore-aft bending moments near 0.3Hz.

6.4.2 Fault Estimation Results

Here, the measurement noise is modelled as white Gaussian Process noise with power $1e-6$. The unknown disturbance d and four different fault cases f_{s_1} for sensor 1 of blade pitch system 1 (thus sensors for the other pitch systems are fault-free) are defined as

Figure 6.7: Frequency spectrum comparison of M_1 in three different pitch controllersFigure 6.8: Frequency spectrum comparison of T_f in three different pitch controllers

$$d(t) = 0.01\sin(t)$$

$$\text{Case 1, Changing bias fault: } f_{s_1} = \begin{cases} 0, & 0 \leq t \leq 700 \\ 8\sin(t), & 700 < t \leq 1000 \end{cases}$$

$$\text{Case 2, Fixed fault at } 23.3^\circ: f_{s_1} = \begin{cases} 0, & 0 \leq t \leq 700 \\ -\beta(t) + 23.3, & 700 < t \leq 1000 \end{cases}$$

$$\text{Case 3, Total failure: } f_{s_1} = \begin{cases} 0, & 0 \leq t \leq 700 \\ -\beta(t), & 700 < t \leq 1000 \end{cases}$$

$$\text{Case 4, Changing multiplicative gain: } f_{s_1} = \begin{cases} 0, & 0 \leq t \leq 700 \\ (0.001t + 0.8 - 1)\beta(t), & 700 < t \leq 1000 \end{cases}$$

By solving proposed LMIs (6.27) and (6.34) using the Matlab LMI Toolbox with $\gamma = 0.85$, $a = -80$, $b = -2.15$, the observer gains for proposed UIO are calculated as:

$$G = \begin{bmatrix} 1.0042 & 0.0042 & 0.0042 & 0 & 0 & 0 & 0.0042 & 0.0042 & 0.0042 \\ 0.0042 & 1.0042 & 0.0042 & 0 & 0 & 0 & 0.0042 & 0.0042 & 0.0042 \\ 0.0042 & 0.0042 & 1.0042 & 0 & 0 & 0 & 0.0042 & 0.0042 & 0.0042 \\ -0.1361 & -0.1361 & -0.1361 & 1 & 0 & 0 & -0.1361 & -0.1361 & -0.1361 \\ -0.1361 & -0.1361 & -0.1361 & 0 & 1 & 0 & -0.1361 & -0.1361 & -0.1361 \\ -0.1361 & -0.1361 & -0.1361 & 0 & 0 & 1 & -0.1361 & -0.1361 & -0.1361 \\ -0.5067 & -0.0067 & -0.0067 & 0 & 0 & 0 & 0.4933 & -0.0067 & -0.0067 \\ -0.0067 & -0.5067 & -0.0067 & 0 & 0 & 0 & -0.0067 & 0.4933 & -0.0067 \\ -0.0067 & -0.0067 & -0.5067 & 0 & 0 & 0 & -0.0067 & -0.0067 & 0.4933 \end{bmatrix}$$

$$L = \begin{bmatrix} 0.1381 & 0.1381 & 0.1381 \\ 0.1381 & 0.1381 & 0.1381 \\ 0.1381 & 0.1381 & 0.1381 \\ -1.3499 & -1.3499 & -1.3499 \\ -1.3499 & -1.3499 & -1.3499 \\ -1.3499 & -1.3499 & -1.3499 \\ 1.5489 & -0.0790 & -0.0790 \\ -0.0790 & 1.5489 & -0.0790 \\ -0.0790 & -0.0790 & 1.5489 \end{bmatrix}, \quad H = \begin{bmatrix} -0.0042 & -0.0042 & -0.0042 \\ -0.0042 & -0.0042 & -0.0042 \\ -0.0042 & -0.0042 & -0.0042 \\ 0.1361 & 0.1361 & 0.1361 \\ 0.1361 & 0.1361 & 0.1361 \\ 0.1361 & 0.1361 & 0.1361 \\ 0.5067 & 0.0067 & 0.0067 \\ 0.0067 & 0.5067 & 0.0067 \\ 0.0067 & 0.0067 & 0.5067 \end{bmatrix}$$

and impose a strong robustness requirement on the FE scheme. In other words the CPC system has simpler dynamics compared with the IPC case (which is actually a complex combination of both the IPC and the CPC).

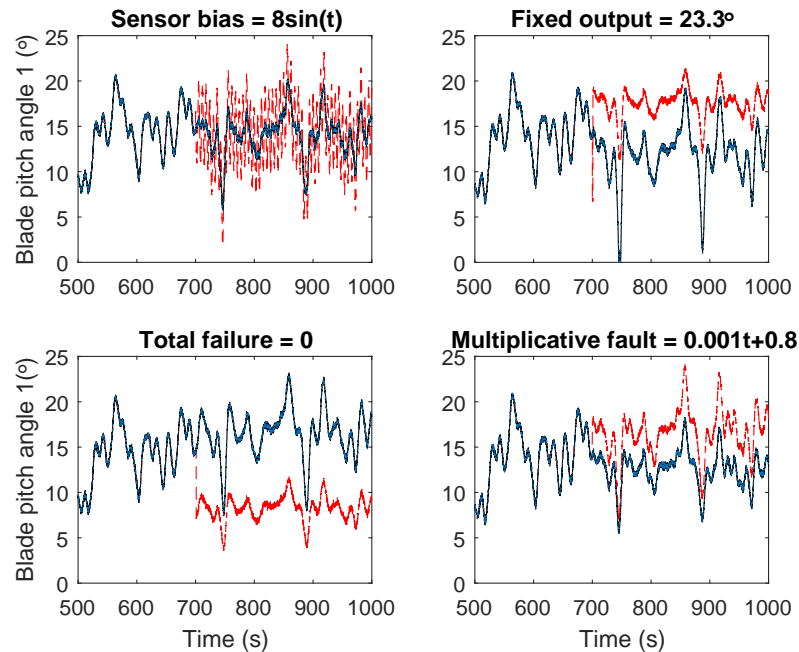


Figure 6.9: Sensor faults in the CPC case

From the above figures, it can be concluded that the designed UIO with H_∞ optimization theory can obtain the decoupling between unknown uncertainties and sensor faults as well as minimise the influence of measurement noises on the FE signal, to achieve a precise sensor fault estimation result in both the CPC and LQR-IPC cases. In this sense, it validates the robustness of proposed FE approach.

6.4.3 Combination between Load Reduction with FE-based FTC

The considered sensor fault occurs in the sensor 1 of blade pitch system 1. With the sensor fault estimation by the UIO strategy, the incorrect measurements is then compensated with the FTC system, completing the proposed FE-based FTC strategy. The simulation results in terms of the standard deviation of the WT power and load performance in the presence of 4 different sensor faults with 3 kinds of pitch controllers (i.e. 27 cases in total) are illustrated in Table 6.5. The CPC_bias denotes the baseline pitch controller, considering the bias faults of sensor 1. CPC_bias_FTC means the case

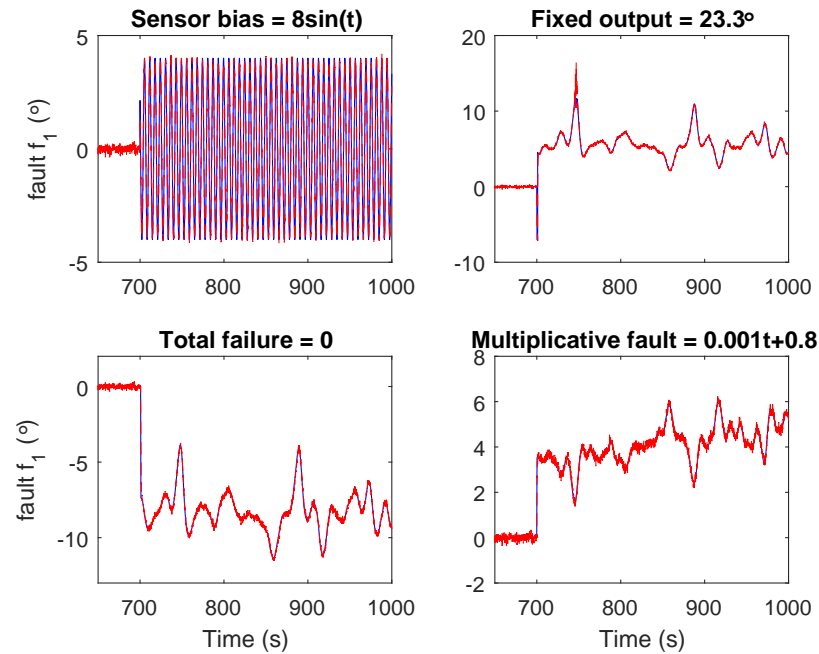


Figure 6.10: Fault estimation results by designed UIO in the CPC case

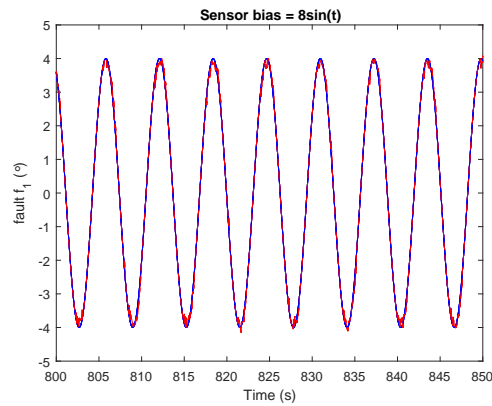


Figure 6.11: A zoom-in figure of sensor bias fault estimation in the CPC case

of CPC_bias with the designed UIO-based FTC system. Similar explanations follow for the other cases. Furthermore, the corresponding spider figures for the normalized performance are illustrated in Figs. 6.14 - 6.16 to provide much clearer comparisons.

From Figs. 6.14-6.16, it can be seen that there are some similarities between the studied pitch controllers in the event of sensor faults. When sensor 1 of pitch system 1 suffers from faults (especially a fixed fault), the standard deviation of the pitch rate has increased by different levels. This shows that the pitch actuator 1 has to work harder to

Table 6.5: Summary of simulation results

Cases	P (KW)	$\dot{\theta}$ (rad/s)	M_1 (kNm)	T_f (kNm)	T_s (kNm)
CPC	88.8	0.0081	2041.1	7816.8	2867.4
PI-IPC	90.9	0.0445	1410.8	8135.7	2981.9
LQR-IPC	51.3	0.0496	1535.0	6778.7	2496.8
CPC_bias	89.5	0.0083	2083.3	8063.7	2985.5
CPC_bias_FTC	88.8	0.0081	2043.3	7814.7	2859.6
CPC_fixed	92.1	0.0095	2431.6	9199.7	4031.6
CPC_fixed_FTC	89.2	0.0082	2046.4	7835.8	2866.1
CPC_total	95.5	0.0086	3029.6	9930.4	5324.0
CPC_total_FTC	89.2	0.0082	2045.8	7841.1	2869.6
CPC_multi	85.8	0.0082	2365.6	8265.3	3727.7
CPC_multi_FTC	88.6	0.0081	2043.1	7792.4	2925.4
PID_bias	91.6	0.0446	1959.8	9420.2	3053.6
PID_bias_FTC	91.7	0.0445	1417.2	8190.3	2968.9
PID_fixed	92.9	0.0469	1648.5	8985.1	3542.8
PID_fixed_FTC	91.5	0.0447	1417.6	8173.9	3031.2
PID_total	101.6	0.0462	2105.3	10363	5468.5
PID_total_FTC	91.4	0.0447	1416.4	8174.6	3008.4
PID_multi	88.6	0.0441	1549.3	8450.4	3507.7
PID_multi_FTC	90.7	0.0444	1408.2	8125.8	2984.6
LQR_bias	66.6	0.0521	1601.0	8323.8	2804.2
LQR_bias_FTC	52.1	0.0500	1541.3	6780.2	2501.5
LQR_fixed	85.7	0.0613	1860.0	8544.4	3225.2
LQR_fixed_FTC	60.9	0.0530	1598.1	6825.4	2550.7
LQR_total	58.9	0.0499	2350.8	8699.5	3824.2
LQR_total_FTC	53.6	0.0508	1570.1	6792.3	2523.4
LQR_multi	56.8	0.0538	1727.9	7976.1	3147.3
LQR_multi_FTC	51.8	0.0501	1539.4	6782.4	2499.1

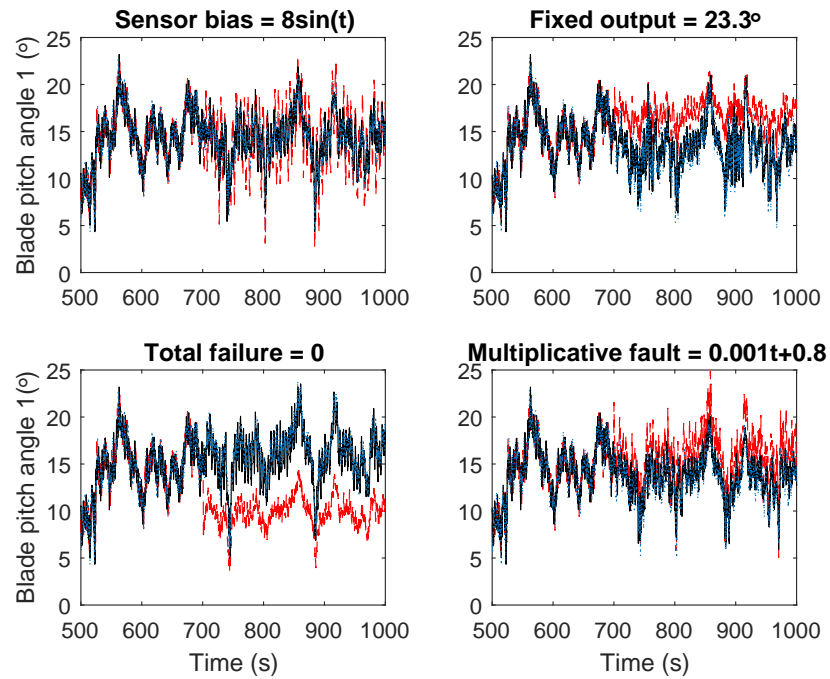


Figure 6.12: Sensor faults in the LQR-IPC case

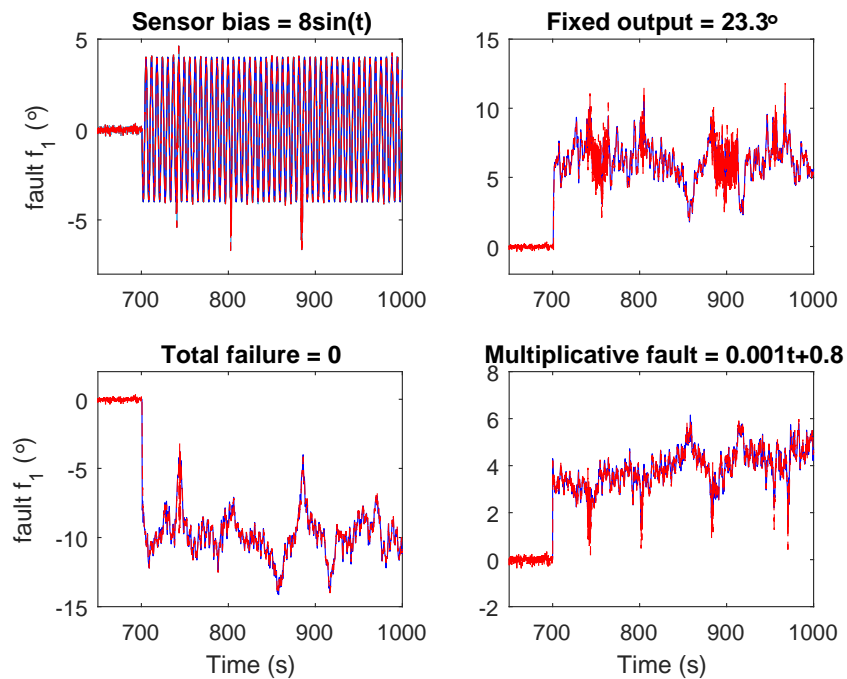


Figure 6.13: Fault estimation results by designed UIO in the LQR-IPC case

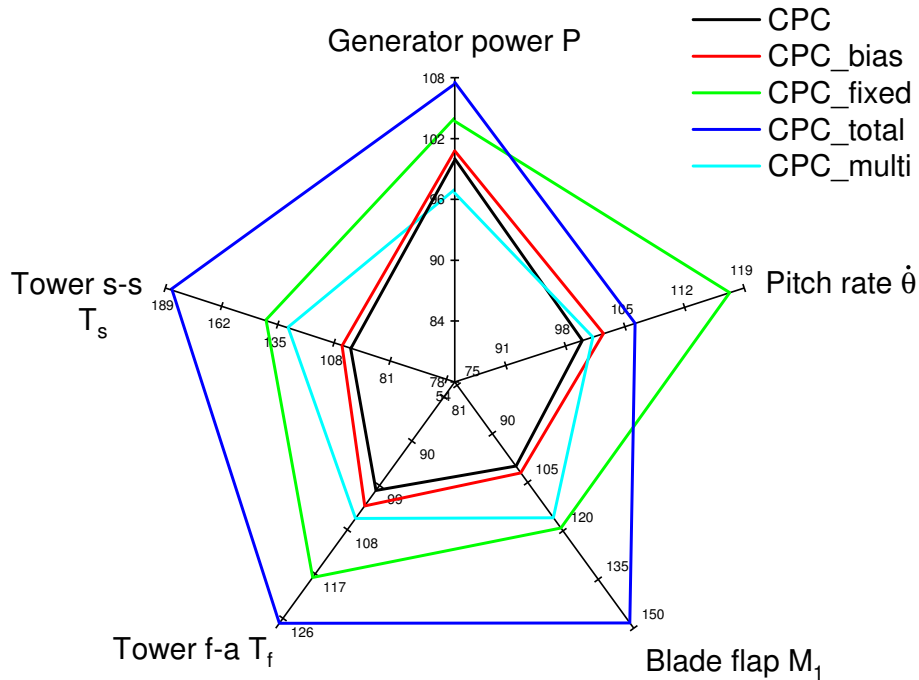


Figure 6.14: Spider figure of normalized performance comparison under 4 different faults of pitch sensor 1 with CPC controller

achieve the reference pitch angle from the associated pitch controller in the presence of sensor faults. Furthermore, it can be seen that different sensor faults have varying degrees of impact on the WT system. Considering the fault levels described in this Chapter, the example of total failure of the pitch sensor shows the greatest influence on the blade and tower loading unbalance. This total failure also has a considerable effect on the generator power.

From Table 6.5, the robustness and effectiveness of the proposed UIO-based FTC strategy is validated. Based on the sensor fault estimation results, the proposed FE-based FTC strategy is feasible and robust to compensate the fault effects in different conditions. For example, the case of CPC_bias_FTC have similar results with the CPC case. Similar results follow for the other cases with the designed FTC strategy. It can be seen that the simulation results in the cases of LQR_fixed_FTC and LQR_multi_FTC after the fault compensation are marginally worse than the baseline LQR-IPC case. This is due to fact that the fault estimation results for these two cases are not as accurate as in other cases. Recall that the quality of the designed FTC scheme relies on the accuracy of the fault estimates generated by the UIO system. The proposed LQR-based IPC system is demonstrated to perform better than the PI-based IPC in terms of reducing the

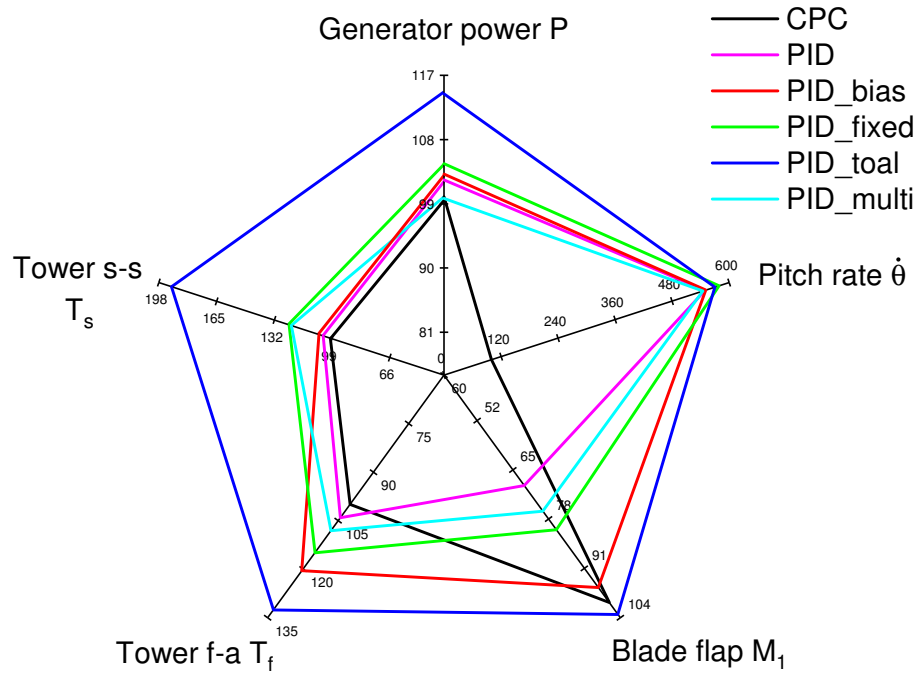


Figure 6.15: Spider figure of normalized performance comparison under 4 different faults of pitch sensor 1 with PID-IPC controller

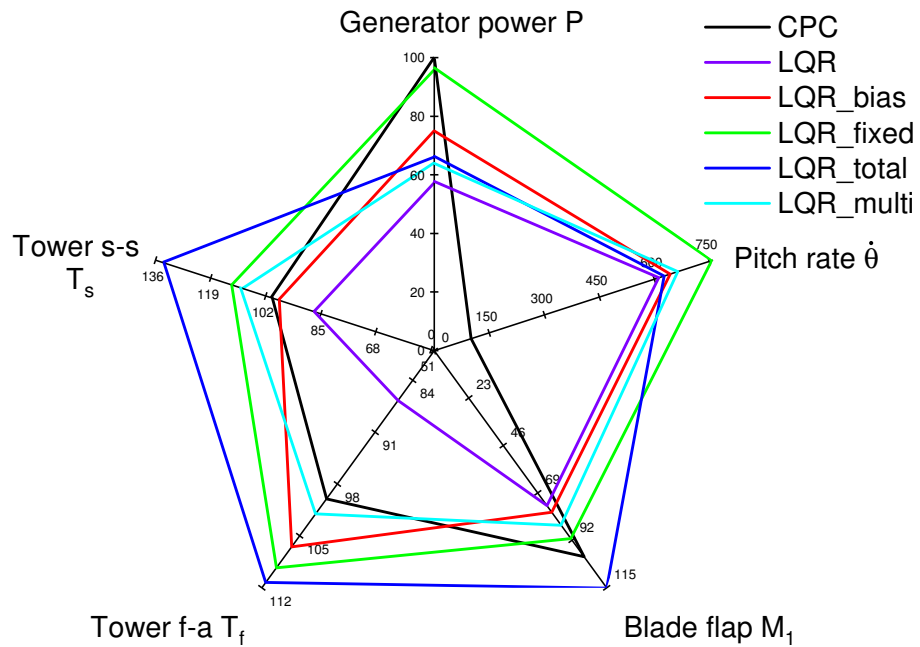


Figure 6.16: Spider figure of normalized performance comparison under 4 different faults of pitch sensor 1 with LQR-IPC controller

fluctuations of generator power, as well as blade and tower loading both in the absence of faults and in the sensor fault case. However, improved load reduction performance comes with the cost of higher pitch rates. The increased pitch usage is still reasonable in the LQR-IPC case, given that the additional pitch angle is aimed at the asymmetrical load mitigation.

Therefore, it is important to consider the performance of the designed load reduction controller for the fault cases to have better all round performance evaluation for the proposed controllers. It can be concluded that the LQR-based IPC system demonstrates an improved performance compared with the PI-based IPC on the whole, including: (i) a better load mitigation performance in reducing the blade and tower bending moments together; (ii) attenuate the negative effects of pitch sensor faults on the turbine structural loading and power output.

6.5 Conclusion

This Chapter proposes the following strategies: i) an LQR-based IPC control strategy for mitigating the blade asymmetrical loads and tower fore-aft loading simultaneously. ii) by considering the hardware redundancy of the pitch sensors, a robust UIO-based FTC system combined with H_∞ optimization theory for accurate sensor fault estimation and compensation is designed. The design also ensures decoupling of the effects of unknown system disturbance and measurement noise from the FE signal. iii) the designed IPC system and sensor FE/FTC strategy are combined together to validate the robustness and achieve a more comprehensive performance evaluation of the proposed strategy.

It is clear that the robust UIO can achieve the sensor fault estimation even when the different pitch controllers are used. The fault estimation results in the CPC case outperform the results for other candidate pitch controllers because the extra pitch angles from the IPC increase the system complexity, hence requiring enhanced robustness. The detailed simulation results verify the effectiveness and robustness of proposed LQR-based IPC and UIO-based FTC strategies. It is concluded that the proposed LQR-based IPC system has a better performance than PI-based IPC not only in mitigating the tower and blade unbalanced loading when it is fault-free but also in the case with pitch sensor faults. This Chapter completes the contribution made by this thesis. A summary of

the research study in this thesis is provided in Chapter 7.

Chapter 7

Summary and Future Work

7.1 Summary

In this thesis, fault tolerant control (FTC) strategies for pitch systems are combined with the individual pitch controller (IPC) for offshore wind turbines in a system level, i.e. considering all the "fault effects" in the rotor or both the rotor and tower systems together aim to:

- Guarantee the mitigation of unbalanced loading in both the fault-free and faulty pitch system, and
- Detect, estimate and compensate some common pitch actuator/sensor fault effects, and
- Reduce the operation & maintenance costs, enhance the lifetime and reliability of offshore wind turbines (OWTs).

The study is based on the (Fatigue, Aerodynamics, Structure and Turbulence) FAST 5MW NREL wind turbine simulator, which is a variable-speed, variable-pitch wind turbine representing the commercial modern wind turbines. This makes it possible to guarantee the effectiveness and reliability of the proposed strategies when applied to a real wind turbine system. This research study contributes to this aim via the following four aspects:

- (1) Proposal of a potential candidate for the expensive and non-universal LiDAR system in the preview control-based IPC strategy.

Due to the inherent delay before the incoming wind exerts effects on WT system, there is growing interest in the preview control, which uses the future knowledge of wind field to enhance the IPC load reduction performance. Model predictive control (MPC) automatically incorporates a feed-forward property and handles system constraints in a systematic way, which makes it popular in the WT preview control scheme. As stressed in the Challenges of Chapter 1, LiDAR can be used to estimate the future wind information but with its limitations (e.g. high operating costs for individual WT, difficult to analyse complex collected data etc.). Therefore, it is worthwhile to investigate popular data-driven methods (i.e. Gaussian process, GP) to obtain very short-time effective wind speed prediction from historical data for the purpose of control and combine this wind prediction with MPC-based preview control. The effectiveness of this strategy is investigated and verified in Chapter 4.

From the simulation results, it can be seen that the MPC-based preview control system with the wind speed forecasting based on the proposed GP model can achieve similar results compared with the ideal future wind speed. This can be compared with another candidate scheme using a cascaded control-based IPC system with additional local blade inflow measurements (Jones et al., 2018). The GP model combined with MPC-based preview control (see Section 4.3 & 4.4) does not require an additional hardware system and can also achieve reasonable results. Therefore, this method can be an alternative to the use of LiDAR when the preview control strategy is considered for the rotor blade load reduction.

(2) Investigation of a multivariable LQR control system for blade and tower loading mitigation.

The importance of reducing the rotor blade and tower unbalanced loading for offshore WTs has been emphasized in this thesis. As discussed in the Challenges of Chapter 1, the current load mitigation technologies for wind turbines generally consider these two problems in separate control loops. There exists strong couplings between the blade flapwise and tower fore-aft bending moments, which are the main source for the blade and tower fatigue. Hence, an LQR-based IPC system is proposed in Section 6.3.1 to reduce these two types of loading simultaneously. This is compared with the alternative two pitch control system which either uses combined collective pitch control (CPC) and PI-IPC control, or simply uses CPC. The promising simulation results validate the feasibility and effectiveness of the proposed LQR-based IPC strategy.

(3) Proposal of different on-line fault monitoring strategies for different pitch system faults.

As discussed in the Challenges of Chapter 1, the introduction of the IPC scheme to offshore WTs achieves the mitigation of not only the rotor blade loading but also the tower loading. However, this strategy inevitably enhances the pitch system movements and increases the possibility of potential pitch system faults. In this thesis, 8 different possible hydraulic pitch system faults are considered and the corresponding fault monitoring strategies are proposed and studied. These are summarised as follows.

- Pitch actuator stuck (PAS) fault.

This is studied in the Section 3.4. The PAS fault means the faulty pitch system fails to regulate the pitch of a particular rotor blade. This is a serious WT actuator fault which is usually caused by valve or pump blockages. A fault detection and isolation (FDI) strategy using the Kalman filter is studied to detect the PAS fault and provides an early-stage alarm for operators to implement an emergency shut-down if there is no hardware redundancy available. Furthermore, the impact of PAS on the turbine loading and power output is also discussed. It is interesting to note that this impact of PAS depends on the angle at which the faulty blade is stuck. If the value of the stuck pitch angle is far away from the nominal required pitch angle, this will result in significant fluctuations of structural loading and generator power output. On the other hand if the stuck pitch angle is close to the required angle, the fluctuations will not be severe.

- Pitch actuator dynamics changing fault.

In this fault mode, three different situations including hydraulic leakage, pump wear and high air content are considered for a fault which essentially comprises changes of the actuator dynamics (see Section 5.2). These faults are often referred to as *actuator component faults*. These three pitch actuator faults are slow and so-called incipient (hard to detect) and result in pitch actuator dynamic variations, which will affect the accuracy and effectiveness of blade pitching system. Here, an observer-based approach using an adaptive sliding mode observer (SMO) is used to obtain the estimation of three different pitch actuator faults. An FTC strategy is designed to compensate for the fault effects.

- Pitch sensor fault.

Four different types of sensor faults including bias fault, stuck with fixed sensor fault, total sensor fault and multiplicative-types of sensor fault are considered in Section 6.2.2. These sensor faults arise from harsh environmental conditions, man-made maladjustment etc., which lead to the incorrect pitch position readings and further affect the accuracy of the pitch controller (including CPC and IPC). Here, a robust unknown input observer (UIO)-based fault tolerant strategy for the pitch system sensor faults is proposed to estimate and compensate the sensor fault effects, taking into account unknown input disturbances and measurement noise. Moreover, the sensor system physical redundancy is also considered as a way of enhancing the sustainability of the proposed control strategy, for real application.

(4) Combined analysis of fault estimation (FE)-based FTC strategy with IPC system.

The pitch system faults will in turn deteriorate the load reduction performance introduced by the IPC system. As discussed in the Challenges of Chapter 1, it is important to integrate the fault-tolerant pitch system with the IPC at a higher level in the system. This is important to verify the robustness and effectiveness of these two systems acting together as well as separately. This goal is investigated in Section 5.4.2 and Section 6.4.3. In these Sections the following are observed: (i) if the different IPC strategies present the same ability to maintain the load reduction performance when the same fault occurs? (ii) does the proposed FE-based FTC strategy have the same performance when different IPC systems are used?

In Section 5.4.2, two traditional Coleman transformation-based IPC systems using PI and H_∞ loop-shaping control approaches are combined with the SMO-based FTC system for pitch actuator component faults. The simulation is verified in two different wind speed conditions of Region 3 with hub-height wind speed 18m/s and 23 m/s, respectively. From the simulation results, the PI-based IPC strategy performs better in the fault-free case. However, the H_∞ loop-shaping based IPC strategy gives better performance in maintaining the load mitigation with respect to incipient pitch actuator faults and also when the FTC scheme is based on FE-based fault compensation. It is interesting to note that the proposed SMO-based FE strategy presents slightly better results in the PI-IPC case compared with the H_∞ loop-shaping based case. Therefore, it can be concluded that the H_∞ loop-shaping based IPC strategy presents better overall benefit compared with the PI-based IPC, both in considering the maintenance of the load mitigation performance in the pitch actuator fault case as well as in restoring the

load mitigation performance (after the fault) with the SMO-based FTC strategy, referring to Fig. 5.14. Moreover, the robustness of this SMO-based FTC strategy has been verified, with reference to Fig. 5.13.

In Section 6.4.3 the proposed LQR-based IPC system is combined with the UIO-based FTC system for four different pitch sensor faults. For comparison, the PI-based IPC system and the CPC pitch system are also combined separately with the UIO-based FTC system. It can be concluded that LQR-IPC performs better than other two pitch systems in mitigating the fluctuations of generator power output, rotor blade and tower loading either in the fault-free or faulty cases, with reference to Figs. 6.14 - 6.16. Moreover, the proposed UIO-based FTC can estimate and compensate different sensor faults in different IPC systems robustly and accurately, with reference to Figs. 6.12, 6.13 and Table 6.5.

7.2 Recommendations for Future Research

In order to make the proposed strategies applicable on the real OWT systems, some further research can be explored to ensure their satisfactory performance:

- (1) To further verify the performance of proposed strategies in this thesis, Monte Carlo simulations should be adopted to evaluate the reliability and robustness of proposed load reduction and FTC systems. Furthermore, the proposed strategies could be performed under more wind conditions including the extreme wind flows (i.e. gusts).
- (2) The effectiveness of IPC has been verified in Chapters 5 & 6 for rotor and tower load reduction but with the sacrifice of high pitch movements which result in a higher potential for the development of pitch system faults. As introduced in Section 2.5.3, the interest is increasing in more advanced load control strategies with built-in intelligent actuators located directly in the blades, named as "smart rotor control". This idea provides some advantages over the IPC system: (i) as only small masses will be regulated and not the total blade mass, and (ii) the extra pitch movements will be saved. This could be a potential topic for future research to make a comparison between the smart rotor control and the IPC system proposed in this thesis.
- (3) Strain gauge and optic fibre sensors are nowadays used to measure the blade moments. However, similar to the pitch sensor faults considered in Section 6.2.2, blade

load sensors suffer from a high-rate of fault development due to high blade strains and harsh environmental factors. These faults will exert bad effects on the IPC load mitigation performance. Therefore, it would be interesting to also consider the blade load sensor faults in the IPC system.

(4) Condition monitoring (CM) is an essential component of an OWT maintenance program. As stated in Section 1.4.1, CM systems normally provide off-line monitoring and basic measurements by sensors to analyse the WT operating status. Control system-based fault monitoring (e.g. FDI/FE-based FTC strategy) operates at a higher system level compared with CM, which could achieve on-line fault diagnosis. However, it would be interesting to make a thorough comparison of the respective advantages and disadvantages of these two monitoring approaches, considering a carefully defined benchmark study focussed on a real OWT application.

(5) Generally, in a wind turbine fault-tolerant system, one fault mode could be recovered by different controllers whilst one scheme could recover several fault modes. For example, as discussed in Section 6.1, the pitch sensor faults can be handled with different strategies, such as Kalman filter, UIO, SMO etc. Moreover, different pitch sensor modes could be estimated using the UIO scheme illustrated in Section 6.3.2. Similarly, a linear parameter-varying (LPV) observer-based active FTC strategy has been proposed for pitch or generator speed sensor faults as well for generator torque actuator faults (Shi and Patton, 2015). The following aspects have not received full attention:

- Optimising the selection of different control-based fault monitoring strategies for suitability for real application, and
- Methods to increase the technology readiness level (TRL) of these techniques.

Appendix A

Baseline controllers

The baseline generator torque controller implemented in MATLAB/Simulink is shown as Fig. A.1 and Fig. A.2. Furthermore, the baseline pitch controller using PI method implemented in MATLAB/Simulink is shown as Fig. A.3 and Fig. A.4:

Baseline Torque Controller

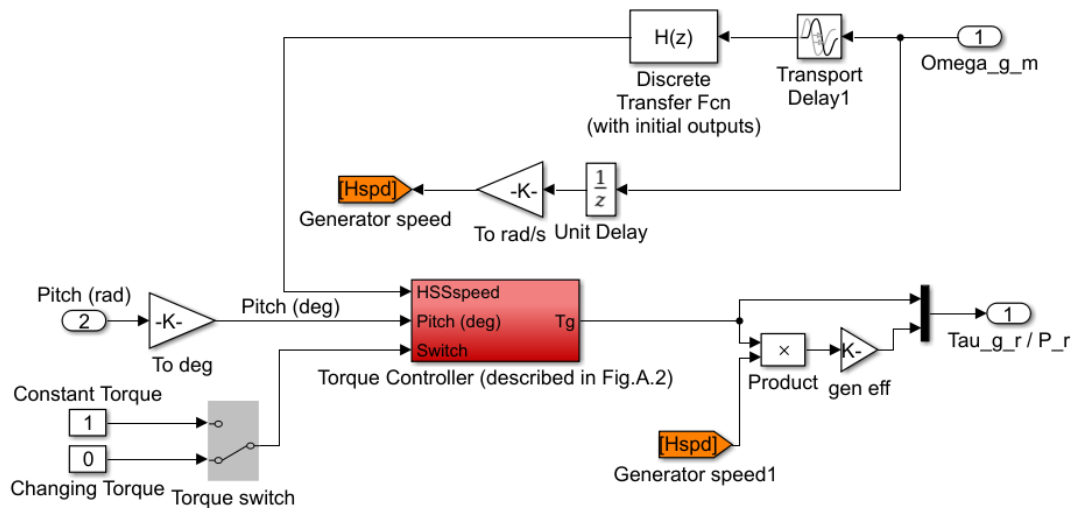


Figure A.1: Baseline Torque Controller in MATLAB/Simulink (continued with Fig. A.2)

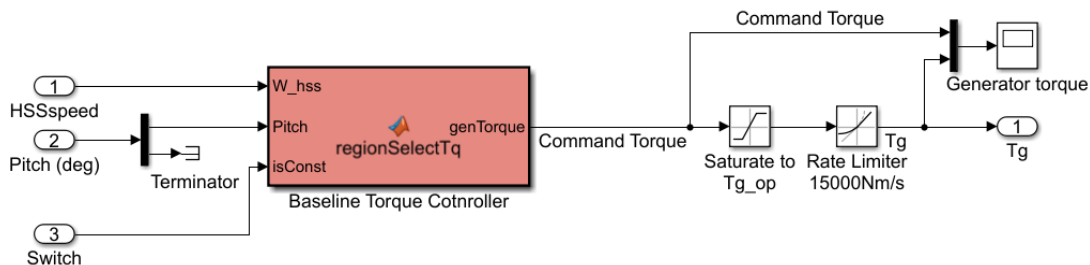


Figure A.2: The detailed torque controller designed in MATLAB/Simulink

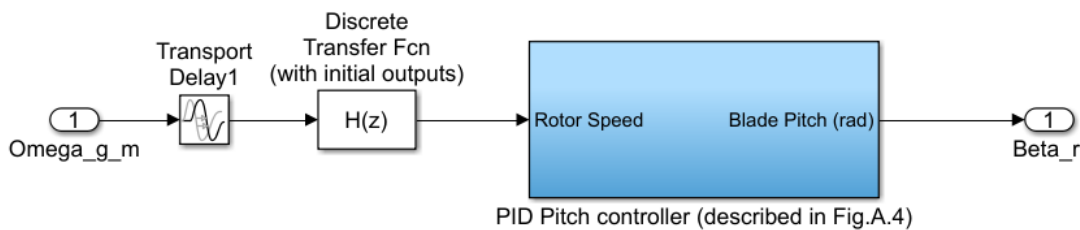


Figure A.3: Baseline Pitch Controller in MATLAB/Simulink (continued with Fig. A.4)

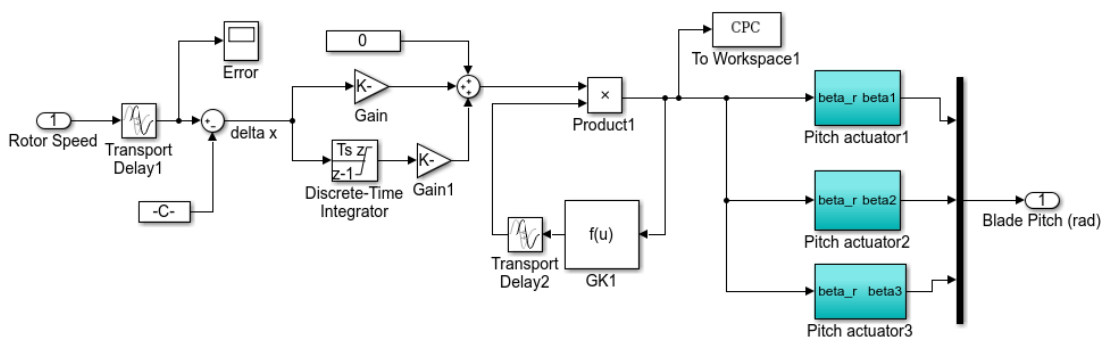


Figure A.4: The detailed pitch controller in MATLAB/Simulink

Appendix B

Frequency Splitting of Coleman transformation

According to the Fourier series expansion, the flapwise bending moments of three blades can be mathematically represented by the sum of fundamental component and high harmonic components (Van Engelen, 2006), shown as follows:

$$\begin{aligned} M_1(\varphi_1) &= M_{0p_1} + \sum_{j=1}^n \left[M_{11_{jp}} \cos(j\varphi_1 + \theta_{1j}) \right. \\ &\quad \left. + M_{12_{jp}} \sin(j\varphi_1 + \theta_{1j}) \right] \\ M_2(\varphi_2) &= M_{0p_2} + \sum_{j=1}^n \left[M_{21_{jp}} \cos(j\varphi_2 + \theta_{2j}) \right. \\ &\quad \left. + M_{22_{jp}} \sin(j\varphi_2 + \theta_{2j}) \right] \\ M_3(\varphi_3) &= M_{0p_3} + \sum_{j=1}^n \left[M_{31_{jp}} \cos(j\varphi_3 + \theta_{3j}) \right. \\ &\quad \left. + M_{32_{jp}} \sin(j\varphi_3 + \theta_{3j}) \right] \end{aligned} \tag{B.1}$$

where M_{0p_1} , M_{0p_2} , M_{0p_3} are the direct components of three flapwise bending moments, respectively. $M_{11_{jp}}$, $M_{12_{jp}}$, $M_{21_{jp}}$, $M_{22_{jp}}$, $M_{31_{jp}}$, $M_{32_{jp}}$ are the Cosine components and Sine components of high harmonic component jP ($j = 1, 2, \dots, n$) (j time the rotational frequency) content of flapwise bending moments of blade 1,2,3 respectively. θ_{1j} , θ_{2j} , θ_{3j} are the initial phase angles of jP content of flapwise bending moments of blade 1, 2, 3.

For wind turbines with well-balanced blades, the magnitudes and initial phase angles of all the harmonic components of the three flapwise bending moments are assumed to be same, namely $M_{0p_i} = M_{0p}$, $M_{i1_{jp}} = M_{c_{jp}}$, $M_{i2_{jp}} = M_{s_{jp}}$, $\theta_{ij} = \theta_j$, ($i = 1, 2, 3$ & $j = 1, 2, \dots, n$).

It follows from the Coleman transform (5.3), inverse Coleman transform (5.4), azimuth angle (5.5) and also (B.1), so that

$$\begin{cases} M_{tilt} = \sum_{i=1}^3 M_i(\varphi_i) \sin \varphi_i \\ M_{yaw} = \sum_{i=1}^3 M_i(\varphi_i) \cos \varphi_i \end{cases} \quad (\text{B.2})$$

The most significant part of structural loading causing the blade fatigue is 1P, and its multiples (0P, 2P, 3P, ..., nP). The impact of all the harmonic components on the tilt and yaw moments can be obtained from (B.1) and (B.2).

a. The impact of the direct components of flapwise bending moments:

$$\begin{cases} M_{tilt} = \sum_{i=1}^3 M_{0p}(\varphi_i) \sin \varphi_i = 0 \\ M_{yaw} = \sum_{i=1}^3 M_{0p}(\varphi_i) \cos \varphi_i = 0 \end{cases} \quad (\text{B.3})$$

b. The impact of the 1P component of flapwise bending moments:

$$\begin{cases} M_{tilt} = -\frac{3}{2}M_{c_{1p}} \sin \theta_1 + \frac{3}{2}M_{s_{1p}} \cos \theta_1 \\ M_{yaw} = \frac{3}{2}M_{c_{1p}} \cos \theta_1 + \frac{3}{2}M_{s_{1p}} \sin \theta_1 \end{cases} \quad (\text{B.4})$$

b. The impact of the 2P component of flapwise bending moments:

$$\begin{cases} M_{tilt} = \frac{3}{2}M_{c_{2p}} \sin(3\varphi + \theta_2) - \frac{3}{2}M_{s_{2p}} \cos(3\varphi + \theta_2) \\ M_{yaw} = \frac{3}{2}M_{c_{2p}} \cos(3\varphi + \theta_2) + \frac{3}{2}M_{s_{2p}} \sin(3\varphi + \theta_2) \end{cases} \quad (\text{B.5})$$

c. The impact of the 3P component of flapwise bending moments:

$$\begin{cases} M_{ilt} = 0 \\ M_{yaw} = 0 \end{cases} \quad (\text{B.6})$$

d. The impact of the 4P component of flapwise bending moments:

$$\begin{cases} M_{ilt} = -\frac{3}{2}M_{c_{4p}} \sin(3\varphi + \theta_4) + \frac{3}{2}M_{s_{4p}} \cos(3\varphi + \theta_4) \\ M_{yaw} = \frac{3}{2}M_{c_{4p}} \cos(3\varphi + \theta_4) + \frac{3}{2}M_{s_{4p}} \sin(3\varphi + \theta_4) \end{cases} \quad (\text{B.7})$$

Appendix C

Lemmas in the Thesis

C.1 Schur Complement

For a symmetric matrix $M_{(p+q) \times (p+q)}$ with the following structure of (Boyd et al., 1994)

$$M = \begin{bmatrix} A_{p \times p} & B_{p \times q} \\ C_{q \times p} & D_{q \times q} \end{bmatrix} \quad (\text{C.1})$$

if A and D are reversible, so that the following properties establish:

$$\begin{aligned} (1) M \prec 0 &\iff A \prec 0 \text{ and } D - CA^{-1}B \prec 0; \\ (2) M \prec 0 &\iff D \prec 0 \text{ and } A - BD^{-1}C \prec 0. \end{aligned} \quad (\text{C.2})$$

C.2 LMI Regional Pole Placement Complement

Assume \mathcal{D} be a sub-region in the left-half part of the complex plane. A system $\dot{x} = Ax$ is termed \mathcal{D} -stable if all its poles (i.e. eigenvalues) of the state matrix A lie in \mathcal{D} . Furthermore, A is also referred to as \mathcal{D} -stable (Chilali and Gahinet, 1996).

Remark C.1 Assume \mathcal{D} is a vertical strip area with $a < \text{Re}(\lambda) < b$, where λ are the eigenvalues of matrix A with a and b are negative limits. The dynamic system $\dot{x} = Ax$ is called \mathcal{D} -stable with the premise of existing a symmetric positive definite matrix P and satisfying the following LMI equation:

$$\begin{bmatrix} He(PA + A^T P) - 2bP & 0 \\ \star & -He(PA + A^T P) + 2aP \end{bmatrix} < 0 \quad (\text{C.3})$$

References

- Alwi, H. and Edwards, C. (2008). Fault tolerant control using sliding modes with on-line control allocation. *Automatica*, 44(7):1859–1866.
- Arnold, U. (2003). Helicopter individual blade control system. US Patent 6,666,649.
- Association, D. W. I. (2003). Wind turbine design: basic load considerations. Available at <http://xn--drmstrre-64ad.dk/wp-content/wind/miller/windpower%20web/en/tour/design/index.htm>. [accessed 16.02.19].
- Badihi, H. and Zhang, Y. (2018). Fault-tolerant individual pitch control of a wind turbine with actuator faults. *IFAC-PapersOnLine*, 51(24):1133–1140.
- Badihi, H., Zhang, Y., and Hong, H. (2013). A review on application of monitoring, diagnosis, and fault-tolerant control to wind turbines. In *IEEE Conference on Control and Fault-Tolerant Systems (SysTol)*, pages 365–370. Nice, October.
- Barlas, T. K. and Van Kuik, G. (2007). State of the art and perspectives of smart rotor control for wind turbines. In *Journal of Physics: Conference Series*, volume 75, page 012080. IOP Publishing.
- Barlas, T. K. and van Kuik, G. A. (2010). Review of state of the art in smart rotor control research for wind turbines. *Progress in Aerospace Sciences*, 46(1):1–27.
- Bemporad, A. and Morari, M. (1999). Robust model predictive control: A survey. In *Robustness in identification and control*, pages 207–226. Springer.
- Berg, J., Resor, B., Paquette, J., and White, J. (2014). Smart wind turbine rotor: design and field test. *SAND2014-0681*, Sandia National Laboratories, Albuquerque, NM.
- Bernhammer, L. O., van Kuik, G. A., and De Breuker, R. (2016). Fatigue and extreme load reduction of wind turbine components using smart rotors. *Journal of Wind Engineering and Industrial Aerodynamics*, 154:84–95.
- Betz, A. (1926). *Wind-energie und ihre ausnutzung durch windmühlen*. Vandenhoeck.
- Bianchi, H. D. B. and Mantz, R. J. (2006). *Wind turbine control systems: Principles, modelling and gain scheduling design*. Springer.

- Bir, G. S. (2008). User's guide to MBC3.
- Bishop, G., Welch, G., et al. (2001). An introduction to the Kalman filter. *Proc of SIGGRAPH, Course*, 8(27599-3175):59.
- Bladed, G. (2019). A design tool for wind turbine performance and loading. Available at <https://www.dnvgl.com/services/bladed-3775>. [accessed 08.02.19].
- Blanke, M., Kinnaert, M., Lunze, J., and Staroswiecki, M. (2006). *Diagnosis and fault-tolerant control*. John Wiley & Sons.
- Blesa, J., Rotondo, D., Puig, V., and Nejjadi, F. (2014). FDI and FTC of wind turbines using the interval observer approach and virtual actuators/sensors. *Control Engineering Practice*, 24:138–155.
- Borraccino, A., Schlipf, D., Haizmann, F., and Wagner, R. (2017). Wind field reconstruction from nacelle-mounted LiDAR short-range measurements. *Wind Energy Science*, 2(1):269–283.
- Bossanyi, E. (2000). Developments in closed loop controller design for wind turbines. In *ASME Wind Energy Symposium*, page 27.
- Bossanyi, E. (2003a). Individual blade pitch control for load reduction. *Wind Energy*, 6(2):119–128.
- Bossanyi, E. (2003b). Wind turbine control for load reduction. *Wind Energy: An International Journal for Progress and Applications in Wind Power Conversion Technology*, 6(3):229–244.
- Bossanyi, E. (2005). Further load reductions with individual pitch control. *Wind Energy*, 8(4):481–485.
- Bossanyi, E., Fleming, P., and Wright, A. (2012). Field test results with individual pitch control on the NREL CART3 wind turbine. In *50th AIAA Aerospace Sciences Meeting including the New Horizons Forum and Aerospace Exposition*, page 1019.
- Bossanyi, E. and Wright, A. (2009). Field testing of individual pitch control on the NREL CART-2 wind turbine. In *European Wind Energy Conference*.
- Bossanyi, E. A., Fleming, P. A., and Wright, A. D. (2013). Validation of individual pitch control by field tests on two-and three-bladed wind turbines. *IEEE Transactions on Control Systems Technology*, 21(4):1067–1078.
- Boyd, S., El Ghaoui, L., Feron, E., and Balakrishnan, V. (1994). *Linear matrix inequalities in system and control theory*, volume 15. Siam.
- Buffington, J., Chandler, P., and Pachter, M. (1999). On-line system identification for aircraft with distributed control effectors. *International Journal of Robust and Nonlinear Control*, 9(14):1033–1049.

- Burton, T., Jenkins, N., Sharpe, D., and Bossanyi, E. (2011). *Wind energy handbook*. John Wiley & Sons.
- Carcangiu, C., Pineda, I., Fischer, T., Kuhnle, B., Scheu, M., Martin, M., et al. (2011). Wind turbine structural damping control for tower load reduction. In *Civil Engineering Topics, Volume 4*, pages 141–153. Springer.
- Castaignet, D., Barlas, T., Buhl, T., Poulsen, N. K., Wedel-Heinen, J. J., Olesen, N. A., Bak, C., and Kim, T. (2014). Full-scale test of trailing edge flaps on a Vestas V27 wind turbine: active load reduction and system identification. *Wind Energy*, 17(4):549–564.
- Castaignet, D., Poulsen, N. K., Buhl, T., and Wedel-Heinen, J. J. (2011). Model predictive control of trailing edge flaps on a wind turbine blade. In *Proceedings of the 2011 IEEE American Control Conference*, pages 4398–4403. San Francisco, June–July.
- Chen, J. and Patton, R. J. (2012). *Robust model-based fault diagnosis for dynamic systems*. Springer Science & Business Media (online). 3rd Edition.
- Chen, J., Patton, R. J., and Zhang, H.-Y. (1996). Design of unknown input observers and robust fault detection filters. *International Journal of control*, 63(1):85–105.
- Chen, L., Shi, F., and Patton, R. (2013). Active FTC for hydraulic pitch system for an offshore wind turbine. In *2013 IEEE Conference on Control and Fault-Tolerant Systems (SysTol)*, pages 510–515. Nice, Oct.
- Chen, N., Qian, Z., Nabney, I. T., and Meng, X. (2014). Wind power forecasts using Gaussian processes and numerical weather prediction. *IEEE Transactions on Power Systems*, 29(2):656–665.
- Chen, P. C. and Chopra, I. (1997). Wind tunnel test of a smart rotor model with individual blade twist control. *Journal of Intelligent Material Systems and Structures*, 8(5):414–425.
- Chen, Z. and Stol, K. (2014). An assessment of the effectiveness of individual pitch control on upscaled wind turbines. In *Journal of Physics: Conference Series*, volume 524, page 012045. IOP Publishing.
- Chilali, M. and Gahinet, P. (1996). H_∞ design with pole placement constraints: an LMI approach. *IEEE Transactions on automatic control*, 41(3):358–367.
- Cho, S., Gao, Z., and Moan, T. (2016). Model-based fault detection of blade pitch system in floating wind turbines. In *Journal of Physics: Conference Series*, volume 753, page 092012. IOP Publishing.
- Cho, S., Gao, Z., and Moan, T. (2018). Model-based fault detection, fault isolation and fault-tolerant control of a blade pitch system in floating wind turbines. *Renewable Energy*, 120:306–321.

- Chow, E. and Willsky, A. (1984). Analytical redundancy and the design of robust failure detection systems. *IEEE Transactions on automatic control*, 29(7):603–614.
- Connectivity, T. (2019). Wind turbine sensors. Available at <https://www.te.com/usa-en/industries/energy-utilities/applications/wind-turbine-sensors.html?tab=pgp-story>. [accessed 10.02.19].
- Daneshi-Far, Z., Capolino, G.-A., and Henao, H. (2010). Review of failures and condition monitoring in wind turbine generators. In *2010 IEEE XIX International Conference on Electrical Machines (ICEM)*, pages 1–6. Rome, Sep.
- Darrow, J., Johnson, K., and Wright, A. (2011). Design of a tower and drive train damping controller for the three-bladed controls advanced research turbine operating in design-driving load cases. *Wind Energy*, 14(4):571–601.
- Deisenroth, M. P. (2010). *Efficient reinforcement learning using Gaussian processes*, volume 9. KIT Scientific Publishing.
- Dong, J. and Verhaegen, M. (2011). Data driven fault detection and isolation of a wind turbine benchmark. In *Proceedings of IFAC World Congress*, volume 2, pages 7086–7091.
- Draxl, C., Hodge, B., Clifton, A., and McCaa, J. (2015). Overview and meteorological validation of the wind integration national dataset toolkit. Technical report, National Renewable Energy Lab.(NREL), Golden, CO (United States).
- Duckwitz, D. and Shan, M. (2014). Active tower damping and pitch balancing—design, simulation and field test. In *Journal of Physics: Conference Series*, volume 555, page 012030. IOP Publishing.
- Dunne, F., Pao, L., Wright, A., Jonkman, B., and Kelley, N. (2010). Combining standard feedback controllers with feedforward blade pitch control for load mitigation in wind turbines. In *48th AIAA Aerospace Sciences Meeting Including the New Horizons Forum and Aerospace Exposition*, page 250.
- Dunne, F., Pao, L. Y., Wright, A. D., Jonkman, B., and Kelley, N. (2011). Adding feedforward blade pitch control to standard feedback controllers for load mitigation in wind turbines. *Mechatronics*, 21(4):682–690.
- Duriez, T., Brunton, S. L., and Noack, B. R. (2017). *Machine Learning Control-Taming Nonlinear Dynamics and Turbulence*. Springer.
- Ebrahimi, A. and Movahhedi, M. (2017). Power improvement of NREL 5MW wind turbine using multi-DBD plasma actuators. *Energy Conversion and Management*, 146:96–106.
- Edwards, C., Spurgeon, S. K., and Patton, R. J. (2000). Sliding mode observers for fault detection and isolation. *Automatica*, 36(4):541–553.

- Esbensen, T. and Sloth, C. (2009). Fault diagnosis and fault-tolerant control of wind turbines. Master's thesis, Aalborg University.
- Etemaddar, M., Gao, Z., and Moan, T. (2014). Structural load analysis of a wind turbine under pitch actuator and controller faults. In *Journal of Physics: Conference Series*, volume 555, page 012034. IOP Publishing.
- Eterno, J. S., Weiss, J. L., Looze, D. P., and Willsky, A. (1985). Design issues for fault tolerant-restructurable aircraft control. In *24th IEEE Conference on Decision and Control*, volume 24, pages 900–905.
- Evans, M. A., Cannon, M., and Kouvaritakis, B. (2015). Robust MPC tower damping for variable speed wind turbines. *IEEE Transactions on Control Systems Technology*, 23(1):290–296.
- Feng, X. (2014). *Predictive control approaches to fault tolerant control of wind turbines*. PhD thesis, University of Hull.
- Feng, X. and Patton, R. (2014). Active fault tolerant control of a wind turbine via fuzzy MPC and moving horizon estimation. *IFAC Proceedings Volumes*, 47(3):3633–3638.
- Fischer, B. and Shan, M. (2013). A survey on control methods for the mitigation of tower loads. *Fraunhofer-Institute for Wind Energy and Energy Systems Technology, IWES Project report*, 1:104–56.
- Fleming, P., Scholbrock, A., Jehu, A., Davoust, S., Osler, E., Wright, A. D., and Clifton, A. (2014). Field-test results using a nacelle-mounted LiDAR for improving wind turbine power capture by reducing yaw misalignment. In *Journal of Physics: Conference Series*, volume 524, page 012002. IOP Publishing.
- Fogh Odgaard, P., Sánchez Sardi, H. E., Escobet Canal, T., and Puig Cayuela, V. (2015). Fault diagnosis and fault tolerant control with application on a wind turbine low speed shaft encoder. In *9th IFAC Symposium on Fault Detection, Supervision and Safety for Technical Processes, SAFEPROCESS 2015, 2-4 september, Paris*, pages 1357–1362.
- Gao, R. and Gao, Z. (2016). Pitch control for wind turbine systems using optimization, estimation and compensation. *Renewable Energy*, 91:501–515.
- Gao, Z., Cecati, C., and Ding, S. X. (2015a). A survey of fault diagnosis and fault-tolerant techniques - Part I: Fault diagnosis with model-based and signal-based approaches. *IEEE Transactions on Industrial Electronics*, 62(6):3757–3767.
- Gao, Z., Cecati, C., and Ding, S. X. (2015b). A survey of fault diagnosis and fault-tolerant techniques - Part II: Fault diagnosis with knowledge-based and hybrid/active approaches. *IEEE Transactions on Industrial Electronics*, 62(6):3768–3774.

- Gao, Z. and Ding, S. X. (2007). Actuator fault robust estimation and fault-tolerant control for a class of nonlinear descriptor systems. *Automatica*, 43(5):912–920.
- Gao, Z., Liu, X., and Chen, M. Z. (2016). Unknown input observer-based robust fault estimation for systems corrupted by partially decoupled disturbances. *IEEE Trans. Industrial Electronics*, 63(4):2537–2547.
- Georg, S. and Schulte, H. (2014). Fault-tolerant control of wind turbines using a Takagi-Sugeno sliding mode observer. In *Journal of Physics: Conference Series*, volume 524, page 012053. IOP Publishing.
- Gertler, J. (1998). *Fault detection and diagnosis in engineering systems*. CRC press.
- Gertler, J. (2015). Fault detection and diagnosis. *Encyclopedia of systems and control*, pages 417–422.
- González-Longatt, F., Wall, P., and Terzija, V. (2012). Wake effect in wind farm performance: Steady-state and dynamic behavior. *Renewable Energy*, 39(1):329–338.
- Guillemin, F., Nguyen, H.-N., Sabiron, G., Di Domenico, D., and Boquet, M. (2018). Real-time three dimensional wind field reconstruction from nacelle LiDAR measurements. In *Journal of Physics: Conference Series*, volume 1037, page 032037. IOP Publishing.
- Habibi, H., Howard, I., and Simani, S. (2018). Reliability improvement of wind turbine power generation using model-based fault detection and fault tolerant control: A review. *Renewable Energy*, pages 877–896.
- Hameed, Z., Hong, Y., Cho, Y., Ahn, S., and Song, C. (2009). Condition monitoring and fault detection of wind turbines and related algorithms: A review. *Renewable and Sustainable energy reviews*, 13(1):1–39.
- Han, Y. and Leithead, W. (2014). Combined wind turbine fatigue and ultimate load reduction by individual blade control. In *Journal of physics: Conference series*, volume 524, page 012062. IOP Publishing.
- Han, Y. and Liu, X. (2014). Collective pitch sliding mode control for large scale wind turbines considering load reduction. In *2014 IEEE International Conference on Mechatronics and Control (ICMC)*, pages 652–656. Jinzhou, July.
- Hassan, H., ElShafei, A., Farag, W., and Saad, M. (2012). A robust LMI-based pitch controller for large wind turbines. *Renewable energy*, 44:63–71.
- Hayman, G. and Buhl Jr, M. (2012). Mlife users guide for version 1.00. *National Renewable Energy Laboratory, Golden, CO*.
- Heredia, G., Ollero, A., Bejar, M., and Mahtani, R. (2008). Sensor and actuator fault detection in small autonomous helicopters. *Mechatronics*, 18(2):90–99.

- Houtzager, I., van Wingerden, J., and Verhaegen, M. (2013). Wind turbine load reduction by rejecting the periodic load disturbances. *Wind Energy*, 16(2):235–256.
- Hua, S., Wang, S., Jin, S., Feng, S., and Wang, B. (2017). Wind speed optimisation method of numerical prediction for wind farm based on Kalman filter method. *The Journal of Engineering*, 2017(13):1146–1149.
- Huang, Z., Patton, R. J., and Lan, J. (2016). Sliding mode state and fault estimation for decentralized systems. In *Variable-Structure Approaches*, pages 243–281. Springer.
- Isermann, R. (2006). *Fault-diagnosis systems: an introduction from fault detection to fault tolerance*. Springer Science & Business Media.
- Isermann, R. (2011). *Fault-diagnosis applications: model-based condition monitoring: actuators, drives, machinery, plants, sensors, and fault-tolerant systems*. Springer Science & Business Media.
- Isermann, R. and Ballé, P. (1997). Trends in the application of model-based fault detection and diagnosis of technical processes. *Control engineering practice*, 5(5):709–719.
- Jena, D. and Rajendran, S. (2015). A review of estimation of effective wind speed based control of wind turbines. *Renewable and Sustainable Energy Reviews*, 43:1046–1062.
- Jiang, X., Dong, B., Xie, L., and Sweeney, L. (2010). Adaptive Gaussian process for short-term wind speed forecasting. In *European Conference on Artificial Intelligence*, pages 661–666. Portugal.
- Johnson, S. J., Baker, J. P., Van Dam, C., and Berg, D. (2010). An overview of active load control techniques for wind turbines with an emphasis on microtabs. *Wind Energy: An International Journal for Progress and Applications in Wind Power Conversion Technology*, 13(2-3):239–253.
- Jones, B. L., Lio, W., and Rossiter, J. (2018). Overcoming fundamental limitations of wind turbine individual blade pitch control with inflow sensors. *Wind Energy*, 21(10):922–936.
- Jonkman, B. J. (2009). Turbsim user’s guide: Version 1.50.
- Jonkman, J., Butterfield, S., Musial, W., and Scott, G. (2009). Definition of a 5-MW reference wind turbine for offshore system development. *National Renewable Energy Laboratory, Golden, CO, Technical Report No. NREL/TP-500-38060*.
- Jonkman, J. M., Buhl Jr, M. L., et al. (2005). FAST user’s guide. *National Renewable Energy Laboratory, Golden, CO, Technical Report No. NREL/EL-500-38230*.

- Kaimal, J. C., Wyngaard, J., Izumi, Y., and Coté, O. (1972). Spectral characteristics of surface-layer turbulence. *Quarterly Journal of the Royal Meteorological Society*, 98(417):563–589.
- Kalman, R. E. (1960). A new approach to linear filtering and prediction problems. *Journal of basic Engineering*, 82(1):35–45.
- Kamal, E., Aitouche, A., Ghorbani, R., and Bayart, M. (2012). Robust fuzzy fault-tolerant control of wind energy conversion systems subject to sensor faults. *IEEE Transactions on Sustainable Energy*, 3(2):231–241.
- Kani, S. P. and Ardehali, M. (2011). Very short-term wind speed prediction: a new Artificial Neural network–Markov chain model. *Energy Conversion and Management*, 52(1):738–745.
- Kiasi, F., Prakash, J., Shah, S., and Lee, J. M. (2011). Fault detection and isolation of benchmark wind turbine using the likelihood ratio test. In *Proceedings of IFAC World Congress*, pages 7079–7085.
- Kim, J., Yang, I., and Lee, D. (2012). Control allocation based compensation for faulty blade actuator of wind turbine. *IFAC Proceedings Volumes*, 45(20):355–360.
- Koerber, A. and King, R. (2013). Combined feedback–feedforward control of wind turbines using state-constrained model predictive control. *IEEE Transactions on Control Systems Technology*, 21(4):1117–1128.
- Koh, J. and Ng, E. (2016). Downwind offshore wind turbines: Opportunities, trends and technical challenges. *Renewable and Sustainable Energy Reviews*, 54:797–808.
- Körber, A. (2014). *Extreme and fatigue load reducing control for wind turbines: a model predictive control approach using robust state constraints*. PhD thesis, Technical University of Berlin.
- Körber, A. and King, R. (2010). Model predictive control for wind turbine. In *European Wind Energy Conference*. Warsaw, April.
- Kragh, K. A. and Hansen, M. H. (2011). Model predictive individual pitch control based on local inflow measurements. In *7th PhD Seminar on Wind Energy in Europe*. Delft University of Technology, organized by the European Academy of Wind Energy.
- Kumar, A., Hugues-Salas, O., Savini, B., and Keogh, W. (2016a). Tower based load measurements for individual pitch control and tower damping of wind turbines. In *Journal of Physics: Conference Series*, volume 753, page 052024. IOP Publishing.
- Kumar, E. V. and Jerome, J. (2013). Robust LQR controller design for stabilizing and trajectory tracking of inverted pendulum. *Procedia Engineering*, 64:169–178.

- Kumar, Y., Ringenber, J., Depuru, S. S., Devabhaktuni, V. K., Lee, J. W., Nikolaidis, E., Andersen, B., and Afjeh, A. (2016b). Wind energy: Trends and enabling technologies. *Renewable and Sustainable Energy Reviews*, 53:209–224.
- Laino, D. J. and Hansen, A. C. (2002). Aerodyn user's guide. *available electronically at <http://wind/designcodes/simulators/aerodyn/AeroDyn.pdf>*.
- Laks, J., Pao, L., Simley, E., Wright, A., Kelley, N., and Jonkman, B. (2011). Model predictive control using preview measurements from LiDAR. In *49th AIAA Aerospace Sciences Meeting including the New Horizons Forum and Aerospace Exposition*, page 813.
- Laks, J., Pao, L. Y., Wright, A., Kelley, N., and Jonkman, B. (2010). Blade pitch control with preview wind measurements. In *Proceedings of the 48th AIAA Aerospace Sciences Meeting Including the New Horizons Forum and Aerospace Exposition*. Florida, Jan.
- Lan, J. (2017). *Robust model-based fault estimation and fault-tolerant control: towards an integration*. PhD thesis, University of Hull.
- Lan, J. and Patton, R. J. (2015). Integrated design of robust fault estimation and fault-tolerant control for linear systems. In *IEEE 54th Decision and Control, CDC 2015*, pages 5105–5110. Osaka, Dec.
- Lan, J. and Patton, R. J. (2016). A new strategy for integration of fault estimation within fault-tolerant control. *Automatica*, 69:48–59.
- Lan, J., Patton, R. J., and Zhu, X. (2018). Fault-tolerant wind turbine pitch control using adaptive sliding mode estimation. *Renewable Energy*, 116:219–231.
- Leithead, W. and Dominguez, S. (2005). Controller design for the cancellation of the tower fore-aft mode in a wind turbine. In *44th IEEE Conference on Decision and Control*, pages 1276–1281. Seville, Dec.
- Leithead, W., Dominguez, S., and Spruce, C. (2004). Analysis of tower/blade interaction in the cancellation of the tower fore-aft mode via control. In *European Wind Energy Conference 2004*. London, Nov.
- Leithead, W., Neilson, V., and Dominguez, S. (2009). Alleviation of unbalanced rotor loads by single blade controllers. In *European Wind Energy Conference (EWEC)*. Marseilles, France.
- Li, D., Song, Y., Cai, W., Li, P., and Karimi, H. R. (2014). Wind turbine pitch control and load mitigation using an L_1 adaptive approach. *Mathematical Problems in Engineering*, pages 719–803. <http://dx.doi.org/10.1155/2014/719803>.

- Li, J., Xu, H., Zhang, L., Hu, S., et al. (2008). Disturbance accommodating LQR method based pitch control strategy for wind turbines. In *2nd IEEE IITA'08 Symposium on Intelligent Information Technology Application*, volume 1, pages 766–770. Shanghai, China.
- Liniger, J., Soltani, M., Pedersen, H. C., Carroll, J., and Sepehri, N. (2017). Reliability based design of fluid power pitch systems for wind turbines. *Wind Energy*, 20(6):1097–1110.
- Lio, W. H., Jones, B. L., Lu, Q., and Rossiter, J. (2017). Fundamental performance similarities between individual pitch control strategies for wind turbines. *International Journal of Control*, 90(1):37–52.
- Lio, W. H. A. (2018). *Blade-Pitch Control for Wind Turbine Load Reductions*. PhD thesis, University of Sheffield.
- Liu, H., Tang, Q., Chi, Y., Zhang, Z., and Yuan, X. (2016). Vibration reduction strategy for wind turbine based on individual pitch control and torque damping control. *International Transactions on Electrical Energy Systems*, 26(10):2230–2243.
- Liu, W., Tang, B., Han, J., Lu, X., Hu, N., and He, Z. (2015). The structure healthy condition monitoring and fault diagnosis methods in wind turbines: A review. *Renewable and Sustainable Energy Reviews*, 44:466–472.
- Liu, Y., Patton, R. J., and Lan, J. (2018a). Fault-tolerant individual pitch control using adaptive sliding mode observer. In *IFAC Safeprocess*, volume 51, pages 1127–1132. Warsaw, Poland.
- Liu, Y., Patton, R. J., and Shi, S. (2018b). Wind turbine load mitigation using MPC with Gaussian wind speed prediction. In *UKACC 12th International Conference on Control, CONTROL 2018, Sheffield*, pages 32–37. Available at IEEE Xplore: <https://ieeexplore.ieee.org/abstract/document/8516882>.
- Lu, B., Li, Y., Wu, X., and Yang, Z. (2009). A review of recent advances in wind turbine condition monitoring and fault diagnosis. In *the IEEE Conference, Power Electronics and Machines in Wind Applications, PEMWA 2009*, pages 1–7. Available at IEEE Xplore: <https://ieeexplore.ieee.org/document/5208325>.
- Lu, Q., Bowyer, R., and Jones, B. L. (2015). Analysis and design of Coleman transform-based individual pitch controllers for wind-turbine load reduction. *Wind Energy*, 18(8):1451–1468.
- Lunze, J. and Richter, J. H. (2008). Reconfigurable fault-tolerant control: a tutorial introduction. *European journal of control*, 14(5):359.
- Lunze, J. and Steffen, T. (2006). Control reconfiguration after actuator failures using disturbance decoupling methods. *IEEE Transactions on Automatic Control*, 51(10):1590–1601.

- Luo, N., Vidal, Y., and Acho, L. (2014). *Wind turbine control and monitoring*. Springer: Heidelberg, Germany.
- Malcolm, D. J. and Hansen, A. C. (2006). Windpact turbine rotor design study: June 2000–June 2002 (revised). Technical report, National Renewable Energy Lab.(NREL), Golden, CO (United States).
- Maybeck, P. S. (1979). Stochastic models, estimation, and control. New York: Academic, 1979, vol.1.
- Maybeck, P. S. and Stevens, R. D. (1991). Reconfigurable flight control via multiple model adaptive control methods. *IEEE Transactions on Aerospace and Electronic systems*, 27(3):470–480.
- Mayne, D. Q., Rawlings, J. B., Rao, C. V., and Sokaert, P. O. (2000). Constrained model predictive control: Stability and optimality. *Automatica*, 36(6):789–814.
- Mendiratta, J. and Jayapal, R. (2010). H_∞ loop shaping based robust power system stabilizer for three machine power system. *International Journal of Computer Applications*, 1:106–112.
- Menezes, E. J. N., Araújo, A. M., and da Silva, N. S. B. (2018). A review on wind turbine control and its associated methods. *Journal of cleaner production*, 174:945–953.
- Mohammadi, E., Fadaeinedjad, R., and Moschopoulos, G. (2018). Implementation of internal model-based control and individual pitch control to reduce fatigue loads and tower vibrations in wind turbines. *Journal of Sound and Vibration*, 421:132–152.
- Morari, M. and Lee, J. H. (1999). Model predictive control: past, present and future. *Computers & Chemical Engineering*, 23(4-5):667–682.
- Naik, G. R. (2017). *Advances in Principal Component Analysis: Research and Development*. Springer Singapore. <https://doi.org/10.1007/978-981-10-6704-4>.
- Namik, H. and Stol, K. (2010). Individual blade pitch control of floating offshore wind turbines. *Wind Energy: An International Journal for Progress and Applications in Wind Power Conversion Technology*, 13(1):74–85.
- Ng, B. F., Palacios, R., Kerrigan, E. C., Graham, J. M. R., and Hesse, H. (2016). Aerodynamic load control in horizontal axis wind turbines with combined aeroelastic tailoring and trailing-edge flaps. *Wind Energy*, 19(2):243–263.
- Odgaard, P. F. and Stoustrup, J. (2009). Unknown input observer based scheme for detecting faults in a wind turbine converter. In *Proceedings of the 7th IFAC Symposium on Fault Detection, Supervision and Safety of Technical processes*, volume 1, pages 161–166. Barcelona.

- Odgaard, P. F. and Stoustrup, J. (2010). Unknown input observer based detection of sensor faults in a wind turbine. In *IEEE International Conference on Control Applications (CCA 2010)*, pages 310–315. <https://ieeexplore.ieee.org/document/5611266>.
- Odgaard, P. F. and Stoustrup, J. (2012a). Fault tolerant control of wind turbines using unknown input observers. In *8th IFAC symposium on fault detection, supervision and safety of technical processes*, pages 313–318. Elsevier Science.
- Odgaard, P. F. and Stoustrup, J. (2012b). Results of a wind turbine FDI competition. In *Proceedings of the 8th IFAC Symposium on Fault Detection, Supervision and Safety of Technical Processes, August*, pages 29–31.
- Odgaard, P. F., Stoustrup, J., and Kinnaert, M. (2013). Fault-tolerant control of wind turbines: A benchmark model. *IEEE Transactions on Control Systems Technology*, 21(4):1168–1182.
- Østergaard, K. Z., Brath, P., and Stoustrup, J. (2007). Estimation of effective wind speed. In *Journal of Physics: Conference Series*, volume 75, page 012082. IOP Publishing.
- Øye, S. (2001). Various flex 5 documentation. DTU Mechanical Engineering.
- Panagopoulos, H. and Åström, K. J. (2000). PID control design and H_∞ loop shaping. *International Journal of Robust and Nonlinear Control*, 10(15):1249–1261.
- Pao, L. Y. and Johnson, K. E. (2011). Control of wind turbines. *IEEE Control systems magazine*, 31(2):44–62.
- Patton, R. J. (1997a). Fault-tolerant control: the 1997 situation. *IFAC Proceedings Volumes*, 30(18):1029–1051.
- Patton, R. J. (1997b). Robustness in model-based fault diagnosis: the 1995 situation. *Annual reviews in control*, 21:103–123.
- Patton, R. J. (2015). Fault-tolerant control. *IEEE Encyclopedia of systems and control*, pages 422–428. <https://link.springer.com/referenceworkentry/10.1007>
- Patton, R. J., Frank, P. M., and Clark, R. N. (2013). *Issues of fault diagnosis for dynamic systems*. Springer Science & Business Media.
- Perrone, F. and Kühn, M. (2015). Offshore wind turbine tower fore-aft fatigue load reduction by coupling control and vibrational analysis. *Journal of Ocean and Wind Energy*, 2(3):168–175.
- Pisu, P. and Ayalew, B. (2011). Robust fault diagnosis for a horizontal axis wind turbine. In *18th IFAC World Congress*, pages 7055–7060. Milan, Aug-Sep.

- Plumley, C., Leithead, W., Jamieson, P., Bossanyi, E., and Graham, M. (2014). Comparison of individual pitch and smart rotor control strategies for load reduction. In *Journal of Physics: Conference Series*, volume 524, page 012054. IOP Publishing.
- Pourmohammad, S. and Fekih, A. (2011). Fault-tolerant control of wind turbine systems - A review. In *Green Technologies Conference (IEEE-Green)*, pages 1–6. <https://ieeexplore.ieee.org/abstract/document/5754880>.
- Privara, S., Široký, J., Ferkl, L., and Cigler, J. (2011). Model predictive control of a building heating system: The first experience. *Energy and Buildings*, 43(2-3):564–572.
- Qi, K., De-hui, S., Zheng-xi, L., Shu-juan, Q., Yan-jiao, H., and Yun-tao, S. (2014). H_∞ fault tolerant control of wind turbine system with actuator faults. In *19th IFAC World Congress*, volume 47, pages 5838–5843. South Africa, Aug.
- Qiao, W. and Lu, D. (2015a). A survey on wind turbine condition monitoring and fault diagnosis - Part I: Components and subsystems. *IEEE Transactions on Industrial Electronics*, 62(10):6536–6545.
- Qiao, W. and Lu, D. (2015b). A survey on wind turbine condition monitoring and fault diagnosis - Part II: Signals and signal processing methods. *IEEE Transactions on Industrial Electronics*, 62(10):6546–6557.
- Qin, S. J. and Badgwell, T. A. (2003). A survey of industrial model predictive control technology. *Control engineering practice*, 11(7):733–764.
- Raach, S., Schlipf, D., Sandner, F., Matha, D., and Cheng, P. W. (2014). Non-linear model predictive control of floating wind turbines with individual pitch control. In *American Control Conference (ACC), 2014*, pages 4434–4439. <https://ieeexplore.ieee.org/document/6858718>.
- Rahnavard, M., Ayati, M., and Yazdi, M. R. H. (2019). Robust actuator and sensor fault reconstruction of wind turbine using modified sliding mode observer. *Transactions of the Institute of Measurement and Control*, 41(6):1504–1518.
- Raković, S. V. (2016). Model predictive control: Classical, robust, and stochastic. *IEEE Control Systems*, 36(6):102–105.
- Riahy, G. and Abedi, M. (2008). Short term wind speed forecasting for wind turbine applications using linear prediction method. *Renewable energy*, 33(1):35–41.
- Richter, J. H. (2011). *Reconfigurable control of nonlinear dynamical systems: a fault-hiding approach*, volume 408. Springer.
- Roberts, S., Osborne, M., Ebden, M., Reece, S., Gibson, N., and Aigrain, S. (2013). Gaussian processes for time-series modelling. *Philosophical Transactions of the*

- Royal Society of London A: Mathematical, Physical and Engineering Sciences*, 371(1984).
- Roddier, D., Cermelli, C., Aubault, A., and Weinstein, A. (2010). Windfloat: A floating foundation for offshore wind turbines. *Journal of renewable and sustainable energy*, 2(3):033104.
- Rossiter, J. A. (2003). *Model-based predictive control: a practical approach*. CRC press.
- Rotondo, D., Nejjari, F., Puig, V., and Blesa, J. (2012). Fault tolerant control of the wind turbine benchmark using virtual sensors/actuators. In *8th IFAC Symposium on Fault Detection, Supervision and Safety of Technical Processes*, pages 114–119. Mexico, Aug.
- Sami, M. and Patton, R. J. (2012a). Fault tolerant adaptive sliding mode controller for wind turbine power maximisation. *IFAC Proceedings Volumes*, 45(13):499–504.
- Sami, M. and Patton, R. J. (2012b). Global wind turbine FTC via TS fuzzy modelling and control. *IFAC Proceedings Volumes*, 45(20):325–330.
- Sami, M. and Patton, R. J. (2012c). An FTC approach to wind turbine power maximisation via TS fuzzy modelling and control. *IFAC Proceedings Volumes*, 45(20):349–354.
- Savvidis, P. (2017). *Nonlinear control: an LPV nonlinear predictive generalised minimum variance perspective*. PhD thesis, University of Strathclyde.
- Schlipf, D. (2016). *LiDAR-assisted control concepts for wind turbines*. PhD thesis, University of Stuttgart.
- Schlipf, D., Fleming, P., Haizmann, F., Scholbrock, A., Hofsäß, M., Wright, A., and Cheng, P. W. (2014). Field testing of feedforward collective pitch control on the CART2 using a nacelle-based LiDAR scanner. In *Journal of Physics: Conference Series*, volume 555, page 012090. IOP Publishing.
- Schlipf, D., Schlipf, D. J., and Kühn, M. (2013). Nonlinear model predictive control of wind turbines using LiDAR. *Wind Energy*, 16(7):1107–1129.
- Scholbrock, A., Fleming, P., Fingersh, L., Wright, A., Schlipf, D., Haizmann, F., and Belen, F. (2013). Field testing LiDAR-based feed-forward controls on the NREL controls advanced research turbine. In *51st AIAA Aerospace Sciences Meeting Including the New Horizons Forum and Aerospace Exposition*, page 818. Texas, Jan.
- Schuler, S., Schlipf, D., Kuhn, M., and Allgower, F. (2010). l_1 -optimal multivariable pitch control for load reduction on large wind turbines. In *European Wind Energy Conference*. Warsaw, April.

- Selvam, K. (2007). Individual pitch control for large scale wind turbines. Master's thesis, Technical University of Delft.
- Selvam, K., Kanev, S., van Wingerden, J. W., van Engelen, T., and Verhaegen, M. (2009). Feedback–feedforward individual pitch control for wind turbine load reduction. *International Journal of Robust and Nonlinear Control*, 19(1):72–91.
- Shan, M., Jacobsen, J., and Adelt, S. (2013). Field testing and practical aspects of load reducing pitch control systems for a 5 MW offshore wind turbine. In *Annual Conference and Exhibition of European Wind Energy Association*, pages 101–105. <http://publica.fraunhofer.de/documents/N-301017.html>.
- Shi, F. and Patton, R. (2015). An active fault tolerant control approach to an offshore wind turbine model. *Renewable Energy*, 75:788–798.
- Shi, S., Patton, R. J., and Liu, Y. (2018). Short-term wave forecasting using Gaussian process for optimal control of wave energy converters. In *11th IFAC Conference on Control Applications in Marine Systems, Robotics, and Vehicles (CAMS 2018)*, pages 44–49. Opatija, Sep.
- Simani, S., Castaldi, P., and Tilli, A. (2011). Data-driven approach for wind turbine actuator and sensor fault detection and isolation. In *Proceedings of IFAC World Congress*, pages 8301–8306. Milan, Sep.
- Simley, E. and Pao, L. (2013). Reducing LiDAR wind speed measurement error with optimal filtering. In *2013 American Control Conference*, pages 621–627. Washington, June.
- Simon, D. (2006). *Optimal state estimation: Kalman, H infinity, and nonlinear approaches*. John Wiley & Sons.
- Sloth, C., Esbensen, T., and Stoustrup, J. (2011). Robust and fault-tolerant linear parameter-varying control of wind turbines. *Mechatronics*, 21(4):645–659.
- Soltani, M. N., Knudsen, T., Svenstrup, M., Wisniewski, R., Brath, P., Ortega, R., and Johnson, K. (2013). Estimation of rotor effective wind speed: A comparison. *IEEE Transactions on Control Systems Technology*, 21(4):1155–1167.
- Soman, S. S., Zareipour, H., Malik, O., and Mandal, P. (2010). A review of wind power and wind speed forecasting methods with different time horizons. In *IEEE North American power symposium (NAPS)*, pages 1–8. Texas, Sep.
- Spencer, M. D., Stol, K. A., Unsworth, C. P., Cater, J. E., and Norris, S. E. (2013). Model predictive control of a wind turbine using short-term wind field predictions. *Wind Energy*, 16(3):417–434.

- Stotsky, A. (2014). Blade root moment sensor failure detection based on multibeam LiDAR for fault-tolerant individual pitch control of wind turbines. *Energy Science & Engineering*, 2(3):107–115.
- Sun, X. and Patton, R. J. (2013). Robust actuator multiplicative fault estimation with unknown input decoupling for a wind turbine system. In *Control and Fault-Tolerant Systems (SysTol)*, pages 263–268. Nice, Oct.
- Tan, C. P. and Edwards, C. (2002). Sliding mode observers for detection and reconstruction of sensor faults. *Automatica*, 38(10):1815–1821.
- Tascikaraoglu, A. and Uzunoglu, M. (2014). A review of combined approaches for prediction of short-term wind speed and power. *Renewable and Sustainable Energy Reviews*, 34:243–254.
- Technology, P. (2017). Horns rev 3 offshore wind farm. Available at <https://www.power-technology.com/projects/horns-rev-3-offshore-wind-farm/>. [accessed 16.02.19].
- Towers, P. and Jones, B. L. (2016). Real-time wind field reconstruction from LiDAR measurements using a dynamic wind model and state estimation. *Wind Energy*, 19(1):133–150.
- Vali, M., van Wingerden, J.-W., and Kühn, M. (2016). Optimal multivariable individual pitch control for load reduction of large wind turbines. In *American Control Conference (ACC), 2016*, pages 3163–3169. <https://ieeexplore.ieee.org/abstract/document/7525404>.
- Van Engelen, T. (2006). Design model and load reduction assessment for multi-rotational mode individual pitch control (higher harmonics control). In *European wind energy conference*. Athens, Feb-March.
- Van Engelen, T. and Van der Hooft, E. (2005). Individual pitch control inventory. *Technical University of Delft, Technical Report No. ECN-C-03-138*.
- Van Kuik, G. A. M., Peinke, J., Nijssen, R., Lekou, D., Mann, J., Sørensen, J. N., Ferreira, C., van Wingerden, J. W., Schlipf, D., Gebraad, P., Polinder, H., Abrahamsen, A., van Bussel, G. J. W., Sørensen, J. D., Tavner, P., Bottasso, C. L., Muskulus, M., Matha, D., Lindeboom, H. J., Degraer, S., Kramer, O., Lehnhoff, S., Sonnenschein, M., Sørensen, P. E., Künneke, R. W., Morthorst, P. E., and Skytte, K. (2016). Long-term research challenges in wind energy – a research agenda by the European Academy of Wind Energy. *Wind Energy Science*, 1(1):1–39.
- Van Wingerden, J., Hulskamp, A., Barlas, T., Marrant, B., Van Kuik, G., Molenaar, D.-P., and Verhaegen, M. (2008). On the proof of concept of a 'Smart' wind turbine rotor blade for load alleviation. *Wind Energy: International Journal for Progress and Applications in Wind Power Conversion Technology*, 11(3):265–280.

- Walford, C. A. (2006). *Wind turbine reliability: understanding and minimizing wind turbine operation and maintenance costs*. Sandia Report, SAND 2006-1100. Sandia National Laboratories, Albuquerque, New Mexico 87185 and Livermore, California. http://www.anecto.com/wp-content/uploads/2012/02/OM_Costs.pdf.
- Wang, H. and Daley, S. (1996). Actuator fault diagnosis: an adaptive observer-based technique. *IEEE Transactions on Automatic Control*, 41(7):1073–1078.
- Wang, L., Cai, M., Zhang, H., Alsaadi, F., and Chen, L. (2017). Active fault-tolerant control for wind turbine with simultaneous actuator and sensor faults. *Complexity*. Article ID 6164841.
- Wang, N., Johnson, K. E., and Wright, A. D. (2012). FX-RLS-based feedforward control for LiDAR-enabled wind turbine load mitigation. *IEEE Transactions on Control Systems Technology*, 20(5):1212–1222.
- Wei, X., Verhaegen, M., and Van den Engelen, T. (2008). Sensor fault diagnosis of wind turbines for fault tolerant. In *17th IFAC World Congress*, pages 3222–3227. Korea, July.
- Wilkinson, M., Hendriks, B., Spinato, F., Harman, K., Gomez, E., Bulacio, H., Roca, J., Tavner, P., Feng, Y., and Long, H. (2010). Methodology and results of the reliawind reliability field study. In *European Wind Energy Conference and Exhibition, EWEC 2010*, volume 3, pages 1984–2004. Warsaw, April.
- Williams, C. K. and Rasmussen, C. E. (2006). Gaussian processes for machine learning. *the MIT Press*, 2(3):4.
- Wilson, A. and Adams, R. (2013). Gaussian process kernels for pattern discovery and extrapolation. In *International Conference on Machine Learning*, pages 1067–1075. Atlanta, June.
- Wright, A. and Fingersh, L. (2008). Advanced control design for wind turbines. *Part I: Control Design, Implementation, and Initial Tests, National Renewable Energy Lab., USA*.
- Wright, A., Fingersh, L., and Stol, K. (2007). Designing and testing controls to mitigate tower dynamic loads in the controls advanced research turbine. In *45th AIAA Aerospace Sciences Meeting and Exhibit*, page 1021. Reno, Jan.
- Wright, A. D. (2004). *Modern control design for flexible wind turbines*. NREL Report No. TP-500-35816, National Renewable Energy Laboratory.
- Xiao, S., Yang, G., and Geng, H. (2013). Individual pitch control design of wind turbines for load reduction using. In *IEEE conference ECCE Asia Downunder (ECCE Asia)*, pages 227–232. Melbourne, June.

- Xie, Y., Zhao, K., Sun, Y., and Chen, D. (2010). Gaussian processes for short-term traffic volume forecasting. *Transportation Research Record*, 2165(1):69–78.
- Yan, X.-G. and Edwards, C. (2007). Nonlinear robust fault reconstruction and estimation using a sliding mode observer. *Automatica*, 43(9):1605–1614.
- Yang, X. and Maciejowski, J. M. (2012). Fault-tolerant model predictive control of a wind turbine benchmark. In *8th IFAC SAFEPROCESS*, pages 337–342. Mexico, Aug.
- Yin, S., Wang, G., and Karimi, H. R. (2014). Data-driven design of robust fault detection system for wind turbines. *Mechatronics*, 24(4):298–306.
- Yuan, Y. and Tang, J. (2017). On advanced control methods toward power capture and load mitigation in wind turbines. *Engineering*, 3(4):494–503.
- Zhang, K., Jiang, B., and Cocquempot, V. (2008). Adaptive observer-based fast fault estimation. *International Journal of Control, Automation, and Systems*, 6(3):320–326.
- Zhang, X., Zhang, Q., Zhao, S., Ferrari, R. M., Polycarpou, M. M., and Parisini, T. (2011a). Fault detection and isolation of the wind turbine benchmark: An estimation-based approach. In *Proceedings of IFAC World Congress*, volume 18, pages 8295–8300. Milan, Sep.
- Zhang, Y., Chen, Z., and Cheng, M. (2013). Proportional resonant individual pitch control for mitigation of wind turbines loads. *IET Renewable Power Generation*, 7(3):191–200.
- Zhang, Y., Chen, Z., Cheng, M., and Zhang, J. (2011b). Mitigation of fatigue loads using individual pitch control of wind turbines based on FAST. In *Proceedings of the 46th VDE International Universities' Power Engineering Conference, UPEC 2011*, pages 1–6. Soest, Sep.
- Zhang, Y., Cheng, M., and Chen, Z. (2014a). Load mitigation of unbalanced wind turbines using PI-R individual pitch control. *IET Renewable Power Generation*, 9(3):262–271.
- Zhang, Y. and Jiang, J. (2001). Integrated active fault-tolerant control using IMM approach. *IEEE Transactions on Aerospace and Electronic systems*, 37(4):1221–1235.
- Zhang, Y. and Jiang, J. (2008). Bibliographical review on reconfigurable fault-tolerant control systems. *Annual Reviews in Control*, 32(2):229–252.
- Zhang, Z., Nielsen, S. R., Blaabjerg, F., and Zhou, D. (2014b). Dynamics and control of lateral tower vibrations in offshore wind turbines by means of active generator torque. *Energies*, 7(11):7746–7772.

-
- Zinober, A. (1990). *Deterministic control of uncertain systems*. London, U.K: P. Peregrinus on behalf of the Institution of Electrical Engineers.
- Zolghadri, A., Henry, D., Cieslak, J., Efimov, D., and Goupil, P. (2014). *Fault diagnosis and fault-tolerant control and guidance for aerospace vehicles*. Springer.
- Zuluaga, C. D., Alvarez, M. A., and Giraldo, E. (2015). Short-term wind speed prediction based on robust Kalman filtering: An experimental comparison. *Applied Energy*, 156:321–330.